Investigating the spatiotemporal dynamics and functional role of sleep oscillations using auditory stimulation and transgenic approaches



Cristina Blanco Duque

New College

Department of Physiology, Anatomy and Genetics

University of Oxford

Thesis submitted for the degree of

Doctor of Philosophy

Trinity 2020

Investigating the spatiotemporal dynamics and functional role of sleep oscillations using auditory stimulation and transgenic approaches

Abstract

Sleep is a fundamental process that appears to be ubiquitous across the animal kingdom. Significant resources are therefore directed towards understanding its underlying neurophysiology and its functional role. Mammals exhibit two kinds of sleep, NREM and REM sleep, which are primarily distinguished by specific patterns of brain activity. During NREM sleep, cortical activity is dominated by slow waves and sleep spindles. While slow-wave activity has been strongly linked with sleep homeostasis, neither the functional role nor regulation of sleep spindles has been fully understood.

Spindles are bursts of neuronal activity, which have been hypothesised to protect sleep from sensory disruption and support memory processing. Due to their potentially important role in normal and impaired brain function, spindles have become an attractive target for neuromodulation technologies. Traditional methods to detect and modulate spindles, however, treat them as all-or-none phenomena, and often do not take into account their complex spatiotemporal dynamics. Here we posit that to achieve a better understanding of the origin and functional significance of sleep spindles, it is necessary to develop novel detection and manipulation approaches that account for their spatiotemporal variability.

In this thesis, we demonstrate, using a novel conceptual and methodological approach, that treating spindles as all-or-none phenomena cannot be justified physiologically or mathematically. At the core of this approach is the *oscillatory-Quality,* which we propose as a parameter to measure the strength and synchrony of neuronal oscillations in quantitative terms. We applied this approach to investigate and characterise the

dynamics of spindles recorded from mice in different brain regions, at different spatial scales and across various experimental manipulations. We used sleep deprivation, auditory stimulation and transgenic mouse models, to investigate some of the hypothesised functional roles of sleep spindles and to evaluate how such interventions affect the global architecture of sleep.

Our data unequivocally suggest that, contrary to the traditional view, spindles cannot be treated as all-or-none phenomena, and neither do they represent strictly local or global events. Instead, spindles show a progressive variability in their spatio-temporal dynamics and other properties, which is captured in their *oscillatory-Quality*. We make novel observations on the cortical laminar dynamics of spindle activity in mice, and assess effects of preceding sleep-wake history and coupling of spindle events with slow waves. Using perturbation approaches, we make a novel observation that spindle activity is homeostatically regulated, independently of the well-established homeostatic regulation of slow-wave activity. Additionally, our preliminary results suggest that spindles play a role in sensory processing during sleep, but the occurrence of spatially synchronised spindle activity does not seem to be necessary for memory function. Overall, we demonstrate here that taking into account the *oscillatory-Quality* and homeostatic regulation of spindles opens up a new and promising avenue towards understanding their origin, dynamics and functional role.

Acknowledgements

First and foremost, I would like to thank Prof. Vladyslav Vyazovskiy and Prof. David Bannerman for being excellent supervisors. This DPhil has been a wonderful experience. With your guidance, enthusiasm, humour, and help, these last four years have been more enjoyable than I could have hoped for. I will always be grateful to you and would like to formally acknowledge your invaluable contribution to this work.

I am deeply grateful to Eckehard Olbrich and Peter Achermann for all of their help and guidance with the spindle detection algorithm, and for their insight into the results presented in Chapter 3. It has been absolutely inspiring to work with you.

I would also like to thank the members of the VV Lab, past and present, for all the support and for brining lots of happiness to my days during these last four years. Special thanks to Martin, Lukas, Laura and Linus, who read parts of this thesis. Thanks for your friendship, for all the laughs, for keeping me happy (and for keeping me sane). I has been an honour to work and collaborate with you.

Beyond the lab, I would like to the thank Leonie and Teele for your friendship, support, for always being there with a smile. Special thanks to Alejandro, my interest in neuroscience was exploited thanks to your support. Your friendship has been a very important key in my life. Special, thanks as well to my family. My family in Colombia and my family in the UK. Mum, dad, Ed, Terry and Thelma you are my core.

I would also like to thank three people who so warmly opened the door to science to me all those years ago: Wilson Lopez, Richard Henson and Andrea Greve. I would not be here without your support. Finally, I am also incredibly grateful with the WellcomeTrust and the Clarendon scholarships that have funded this work.

I would also like to thank Prof. Chiara Cirelli and Prof. Edward Mann for agreeing to be my examiners

Declaration and attributions

I declare that no part of this thesis has been, or is being, submitted for any qualification other than the degree of Doctor of Philosophy at the University of Oxford.

Research presented in this thesis was carried out under the supervision of Prof. Vladyslav Vyazovskiy and Prof. David Bannerman. All work presented is my own except were explicitly stated in the text our as detailed below:

- Prof. Eckehard Olbrich and Peter Achermann developed the original algorithm to detect spindles that was extended in this work.

- Dr. Lukas Krone, Dr. Martin Kahn, Linus Milinski and Jose Prius Mengual assisted with the surgeries and histology presented in Chapters 3 and 5.

Table of Contents

CHAPTER 1 - General Introduction 1

1.1. SLEEP OVERVIEW 1

1.1.1. Behavioural and electrophysiological characterization of sleep 2

1.1.2. Neuronal regulation of sleep 3

1.1.3. Sleep architecture in rodents and humans 4

1.2. ELECTRICAL RECORDINGS OF NEURONAL NETWORKS 6

1.2.1. Non-invasive extra-cortical recordings (EEG and ECoG) 7

1.2.2. Extra-cellular recordings (low and high frequency components) 8

1.3. NEUROPHYSIOLOGY OF SLEEP 8

1.3.1. Neurophysiology of spindles 9

1.3.2. Neurophysiology of the slow-oscillation 14

1.4. HOMEOSTATIC AND CIRCADIAN CONTROL OF SLEEP 17

1.5. POTENTIAL FUNCTION OF SLEEP IN HOMEOSTASIS AND COGNITION 19

1.5.1. Sleep and plasticity 19

1.5.2. Sleep and memory 20

1.6. SPINDLES IN PATHOLOGY 21

1.7. MODULATION OF SLEEP OSCILLATIONS 22

1.8. RATIONALE AND AIMS OF THIS THESIS 23

CHAPTER 2 - General Methods 25

2.1. Experimental Animals 25

2.2. Surgical Procedure 26

2.3. Histological verification of recording site 27

2.4. Identification of cortical layers 27

2.5. Signal processing and sleep scoring 28

2.6. Analysis of extracellular neuronal activity 29

2.7. Spindle detection 29

2.8. Slow wave detection 30

2.9. Sleep deprivation techniques 31

2.10. Statistical Analyses 31

CHAPTER 3 - *Oscillatory-Quality*: A fundamental parameter to understand the spatiotemporal dynamics of rhythmic neuronal oscillations like sleep spindles 34

3.1. INTRODUCTION 34

3.1.1. Approaches to study neuronal oscillations: commonly used and unused parameters 34

3.1.2. Traditional approaches for studying oscillations such as sleep spindles 36
3.1.3. What we know about spindle spatio-temporal dynamics based on traditional approaches 38
3.1.4. Our proposed approach: studying spindles while taking into account their oscillatory strength 42
3.2. METHODS 43
3.2.1. Animals 43
3.2.2. Surgical Procedure 44
3.2.3. Spindle Detection 45
3.2.4. Surrogate signal generation 49
3.3. RESULTS 50
3.3.1. Spindles are not all-or-none phenomena but there is substantial variability in their properties 52
3.3.2. The Oscillatory Quality (o-Quality): A quantitative metric for the strength of oscillatory activity 61
3.3.3. The Oscillatory-Quality reflects local and global synchrony of the spindle generating network 63
3.3.4. The Oscillatory-Quality reveals a thorough picture of the topography of spindles .. 72
3.3.5. The o-Quality of spindles is directly related to the occurrence of slow-waves and is sensitive to the levels of homeostatic sleep need 79
3.3.6. The o-Quality of spindles varies as a function of the infra-slow oscillation 92
3.4. DISCUSSION 99
3.4.1. Spindles are not all-or-none phenomena but there is high variability in their properties such as oscillatory-Quality 99
3.4.2. The Oscillatory-Quality gives an index of the local and global synchrony of the spindle generating network 101
3.4.3. The Oscillatory-Quality reveals a more complete picture of the topography of spindles 102
3.4.4. The o-Quality of spindles is directly related to the occurrence of slow waves and is sensitive to the levels of homeostatic sleep need 103
3.4.5. The quality of spindles varies as a function of the infra-slow oscillation 105
CHAPTER 4 – Investigating spindle-related deficits in GRIA1$^{-/-}$ mice, a mouse model relevant for schizophrenia 107
4.1. INTRODUCTION 107
4.2. METHODS 113
4.2.1. Animals 114
4.2.2. Surgical Procedure 115
4.2.3. Histological verification of recording sites 116
4.2.4. Behavioural tasks 118

4.2.5. Spindle detection 123
4.3. RESULTS 124
4.3.1. GRIA1$^{-/-}$ mice show a profound reduction in EEG spindle activity 126
4.3.2. Despite the reduction in EEG spindles, local LFP spindles are preserved in GRIA1$^{-/-}$ mice 130
4.3.3. The deletion of GluA1 affects the large scale synchronization of spindles..... 134
4.3.4. GluA1 deletion affects the association between spindle o-Quality and both the incidence of slow-waves and the levels of homeostatic sleep need 137
4.3.6. Despite showing deficits in spindle dynamics, long-term memory is preserved in GRIA1$^{-/-}$ mice 152
4.4. DISCUSSION 155
4.4.1. Potential neural mechanisms underlying spindle dynamics and deficits 156
4.4.2. Potential neural mechanisms underlying local and global sleep spindles 158
4.4.3. Potential effects of the deletion of GluA1 on the association between slow waves and spindles 159
4.4.4. Potential effects of the deletion of GluA1 on the association between the infra-slow oscillation and the spindle o-Quality 162
4.4.5. Clinical significance of the pattern of spindle deficits in GRIA1$^{-/-}$ mice..... 163
4.4.6. Functional significance of the spindle deficits in GRIA1$^{-/-}$ mice 164
CHAPTER 5 - Insights into the dynamics and function of spindles using auditory stimulation during sleep 167
5.1. INTRODUCTION 167
5.1.1. A potential role of spindles in the protection of sleep from sensory disruption 169
5.1.2. The effect of auditory stimulation on spindle activity 171
5.2. METHODS 176
5.2.1. Animals 176
5.2.2. Surgical Procedure 178
5.2.3. Auditory Stimulation 180
5.2.4. Spindle detection 189
5.3. RESULTS 190
5.3.1. Evidence of a homeostatic regulation of spindles in granular layers of S1 and in the frontal cortex after disruption caused by auditory stimulation 190
5.3.2. Auditory stimulation induces a reduction in multi-unit activity in granular layers of S1 209
5.3.3. Preliminary insights based on auditory closed-loop stimulation targeting spindle events 214
5.4. DISCUSSION 227

5.4.1. Potential mechanisms implicated in the association between spindle activity and auditory stimulation 228
5.4.2. The spindle activity seems to show a homeostatic regulation 231
5.4.3. Potential role of spindles protecting sleep from sensory disruption..... 232
CHAPTER 6 - General Discussion and Future Directions..... 235
6.1. Methodological advances..... 235
6.2. Insights into the spatio-temporal dynamics of spindles 237
6.2.1. The progressive occurrence of spindles in space and time 237
6.2.2. Spindle o-Quality and network synchrony..... 238
6.2.3. Characterising spindles: from global, to local, to dynamic 240
6.3. Insights into the homeostatic regulation of spindles 241
6.4. Insights into the functional role of sleep spindles..... 243
6.5. Practical and clinical implications of these advances 245
APPENDIX CHAPTER 3: STATISTIC TABLES..... 246
APPENDIX CHAPTER 4: STATISTIC TABLES..... 259
APPRENDIX CHAPTER 5: STATISTIC TABLES 270
BIBLIOGRAPHY 280

List of tables containing statistical analyses

TABLE 1. STATISTICAL ANALYSES FOR **FIGURE 8.E** 246
TABLE 2. STATISTICAL ANALYSES FOR **FIGURE 11.A** 246
TABLE 3. STATISTICAL ANALYSES FOR **FIGURE 11.B** 247
TABLE 4. STATISTICAL ANALYSES FOR **FIGURE 11.B** 248
TABLE 5. STATISTICAL ANALYSES FOR **FIGURE 11. A - B** 248
TABLE 6. STATISTICAL ANALYSES FOR **FIGURE 12.A (TOP PANEL)** 249
TABLE 7. STATISTICAL ANALYSES FOR **FIGURE 12.A (BOTTOM PANEL)** 249
TABLE 8. STATISTICAL ANALYSES FOR **FIGURE 12.B** 250
TABLE 9. STATISTICAL ANALYSES FOR **FIGURE14.*B (LEFT)*** 250
TABLE 10. STATISTICAL ANALYSES FOR **FIGURE14.B *(RIGHT)*** 251
TABLE 11. STATISTICAL ANALYSES FOR **FIGURE14.C *(LEFT)*** 251
TABLE 12. STATISTICAL ANALYSES FOR **FIGURE14.C (RIGHT)** 252
TABLE 13. STATISTICAL ANALYSES FOR **FIGURE 15.B** 252
TABLE 14. STATISTICAL ANALYSES FOR **FIGURE 15.B** 252
TABLE 15. STATISTICAL ANALYSES FOR **FIGURE 15.B** 252
TABLE 16. STATISTICAL ANALYSES FOR **FIGURE 15.B** 253
TABLE 17. STATISTICAL ANALYSES FOR **FIGURE 16.A** 253
TABLE 18. STATISTICAL ANALYSES FOR **FIGURE 16.B** 253
TABLE 19. STATISTICAL ANALYSES FOR **FIGURE 16.C** 254
TABLE 20. STATISTICAL ANALYSES FOR **FIGURE 16.D** 254
TABLE 21. STATISTICAL ANALYSES FOR **FIGURE 16.E** 255
TABLE 22. STATISTICAL ANALYSES FOR **FIGURE 16.F** 256
TABLE 23. STATISTICAL ANALYSES FOR **FIGURE 16.G** 256
TABLE 24. STATISTICAL ANALYSES FOR **FIGURE 16.F** 256
TABLE 25. STATISTICAL ANALYSES FOR **FIGURE 18.B** 257
TABLE 26. STATISTICAL ANALYSES FOR **FIGURE 18.C** 257
TABLE 27. STATISTICAL ANALYSES FOR **FIGURE 18.C** 258
TABLE 28. STATISTICAL ANALYSES FOR **FIGURE 18.D** 258
TABLE 29. STATISTICAL ANALYSES FOR **FIGURE 22.A** 259
TABLE 30. STATISTICAL ANALYSES FOR **FIGURE 22.B** 260
TABLE 31. STATISTICAL ANALYSES FOR **FIGURE 22.C** 260
TABLE 32. STATISTICAL ANALYSES FOR **FIGURE 22.E** 260
TABLE 33. STATISTICAL ANALYSES FOR **FIGURE 23.B** 261
TABLE 34. STATISTICAL ANALYSES FOR **FIGURE 23.C,E** 261
TABLE 35. STATISTICAL ANALYSES FOR **FIGURE 23.D** 261
TABLE 36. STATISTICAL ANALYSES FOR **FIGURE 23.F** 262
TABLE 37. STATISTICAL ANALYSES FOR **FIGURE 24.A** 262
TABLE 38. STATISTICAL ANALYSES FOR **FIGURE 24.B** 262
TABLE 39. STATISTICAL ANALYSES FOR **FIGURE 24.D** 263
TABLE 40. STATISTICAL ANALYSES FOR **FIGURE 24.E** 263
TABLE 41. STATISTICAL ANALYSES FOR **FIGURE 25.A** 263
TABLE 42. STATISTICAL ANALYSES FOR **FIGURE 25.A** 263
TABLE 43. STATISTICAL ANALYSES FOR **FIGURE 25.C** 264
TABLE 44. STATISTICAL ANALYSES FOR **FIGURE 25.C** 264
TABLE 45. STATISTICAL ANALYSES FOR **FIGURE 25.D** 264
TABLE 46. STATISTICAL ANALYSES FOR **FIGURE 25.D** 265
TABLE 47. STATISTICAL ANALYSES FOR **FIGURE 26.A** 265

Table 48. Statistical analyses for **Figure 26.A** 265
Table 49. Statistical analyses for **Figure 26.B** 266
Table 50. Statistical analyses for **Figure 26.C** 266
Table 51. Statistical analyses for **Figure 26.C** 266
Table 52. Statistical analyses for **Figure 26.D** 267
Table 53. Statistical analyses for **Figure 26.E** 267
Table 54. Statistical analyses for **Figure 26.E** 267
Table 55. Statistical analyses for **Figure 26.F** 268
Table 56. Statistical analyses for **Figure 26.G** 268
Table 57. Statistical analyses for **Figure 26.G** 268
Table 58. Statistical analyses for **Figure 27.D** 269
Table 59. Statistical analyses for **Figure 28.A** 269
Table 60. Statistical analyses for **Figure 28.B** 269
Table 61. 270
Table 62. Statistical analyses for **Figure 33**.C 271
Table 63. Statistical analyses for **Figure 33**.D 271
Table 64. Statistical analyses for **Figure 33**.E 271
Table 65. Statistical analyses for **Figure 34**.A 272
Table 66. Statistical analyses for **Figure 34**.B 272
Table 67. Statistical analyses for **Figure 34**.C 273
Table 68. Statistical analyses for **Figure 34**.D 273
Table 69. Statistical analyses for **Figure 34**.E 273
Table 70. Statistical analyses for **Figure 34**.F 274
Table 71. Statistical analyses for **Figure 34**.G 274
Table 72. 274
Table 73. Statistical analyses for **Figure 35**.D 275
Table 74. Statistical analyses for **Figure 36**.A 275
Table 75. Statistical analyses for **Figure 36**.B 275
Table 76. Statistical analyses for **Figure 36**.C 276
Table 77. Statistical analyses for **Figure 36**.D 276
Table 78. Statistical analyses for **Figure 36**.E 276
Table 79. Statistical analyses for **Figure 36**.F 277
Table 80. Statistical analyses for **Figure 37**.A 277
Table 81. Statistical analyses for **Figure 37**.B 277
Table 82. Statistical analyses for **Figure 42**.C 278
Table 83. Statistical analyses for **Figure 42**.C 278
Table 84. Statistical analyses for **Figure 42**.C 278
Table 85. Statistical analyses for **Figure 42**.D 278
Table 86. Statistical analyses for **Figure 42**.D 278
Table 87. Statistical analyses for **Figure 42**.D 279
Table 88. Statistical analyses for **Figure 42**.E 279
Table 89. Statistical analyses for **Figure 42**.E 279
Table 90. Statistical analyses for **Figure 42**.E 279
Table 91. Statistical analyses for **Figure 43.B** 279



CHAPTER 1 - General Introduction

This chapter presents an overview of the scientific background upon which this thesis is based. Specific introductions are presented at the beginning of each chapter.

1.1. SLEEP OVERVIEW

Sleep is something of an evolutionary paradox. During sleep, organisms are vulnerable to external threat, yet sleep seems to be necessary to support fundamental functions of the brain and body (Rechtschaffen, 1998; Siegel, 2005; Tononi and Cirelli, 2014; Krueger et al., 2016). From a phenomenological perspective, it may seem clear that sleep is important: when we do not sleep, we experience an array of negative physical, cognitive and emotional effects. Whether sleep is strictly necessary for survival, and the specific functions it may fulfil, are matters of intense debate (Rial et al., 2007; Cirelli and Tononi, 2008; Mignot, 2008; Dubouć et al., 2011; Anafi et al., 2019)

One of the strongest indications that sleep fulfils an important biological role is that it seems to be conserved across the animal kingdom (Campbell and Tobler, 1984; Cirelli and Tononi, 2008; Anafi et al., 2019). Furthermore, sleep loss seems to be homeostatically compensated in all species (Borbely, 1982; Franken et al., 1991; Achermann and Borbély, 2003; Cirelli and Tononi, 2008), and the lack of sleep objectively generates deleterious effects (Rechtschaffen and Bergmann, 2002; Tartar et al., 2006; Cirelli and Tononi, 2008). Investigating the dynamics and potential function of sleep-related brain activity, is therefore a worthwhile effort, with apparent fundamental implications.

1.1.1. Behavioural and electrophysiological characterization of sleep

Despite its universal nature, the expression of sleep varies widely across species (Campbell and Tobler, 1984; Cirelli and Tononi, 2008; Anafi et al., 2019). The main behavioural criteria that have been proposed to define sleep across species, define it as a reversible state of quiescence that involves species-specific postures, reduced responsiveness to external stimuli, is homeostatically regulated, and occurs at species-specific times of the day (Campbell and Tobler, 1984; Deboer, 2013).

The recording of electrophysiological activity from the mammalian and avian brain has been a useful tool to characterise and study sleep in these species. For instance, based on electroencephalographic (EEG) recordings in humans and rodents, it has been established that sleep in these species is composed of two core stages, defined as rapid eye movement sleep (REM) and non-rapid eye movement sleep (NREM), which

alternate in a semi-cyclical manner (Loomis et al., 1937; Dement and Kleitman, 1957; Saper et al., 2010).

On the one hand, NREM is mainly characterised by the regular occurrence of large amplitude slow waves, with a frequency of ~0.5-4 Hz (Destexhe et al., 1999; Massimini et al., 2004), and waxing-and-waning 10-15 Hz spindle oscillations (Loomis et al., 1935; Steriade et al., 1987; Steriade, 2003), which recur with a cycle length of around 50-s (Lecci et al., 2017; Lázár et al., 2019). On the other hand, during REM sleep the brain displays wake-like activity, particularly at theta (4-8 Hz) and faster frequencies, accompanied by a general reduction in muscle tone and rapid movement of the eyes (Dement and Kleitman, 1957; Zamboni et al., 1999; Cantero et al., 2003; Vyazovskiy et al., 2004b).

1.1.2. Neuronal regulation of sleep

Beginning with von Economo's observations in patients suffering from encephalitis lethargica, the hypothalamus has been studied as a key regulator of sleep and wakefulness (Economo, 1930). Since then, numerous hypothalamic structures have been shown to play an important role in sleep regulation. For instance, the ventrolateral preoptic area (VLPO) contains sleep active neurons (Sherin et al., 1996) and lesions to this region reduce the amount of NREM sleep (Lu et al., 2000). On the other hand, various circuits within and outside the hypothalamus are wake-promoting, such as hypocretin neurons, the Locus Coeruleus (Carter et al., 2010), or several regions of the thalamus (Honjoh et al., 2018).

A prominent circuit model of sleep-wake regulation (Saper et al., 2001, 2010) postulates a neuronal flip-flop switch, whereby wake- and sleep-promoting neurons mutually inhibit each other and thus produce stable brain states. While it is a valuable model, it cannot account for the large number of sleep-related structures identified so far (Liu and Dan, 2019) and explicitly does not account for the fact that sleep is far more nuanced than a dichotomous state appearing as either NREM or REM. As we will see later in this thesis, NREM sleep alone displays a humbling diversity of neuronal phenomena, each of which appears to be regulated individually and in complex interaction with each other. There is currently little known about if and how circuits that regulate sleep/wake transitions overlap with the regulatory elements in control of sleep-specific phenomena discussed in this thesis.

1.1.3. Sleep architecture in rodents and humans

Interestingly, despite the substantial variability that exists between mammals in terms of brain structure, the frequency characteristics (e.g. frequency bands) and temporal dynamics of information processing remain largely similar (Buzsáki et al., 2013). Consequently, brain activity patterns observed in the human brain are similarly present in other mammals. This makes non-human mammals useful models for providing physiological insights into human sleep. It is still relevant to highlight, however, that several differences exist in the architecture of sleep and circadian patterns between species (Lesku et al., 2006; McNamara et al., 2008).

For example, humans are normally diurnal (i.e. mainly active in daytime) (Ripperger et al., 2011; Refinetti et al., 2016) and during sleep show NREM-REM cycles of ~90

minutes (Loomis et al., 1937; Dement and Kleitman, 1957; Olbrich et al., 2011). Moreover, according to the American Academy of Sleep Medicine, NREM sleep in humans is subdivided into three stages (i.e. stages 1, 2 and 3), which show progressive depth and are comprised of different electrophysiological patterns (Olbrich et al., 2011). In contrast, laboratory mice (the species used in the present thesis) are predominantly nocturnal (i.e. mainly active at night-time) and polyphasic, meaning that (relative to humans) they express more fragmented sleep and wake periods, and during sleep, show NREM-REM transitions with shorter cycles lengths (i.e. ~10 minutes) (Campbell and Tobler, 1984). Additionally, rodent NREM sleep is not commonly subdivided into different stages (Lampert et al., 2015).

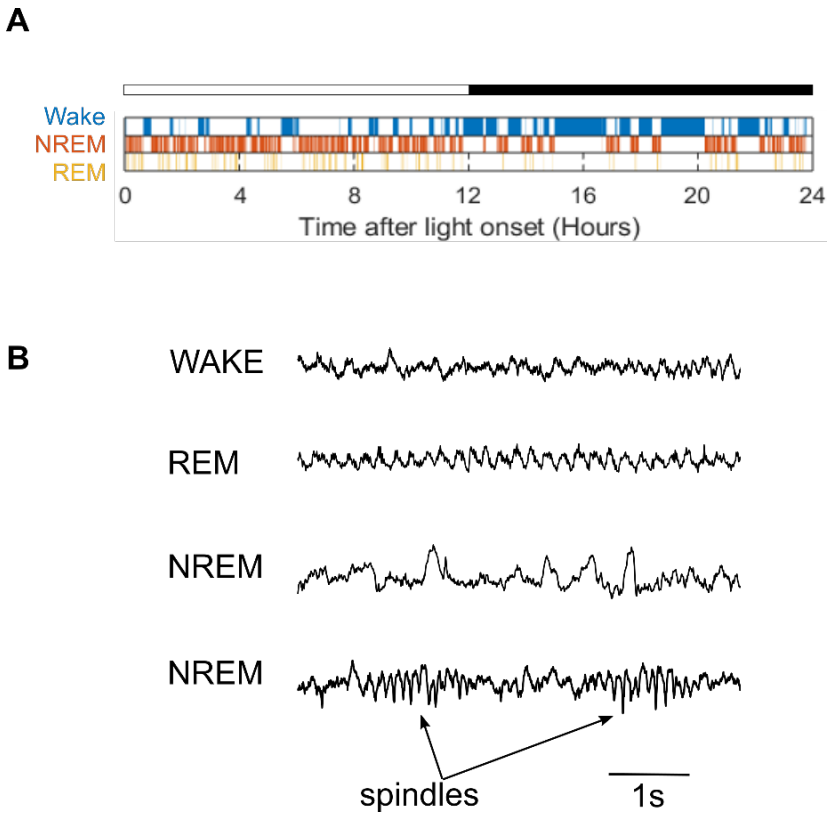


Figure 1. Sleep architecture in the rodent. (A) *Example hypnogram for an undisturbed 24-hour period (12h light/12h dark cycle represented by the white/black frame on top) in one mouse. This examples shows the cyclical nature of sleep in rodents.* ***(B)*** *Examples of different arousal stages in*

one mouse during wake, REM (high theta activity 6-9 Hz), NREM (0.5 – 4 Hz) and NREM sleep with pronounced sigma-frequency activity (I.E. spindles 10-15 Hz).

Extensive advances in the understanding of sleep have been made with the advent of technologies to record brain activity with high spatial and temporal resolution. Below, we discuss some of the main approaches to measure neuronal activity, before proceeding to discuss some of the advances made to understand the neuronal mechanisms implicated in sleep.

1.2. ELECTRICAL RECORDINGS OF NEURONAL NETWORKS

Neuronal networks in the mammalian brain have an intrinsic capacity to generate and sustain a wide range of rhythmic activity patterns. These patterns, reflected as neuronal oscillations, occur at different levels of organisation in the nervous system (Buzsáki and Draguhn, 2004). Thanks to different electrophysiological techniques that can achieve temporal resolutions matching the operation speed of neurons, we know that these oscillations can be observed from the level of single cells to widespread neuronal networks (Buzsáki, 2004).

Extracellular electrophysiological recordings are based on the premise that the superposition of electrical currents arising from cellular processes within a volume of neural tissue generate a potential at any given location (Buzsáki et al., 2012). The difference in potential between different locations gives rise to an electrical field, which can be recorded with different types of electrodes. Electric fields are thought to reflect multiple cellular sources and properties of the recorded brain tissue (Buzsáki et al.,

2012; Herreras, 2016; Telenczuk et al., 2017). Synaptic potentials (Nunez and Srinivasan, 2009)(Telenczuk et al., 2017)have been proposed to be the dominant contributors to these local electric fields.

Recordings of electric fields have traditionally been called: 'electro-encephalogram' (*EEG* - when recorded non-invasively from electrodes placed on the scalp), 'electro-corticogram' (*ECoG* – when recorded from the cortical surface), and 'local field potentials' (*LFP* – when recorded with intracranial electrodes implanted into the extracellular space). The main principle behind these different recording techniques is similar, however they reflect different patterns of activity due to their inherent differences in electrode size and location.

1.2.1. Non-invasive extra-cortical recordings (EEG and ECoG)

The EEG and, to a certain degree, the ECoG are some of the most widespread techniques used in clinical environments to record neuronal electrical activity (Freeman, 2006). Although they possess a high temporal resolution, their spatial resolution is low (appearing as a smoothed version of the LFP activity across ~10cm^2) (Buzsáki et al., 2012). This reduced spatial resolution largely results from distortions caused by the scalp and/or soft tissue (Buzsáki et al., 2012). Additionally, given the large distance of EEG/ECoG electrodes from the current generators, these techniques detect the activity of neurons over widespread fields and reflect activity from superficial layers of the cortex. The EEG/ECoG, therefore, reflect cortical activity that is highly synchronized and spatially homogeneous (Musall et al., 2014).

1.2.2. Extra-cellular recordings (low and high frequency components)

A wide variety of multi-site recording electrodes can be implanted intra-cortically into the extra-cellular space of the brain to study electrical events occurring in deeper layers of the cortex or regions of the brain. Depending on the filters applied to the electrical signal, both LFP signals or extracellular action potentials (i.e. multi-unit activity, MUA) can be recorded. On the one hand, lower frequency components (<500 Hz) of the LFP are believed to reflect the summed electrical activity of cell populations within distances ranging from ~200-400 μm (lateral plane) to millimetres (vertical plane) (Destexhe et al., 1999; Katzner et al., 2009; Xing et al., 2009; Kajikawa and Schroeder, 2011). On the other hand, the high frequency components (500-3000 Hz) of the LFP reflect more localised activity resulting from action potentials and other membrane potentials (Buzsáki et al., 2012). Such local high frequency activity (i.e. MUA) has been found to reflect local activity with a radius of ~100μm (Buzsáki, 2004; Kajikawa and Schroeder, 2011).

1.3. NEUROPHYSIOLOGY OF SLEEP

The electrical recording of brain activity has been a fundamental technique to investigate both whether and how the spatiotemporal orchestration of neuronal activity across large networks supports wake and sleep related processes and behaviours. In the mammalian brain, neuronal networks demonstrate different oscillatory bands ranging from around 0.05Hz to 500 Hz (Buzsáki and Draguhn, 2004). Sleep-related oscillations, and in particular spindles and slow-waves which are the two

most prominent hallmarks of NREM sleep, are the main focus of this thesis. The mechanisms implicated in the generation and maintenance of these oscillations are discussed below.

1.3.1. Neurophysiology of spindles

Spindles were first described by the American polymath Alfred Lee Loomis in 1935 and were the first network oscillations for which a putative neuronal mechanism was identified (Loomis et al., 1937; Steriade et al., 1987; Destexhe et al., 1993; Steriade et al., 1993a; Contreras et al., 1996; Destexhe et al., 1996; McCormick and Bal, 1997). The American Academy of Sleep Medicine manual for sleep scoring defines spindles as a "train of distinct waves with frequency 10-15 Hz, with a duration of >=0.5 s, most prominent in central derivations" and identifies them as a key marker of NREM stage 2 sleep in humans. Spindles have been clearly identified across different mammalian species (Fernandez and Lüthi, 2020; Schneider et al., 2020), and evidence of spindle-like activity has also been reported in amphibians (Fang et al., 2012) and reptiles (De Vera et al., 1994).

According to the most established view, EEG spindles are the cortical manifestation of synchronized neuronal activity, induced by the rhythmic interaction of cells within the thalamo-cortical network (Steriade et al., 1993a). The main cellular mechanisms implicated in the generation of these oscillations are presented below.

1.3.1.1. Cellular mechanisms implicated in the generation of spindles

The generation of spindles is thought to rely on two types of cells present in the thalamo-cortical network: 1) GABAergic cells located in the reticular nucleus of the thalamus (TRN), and 2) glutamatergic thalamo-cortical projection cells (TC) (Steriade et al., 1987). The TRN is a thin layer of GABAergic neurons (mainly parvalbumin-positive) that surrounds the dorsal thalamus. These neurons are the principal source of inhibition for glutamatergic thalamo-cortical projection neurons (Steriade et al., 1987; Kim and McCormick, 1998; Pinault, 2004). TRN and TC neurons can display two distinct firing modes: tonic and burst (Kim and McCormick, 1998). Tonic firing is a sustained response activated during the course of a stimulus, while during burst firing cells exhibit periods of rapid action potential output, which alternate with alternate with quiescent periods.

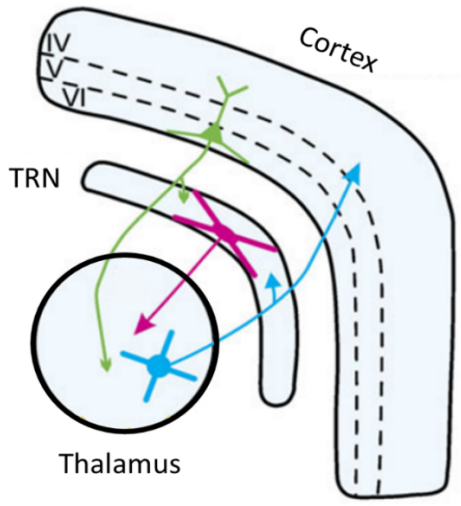


Figure 2. Thalamo-cortical and cortico-thalamic circuits. *The reticular nucleus of the thalamus (TRN) surrounds the dorsal thalamus and provides its main sources of inhibition (GABAergic input= magenta). Glutamatergic thalamo-cortical (TC) neurons (blue) project mainly to upper layers of the cortex (layer IV here for the primary somato-sensory cortex). The*

cortex send projections to the thalamus and TRN through glutamatergic projections cells, which mainly descend from layer VI of the cortex. Schematic adapted from (Pinault, 2011).

Neurons in the TRN and TC express an assembly of cellular mechanisms that make them capable of sustaining rhythmic burst activity. Amongst the most important mechanisms implicated in the generation of burst firing in these neurons are low-threshold-activated voltage-gated Ca^{2+} channels (i.e. T-type channels: CaV3.2 and CaV3.3) (Talley et al., 1999; Astori et al., 2011), and small-conductance Ca^{2+}-activated type-2 K^+ (SK2) channels (Crunelli et al., 1989; Huguenard, 1996; Crunelli et al., 2006).

During wake, when the release of monoaminergic neurotransmitters into thalamic neurons keeps resting membrane potentials in a depolarised state (i.e. above ~ -50mV), the SK2 and T-type channels remain inactivated (Crunelli et al., 1989, 2006). NREM sleep, however, is characterised by a reduced activity in the monoaminergic systems (Saper et al., 2010), which induces hyperpolarization in thalamic neurons. At hyperpolarised states (~65mV or below), T-channels in TRN de-inactivate and generate Ca^{2+} currents, which depolarise the membrane voltage, activate small-conductance Ca^{2+}-activated type-2 K^+ (SK2) channels, and thereby facilitate the initiation of bursts of action potentials (Crunelli et al., 1989, 2006; Huguenard, 1996).

The bursting activity arising from the TRN evokes burst activity in glutamatergic TC projection neurons, which in return evoke excitatory postsynaptic potentials in TRN neurons (Destexhe et al., 1993; Huguenard, 1996). This interaction creates an intra-

thalamic loop of activity, which is thought to be the basis for spindle generation (Steriade et al., 1987; McCormick and Bal, 1997). Additionally, it has been suggested that TRN-TC rebound activity follows a 10-15Hz frequency, due to the time it takes for TC neurons to repolarise from the TRN inhibitory inputs (Von Krosigk et al., 1993).

1.3.1.2. Spindle synchrony in thalamo-cortical networks

The interaction between the thalamus and cortex is believed to play a crucial role in the generation and expression of spindles. It is known that spindles are preserved in the thalamus of decorticated cats (Steriade et al., 1987). However, glutamatergic cortical projections to the thalamus, which mainly descend from layer VI of the cortex (Bromberg et al., 1981; Fonnum et al., 1981), are necessary to provide temporal synchrony and spatial coherence to spindle activity (Contreras and Steriade, 1996; Steriade, 2006).

Interestingly, the TRN is subdivided into different modality-specific areas (i.e. sensory, motor, limbic), which arise from their projection to particular thalamic nuclei, and innervation from topographically aligned cortical (VI) layer regions (Jones, 1975; Pinault, 2004; Halassa and Acsády, 2016). It has been proposed that local spindles can be generated within the boundaries of these different sectors in the TRN (Contreras and Steriade, 1996), and that gap junctions promote synchrony of spindle activity within the TRN.

Additionally, it has been suggested that the synchrony of spindles within the TRN is reflected in the spatial extent they show in the cortex (Fernandez et al., 2018). However, the mechanisms underlying a potential relationship between the synchrony of spindles in TRN and the synchrony of cortical spindles is largely unknown. In fact, the mechanisms implicated in the propagation of spindles to the cortex are not yet as well understood as their generation mechanisms. Moreover, (Feldmeyer et al., 2013) thalamo-cortical connectivity is highly divergent across different brain regions, which is likely to cause regional differences in the mechanism driving spindles (Halassa and Acsády, 2016; Piantoni et al., 2017) .

1.3.1.3. Spindle expression in the cortex

Overall, previous studies have shown that TRN cells do not project to the cortex but to modality-specific thalamic nuclei (Jones, 1975; Pinault, 2004; Halassa and Acsády, 2016). As shown in rodent studies, TC cells in these areas project to excitatory and inhibitory fast-spiking interneurons of all cortical layers, but in the case of the barrel cortex, the majority of synapses are formed in layers 4 and 5a (Sakmann, 2017). Parvalbumin-positive interneurons are very likely to discharge action potentials upon arrival of TC excitatory projections. Amongst the many cellular mechanisms implicated in the cortical expression of spindles, parvalbumin-positive interneurons and cells expressing AMPA receptors lacking the GluA2 subunit, have been found to be important sources of propagation. Specifically, while the TC effect on excitatory neurons is low, AMPA receptors in the cortex provide rapid signal conductance and kinetics capable of recruiting cortical circuits (Fernandez et al., 2018).

In the primary somatosensory and pre-frontal cortices, spindle activity is associated with rhythmic activity that entrains ~30% of excitatory and ~80% of fast spiking interneurons (mainly parvalbumin-positive) of granular cortical layers (Peyrache et al., 2011). Interestingly, additional current sinks (i.e. current reception points) and rhythmic activity can be appreciated in layers II-III and layers V-VI within milliseconds, which suggests that cortico-cortical connectivity also contributes to the expression of spindles in the cortex (Kandel and Buzsaki, 1997).

In the cortex, spindles express as waxing-and-waning oscillations with frequency around 10-15Hz. These oscillations are faster and show higher density in parietal relative to frontal regions (Piantoni, 2017), although topographical changes in frequency are not present in mice (Kim et al., 2015). Interestingly, human EEG and rodent LFP recordings from sensory cortical areas have revealed that spindle activity follows an infra-slow oscillation with frequency of 0.02Hz (Achermann and Borbély, 1997; Lecci et al., 2017; Lázár et al., 2019). This means that bursts of spindle events recur every ~50s, and are interspersed by periods of reduced spindle activity. The spatiotemporal dynamics of spindle activity in the cortex will be further discussed in Chapter 3.

1.3.2. Neurophysiology of the slow-oscillation

Slow waves (0.5–4.0 Hz) are the most prominent electroencephalographic activity of NREM sleep. This type of activity was identified as early as 1929, when Hans Berger the

pioneer of the EEG recognised that different brain states generate waveforms with characteristic amplitudes and frequencies (Berger, 1929). The first recordings of the slow wave (0.5–4.0 Hz) during sleep were performed by Alfred Lee Loomis in 1937 (Loomis et al., 1937) and, since then, the recording of EEG slow wave activity has been central to the understanding of sleep/wake states.

1.3.2.1. Potential origins of the slow wave

The first insights into the cellular origins of the slow wave come from intracellular recordings of cortical and thalamic networks in anaesthetised cats and rats (Wilson and Groves, 1981; Steriade et al., 1993b). These studies demonstrated that the EEG slow waves highly correlate with slow oscillations in single neurons (<1Hz), which follow a bi-stable alternation in membrane potential between depolarised (i.e. Up or ON state: active neuronal firing) and hyperpolarised (i.e. Down or OFF state: absent neuronal firing) states (Wilson and Groves, 1981; Steriade et al., 1993b). Further work has confirmed the relationship between Down-Up neuronal firing patterns and the slow wave activity during natural (NREM) sleep in rodents (Vyazovskiy et al., 2009b) and human patients with epilepsy (Nir et al., 2011). These results further confirmed that Down states of cortical activity appear as negative deflections in recordings of scalp EEG or superficial cortical layers, or as positive potentials when recorded from deep layers of the cortex (Steriade et al., 1993b; Vyazovskiy et al., 2009b).

The precise mechanisms underlying the generation of the slow wave have proved challenging to identify, however different studies suggest that cortical and thalamic networks play an important role. For instance, previous studies have also demonstrated

that the slow oscillation persists after thalamic lesions (Steriade et al., 1993b), and is present in cortical slabs (Timofeev et al., 2000) and in *ex vivo* cortical preparations (Sanchez-Vives and McCormick, 2000), i.e. in the absence of thalamic inputs. This suggests that the cortex is sufficient to generate (at least a certain type of) slow-oscillations. Specifically, layer 5 of the cortex has been proposed as a likely generator of slow waves (Sanchez-Vives and McCormick, 2000). However, different studies have shown that the inactivation of thalamic nuclei can reduce the incidence of slow waves during natural sleep (David et al., 2013). This further suggests that, apart from the cortical contributions, the thalamo-cortical network plays an important role in the modulation of slow wave activity.

1.3.2.2. Slow wave and network synchrony

Slow waves were initially considered global and synchronous events spanning mainly large cortical-thalamic areas (Contreras and Steriade, 1995; Neske, 2016). In fact, slow waves can achieve large-range coherence through horizontal axonal projections of pyramidal cells, which can span millimetre-long distances (Amzica and Steriade, 2000) or diffuse thalamo-cortical projections (Sheroziya and Timofeev, 2014). Different studies have found, however, that slow waves mostly express in confined local regions in the brain (Nir et al., 2011; Vyazovskiy et al., 2011; Funk et al., 2016). Interestingly, even at this level, the amplitude and slope of LFP slow waves can reflect the level of synchrony across neuronal populations (Vyazovskiy et al., 2009b; Nir et al., 2011). Moreover, it has been proposed that apart from reflecting synchrony, slow rhythms affect large proportions of local neurons and can thus provide network synchronization to higher frequency oscillations, such as spindles (Contreras and Steriade, 1996;

Buzsáki and Draguhn, 2004; Staresina et al., 2015). Indeed, previous studies suggest that spindles are driven by the depolarising up state of the slow-oscillation (Niethard, Ngo, Ehrlich, & Born, 2018). The interaction between these two oscillations will be further explored in Chapter 3.

The study of slow waves has opened a path towards the understanding of a fundamental component of sleep: its homeostatic regulation. Specifically, previous studies have shown that the EEG slow wave activity (Borbely, 1982; Borbély et al., 2016), as well as the distribution of ON and OFF states of cortical neuronal populations (Vyazovskiy et al., 2009), change as a function of sleep/wake history and can be used as indicators of sleep need and homeostatic regulation. The main principles of the homeostatic regulation of sleep are presented below.

1.4. HOMEOSTATIC AND CIRCADIAN CONTROL OF SLEEP

Sleep is strictly regulated (Borbely, 1982; Borbély et al., 2016), which is one of the key properties that suggests it has an essential biological relevance. Alexander Borbély investigated the basic principles of sleep regulation and in 1982 proposed the "two-process model of sleep regulation" (Borbely, 1982; Borbély et al., 2016). Based on animal and human studies (Borbely, 1980, 1982), as well as quantitative modelling (Daan et al., 1984), this model proposes that homeostatic (Process S) and circadian (Process C) processes interact to regulate sleep/wake cycles, and more specifically the intensity, duration and timing of sleep.

On the one hand, the duration and timing of sleep is thought to be regulated by Process C. In short, it has been found that circadian pacemakers, which are entrained to external cues (Zeitgebers), are present throughout the body and regulate several processes including the sleep/wake timings at certain circadian phases. The master clock for all the body pacemakers has been located in the suprachiasmatic nucleus (Ralph et al., 1990). The molecular mechanisms controlling circadian cycles have been studied extensively, leading to the 2017 Nobel Prize in Physiology or Medicine.

On the other hand, according to the "two-process model" the intensity of sleep is believed to be reflected in Process S, the homeostatic process (Borbely, 1982). Homeostasis, as initially described by Claude Bernard in 1849, represents regulatory mechanisms, which drive physiological processes towards a stable equilibrium. Alexander Borbély (1982) applied this concept to describe the regulated balance that exists between sleep and wake states. Extensive experimental and modelling work, has since then demonstrated that Process S increases exponentially during wakefulness and decreases exponentially during sleep (Tobler et al., 1983; Feinberg et al., 1985; Dijk et al., 1987; Achermann et al., 1993; Werth et al., 1997).

The biological mechanism behind Process S remains mysterious, as does the function of sleep itself. One line of evidence suggests that extracellular levels of the ATP metabolite adenosine may be reflecting sleep pressure and thus potentially link sleep need to brain energy stores (Porkka-Heiskanen and Kalinchuk, 2011). Another well supported idea is that that sleep need and intensity is directly linked to the net strength of forebrain synapses. This theory is called the sleep homeostasis hypothesis (SHY), and

elegantly brings together several key characteristics of sleep (Tononi and Cirelli, 2003, 2006), and will be described next.

1.5. POTENTIAL FUNCTION OF SLEEP IN HOMEOSTASIS AND COGNITION

Central to the study of sleep is the question regarding its purpose or functions. Mounting evidence points towards a role of sleep in immune, metabolic, homeostatic and neuronal regulation, as well as cognitive functions (Krueger et al., 2016). We will focus here on the last three processes.

1.5.1. Sleep and plasticity

The sleep homeostasis hypothesis (Tononi and Cirelli, 2003, 2006) proposes that a key function of sleep is to facilitate a net weakening of synaptic weights and to restore cellular homeostasis, and thus counteract the net synaptic strengthening and energy demands brought about through daytime experiences. According to this hypothesis, increases in slow wave activity after prolonged wakefulness are due to increased synaptic weights. As sleep progresses, synapses become weaker and thus slow wave activity decreases.

Notably, SHY can account for both local and global changes in sleep intensity. Moreover, it proposes that slow waves could be directly facilitating synaptic weakening, which would allow for an elegant self-regulatory system whereby strong synapses promote strong slow oscillations, which in turn promote strong synaptic weakening. In recent years, several central aspects of the sleep homeostasis hypothesis have been supported, such as the dependency of net synaptic weights on sleep/wake history (Vyazovskiy et

al., 2008; De Vivo et al., 2017; Diering et al., 2017) or a contribution of slow oscillations to synaptic weakening (Bartram et al., 2017; González-Rueda et al., 2018; Kim et al., 2019).

The possibility that sleep is accompanied by net synaptic weakening does not preclude the prospect of synaptic potentiation during sleep, which may be crucial for its role in memory consolidation (Born and Feld, 2012). Indeed, it has been reported that spindles can facilitate synaptic plasticity. On the one hand, spindles are thought to generate favourable conditions to induce synaptic potentiation. For instance, spindle occurrence is associated with increases in cortical unit spiking and co-firing (i.e. simultaneous spiking on different electrodes in a microarray) within ~25ms (Dickey et al., 2020). Moreover, the excitation imposed by TC afferents into the cortex, can result in strong Ca2+ influx into cortical dendrites (Contreras et al., 1997b), and calcium signals recorded from pyramidal cells substantially increases during spindles nested in slow oscillation up-states (Niethard et al., 2018). Finally, in vitro studies have shown that the reproduction of spindle-patterns, recorded in vivo, in cortical slices can induce long-term potentiation (Rosanova and Ulrich, 2005). On the other hand, however, stimulation at spindle-like frequencies (i.e. 10Hz) can also induce depression in cortical neurons depending on the intensity of stimulation and the background level of neuronal activity in vivo (Crochet et al., 2006).

1.5.2. Sleep and memory

According to SHY, processes that have been proposed to benefit from sleep, like memory consolidation, could also rely on synaptic renormalization (Tononi and Cirelli,

2014). An alternative, and possibly complementary, hypothesis suggests that sleep oscillations are key physiological features that actively support processes like memory consolidation (BuzsÁk, 1998; Born et al., 2006). According to this hypothesis, the spatiotemporal orchestration of slow waves, spindles, and sharp-wave ripples (i.e. 150-250 Hz oscillations arising in the hippocampus) could actively promote the transfer of information from temporary to long-term storage in distributed cortical regions (BuzsÁk, 1998; Battaglia et al., 2004; Marshall et al., 2006; Rasch and Born, 2013).

Additionally, it has been proposed that spindles protect sleep from sensory disruption (Dang-Vu et al., 2010; Schabus et al., 2012). Based on this, it has been suggested that spindle oscillations are part of a network that regulates two opposing needs of the brain, i.e. maintaining sensory reactivity to the environment while promoting off-line periods during which recovery and memory consolidation can take place (Lecci et al., 2017; Fernandez and Lüthi, 2020). Evidence supporting these hypotheses are discussed in Chapters 4 and 5.

1.6. SPINDLES IN PATHOLOGY

Alterations in spindle activity have been identified in different disorders, usually as one of several sleep abnormalities. On the one hand, hyper-synchronisation of thalamic-related oscillations, which can present as spike-wave discharges are apparent in patients with epilepsy (Beenhakker and Huguenard, 2009) and children with Down's syndrome (Gibbs and Gibbs, 1962). Additionally, a number of neurological and neuropsychiatric disorders are associated with a reduction in spindle activity. Amongst these disorders are schizophrenia (Ferrarelli, 2007), Alzheimer's disease (Gorgoni et

al., 2016), Creutzfeldt–Jakob disease (Landolt et al., 2006), and children with different developmental disorders (Bódizs et al., 2012; Farmer et al., 2018).

Spindle deficits in schizophrenia have been widely studied (Ferrarelli, 2007; Ferrarelli and Tononi, 2016) and have been proposed to provide important insights into the mechanisms implicated in this disorder (Ferrarelli and Tononi, 2016; Manoach et al., 2016; Ferrarelli and Tononi, 2017; Ang et al., 2018). Spindle deficits have been also reported in mouse models relevant for schizophrenia, such as mice lacking the GluA1 subunit of the AMPA receptor (Ang et al., 2018) or mGluR5 knockout mice (Aguilar et al., 2020). The study of these mouse models could also provide an opportunity to obtain mechanistic insights into spindle dynamics and their relevance for schizophrenia. This topic will be further studied and discussed in Chapter 4.

1.7. MODULATION OF SLEEP OSCILLATIONS

Due to their hypothesised cognitive and clinical relevance, spindles have become an attractive target for neuromodulation. Regarding rodent research, manipulations of the expression of ion channels involved in the rhythmic bursting of TRN, such as $Ca_v3.3$ and SK2 (Astori et al., 2011; Wimmer et al., 2012), have offered an initial tool to investigate the dynamics and potential functional role of spindles. The advent of optogenetic approaches to manipulate the activity of TRN neurons (Halassa et al., 2011; Latchoumane et al., 2017) has allowed for more targeted manipulations of the spindle-generating system. Targeted enhancement in spindles has also been reported in humans by implementing feedback-controlled electrical brain stimulation (Lustenberger et al., 2016) or auditory stimulation during sleep using stimuli

modulated at the spindle-related frequencies (Antony and Paller, 2017; Antony et al., 2018; Lustenberger et al., 2018). Discussion of spindle and slow wave modulation technologies will be presented in Chapter 5.

1.8. RATIONALE AND AIMS OF THIS THESIS

Advances in the physiological understanding of sleep oscillations, combined with the evolving progress of technologies for modulating spindles, have opened an avenue for further understanding their functional role and biological relevance. Moreover, these advances have the potential to become effective tools for treating different disorders. This is a timely moment, therefore, to evaluate the approaches we are implementing to detect, characterise, and manipulate sleep oscillations like spindles. It is important to assess, for instance, how our conceptual and methodological approaches influence how we define and hence understand these oscillations. Moreover, it is important to understand how the manipulations we are inducing in sleep oscillations, like spindles, affect the structure and dynamics of sleep, which is a process known to be dynamic yet strictly regulated.

Following on from this, the specific aims of this thesis are:

Aim 1: Develop a methodological and conceptual framework to detect and characterise sleep spindles that takes into account their complex spatio-temporal properties, and apply this approach to expand our understanding of their network dynamics (**Chapter 3)**.

Aim 2: Investigate spindle-related deficits in GRIA1$^{-/-}$ mice, a mouse model relevant for schizophrenia, using the methodological and conceptual framework developed in Chapter 3 (**Chapter 4).**

Aim 3: : Investigate the effects of modulating sleep oscillations on the architecture and dynamics of sleep, and test the hypothesis that spindles protect sleep from sensory disruption using auditory stimulation (**Chapter 5)**



CHAPTER 2 - General Methods

This chapter presents an overview of the general methods used in this thesis. Specific methods sections are presented at the beginning of each chapter explaining detailed procedures performed for each one of them. Additionally, note that detailed descriptions of the statistical results for each analysis are shown in tables reported in the APPENDIX.

2.1. Experimental Animals

During the experiments, mice were individually housed in plexi-glass cages (20.3 x 32 x 35cm) under a 12:12 light-dark cycle (lights on at 9am). Cages were housed in sound-attenuated, ventilated Faraday chambers. Food and water were available ad libitum. Room temperature and relative humidity were maintained at 20 ± 1°C and 60 ± 10%, respectively. Experimental procedures were performed in accordance with the Animal (Scientific Procedures) Act 1986 under a UK Home Office Project Licence and were in accordance with institutional guidelines. The specific number and strain of mice used for each experiment are reported in the *Methods* section presented in each chapter.

2.2. Surgical Procedure

Surgical procedures were performed under isoflurane anaesthesia. All mice were implanted: 1) epidural screws to record EEG signals, 2) intra-cortical probes to record LFP and MUA signals, and 3) tungsten wires in the nuchal muscle to record the EMG. The extra-cellular LFP and MUA recording were performed from different cortical regions in different experiments. Therefore, the surgical procedures performed to implant these intra-cortical probes will be described separately in each chapter.

The EEG and EMG recording were performed for all mice. To obtain these signals, mice were implanted with EEG/EMG mounts, composed of stainless-steel screws (shaft diameter 0.86mm, InterFocus Ltd, UK) and two single stranded stainless-steel wires, attached to an 8-pin mount connector (8415-SM, Pinnacle Technology Inc, USA). EEG screws were implanted epidurally over frontal (motor area, anteroposterior (AP) +2mm, ML 2 mm, relative to bregma) and occipital (visual area, anteroposterior - 3.5–4 mm, mediolateral (ML) 2.5 mm) cortical regions. A reference screw was implanted over the cerebellum and an anchor screw was implanted contralaterally to the EEG screws to provide stability to the implant. Finally, the EMG was recorded from the two stainless steel wires inserted on both sides of the nuchal muscle. All the screws and wires were attached to the skull using dental cement.

Note: In this thesis, we refer to the EEG as 'global signal' and the LFP as 'local signal'. While subjective, we use these terms to highlight the different spatial scales involved in our recordings.

2.3. Histological verification of recording site

To confirm the location of the electrodes, all laminar probes and micro-wire array wires were coated with DiI fluorescent dye (DiIC18(3), Invitrogen), prior to their implantation. At the end of the experiment, mice were deeply anaesthetised, electrolytic micro-lesions (10μA, 20s) were performed at specific sites to be used as landmarks to verify the recording locations (NanoZ, Neuralynx), and mice were transcardially perfused (0.9% saline, 4% paraformaldehyde). Brains were sliced to obtain 50μm coronal slices, using a Vibratome (Leica VT1000 S, Germany). The brain slices were stained with DAPI, mounted on slides, and imaged with a fluorescence microscope (Olympus Bx51, Japan), using 1.6, 2.5, and 5x magnifications. The electrode locations were mapped using the Dil stain and microlesion traces and the coordinates of the recording sites were identified using the Allen mouse brain atlas (Lein et al., 2007).

2.4. Identification of cortical layers

For recordings performed with 16-channel laminar probes and micro-wire arrays, the cortical layer recorded by each electrode was identified in 5x-magnification fluorescence images. Specifically, the sites of the micro-lesion were identified on the DAPI fluorescence images. The Dil stain trace, the length of the electrode, and the position of micro-lesions, were then used to determine the layer recorded by each contact. Layer 1 was identified based on the low density of neurons compared to Layer 2/3. The beginning and end of Layer 4 were identified based on an increase in cell density relative to Layers2/3 and Layer 5. It has been debated whether Layer 4 exists in M1. Mounting evidence suggests that, although small in thickness, Layer 4 does exist in M1 and can be identified as a small increase in cell density right above Layer 5

(Yamawaki et al., 2014; Bopp et al., 2017). Significantly different physiological behaviour related to spindles and the slow-wave activity, were identified between superior and inferior channels implanted in both Layer 2/3 and Layer 5. Based on previous literature indicating that differential structural, connectomic, and computational properties can be found between Layers 2 and 3 (Karimi et al., 2019), and between Layers 5a and 5b (Krieger et al., 2017), we analysed these as separate layers.

2.5. Signal processing and sleep scoring

Electrophysiological recordings were acquired with a RZ2 High Performance Processor and Synapse software (Tucker-Davis Technologies Inc., Alachua, FL, USA). LFP, EEG and EMG data were continuously recorded with low-pass filtering at 128 Hz, amplified (PZ5 NeuroDigitizer pre-amplifier, TDT, USA), and stored at a sampling rate of 305 Hz. The signals were resampled offline at a sampling rate of 256 Hz using custom-made Matlab (The MathWorks Inc, Natick, Massachusetts, USA) scripts and were then transformed into European Data Format (EDF) using open source Neurotraces software.

Sleep scoring was performed offline and manually. EEG, LFP and EMG signals were visualized in 4-s epochs using the software SleepSign (Kissei Comtec Co, Nagano, Japan). Wake was defined as low voltage, high frequency EEG activity accompanied by a high level of EMG activity lasting more than 4 epochs. NREM sleep was defined as signal with high voltage and slow frequency, predominantly characterised by the occurrence of slow-waves (0.5-4Hz) and sleep spindles (10-15Hz). REM sleep was defined as low

voltage, high frequency oscillations, with predominance of theta activity in occipital derivations, which was distinguished from waking by the reduced level of EMG activity. Brief awakenings (also called micro-arousals here) were defined as periods of low voltage, high frequency oscillations in the EEG and LFP signals accompanied by movement, lasting ≤16 seconds. Epochs containing artefacts were identified and removed from the analyses. SleepSign software was also used to calculate the power spectra of the scored 4-s epochs, using a Fast Fourier Transform (FFT for 4-s epochs, Hanning window: 0.25Hz resolution).

2.6. Analysis of extracellular neuronal activity

Extracellular neuronal activity was continuously recorded at a sampling rate of 25 kHz and filtered between 300 Hz and 5 kHz, concomitantly with the LFPs from the same electrodes (described in Chapter 2. General Methods). For each recording channel, amplitude thresholds were manually set on Synapse, at least two standard deviations above the noise level. When the recorded voltage crossed this predefined set threshold, 46 samples around the event (0.48ms before, 1.36 ms after the threshold crossing) were extracted. Spike waveforms were processed using a custom-made Matlab scripts. Events with artefactual waveforms were excluded from further analysis.

2.7. Spindle detection

Oscillatory events were detected with an algorithm developed by Olbrich and Achermann (2005), and adapted by us to detect spindle events with varying damping. This algorithm treats electrophysiological brain signals as a superposition of

stochastically-driven harmonic oscillators with damping and frequency varying in time. Briefly, an autoregressive model of order 8 was fitted to overlapping (shifted by 1 sample interval) 1-s segments of LFP and EEG signal. Oscillatory events were detected whenever the damping at one or more frequencies exceeded one of five r_b thresholds (r_b = 0.92, 0.93, 0.94, 0.95, 0.96). Detected oscillatory events that had a frequency of around 10 to 15 Hz were selected as 'putative spindles'. This algorithm and the logic behind the spindle detection approach used in this thesis is explained in detail in Chapter 3 (and more specifically in Methods, section *3.2.7. Spindle detection*).

2.8. Slow wave detection

Slow-waves were detected in the EEG and LFP signals following the method presented in Vyazovskiy et al. (2007). Specifically, slow waves were detected in the signals after band pass filtering between 0.5 and 4 Hz, using a phase-neutral Chebyshev Type II filter, with stopband edge frequencies at 0.3 and 8 Hz. The parameters of the filter were optimized visually to obtain the maximal resolution of the wave shape, as well as to minimise intrusions of fast frequencies (i.e. spindles). Slow waves were detected as positive deflections in the signal, amongst two consecutive negative deflections (separated by at least 0.1-s). For our analyses, we selected slow waves with peak amplitude greater than the median amplitude detected across all slow waves. These slow waves are the ones that most accurately reflect homeostatic sleep pressure (Vyazovskiy et al., 2007).

2.9. Sleep deprivation techniques

In order to investigate the effect of preceding sleep/wake history and increasing sleep pressure on different parameters, sleep deprivation was performed using the well-established technique that consists of exposing mice to novel stimuli. This technique has been previously described in (Fisher et al., 2016). This procedure is based on the natural tendency of mice to exhibit exploratory behaviour when presented with novel objects. Sleep deprivation was performed in the home cages of mice, where they were presented with novel stimuli to elicit exploratory behaviour and induce wakefulness in an ecological manner. This intervention was performed the day following a 24-h undisturbed (baseline) recording.

2.10. Statistical Analyses

Data were analysed using MATLAB and Statistics Toolbox, (The MathWorks, Inc) and IBM SPSS Statistics (IBM Corp). Relevant results of statistical analyses are shown in the text and figures, and ***more detailed descriptions of the statistical results are shown in tables reported in the APPENDIX*.** Details regarding the numbers of animals used in each one of the analyses are stated in the specific figure legends.

Overall, linear mixed models, analysis of variance (ANOVA), factorial repeated measures ANOVA, repeated measures ANOVA, t-tests, and respective non-parametric tests were used as appropriate. To assess differences between specific groups, post-hoc tests were performed. The Tukey test was used to compare between groups when equal variances were assumed. The Sidak test was used to do multiple comparisons in cases

where equal variances were assumed. Finally, the Games Howell test was used when equal variances were not assumed.

The parametric analyses mentioned above (ANOVA-based, t-test, and linear mixed models) require dependent variables to be normally distributed (although they are robust to violations in this assumption when group sizes are equal) (Field, 2005). Shapiro-Wilk normality tests were used to determine whether the data were normally distributed. In cases where the normality assumption was highly violated (and the size of the compared groups was different) the data was transformed or non-parametric statistics were performed (i.e. Friedman test or Games-Howell post hoc test).

Mixed and multivariate tests require the variances for each combination of the groups to be homogenous. The Levene statistic was used to test for homogeneity of variance in the different assessed variables (Field, 2005). In cases where the homogeneity of variance assumption was violated, Welch's F test or non-parametric posthoc tests (Games-Howell) were used. In the case of mixed models and repeated measures, the variances of the differences between groups of the within-subject factor (across the between-subjects factor) is required to be homogenous (i.e. sphericity assumption) (Field, 2013). Mauchley's test of sphericity was used to assess whether the population variances of all possible different variable combinations were equal. In cases where the sphericity assumption was violated, the Greenhouse-Geisser (referred to as 'GG') correction was used. This method corrects for the inflation in the F-value caused by lack of sphericity (unequal population variance at all variable levels) by multiplying the Greenhouse–Geisser estimate by the degrees of freedom used to calculate the F-value (Field, 2005).

Important note: ***the results of all statistical analyses are reported in tables in the Appendix section.*** **Where statistical results are reported in the text, we indicate the specific appendix table summarising the test performed, variables included, and results.** Additionally, in tables and figures showing statistical results, means denoted by a different letter (i.e. a, b, c) indicate a significant difference. Finally, the following symbols will be used: *p<0.05, **p<0.001, ***p<0.0001.



CHAPTER 3 - *Oscillatory-Quality*: A fundamental parameter to understand the spatiotemporal dynamics of rhythmic neuronal oscillations like sleep spindles

3.1. INTRODUCTION

3.1.1. Approaches to study neuronal oscillations: commonly used and unused parameters

Since neuronal oscillations were first reported by Hans Berger in 1924, a major area of study in neuroscience has focused on understanding their origins and functions. Mounting evidence suggests that these rhythmic patterns of neuronal activity play a causal role in behaviour by facilitating communication within and between different brain regions (Sejnowski and Paulsen, 2006; Buzsáki and Watson, 2012). The characteristics and functional role of neuronal oscillations substantially depend, however, on the topography, time constants and initial conditions of the brain systems that support them (Buzsáki and Draguhn, 2004). These variables are not always taken

into consideration and thereby neuroscience still lacks unified interpretations of how neuronal circuits operate and generate behaviour. To address this, it is therefore crucial to understand the spatiotemporal dynamics of neuronal oscillations, and to develop conceptual and methodological frameworks to characterise and manipulate them that take into account the complexity in their dynamics.

In practice, spectral analyses (i.e. Fourier, Hilbert and wavelet transforms) and band-pass filters have been predominantly used to detect neuronal oscillations and study their spatiotemporal properties and functional role (Buzsáki and Draguhn, 2004; Siegel et al., 2012). These analyses have mainly focused on establishing the functional relevance of the spectral, phase, amplitude and frequency properties of neuronal oscillations (van Vugt et al., 2007). Band-pass filters, however, can considerably distort the temporal structure and amplitude of electrophysiological signals (VanRullen, 2011; Widmann et al., 2015) and introduce oscillatory artefacts in the absence of biological oscillators (He, 2014). Additionally, neuronal oscillations are superimposed on a stochastic background, and spectral analyses are not well-suited to distinguish between these two (Wen and Liu, 2016).

Furthermore, there are additional parameters that describe fundamental properties of oscillatory systems, which are not fully captured by spectral analyses. For instance, the very same network may exist in different oscillatory states and, importantly, oscillatory activity can vary in terms of strength and stability. The stability and strength of oscillations are measurements routinely used in engineering and physics to assess oscillatory dynamics (Harlow, 2004). These measurements, and their physiological relevance, have not been widely studied in the field of neuroscience, although a few

methods have been developed to measure the strength and stability of neuronal oscillations at a single cell (Mureşan et al., 2008) and EEG level (Achermann & Olbrich, 2004; Olbrich & Achermann, 2005).

In the case of the EEG, Achermann and Olbrich (2004, 2005) developed an algorithm that fits auto-regressive (AR) models to electrophysiological signals and determines the strength at which neuronal networks are oscillating at a certain frequency by measuring the damping of the signal. Damping is a dimensionless measure that describes the decay of oscillations (Alciatore, 2002), and is parameterised in terms of a Quality-Factor (Harlow, 2004; Marmion, 2007). The Quality-Factor compares the exponential time constant for the decay in amplitude of an oscillation to its period and, therefore, gives an index of the strength and stability of an oscillation. Due to their stochastic nature, electrophysiological signals in the brain are thought to show high variability in their frequency and oscillatory strength (Olbrich & Achermann, 2005; Pardey et al., 1996). While the functional relevance of the variability of oscillations in terms of frequency has been widely studied, their variability in oscillatory strength has not. Consequently, it remains largely unknown whether the variability in their oscillatory strength (i.e. damping) has a relevant physiological meaning.

3.1.2. Traditional approaches for studying oscillations such as sleep spindles

One of the main reasons why the variability in the strength (i.e. damping) of neuronal oscillations remains unknown, is likely due in part to the way in which many of these oscillations are conceptualised and studied. To illustrate this, we take the example of sleep spindles, which are one of the most widely studied sleep oscillations. Since

spindles were first described by the pioneers of EEG recordings (Loomis et al., 1935), these oscillations have been considered to be all-or-none phenomena. As a result, the methods developed to automatically detect these oscillations have been predominantly based on single fixed thresholds.

For instance, as shown in

Figure 3, spindles are traditionally detected when parameters, such as their amplitude or damping, surpass a fixed threshold (Devuyst et al., 2006; Eero Huupponen et al., 2007; Olbrich & Achermann, 2005; Ray, Fogel, Smith, & Peters, 2010; Schimicek, Zeitlhofer, Anderer, & Saletu, 1994). Therefore, a binary classification is made where events are either accepted or rejected as 'spindles' based on a single constant value. The problem, however, is that such a binary classification disregards the substantial variability that might exist in properties, such as the strength and stability of spindle activity, which give additional insight into the network dynamics of these oscillations, as we will show throughout this chapter.

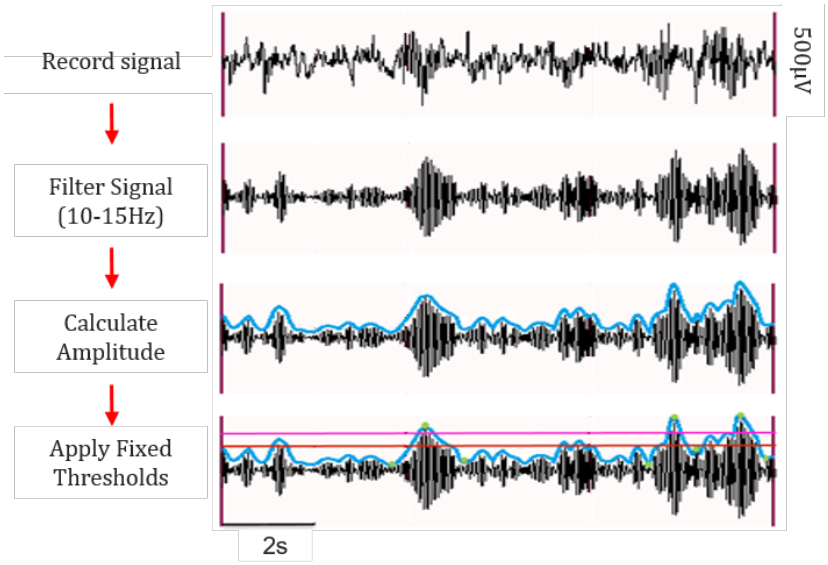


Figure 3. Traditional approach to detect sleep spindles based on their amplitude. *Electrophysiological signals are filtered at the spindle frequency range (10-15 Hz) and the envelope or instantaneous amplitude of the signal (blue line) is calculated. Upper (magenta line) and lower (red line) amplitude-based thresholds are set (generally at around two and five times the mean amplitude of the signal). The upper threshold is used to detect spindle events and the lower threshold is used to determine spindle start and end times.*

3.1.3. What we know about spindle spatio-temporal dynamics based on traditional approaches

Using the aforementioned traditional spindle detection approach, there have been several important advances in understanding the network dynamics of spindles. We discuss some of these below before proceeding to show (throughout this chapter) that taking into account the variability of spindles, in terms of their oscillatory strength, can expand our understanding of their spatio-temporal dynamics.

3.1.3.1. Spindle spatial dynamics

Following this traditional approach contributed to the idea that spindles constitute patterns of activity that are mainly spatially coherent and synchronised throughout widespread cortical areas (Contreras et al., 1997a; Achermann and Borbély, 1998; Sejnowski and Destexhe, 2000; Steriade, 2003). This observation was supported by studies based on human extra-cortical EEG recordings and fMRI data (Andrade et al., 2011). Mounting evidence based on intra-cortical human and rodent recordings, however, suggests that most spindles occur and are modulated locally (Andrillon et al., 2011; Nir et al., 2011; Piantoni et al., 2017; Fernandez et al., 2018). In attempting to reconcile these observations, it has been suggested that spindles might represent a mixture of local and global phenomena, possibly due to the diversity of thalamo-cortical (Bonjean et al., 2011) and cortico-cortical (Kandel and Buzséki, 1997) connections. Furthermore, it has been proposed that the properties of spindles, such as their frequency, density and power, are strongly influenced by spatial and temporal factors (Finelli et al., 2001; Andrillon et al., 2011; Piantoni et al., 2017; Hagler et al., 2018; Krishnan et al., 2018).

3.1.3.2. Spindle temporal dynamics

Regarding temporal dynamics, evidence suggests spindle density and sigma activity power increase within and across NREM episodes, are prominent prior to NREM-to-REM transitions (Gottesmann, 1996; Vyazovskiy et al., 2004a), and are higher during light sleep relative to deeper sleep (Trachsel et al., 1988; Himanen et al., 2002; Vyazovskiy et al., 2004a; Andrillon et al., 2011). The frequency of spindles also seems

to increase during light sleep relative to deeper sleep (Himanen et al., 2002; Andrillon et al., 2011). Moreover, recent findings suggest that bursts of spindles recur at intervals of ~50 seconds and follow an infra-slow oscillation with a frequency of ~0.02 Hz (Lecci et al., 2017; Lázár et al., 2019), where individual spindles recur approximately every 4 seconds (Achermann and Borbély, 1997). This infra-slow oscillation has been proposed to divide NREM sleep into phases of high and low susceptibility to sensory stimulation and memory processing (Lecci et al., 2017).

3.1.3.3. Topography of spindle activity

Spindles are thought to arise in the reticular nucleus of the thalamus (Morison and Bassett, 1945; Steriade et al., 1987), and express across local (Andrillon et al., 2011; Nir et al., 2011; Fernandez et al., 2018) and widespread (Contreras *et al.*, 1997; Achermann and Borbély, 1998) thalamic and cortical areas. The dynamics of spindle propagation in the cortex are uncertain, however growing evidence suggests that spindle density and frequency are high in parietal areas, somewhat reduced in frontal areas and further reduced in temporal areas (Andrillon et al., 2011; Piantoni et al., 2017). Similarly, the power of the infra-slow oscillation of spindle activity seems to be higher in parietal relative to frontal regions (Lecci et al., 2017).

As for the topographical dynamics of spindles at a more local level, a recent study based on intracranial recordings of 4 patients with epilepsy, reported that spindles are most common and prominent in middle-upper cortical layers, with a reduced involvement of deeper layers (Hagler et al., 2018). Similarly, an earlier study performed in un-anaesthetised rats, suggests that the major extracellular currents underlying spindles

in the somatosensory cortex consist of a combination of multiple cortical dipoles, with strongest sinks in L4, followed by L5-6, and lastly a delayed sink in L2/3 (Kandel and Buzséki, 1997). However, detailed studies of the spatiotemporal dynamics of LFP spindles recorded from different cortical layers in different brain regions are currently lacking.

3.1.3.4. Interactions of spindles with other sleep oscillations

Accumulating evidence suggests that, despite being predominantly local phenomena, the spindle system follows a global organisation, which is driven by their interaction with other sleep oscillations. Cortical slow-waves (0.5–4.0 Hz) reflect widespread synchronous neuronal activity which, given their high power, can provide network synchronization to higher frequency oscillations, such as spindles (Contreras and Steriade, 1996; Buzsáki and Draguhn, 2004; Staresina et al., 2015). Specifically, numerous studies have reported that, although spindles can be generated autonomously in the thalamus, these oscillations can be nested (Staresina et al., 2015; Klinzing et al., 2016) and their synchrony is mainly driven by the depolarising up state of the slow-oscillation (Steriade, 1993; Niethard et al., 2018). Other studies, however, suggest that an inverted-u relationship exists between spindles and slow waves. These studies have found that the incidence of spindles decreases in conditions during which the slow wave incidence and power is increased (i.e. during the initial hours of sleep and after sleep deprivation), but decrease when the slow-wave power is too high (Dijk, Hayes and Czeisler, 1993; Vyazovskiy *et al.*, 2004).

3.1.4. Our proposed approach: studying spindles while taking into account their oscillatory strength

Despite considerable knowledge on the spatiotemporal variability that spindles show in terms of their density, amplitude, frequency and power, research to date has not yet determined whether the oscillatory strength and stability of spindles varies in space and time, and whether this has any biological and physiological relevance. Additionally, if spindles indeed vary in terms of their oscillatory strength, the fixed amplitude-based thresholds that have predominantly been used in the literature would preferentially detect spindles with a certain (typically high) oscillatory strength. This would bias any conclusion subsequently made on the spatiotemporal dynamics and functional role of sleep spindles.

To address this, we developed a methodological and conceptual framework to detect and characterise spindles that takes into account their variability in oscillatory strength and stability. As such, this new approach allows us to deal with oscillations as gradual phenomena Specifically, we extended a linear stochastic model with time-dependent coefficients introduced by Olbrich & Achermann (2005) to detect and characterise spindles based on their variable damping, and applied this for the first time in mice. No specific assumptions about the oscillatory frequency or waveform are needed with this approach, overcoming the shortcomings of spectral analyses.

Our observations show that spindles are clearly not all-or-none phenomena but rather they show a continuum in terms of their damping (i.e. oscillatory strength and stability). To parameterise this property, we propose a new metric, which in analogy to the

Quality-Factor, we call *oscillatory-Quality (o-Quality).* This approach allowed us to investigate the physiological relevance of the oscillatory strength and stability of spindles, and discover new aspects of their spatiotemporal dynamics. Specifically, we used the *o-Quality* of spindles to further understand their dynamics across brain regions and cortical layers (spatial), and their change in time relative to the sleep-wake history and the dynamics of other sleep oscillations, such as the slow-wave activity and infra-slow oscillation (temporal).

We found that the *o-Quality* of spindles reflects synchrony within cortical networks, reveals a thorough picture of the spatiotemporal dynamics of the spindle network, is directly related to the occurrence of slow waves, and is sensitive to the levels of sleep need. Overall, taking into account the variability of spindles in terms of *o-Quality* offers a more complete and thorough picture of the spatiotemporal dynamics of the spindle system, which is a fundamental step to understand their biological and physiological role.

3.2. METHODS

3.2.1. Animals

Experiments were performed in adult 3-4 months old male C57BL/6 mice (Harlan UK Ltd, Bicester, United Kingdom). Twenty-one mice were used in total. Seven of these mice (n=7) were implanted with laminar probes in S1, seven mice (n=7) were implanted with microwires arrays in S1, and mice (n=7) were implanted with laminar probes in M1.

3.2.2. Surgical Procedure

Surgical procedures were performed under isoflurane anaesthesia. All mice were implanted: 1) epidural screws to record EEG signals, 2) intra-cortical probes to record LFP and MUA signals, and 3) tungsten wires in the nuchal muscle to record the EMG. See Chapter 2 - *Surgical Procedure*, for details on the EEG and EMG implants. The LFP and MUA recordings for the experiments described in this chapter were obtained across or within layers of the cortex. These recording were made contralateral to the EEG screws.

Recordings using laminar probes: To record signals across layers of the cortex, two-thirds of the mice (n=14) were implanted with 16-channel laminar probes (NeuroNexus, A1x16-3mm-100-703, 100µm spacing) either in the primary somatosensory cortex (S1, n=7 mice, -0.5mm AP and −3.25mm ML) or the primary motor cortex (M1, n=7, 1.5mm AP and -2mm ML).

Recordings using micro-wire arrays: To record signals within layers of the cortex, one third of the mice (n=7) were implanted with a polymide-insulated tungsten micro-wire arrays (Tucker-Davis Technologies Inc (TDT), USA) into deep layers (target: layers 4 and 5) of S1, where previous studies have identified well-defined spindles (Kim et al., 2015; Fernandez et al., 2018). The array consisted of 16-channels with properties as follows: two rows of eight wires, wire diameter 33µm, electrode spacing 250µm, row separation L-R: 375µm and tip angle 45 degrees. Arrays were customised so the left row was 250µm longer. A craniotomy of approximately 1x2mm was made and the midpoint of the craniotomy was located relative to bregma: -1mm AP and −3.25mm ML.

A schematic of implantation locations is shown in

Figure 4. Mice were given at least two weeks to recover and were habituated to the recording cage and cables for a minimum of four days prior to recording. For details on the histological verification of recording sites, see Chapter 2 – *Histological verification of recording sites*.

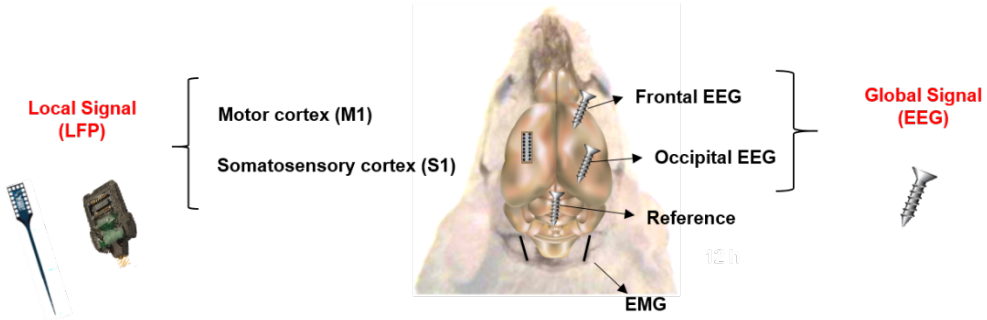


Figure 4. Schematic of implantation sites. *EEG screws were implanted epidurally over frontal and occipital regions. A reference screw was implanted over the cerebellum. EMG was recorded from the two stainless steel wires inserted on both sides of the nuchal muscle. LFP and MUA were recorded from laminar probes (blue elongated 'LFP' probe - left) and micro-wire arrays (black and green 'LFP' array - right) implanted into S1 or M1.*

3.2.3. Spindle Detection

Oscillatory events were detected in all EEG and LFP signals by applying a previously published algorithm (Achermann and Olbrich, 2004; Olbrich and Achermann, 2005; see Olbrich *et al.*, 2017 for the most recent revision), based on autoregressive (AR) modelling of human EEG (Pardey et al., 1996). This algorithm models electrophysiological brain signals as a superposition of stochastically driven harmonic

oscillators (f > 0Hz) and relaxators (f = 0Hz) with damping and frequency varying in time. Based on this, EEG and LFP times-series *x(t)* were resampled at 128 Hz and overlapping 1-s segments, shifted by 1 sampling interval, were modelled with an AR-model of order p=8. As such, the AR(8)-model uses the weighted sum of the preceding p samples to predict the value of the n^{th} sample of the time series $x(t_n)$:

$$x(t_n) = \sum_{i=1}^{p} a_i x(t_n - i) + \varepsilon(t_n)$$

where a_i denotes the AR coefficients and $\varepsilon(t_n)$ the residuals. The model was estimated using the Burg algorithm (Nathan and Scobell, 2012). These a_i coefficients are used to calculate the frequency $f_k = \emptyset_k(2\pi\Delta)$ and damping coefficient $\gamma_k = \frac{1}{t_k} = -\Delta^{-1}\, ln\, r_k$ ($\Delta = t_n - t_{n-1}$ denotes the sampling interval) using:

$$z^p - \sum_{k=1}^{p} a_k z^{p-k} = \prod_{k=1}^{p} (z - z_k), \qquad z_k = r_k e^{i\emptyset_k}$$

Note that r_k is exponentially related to the damping coefficient γ_k, such that a decrease in γ_k is reflected as an increase in r_k. Additionally, the order of the AR-model (p) determines the total number of poles z_k (by *p=2m + n,* with *m* oscillators and *n* relaxators), such that our AR(8)-model could generate up to four different oscillatory poles z_k. In this way, when the signal is dominated by a rhythmic and stable oscillation

with frequency f_k, like a spindle (10-15 Hz), this activity will be reflected by a reduction in damping coefficient γ_k and an increase in r_k of a pole z_k with the corresponding frequency f_k (**Figure 5**).

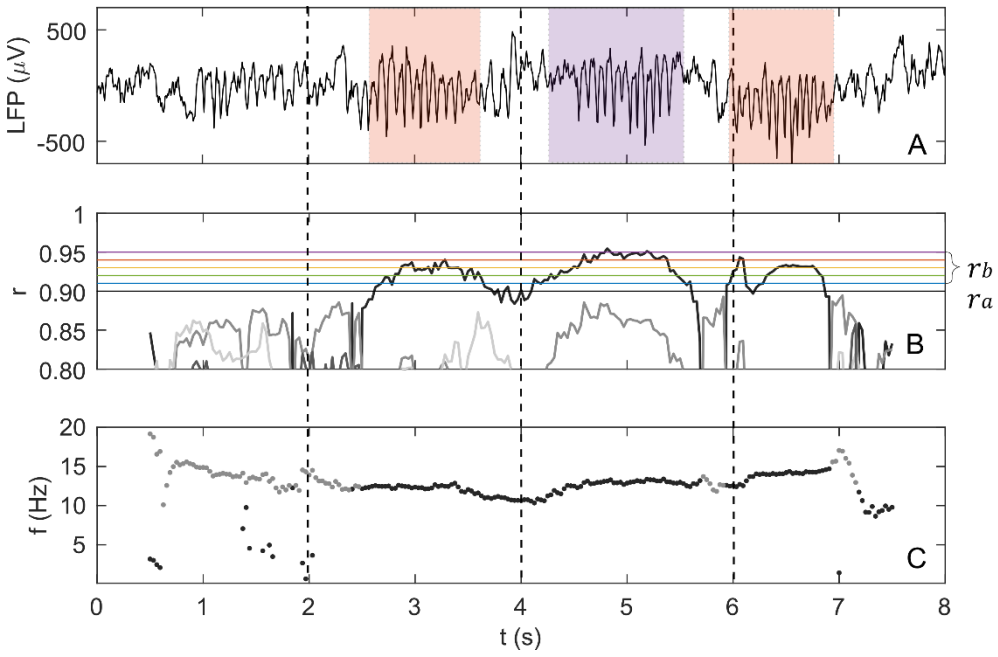


Figure 5. Principle of the AR-model used to detect oscillatory events. (A) *Eight-second segment of LFP data during NREM sleep showing a sequence of detected spindle events, highlighted by shaded coloured boxes. The red boxes indicate spindle events whose r_t values reached the upper threshold r_b=0.94, while the purple box indicates a spindle event whose r_t values reached the upper threshold r_b=0.95.* ***(B)*** *Absolute r_t values for the four poles estimated by the AR(8)-model. Each pole is represented with a different shade of grey. The horizontal coloured lines represent the different upper thresholds used for detection of oscillatory events (i.e. r_b=0.96, 0.95, 0.94, 0.93, 0.92). The horizontal black line represents the lower threshold (r_a=0.90) used to merge or separate consecutive oscillatory events.* ***(C)*** *Frequencies f_k of the poles estimated by the AR(8)-model that showed highest r_t values represented with a different shade of grey as in (B). In* ***(B,C)*** *The black line and dots represent the pole with lowest damping at spindle-related frequencies.*

Based on this, two types of thresholds were used to detect events. On the one hand, oscillatory events were detected when the damping coefficient γ_k at frequency f_k

decreased and, therefore, r_k surpassed a predefined upper threshold r_b. In previous applications to human EEG signals (Olbrich and Achermann, 2005; Olbrich et al., 2017), the upper threshold was set to r_b=0.95. Here, five different upper thresholds (r_b) were used to detect events with varying damping, namely r_b=0.96, 0.95, 0.94, 0.93, 0.92. Additionally, the duration of events was determined by the lower r_b threshold. Specifically, for each event, the start time (t_1) was considered the time point when r_k exceeded r_b=0.92, while end time (t_2) was considered the time point when r_k fell below r_b=0.92.

On the other hand, a lower threshold r_a was used to deal with the fluctuations of *r* and to merge or separate consecutive events with overlapping time and frequency. Specifically, consecutive oscillatory detections were considered a single event if r_k stayed above the lower threshold r_a, or were considerate separate events if r_k fell below r_a. Similar to previous applications (Olbrich and Achermann, 2005; Olbrich et al., 2017), we set the lower threshold to r_a=0.90. The choice of these thresholds was based on data-driven and visual validation (which will be further explained in **Figure 8**).

The oscillatory events detected by this algorithm in the human sleep EEG correspond to the classically defined EEG frequency bands: e.g. delta (0 -4.5 Hz), alpha (8-11.5 Hz), and sigma (11-15 Hz) (Achermann, Rusterholz, Stucky, & Olbrich, 2019; Olbrich & Achermann, 2005; Olbrich, Landolt, & Achermann, 2014). Detected oscillatory events that showed a mean frequency f_k between 10-15 Hz were defined as putative 'spindle events'. **Figure 5** illustrates the principle of the algorithm and demonstrates the detection of several spindle events in an 8-s segment of an LFP signal. Notably, this spindle detection approach does not require signal filtering in any specific frequency

band and does not assume any specific oscillatory waveform. This is highly relevant as filtering can considerably distort the temporal structure, onset latency, and amplitude of electrophysiological signals (VanRullen, 2011; Widmann et al., 2015).

3.2.4. Surrogate signal generation

In order to test the hypothesis that the detected spindle events and observed spindle dynamics were not obtained by chance, but rather represent true physiological phenomena, we created surrogate data (artificial signals) of the EEG (n=19) and LFP (n=19) signals. These surrogate signals were created based on an improved version of the Iterative Amplitude Adjusted Fourier Transform (IAAFT) algorithm developed by Schreiber and Schmitz, (2000). Specifically, for 10-minute segments of signal (EEG or LFP) the windowed Fourier transform was calculated. The resulting Fourier phases were randomized and the inverse of the Fourier transform was calculated. Then the amplitudes of the resulting time series were adapted to match the original amplitude distribution. This was done by rank ordering the resulting time series and replacing the data points with the data point of the original time series with the same rank. This procedure was performed in an iterative manner in order for the surrogate signals to achieve a closer match to the amplitude distribution and the power spectra of the original signals.

IAAFT surrogates test the null hypothesis that the data represent a stationary linear Gaussian process observed with a monotone, but potentially nonlinear, measurement function. In our case, we used the nineteen LFP (n=19) and EEG (n=19) surrogate signals to assess whether the spindle events and spindle dynamics detected in the real

signal represented true characteristics of an underlying physiological system, or whether they could simply be described by a stationary linear stochastic process (i.e. were obtained by chance). The selected number of surrogates per signal (19) comes from a 5% significance level for a one sided test. In other words, if the observable is larger than the value for all surrogates, the null hypothesis can be rejected (i.e. the results are not random).

Specifically, the context where we used the surrogates in this chapter were: (1) applying our spindle detection AR-model to the original and surrogate signals, and assessing whether spindles were mainly detected in the original signals. This gave us an index of the accuracy of our spindle detection AR(*p)*-model. (2) Additionally, we compared properties such as the sigma peak distribution and the infra-slow spectral dynamics of both real and surrogate signals (for both EEG and LFP).

3.3. RESULTS

We analysed EEG, EMG, and intra-cortical multi-electrode LFP and MUA recordings from the brain of freely moving mice during natural sleep. EEG signals were recorded from frontal and occipital derivations (**Figure 6.A**). Intra-cortical recordings were performed from the primary somatosensory (S1, n=7, **Figure 6.C**) and motor (M1, n=7, **Figure 6.D**) cortices, using 16-channel laminar probes with 100μm inter-electrode separation, and micro-wire arrays implanted into deep layers (L4 and L5) within S1 (**Figure 6.E**). Note that throughout this chapter we refer to EEG as "global" signals and the LFP as "local" signals. Although these are subjective terms, we use them to highlight the different spatial scales involved in our recordings. All animals (n=14) showed

expected EEG and LFP signatures of waking, NREM sleep and REM sleep (**Figure 6.B**). Waking and REM sleep were characterised by low voltage, high frequency oscillations, while NREM sleep was characterised by high voltage slow-waves (0.5-4Hz) and sleep spindles (10-15Hz) (**Figure 6.F**).

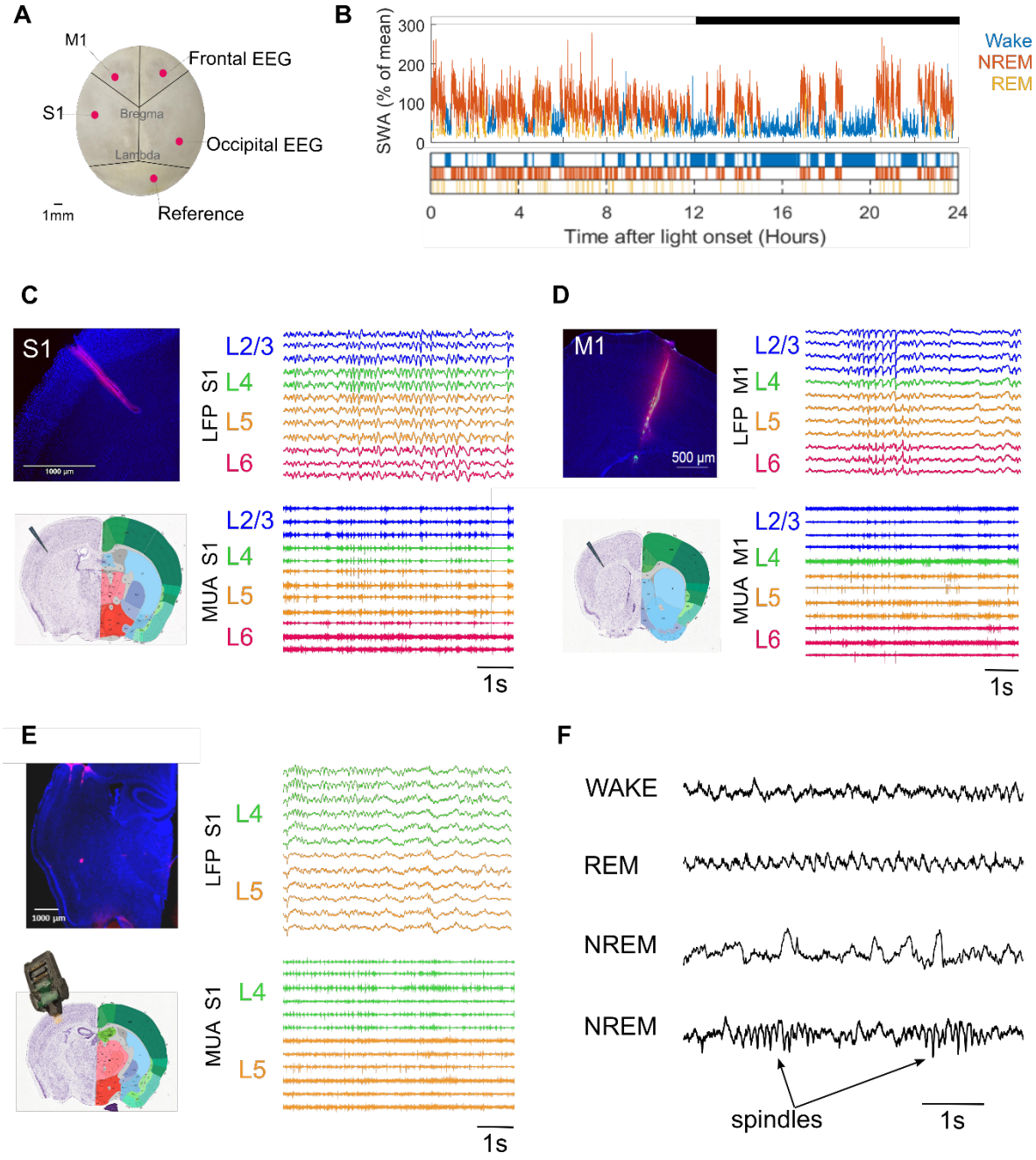


Figure 6. Recording sites and recordings of cortical activity during wake and sleep. (A) *Locations where the EEG screws (frontal, occipital and cerebellar reference) and LFP probe/micro-wire arrays (S1 or M1) were implanted.* ***(B)*** *Profile of EEG slow-wave activity (SWA EEG power between 0.5–4.0 Hz, represented as % of 24-h mean (top) and respective hypnogram (bottom) for one mouse during an undisturbed 24-hour period (12h light/12h dark cycle represented by the white/black frame on top).* ***(C,D,E)*** *Twenty-one mice were implanted with either: a 16-channel laminar probe in S1 cortex (n=7)* ***(C)*** *or in M1 cortex (n=7)* ***(D),*** *or a 16-channel micro-wire array in deep layers of S1 (n=7)* ***(E)****. In (C,D,E),* ***t****he location of the electrodes across or within S1 and M1 cortical layers was verified with histological evidence of electrolytic microlesions and Dil stain electrode traces (magenta) on brain slices stained with DAPI (blue). The recording coordinates for each implant type were identified using the Allen mouse brain atlas. Representative 7-s segments of LFP and MUA signals (recorded during NREM) sleep across electrodes is shown for the different implants.* ***(F)*** *A 5-s representative example for LFP recordings in one mouse during wake, REM (high theta activity 6-9 Hz), NREM (0.5 – 4 Hz) and NREM sleep with pronounced sigma-frequency activity (10-15 Hz).*

3.3.1. Spindles are not all-or-none phenomena but there is substantial variability in their properties

As expected, putative spindle events were observed in both the EEG and LFP signals. However, in contrast to the traditional view that spindles are all-or-none phenomena, we observed that spindles are highly idiosyncratic and dynamic entities, showing substantial variability in their characteristics. This variability in properties such as their amplitude, duration, shape and frequency was visually evident across both time and spatial location. This raises an important question about whether, and to what extent, such variability is noise or is biologically meaningful. At any rate, this variability represents an important methodological problem for the reliable and unbiased detection of spindles.

Automated spindle detectors have traditionally been based on a band-pass filtering and amplitude-threshold approach (Warby et al., 2014). Similar to other detection approaches, this approach is based on a binary classification where events are either accepted or rejected as 'spindles' based on a single constant value (Warby et al., 2014); in this case based on a single sigma amplitude threshold. For such a binary classification to be accurate and objective, the distribution of peak amplitudes of the filtered (10-15 Hz) signals or the damping of the signal should show a single clear boundary that accurately distinguishes 'spindles' from other signal states. We proceeded, therefore, to investigate whether we could identify a single boundary to detect spindles accurately based on fundamental properties like their damping.

3.3.1.1. There is no obvious single boundary to detect spindles based on their amplitude

We started by applying the approach that is most traditionally used in the literature (Warby et al., 2014). We band-pass filtered (10-15 Hz) mouse EEG and LFP signals, recorded over 12-hour light periods (**Figure 7**.**A**), and explored whether we could find a single amplitude-based threshold to discriminate between spindle oscillations and background variations in sigma frequency. We calculated the amplitude of sigma peaks, during NREM sleep, from rectified band-pass filtered (10-15Hz) EEG and LFP signals (recorded during 12 hours in the light period), and plotted their distribution. We found that the distribution of sigma peak amplitudes of EEG (frontal and occipital) and LFP (S1 and M1) signals, shows a log-normal distribution (i.e. when mentioning log-normal we refer to a normal gaussian distribution for data transformed in a logarithmic scale,

further analyses need to be performed to confirm log-normality) (**Figure 7.B**). No indication of bimodality was evident in this distribution.

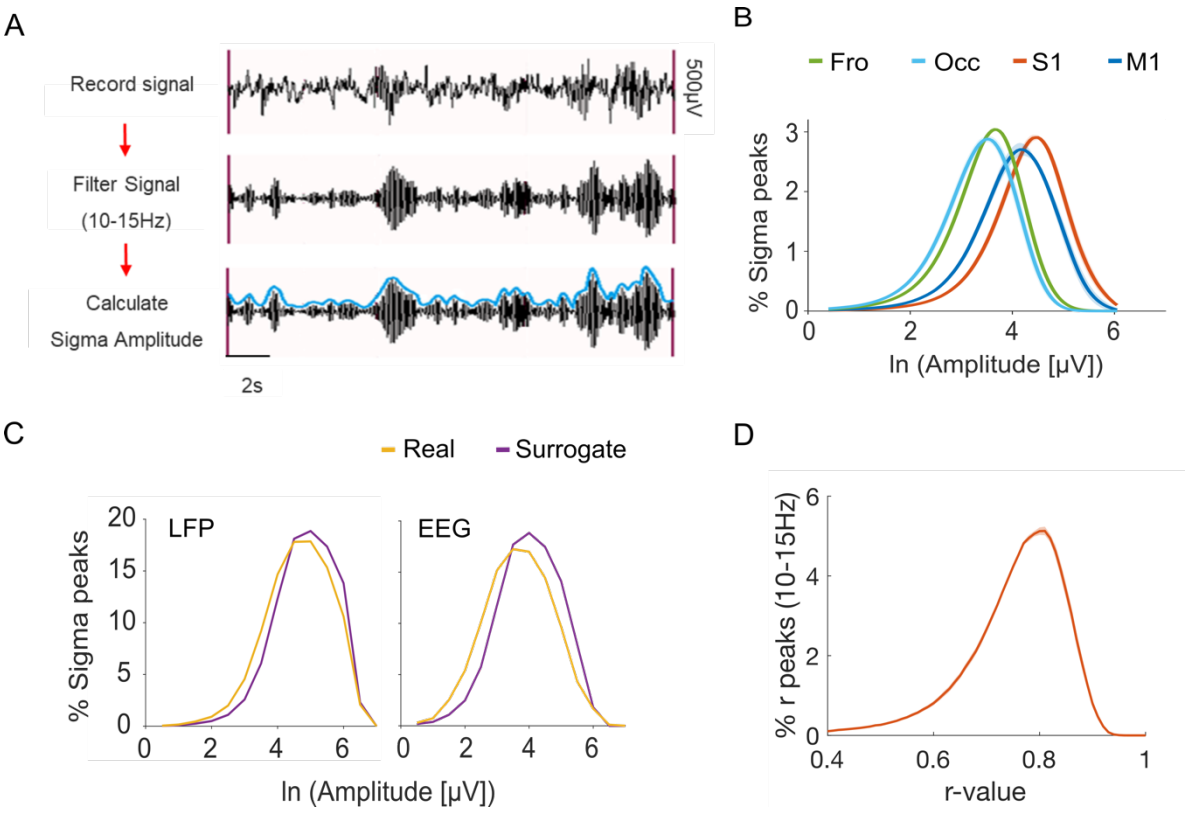


Figure 7. Lognormal distribution in the amplitudes of sigma activity. (A) *Mouse EEG and LFP signals were band-pass filtered between 10-15 Hz. The instantaneous amplitude of the filtered signal was calculated using a Hilbert transform and the peak amplitudes, during NREM sleep, were identified.* ***(B)*** *Peak sigma (10-15 Hz) amplitude distribution for EEG (Fro= frontal; Occ= occipital) and LFP (S1= primary somatosensory cortex; M1= primary motor cortex) signals (mean and SE – shaded area- across mice).* ***(C)*** *Peak sigma (10-15 Hz) amplitude distribution calculated from a 10-minute segment of EEG and LFP real signal (in one mouse) and 19 respective surrogate (EEG and LFP) signals (mean across surrogates).* ***(D)*** *Distribution of peaks on continuous r_k values from an oscillator with frequency 10-15 Hz calculated with the AR-model. Note that r_k is inversely related to the damping of the signal.*

We also found this log-normal distribution in the peak amplitudes of rectified band-pass filtered (10-15 Hz) surrogate signals (which corresponded to 10s of EEG or LFP signals recorded during NREM sleep, see Methods. *Surrogate signal generation*) (**Figure 7.C**). There was no significant difference between the peak amplitude distributions of the real EEG and LFP and surrogate filtered (10-15 Hz) signals (EEG real vs EEG surrogate, z=1.23, p<0.01; LFP real vs LFP surrogate, z=0.45, p<0.01). These results suggest that, despite being an approach traditionally used in the literature, it is not possible to define a meaningful threshold that separates fully-fledged spindle events from background variations in sigma frequency amplitude.

3.3.1.2. There is no obvious single boundary to detect spindles based on their damping

Other spindle detection approaches have been developed to circumvent the potential signal distortion that band-pass filters can generate (Achermann and Olbrich, 2004; Olbrich and Achermann, 2005). We proceeded by applying the spindle detection approach developed by Olbrich and Achermann (2005), which applies a linear model to detect spindle oscillations based on the signal damping, a fundamental property of harmonic oscillators. For the first time, we used this linear model to detect oscillatory events on mouse EEG (i.e frontal and occipital) and LFP (i.e. S1 and M1) signals. Specifically, we used an AR algorithm of order p=8 to model 1s segments of the signals. The signal frequencies and damping coefficients were estimated from the coefficients a_i of the AR(8)-model. An rk coefficient was calculated to represent the damping strength of the signal, such that an exponential decrease in damping is reflected as an increase in rk (**Figure 7.D**). We plotted the rk distribution of oscillators with frequency

between 10-15Hz calculated from the LFP S1 signal (showing highest spindle incidence per mouse). Similar to the results presented above (based on the damping of signals filtered at the spindle frequency range), it was apparent that oscillatory activity occurring between 10-15 Hz shows a continuous variation in its damping (Fig.2D). These results suggest that there is not a single clear boundary that unequivocally determined the occurrence or absence of spindles based on their amplitude or damping. Note that we are not comparing here the performance of different spindle detection methods but rather highlighting that no single fixed amplitude-based or damping-based threshold can unequivocally distinguish between fully-fledged spindles and 'background' sigma activity. A comparison between amplitude-based and damping-based spindle detection methods would be useful for investigating what properties of spindles are differentially captured by each one of them. This is not the scope of the present thesis but will be an informative analysis for future work.

Oscillatory events in the range of 10-15 Hz were considered to correspond to spindles and were detected whenever the r_k coefficient surpassed a predefined upper threshold r_b. To examine the effect of using different thresholds and detect events with varying damping, we used five different upper thresholds (r_b), namely r_b=0.92, 0.93, 0.94, 0.95, 0.96. These corresponded to high-to-low damping in the descending order, i.e. weak-to-strong oscillatory strength (see **Figure 5** and Methods section - *Spindle Detection*).

First, we explored the incidence of detected events as a function of their frequency **(Figure 8.A)**. As expected, a major peak in the incidence of events in the traditionally accepted spindle-frequency range (10-15 Hz) was apparent during NREM sleep, particularly in the LFP (middle upper cortical layers: S1 layer 4 and M1 layer 5), and

EEG (frontal and occipital) signals **(Figure 8.A)**. Interestingly, this peak was absent for detections made on LFP signals recorded from deeper cortical layers (S1 and M1: layer 6) **(Figure 8.A)**. Moreover, the peak was most prominent in S1 relative to M1, as well as relative to EEG frontal and occipital derivations, where the incidence of spindles has been reported to be low compared to parietal and frontal regions in both humans (Piantoni et al., 2017) and rodents (Ang et al., 2018). In contrast, an occurrence of oscillatory events within the theta frequency range (4-7 Hz) was apparent during REM sleep, especially in the occipital EEG and LFP signals **(Figure 8.A)**. Note that we did not analyse the *o-Quality* of slow-waves (or other oscillations) as this was outside the scope of the present thesis. Additionally, it is important to note that the AR-model is not ideal to study slow-oscillations as we model the data in 1-s segments and therefore activity below this time-window would not be modelled properly.

It was also apparent that detected spindles varied substantially in terms of their damping strength. Specifically, some events that were unequivocally visually discernible from the background activity were detected with a low damping coefficient threshold (i.e. $r_b = 0.92$) but were missed if the threshold was increased (i.e. $r_b = 0.95$). Other events were much more robust and detected reliably even with a higher r_b threshold **(Figure 8.B).**

We were interested, therefore, in investigating the effects of varying the r_b thresholds (r_b 0.92-0.96) on the metrics of the detected spindles. The choice of these different thresholds was arbitrary but meant to highlight the effect that using fixed thresholds has on the parameters of detected events.

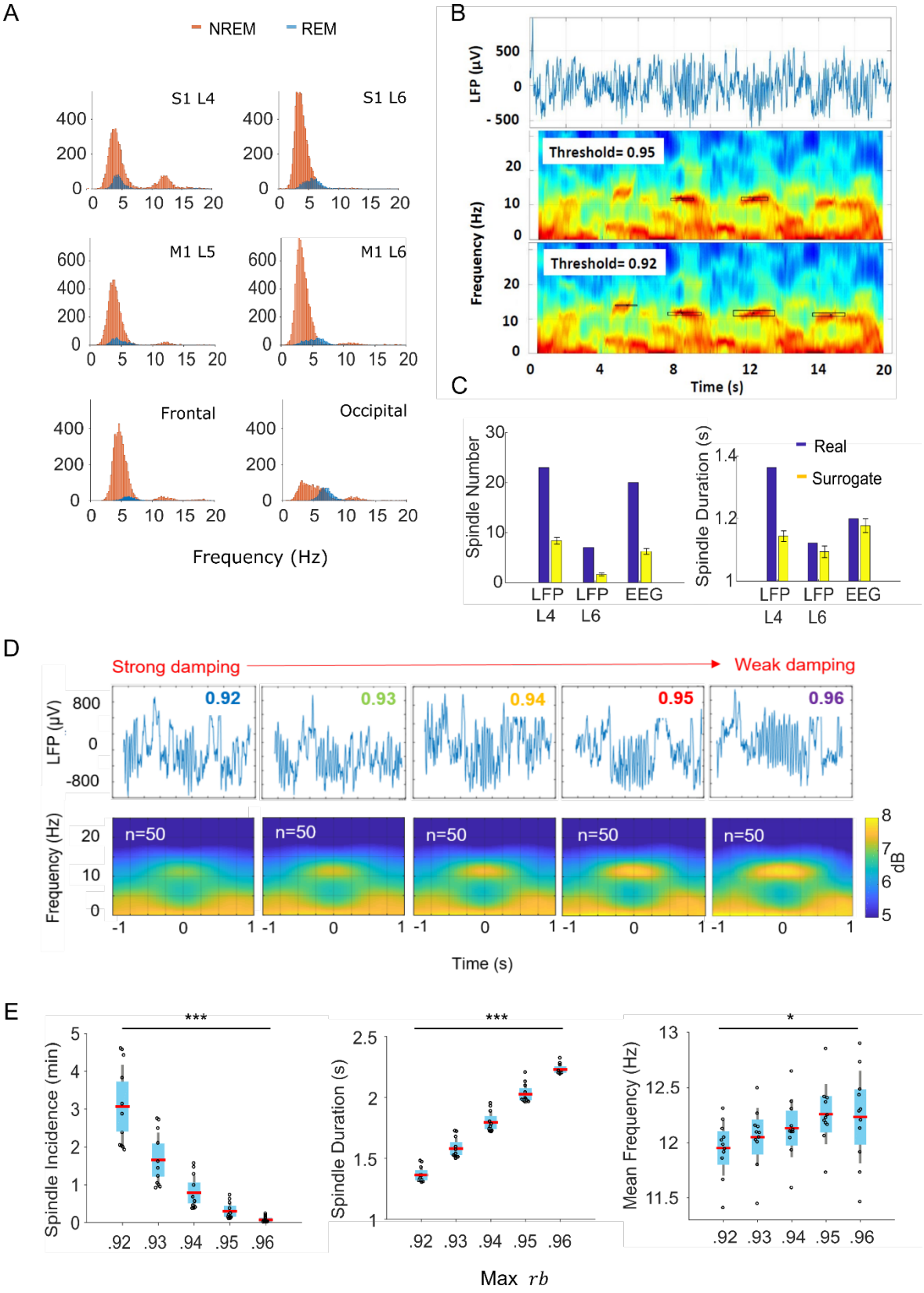


Figure 8. Characteristics of the events detected with the AR-model. (A) *Frequency distribution of the events detected with the lowest r_b threshold of the AR-model (r_b=0.92) during NREM (blue) and REM (red) sleep. (Top) LFP S1 signal (In the layer with highest*

incidence of spindles –i.e. Layer 4- and the layer with least spindles –i.e. Layer 6). (Middle) LFP M1 signal (In the layer with highest incidence of spindles –i.e. Layer 5- and the layer with least spindles –i.e. Layer 6. (Bottom) frontal and occipital EEG signals. ***(B)*** *(Top) 20-s segment of the LFP signal from one mouse. (Middle and Bottom) spectrograms corresponding to the LFP signal. The black boxes indicate spindle events detected when upper thresholds r_b=0.95 and r_b=0.92, respectively, are used for detection. This figure was produced together with Eckehard Olbrich.* ***(C)*** *Comparison of the number and duration of spindles detected (with the r_b=0.92 upper threshold) in the real LFP (S1, layers 4 and 6) and EEG signals (from one mouse) and the respective surrogates (mean and SEM across n=19 per derivation).* ***(D)*** *Examples of spindle events detected with the different r_b* thresholds *(note: spindles detected at a specific r_b threshold level, were those that reached all the lower r_b thresholds up to that specific r_b threshold – therefore we call it here Max r_b).* ***(E)*** *Mean number of spindles per minute (left), mean duration in seconds (middle), and mean frequency (right) of spindles detected by the different r_b thresholds. n=11 mice (n=7 laminar probes in S1; n=4 micro-wire arrays in S1). Red lines= mean across mice; blue boxes= SEM; grey bars= 95% confidence intervals; dots= individual values for each mouse). *p<0.05, **p<0.001, ***p<0.0001.*

It is important to mention that reducing detection thresholds can render algorithms prone to false positive detections. We therefore chose the lowest upper threshold r_b using two criteria. First, we compared the performance of the AR-based detector with human expert visual detection of 'spindle events'. Based on this, we identified the lowest r_b threshold (i.e. r_b = 0.92) for the AR-model, which did not detect putative 'spindle events' that did not clearly resemble 10-15Hz oscillatory events. We proceeded by running the AR-based detector on 10-minute segments of real LFP and EEG signals and their respective surrogates (n=19 for each signal), using the lowest r_b threshold (i.e. r_b = 0.92). We confirmed that spindles were mainly detected, and showed higher durations, in the original signals than in the surrogates **(Figure 8.C)**. Based on this, we selected a series of r_b thresholds above the lowest selected value (i.e. r_b= 0.92, 0.93, 0.94,

0.95, 0.96) and explored whether the properties of detected spindles varied as a function of the different r_b thresholds.

We grouped spindles based on the highest r_b threshold that they passed. For example, spindles with r_k coefficient 0.923, 0.938 and 0.947 would be considered to be detected with r_b thresholds 0.92, 0.93 and 0.94, respectively. Note that a spindle detected with a higher threshold (e.g. 0.94) is not part of the lower threshold groups (i.e. 0.92 and 0.93 in this case).

We found that spindles that were detected with low r_b threshold occur at a significantly higher rate ($F_{4,40}$=98.6, p<0.0001, ***Table 1***) **(Figure 8.E)**, but show reduced power **(Figure 8.D)** and duration ($F_{4,40}$=237.9, p<0.0001, ***Table 1***) **(Figure 8.F),** relative to spindles detected with higher r_b thresholds. Notably the incidence, duration and power varied gradually across spindles detected with different r_b thresholds, instead of showing a distribution with a clear-cut boundary (between spindles and other signal states), which would be expected if spindles were indeed all-or-none phenomena **(Figure 8.D)**. Additionally, there was a slight but significant difference in the spindle mean frequency as a function of r_b threshold ($F_{4,40}$=8.5, p<0.05, ***Table 1***). Specifically, spindles detected with the highest threshold (r_b=0.96) were on average 0.29 ± 0.16 Hz (mean ± SEM) faster than spindles detected with the lowest threshold (r_b=0.92) **(Figure 8.E).**

Overall, these results show that the choice of threshold directly affects the metrics of detected spindles. Low r_b thresholds allow the AR-model to detect a high rate of spindles that are short in duration and power. As these r_b thresholds are increased, the

incidence of detected spindles decreases (following a linear trend, $p<0.0001$) while their duration, power and frequency increase (following linear and cubic trends $p<0.001$), in a gradual manner.

3.3.1.3. Interim summary

From this section, we conclude that contrary to the assumption widely used in the field (Wamsley et al., 2012; Warby et al., 2014; Gemignani et al., 2015; Lajnef et al., 2015), spindles form a continuum rather than representing all-or-none phenomena. Binary classification of spindles based on single fixed thresholds is arbitrary and can bias algorithms towards the detection of spindles within a narrow section of their distribution. These results also highlight the possibility that the variability in spindle characteristics has an important physiological meaning.

3.3.2. The Oscillatory Quality (o-Quality): A quantitative metric for the strength of oscillatory activity

We proceeded to explore whether the variability in the characteristics of sleep spindles has indeed any physiological relevance. To do so, we developed a methodological and conceptual framework to characterise spindles taking into account the variability in their properties. To develop this framework, we made use of measurements routinely used in engineering and physics to assess oscillatory dynamics. In these fields, *damping* is used to measure the robustness and duration of an oscillation (Alciatore, 2002). Additionally, the *Quality-Factor* is a parameter used to calculate the level of damping of

an oscillation (Harlow, 2004; Marmion, 2007). Therefore, in analogy to the *Quality-Factor (Q)*, we propose to use the damping strength of neural oscillations (i.e. in this case 10-15 Hz events), as a measure of their *Oscillatory-Quality* (*o-Quality*). Essentially, strong-to-weak damping corresponds to low-to-high *o-Quality* **(Figure 9).** In this way, we classified all spindles detected in the LFP and EEG signals into one of five *o-Quality* levels (*o-Q1* to *o-Q5*), based on the highest r_b threshold they reached (i.e. based on their oscillatory strength). Spindles with low oscillatory strength (which based on the previous section we know are those with short duration, low amplitude and low power) received a low *o-Quality* index, while spindles with high oscillatory strength (i.e. those with long duration, high amplitude and high power) received a high *o-Quality* index. For instance, using the same examples as above, spindles with r_k coefficient 0.923, 0.938 and 0.947, would be considered to be detected with r_b thresholds 0.92, 0.93 and 0.94, and would be classified with *o-Quality* levels: *o-Q1*, *o-Q2* and *o-Q3*, respectively. Note that a spindle detected with a higher threshold (e.g. 0.94) is not part of the lower threshold groups (i.e. 0.92 and 0.93 in this case).

Importantly, this new metric for the first time describes the oscillatory strength of sleep spindles in quantitative terms. Note that the AR-model used to detect spindles was previously published by Olbrich and Achermann (2005). Here we do not claim that this model is overall superior to other approaches (i.e. amplitude-based approaches). Instead we suggest that the use of single thresholds is not justified physiologically or mathematically, and that the variability of spindles in properties (like the oscillatory strength, i.e. *o-Quality*) may have a meaning that has been underappreciated.

We continued, therefore, by investigating whether the variability of spindles in terms of *o-Quality* has any physiological, network or functional relevance. Indeed, we found that taking into account the variability of spindles in terms of *o-Quality*, opens a new and crucial avenue to understand their network dynamics and functional role. We will proceed to show evidence supporting the relevance and utility of the *o-Quality* metric, and will report novel findings on the dynamics and function of spindle oscillations obtained by applying it.

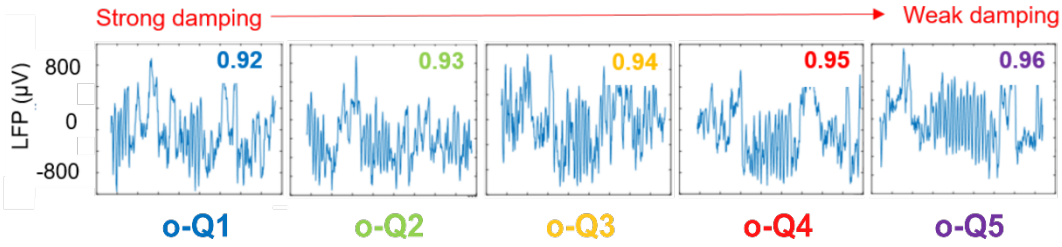


Figure 9. Illustration of the oscillatory-Quality (o-Quality) concept. *Each spindle received an o-Quality score such that strong-to-weak damping corresponded to low-to-high o-Quality. Spindles that exhibited strong damping, which means low oscillatory strength and hence reached only the lowest* r_b *thresholds, would receive a low o-Quality score (e.g. o-Q1 for spindles that reached only the lowest threshold* r_b*=0.92). On the contrary, spindles that exhibited weak damping, which means high oscillatory strength, and were detected by the highest* r_b *thresholds, would receive a high o-Quality score (e.g. o-Q5 for spindles that reached the highest threshold* r_b*=0.96).*

3.3.3. The Oscillatory-Quality reflects local and global synchrony of the spindle generating network

For several decades after spindles were described for the first time by the pioneers of EEG recordings (Loomis et al., 1935), spindles were thought to be widespread and synchronized throughout large cortical areas (Achermann & Borbély, 1998; Contreras

et al., 1997). Mounting evidence based on intra-cortical human and rodent recordings suggests, however, that although spindles can occur in widespread areas, most spindles occur and are modulated locally (Andrillon et al., 2011; Piantoni et al., 2017; Fernandez et al., 2018). This is indeed what we found in our recordings.

3.3.3.1. Visual evidence of local and global spindles in the local field potentials and multiunit activity

In line with previous evidence, visual inspection of LFP and MUA signals revealed that spindles in S1 and M1 display a significant diversity in their spatial extent at the mesoscopic level. Signals that were recorded with 16-channel laminar probes (100µm inter-electrode spacing) and 16-channel micro-wire arrays (250µm inter-electrode spacing) show a large diversity in the percentage of channels that are involved in a spindle event simultaneously **(Figure 10.A)**. Some LFP spindles are extra-local and express in just a few recording channels, without evidence of spindling at other recording sites located a couple hundred micrometres away. Some other LFP spindles, in the same animal, show greater spatial extent and express in a greater proportion of these recording channels. Interestingly, visual inspection revealed that spindles events, which appear to have the greatest spatial extent and prominence (i.e. highest duration and amplitude), show concordant spindling in the global frontal EEG **(Figure 10.A).** This was the case for local spindles recorded both across and within cortical layers.

Previous studies suggest that LFP signals can spread to sites away from their neuronal generators by a passive process of volume conduction (Buzsáki, 2004; Kajikawa and Schroeder, 2011). Such spread has been found to reach distances as long as 200-400

μm (horizontally) to many millimetres (vertically). Therefore, a question that naturally arises at this point is whether the variability in the spatial extent of LFP spindles reflects a physiological phenomenon or results from volume conduction. To assess this, we investigated whether the distribution of LFP spindles related to locally recorded MUA, which reflects more local spiking activity with a radius of ~100μm (Buzsáki, 2004; Kajikawa and Schroeder, 2011) and therefore is not likely to be affected by volume conduction.

Indeed, we visually confirmed that local spindle events detected in a reduced number of LFP channels (i.e. 3 or 4) showed corresponding MUA activity restricted to the same channels. Similarly, more global spindle events expressing across several LFP channels showed corresponding MUA extending to those channels **(Figure 10.B)**. Moreover, these local events, expressed in both the LFP and MUA signals, give rise to a marked increase in spectral power at the spindle frequency range (10-15Hz), which is not evident during the same epoch in other channels where spindles are not visibly evident ($F_{80,880}$= 8.97, p<0.0001; p<0.05 for frequencies 10.25 to 20), **(Figure 10.C,D)**.

These preliminary results suggest that the pronounced variability in the spatial extent of spindles, at a mesoscopic level, cannot be explained by volume conduction, and furthermore that spindles can occur within highly restricted local cortical areas. In order to fully determine this, however, further analyses need to be performed to confirm that the extend of LFP spindles is not only reflecting volume condition. Spindles will be detected based on the MUA in order to confirm the results observed here based on visual inspection. Additionally, current source density analyses could be applied to

our data to address whether the activity observed in just a few recording channels does indeed reflect "local" activity in the cortex.

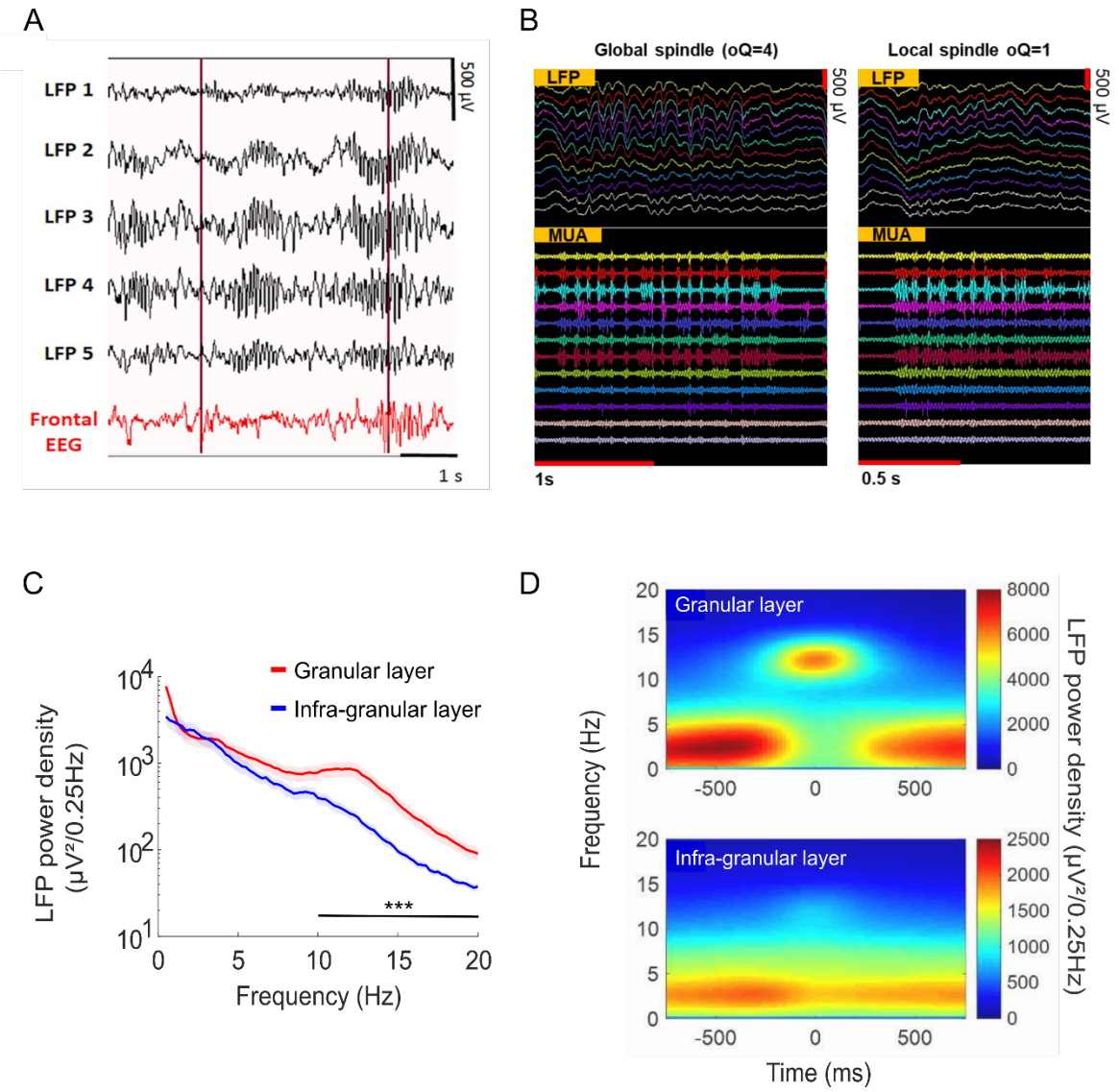


Figure 10. Evidence of global and local spindles in the LFP/EEG and MUA signals. (A) *Representative LFP signals (7-s of NREM sleep in one mouse) recorded from five contiguous electrodes within a micro-wire array implanted in S1 (black) and corresponding frontal EEG signal (red). These traces show examples of local spindles (restricted to a few LFP channels) and a global spindle that expresses in all the LFP channels and the EEG.* ***(B)*** *Examples of a global (left) and a local (right) spindle. Top panels show LFP signals across 12 consecutive channels of a micro-*

wire array implanted in S1 in one mouse. Bottom panels show corresponding MUA traces across these channels. Note that spindle events detected in a reduced amount of LFP channels showed corresponding MUA activity restricted to the same channels. ***(C)*** *Mean LFP power density spectra in the LFP (S1) channel with highest spindle density per mouse (red – LFP recording electrode located in the granular layer of S1) and in an LFP (S1) channel with low spindle density (blue – LFP recording electrode located in Layer 6 of S1), during 4-s epochs where spindles were detected with the AR model. (Mean and shaded area= SEM across mice).* ***(D)*** *Average spectrograms of 2-s segments of LFP signals recorded from the electrodes located in the granular and infra-granular layers of S1. n= 7 mice implanted with laminar probes in S1. Spectrograms are aligned to the midpoint of each spindle event. This specific spectrogram was developed suing Dr. Ross Purple's script. Note: *p<0.05, **p<0.001, ***p<0.0001.*

We proceeded then to further explore the spatiotemporal dynamics of spindles at a local and a global level, and to investigate whether and how this is related to the *o-Quality* of spindles.

3.3.3.2. The Oscillatory-Quality of spindles is an index of the LOCAL synchrony of the spindle generating network

Based on the visual inspection of the recorded EEG and LFP signals, we hypothesised that spindles with high *o-Quality* index would encompass larger cortical networks than spindles with low *o-Quality.* To test this quantitatively, we investigated how the spatial extent of spindles varied as a function of spindle *o-Quality*. The spatial extent of spindle expression was calculated based on the number of local LFP recording electrodes involved in a spindle event and the spacing between these electrodes (100 μm for the laminar probes, and 250 μm for the horizontal micro-wire arrays). For example, a spindle detected in three recording electrodes of a laminar probe (inter-electrode spacing = 100 μm) would be considered to express within a radius of ~200 μm.

Our results revealed a significant positive association between spindle *o-Quality* and the spatial extent of LFP spindle events both in S1 (recorded within and across cortical layers) and M1 (x^2_4=109.1 p<0.0001, multinomial logistic regression, ***Table 5***) **(Figure 11.A)**. In other words, as the *o-Quality* increased, more LFP channels were involved in the spindle event ($F_{4,72}$=132.4, *p*<0.0001, ***Table 2***). Moreover, the spatial extent of spindle expression varied as a function of cortical region, being significantly higher in S1 relative to M1 across all *o-Quality* levels ($F_{4,17}$=27.5, p<0.0001, ***Table 2***).

Overall, spindles with low *o-Quality* were predominantly local and expressed within a radius ~300 μm in S1 and ~200 μm in M1 (i.e. expressed in ~22% to 50 % of all LFP channels). As the *o-Quality* of spindles increased, the spatial extent of their expression gradually increased, until this reached a radius of ~700 μm in S1 and ~550 μm in M1. This result suggests that the *o-Quality* of local LFP spindles reflects the level of synchrony in the local networks involved in the expression of spindles. High *o-Quality* spindles show a high spatial extent, suggesting that the local network is in a highly synchronous state, while low *o-Quality* spindles reflect a low local synchrony state.

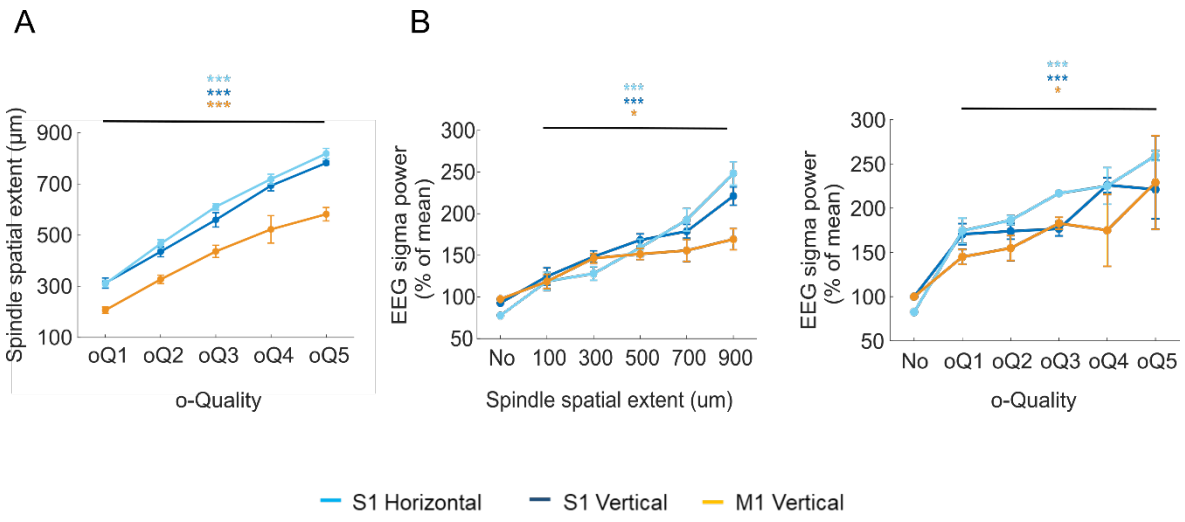


Figure 11. The spindle o-Quality is a measure of synchrony within local and global cortical networks. (A) *Mean spatial extent of LFP spindles recorded from both laminar probes (in S1 – dark blue- and M1 - orange) and micro-wire arrays (S1 –orange), as a function of o-Quality. The spatial extent of a spindle is calculated from the number of LFP electrodes involved in that spindle event.* ***(B)*** *Mean EEG sigma power in the frontal derivation during epochs with detected spindles as a function of spindle spatial extent (left) and o-Quality of local LFP spindles (right) detected in S1 (dark blue= laminar probe; light blue= micro-wire array) and M1 (orange). Note: figures show mean and SEM across mice. NOTE:* S1 laminar: n=7; S1 micro-array: n=7; M1 laminar= S1 laminar: n=7. **p<0.05, **p<0.001, ***p<0.0001.*

3.3.3.3. The Oscillatory-Quality of spindles is an index of the GLOBAL synchrony of the spindle generating network

An important question that arises at this point is to what extent oscillatory synchrony within local circuits is reflected within more extended cortical networks. As previously mentioned, visual inspection of the EEG and LFP signals hinted that only the most pronounced local LFP spindles would manifest in the global frontal EEG signal. We therefore continued by exploring the association between both the spatial extent and

o-Quality of spindles, as well as their propensity to express at the global EEG level (in the frontal derivation). To do this, we calculated the mean frontal EEG power spectra across 4-s epochs where LFP spindles were detected, and measured how the power at the spindle frequency range varied based on the spatial extent and *o-Quality* of spindles.

Using a multinomial regression approach, we observed a significant positive association between sigma power in the frontal EEG and both the spatial extent (x^2_4=163.3, p<0.0001, ***Table 5***) and *o-Quality* (X^2_4=163.3, p<0.001, ***Table 5***) of LFP spindles. Specifically, mixed ANOVA and follow-up repeated measure analyses revealed that the frontal EEG sigma power significantly increased as the spatial extent of local spindles increased **(Figure 11.B)** (S1 laminar: $F_{4,72}$=20.5, p<0.0001; S1 horizontal: $F_{4,72}$= 11.6, p<0.0001; M1 $F_{4,72}$=2.7 p<0.05, ***Table 3***). However, this effect was significantly stronger in S1 relative to M1 ($F_{4,72}$=3.1, p<0.05, ***Table 3***), where spindles with high spatial extent (i.e. 700-900 μm) were rare and were associated with significantly lower frontal EEG sigma power relative to high spatial extent spindles in S1.

In a similar way, the sigma power significantly increased in the EEG as the *o-Quality* of LFP spindles in S1 and M1 increased **(Figure 11.B)** ($F_{4,72}$=2.97, p<0.05, ***Table 4***). In this case no interaction was evident between the *o-Quality* level and the recording configuration, i.e. S1 laminar, S1 micro-array, M1 ($F_{4,72}$=0.3, p=0.97, ***Table 4***). Overall, this confirms our hypothesis that low *o-Quality* spindles are local and transient while spindles with higher *o-Quality* last longer, encompass larger cortical regions and, therefore, manifest at a global EEG scale. Together, these results show that the size of the neuronal population that oscillates at the spindle-frequency range is reflected in the

o-Quality of spindles. In other words, the *o-Quality* is a direct measure of the local and global synchrony of the network involved in the expression of spindles.

Extensive research targeting oscillations like sleep spindles is based on extra-cranial recordings, like the EEG, which measures electrical activity of synchronised neurons within widespread cortical networks (Buzsáki, 2004). Our results show, however, that ~91.7% ± 1.27 (mean ± SEM, n=7 mice, S1 LFP channel) of LFP spindles are highly local and remain undetected in the frontal EEG (recorded contralaterally from the source of LFP signal). The expression of spindles throughout global cortical networks becomes more likely as the *o-Quality* of spindles increases. However, these high *o-Quality* global spindles comprise only ~8.35% ± 0.78 (mean ± SEM, n=7 mice) of the total spindle population. This means that within a 12-hour light period, approximately 800 spindles (considered local because they express within a radio of ~400 μm mainly in granular layers, a singnal that would not be detected by high density EEG recordings, Buzsáki, 2004b), are missed (as recorded from the contralateral hemisphere) when only extra-cranial recordings, like the EEG, are used to assess spindle dynamics in mice (relative to LFP channels with highest spindle incidence). It is crucial, therefore, that EEG-based studies take into consideration the fact that they are dealing with only a small proportion of sleep spindles and are detecting only high *o-Quality* events that arise within highly synchronous networks.

This result suggests that the *o-Quality* of local LFP spindles reflects the level of synchrony in the local networks involved in the expression of spindles. These results also highlight the relevance of taking into account the *o-Quality* of spindles in order to understand their network dynamics. Fixed amplitude-based or damping-based

thresholds, set to detect EEG global spindles, are likely to reject local LFP spindles, which comprise the majority of the spindle population but show low amplitudes and high damping.

3.3.3.4. Interim summary

The results from this section are in line with previous evidence suggesting that spindles are predominantly local phenomena, which sometimes express in widespread cortical regions (Nir et al., 2008; Andrillon et al., 2011; Piantoni et al., 2017). It follows, therefore, that the majority (~91.7%) of local LFP spindles remain undetected at the global EEG level (where they are generally recorded from in humans). Additionally, our results suggest that the *o-Quality* of local LFP spindles reflects the level of synchrony in the local networks involved in the expression of spindles. We proceeded, therefore, to further explore the topography of spindles at local and global levels, taking into consideration the *o-Quality* of spindles and its relationship to the network spatiotemporal dynamics.

3.3.4. The Oscillatory-Quality reveals a thorough picture of the topography of spindles

Mounting evidence suggests that the properties of spindles are highly dependent on their underlying macroscopic (Nir et al., 2011; Piantoni et al., 2017) and mesoscopic (Hagler et al., 2018; Ujma et al., 2019) topography. For instance, in human subjects spindle density, amplitude and frequency have been reported to be high in parietal

areas, somewhat reduced in frontal areas, and further reduced in temporal areas (Finelli et al., 2001; Andrillon et al., 2011; Piantoni et al., 2017). Similar results have been observed in rodents (Kim et al., 2015), which have further reported that spindles seem be to highly prominent in primary sensory regions (Fernandez et al., 2018). Differences in spindle properties, however, could reflect differences in factors that affect detectability, such as their *o-Quality*. We proceeded, therefore, to investigate the macroscopic (millimetre scale, i.e. comparing different brain regions: S1 vs M1) and mesoscopic (micrometer scale, i.e. comparing different cortical layers) topography of spindles taking into account their variability in terms of *o-Quality*.

3.3.4.1. Topography of spindles at a macroscopic level

We found that the incidence and duration of spindles varies as a function of their *o-Quality* and this variation depends on the cortical derivation from which spindles are recorded ($F_{4,128}$=22.11, p<0.0001 and $F_{4,128}$=1.89, p<0.05; effect of *o-Quality**derivation on spindle incidence and duration, respectively, ***Table 6***). As expected from previous literature (Fernandez et al., 2018), spindles were significantly more frequent **(Figure 12.A)** (p<0.0001, see posthoc tests in ***Table 6***) and on average showed higher *o-Quality* in S1 relative to M1 and to global spindles detected in the frontal and occipital EEG **(Figure 12.B)** ($F_{3,33}$= 10.12, p<0.0001, ***Table 8***). Moreover, S1 spindles were overall longer in duration than M1 and EEG spindles **(Figure 12.A)** (p<0.0001, see posthoc tests in ***Table 7***). No differences in spindle incidence, duration or *o-Quality* were evident between spindles detected in M1 and the frontal and occipital EEG (see posthoc tests in ***Table 6, Table 7, and Table 8***). These results are in line with previous human (Finelli

et al., 2001; Andrillon et al., 2011; Piantoni et al., 2017) and rodent (Kim et al., 2015; Fernandez et al., 2018) studies, and further support the argument that spindles are not all-or-none phenomena but rather properties such as their incidence, duration, and *o-Quality,* vary as a function of their cortical topography.

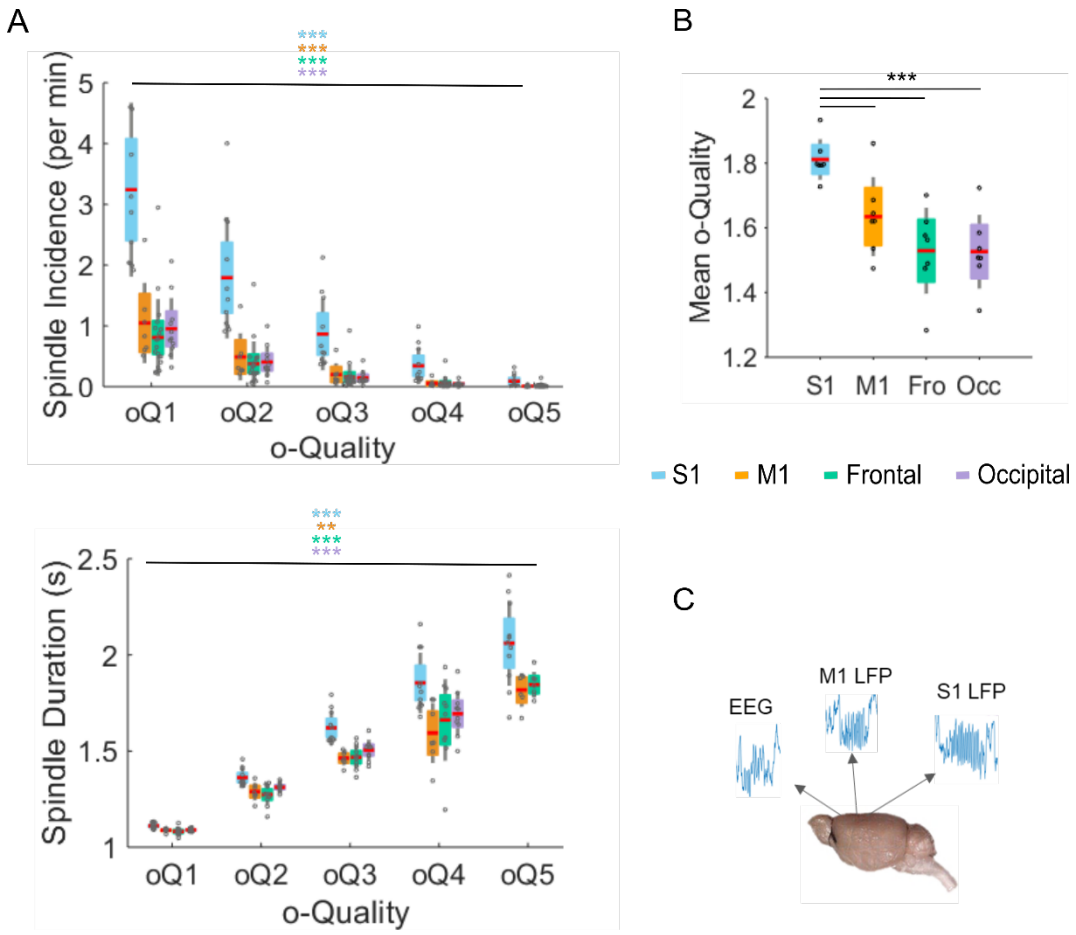


Figure 12. The o-Quality gives a more complete picture of the topography of spindles at a macroscopic level. (A) *Incidence (top) and duration (bottom) of spindles detected in the LFP (S1 and M1) and EEG (frontal and occipital) derivations as a function of spindle o-Quality.* ***(B)*** *Mean spindle o-Quality across brain regions. S1 (n=11 [laminar n=7; micro-array n=4]), M1 (n=7), Fro (n=11), Occ (n=11).* ***(C)*** *Illustration showing examples of spindle events detected in the different brain areas (frontal EEG, S1 LFP and M1 LFP). NOTE: (S1= primary somatosensory, M1= primary motor, Fro= frontal, Occ= occipital cortex). S1 (n=7, laminar), M1 (n=7), Fro (n=7), Occ (n=7). Box-*

*plots: red lines= mean across mice; blue boxes= SEM; grey bars= 95% confidence intervals; dots= individual values for each mouse. *p<0.05, **p<0.001, ***p<0.0001.*

3.3.4.2. Topography of spindles at a mesoscopic level

In contrast to the variability of spindles across macroscopic cortical regions, their variability at a mesoscopic level (i.e. within areas extending a few hundred micrometres) has not been extensively studied. One study based on intracranial recordings in human epileptic patients, suggested that spindles are most frequent and prominent in middle cortical layers, slightly weaker in upper layers and further reduced in deep layers (Hagler et al., 2018). Similarly, current-source density analyses performed in the somatosensory cortex of anaesthetised rats, suggest that a major dipole associated with spindles arises in Layer 4 (Kandel and Buzséki, 1997). Previous studies have not explored, however, whether the laminar profile of spindles varies as a function of their macroscopic location. Moreover, it is still not known whether the oscillatory strength (i.e. *o-Quality*) of spindles varies as a function of the cortical depth. We investigated, therefore, the laminar profile and *o-Quality* dynamics of spindles, recorded from 16-channel laminar probes (100 μm inter-contact spacing) during NREM sleep, in two different brain regions (i.e. S1 and M1). The cortical layer recorded by each laminar electrode was determined based on histological and electrophysiological landmarks, as explained in the methods section.

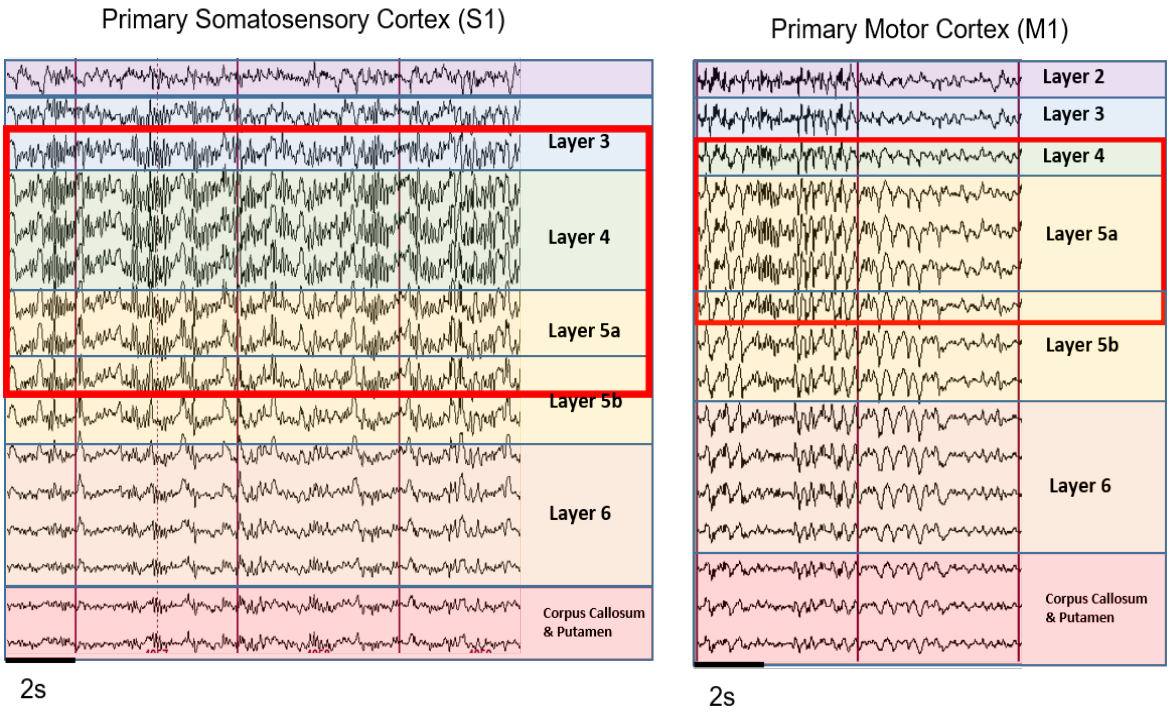


Figure 13. Visual inspection of LFP signals in S1 and M1 across cortical layers. *Raw LFP signals recorded from laminar probes during NREM sleep in two different mice from the primary somatosensory and primary motor cortices. The red boxes highlight the layers where spindles are visibly most common in either brain region.*

In line with previous findings, visual inspection of LFP signals suggests that spindles in S1 are more prominent in Layer 4, and 3 while in M1 they are more prominent in Layers 5 and 4 **(Figure 13).** Interestingly, quantitative analyses suggest that the laminar profile of spindles changes as a function of the cortical area (Laminar profile * derivation= $F_{5,60}$=19.58, p<0.0001, ***Table 9***). A laminar analysis including spindles with all *o-Quality* levels, showed that in S1 the incidence ($F_{5,60}$=19.9, p<0.0001, ***Table 9***) and *o-Quality* ($F_{5,60}$=27.88, p<0.0001, ***Table 10***) of spindles is highest in Layers 3, 4, and 5a, somewhat reduced in Layers 2 and 5b, and further reduced in Layers 1 and 6 **(Figure 14.B)**.

Figure 14.C (left panel) shows that the proportion of high *o-Quality* spindles (oQ4 and oQ5) in S1 is higher in Layers 3, 4, and 5a relative to all the other layers ($F_{20,80}$=2.8, p<0.05, ***Table 9***), which could explain the increased mean *o-Quality* in these layers. These results are consistent with previous laminar analyses performed in humans (Hagler et al., 2018) and anaesthetised rats (Kandel and Buzséki, 1997). Moreover, they are consistent with evidence demonstrating that the density of thalamo-cortical inputs to S1 is highest in Layer 4, followed by Layers 3 and 5 (Killackey, 1973; Jensen and Killackey, 1987).

Similar to S1, a laminar analysis including spindles with all *o-Quality,* showed a significant effect of cortical layer on both the incidence ($F_{5,60}$=2.8, p<0.05, ***Table 9***) and mean *o-Quality* ($F_{5,60}$=2.68, p<0.05, ***Table 10***) of spindles in M1. In contrast to S1, however, the incidence and *o-Quality* of spindles was slightly higher in Layers 4 and 5a (

Figure 14.B). Moreover, the proportion of low and high *o-Quality* spindles relative to the total number of spindles was similar across layers ($F_{20,80}$=1.6, p=0.18, ***Table 12***). No detailed analysis of the laminar profile of spindles had been performed in the literature on M1, but interestingly these results are consistent with previous anatomical evidence indicating that thalamo-cortical projection to M1 form the majority of synapses in Layers 5 and 4, and to a lesser extent in Layers 2 and 3 (Hooks et al., 2013).

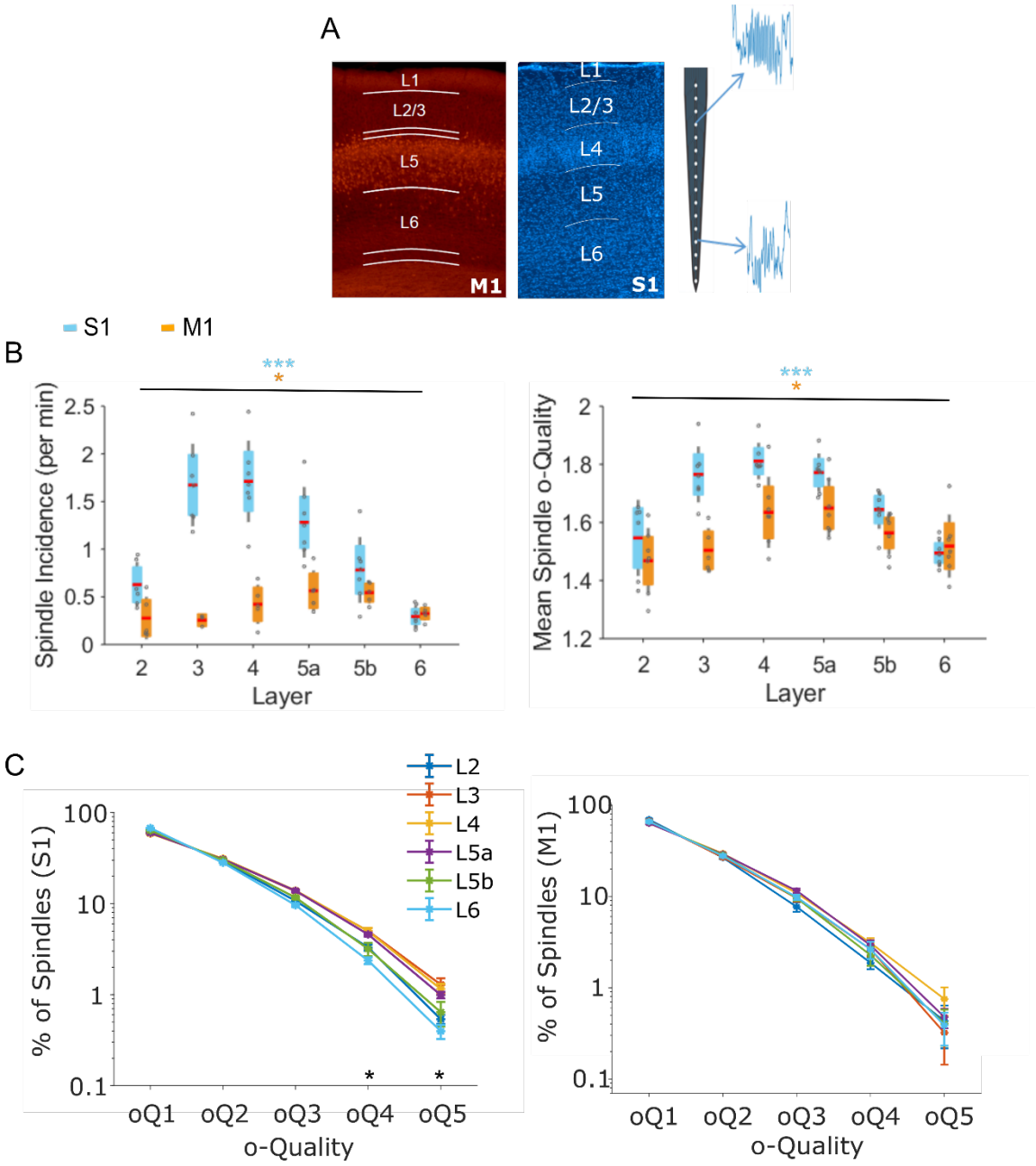


Figure 14. The o-Quality gives a more complete picture of the topography of spindles at a macroscopic level. (A) *Histological verification of probe location across cortical layers in S1 and M1. Note: the histological analysis of the slices acquired in M1 and the generation of the respective image was done by Lukas Krone.* ***(B)*** *Mean incidence (left) and o-Quality (right) of spindles detected across different cortical layers of the primary somatosensory (S1) and primary motor (M1) cortices. (Box-plots: red lines= mean across mice; blue boxes= SEM; grey bars= 95% confidence intervals; dots= individual values for each mouse).* S1 (n=7); M1 (n=7). ***(C)*** *Percentage of spindles (out of the total number of spindles detected across layers) detected at each o-Quality level across the different cortical layers of S1 (left) and M1 (right), (showing mean across mice*

*and SEM). NOTE: *p<0.05, **p<0.001, ***p<0.0001.* Channels per layer: L2 (n=11), L3 (n=10), L4 (n=12), L5a (n=12), L5b (n=12), L6 (n=12).

3.3.4.3. Interim summary

Overall, the results from this section support the view that spindles are mostly local phenomena (Andrillon et al., 2011; Nir et al., 2011; Piantoni et al., 2017; Fernandez et al., 2018). Moreover, they suggest that properties such as their prominence and oscillatory strength and stability (i.e. *o-Quality*) do not vary only between macroscopic regions but can also show substantial variability within microscopic regions separated by just a few hundred micrometre distances in the cortex.

3.3.5. The o-Quality of spindles is directly related to the occurrence of slow-waves and is sensitive to the levels of homeostatic sleep need

Despite being mainly local phenomena, the spatial and temporal synchrony of spindles within and across thalamo-cortical networks has been proposed to be driven by the depolarising up state of slow-waves (Contreras and Steriade, 1996; Buzsáki and Draguhn, 2004; Staresina et al., 2015; Klinzing et al., 2016; Niethard et al., 2018). Based on this and our previous results, which indicate that the spindle *o-Quality* reflects local and global synchrony of the spindle-generating network, we hypothesised that the occurrence of slow-waves (0.5 – 4 Hz) would be directly related to the *o-Quality* of spindles, and proceeded to investigate this.

Slow-waves were detected in band-pass filtered (0.5-4 Hz) EEG and LFP signals, as positive deflections between two consecutive negative deflections (separated by at least 0.1 s). We calculated the association between slow-waves and spindles in both the EEG and the LFP recording channel showing the highest incidence of spindles per mouse. Spindles were considered to co-occur with slow-waves if their onset occurred within a window of 0.12-s after the detection of a slow-wave (see Methods: *Slow-wave detection*). A window of 0.12-s was used so that the coupling between spindles would match even slow-waves with a frequency of 4Hz (0.12Hz would fall within ½ of one cycle of the 4Hz oscillation and within 1/8 of a 0.5Hz oscillation).

We found, indeed, that the *o-Quality* of spindles is positively associated with the occurrence of slow-waves (x^2_3= 11.66, p<0.01, R^2=0.36), both recorded from local (LFP) areas. High *o-Quality* LFP spindles are more likely to be preceded by local slow-waves than low *o-Quality* spindles in S1 ($F_{4,28}$= 5.64, p<0.001, ***Table 13***) **(Figure 15.A,B)**. This association was also present between slow-waves and the *o-Quality* of spindles in M1 ($F_{4,28}$= 3.28, p<0.05, oQ1-4, ***Table 14***), the frontal EEG ($F_{3,21}$= 8.97, p<0.01, oQ1-4, ***Table 15***), and the occipital EEG ($F_{3,21}$=37.6, p<0.0001, oQ1-3, ***Table 16***). In these derivations, however, high *o-Quality* spindles were very rare and hence were excluded from the analysis (see statistic *Tables 14-16* for details). We proceeded, therefore, to investigate how the sigma power, spindle incidence, and spindle *o-Quality* varied in conditions where the slow-wave activity varies as well (i.e. during natural sleep or resulting from sleep deprivation, as discussed below) (Dijk et al., 1993; Knoblauch et al., 2003; Vyazovskiy et al., 2004). We focused these analyses mainly on S1 (primary somatosensory cortex), because spindles are most pronounced and show a greater variability in terms of *o-Quality* in this region.

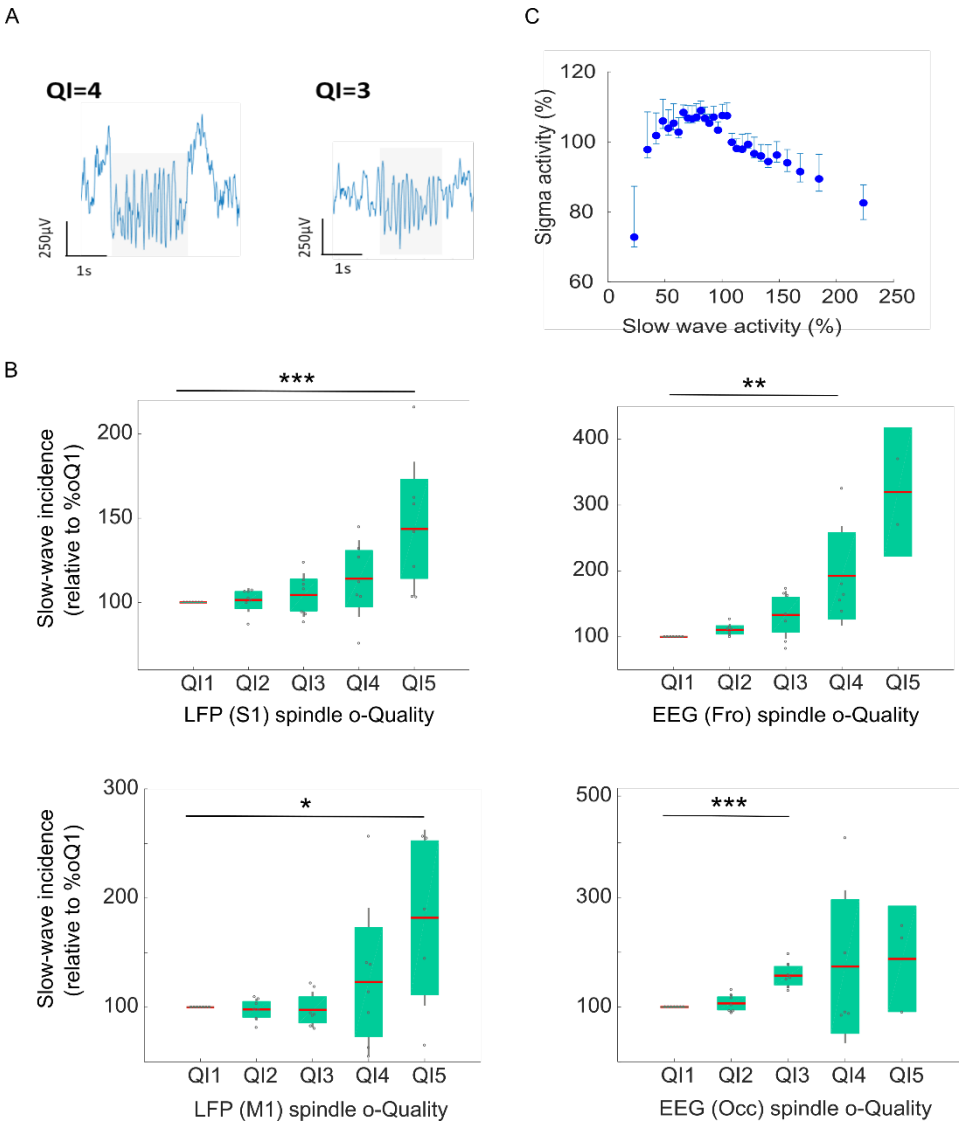
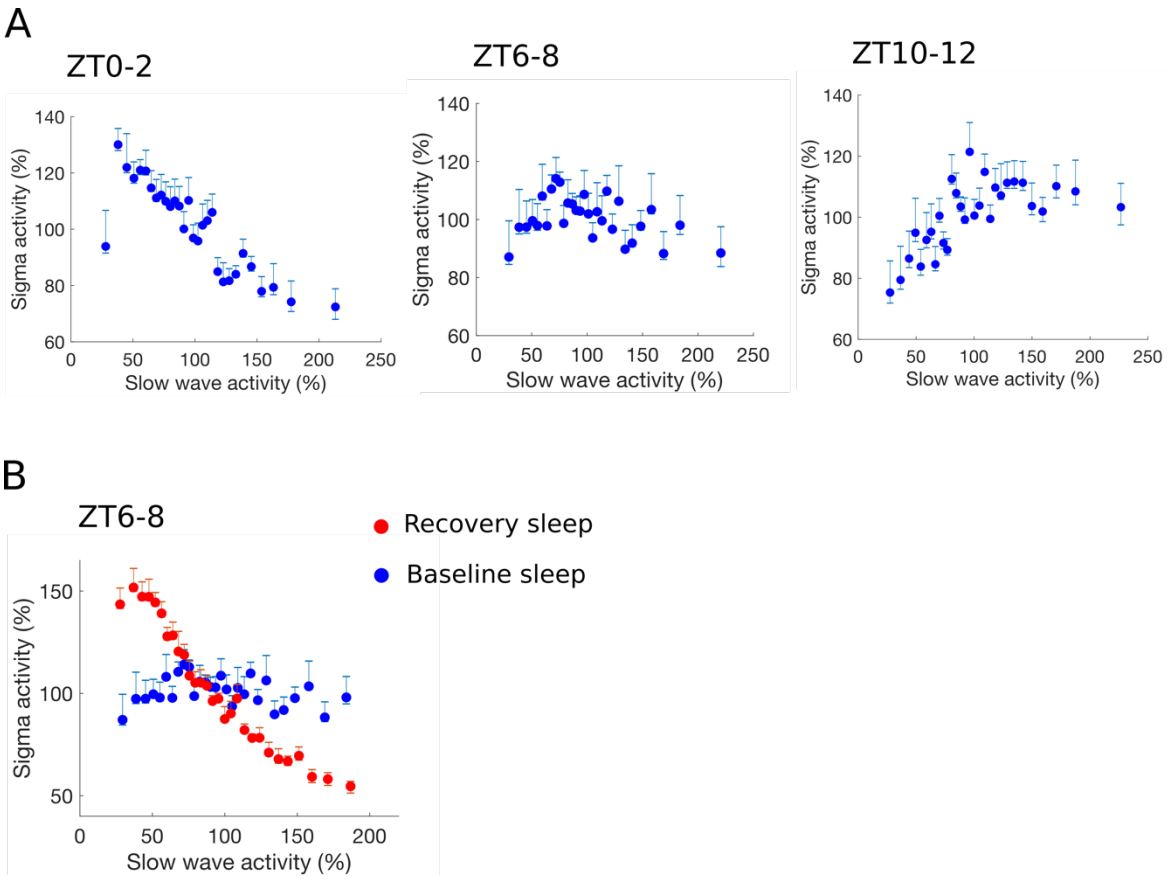


Figure 15. The o-Quality of spindles is directly related to the occurrence of slow-waves. (A) *Representative examples of spindle events with high (oQ4) and lower (oQ3) o-Quality detected in S1. This illustrates that high-quality spindles are more likely to be preceded by slow-waves than lower quality spindles. n= 7 mice laminar implant in S1.* ***(B)*** *Percentage of spindles preceded by slow-waves (in LFP and EEG derivations, respectively), as a function of o-Quality. Values in the y-axis are shown relative to the percentage of the lowest o-Quality spindles (oQ1) preceded by slow-waves, i.e. values>100 indicate a higher relative occurrence. S1= primary somatosensory n=7; M1= primary motor n=7; Fro= frontal n=7; Occ= occipital cortex n=7.* ***(C)*** *Relationship between LFP slow-wave activity (SWA, 0.5–4.0 Hz) and LFP sigma activity (activity at the spindle-frequency range, 10–15 Hz) during baseline. Four second epochs of NREM sleep recorded from 12h light periods were subdivided into thirty 5% bins as a function of SWA sorted from lowest to highest values, and corresponding sigma activity values were averaged for the same epochs prior to averaging across animals. NOTE: (Box-plots: red lines= mean across mice; blue boxes= SEM; grey*

*bars= 95% confidence intervals; dots= individual values for each mouse). *p<0.05, **p<0.001, ***p<0.0001.*

3.3.5.1. The slow-wave and sigma activity show an inverted-U shaped relationship within short (4-s) time intervals

We started by assessing the association between slow-wave and sigma activity within 4-s epochs. Specifically, we calculated the spectral power of EEG and LFP (S1) signals across mice using FFT on 4-s epochs. We chose the LFP channel that showed the highest incidence of spindles for each mouse, which in all cases was located in Layer 4. Using a multinomial regression, we calculated the association between relative spectral power densities in frequencies between 0.5-4Hz (slow-wave activity) and 10-15Hz (sigma activity) by grouping all 4-s epochs during NREM into thirty bins based on their slow-wave activity. In line with previous literature (Ang *et al.*, 2018), we found that slow-wave activity and sigma activity (recorded throughout 12h of rest, i.e. light period) were positively associated (x^2_{15}=73.78, p<0.0001, R^2=0.95 Cox and Snell) when slow-wave activity (normalised to mean slow-wave activity during NREM) was below 88%. Above 88%, however, the relationship inverted and we observed a negative association between slow-wave activity and sigma activity (x^2_{15}=88.7, p<0.0001, R^2=-0.97 Cox and Snell) **(Figure 15.C)**.



Supplementary Figure 15. Relationship between slow-wave and sigma activitya across time and conditions. (A) *Relationship between LFP slow-wave activity (SWA, 0.5–4.0 Hz) and LFP sigma activity (activity at the spindle-frequency range, 10–15 Hz) during the first two hours (left, ZT0-1), the middle (central, ZT6-8), and the last two hours (right, ZT10-12) of sleep baseline.* ***(B)*** *Relationship between LFP slow-wave activity (SWA, 0.5–4.0 Hz) and LFP sigma activity (activity at the spindle-frequency range, 10–15 Hz) during the 12h periods of sleep baseline (blue) and sleep deprivation (red).* ***(A-B)*** *Four second epochs of NREM sleep recorded from different time-segments of 12h light periods were subdivided into thirty 5% bins as a function of SWA sorted from lowest to highest values, and corresponding sigma activity values were averaged for the same epochs prior to averaging across animals.*

Interestingly, as reported in previous studies the association between sigma and slow-wave activity at a 4-s scale changes throughout the light period (i.e. across different time-points when the sleep pressure varies as well) (**Supplementary Fig.15A**). During the first two hours of sleep (ZT0-2) sigma and slow-wave activity show an inverse relationship (R^2=-0.87 Cox and Snell, p<0.0001). Halfway throughout the light period (i.e. ZT6-12) an inversed U-shaped relationship between slow-wave and sigma activity was apparent. Specifically, slow-wave activity and sigma activity were positively associated (R^2= 0.71 Cox and Snell, p<0.01) when slow-wave activity (normalised to mean slow-wave activity during NREM) was below 88%. Above 88% however the relationship inversed, and we observed a negative association between slow-wave activity and sigma activity (R^2= -0.65 Cox and Snell, p<0.01). Lastly, during the last 2 hours of the light period (ZT10-12) sigma and delta activity showed a positive relationship, which was most pronounced when the slow-wave activity was below 88%; R^2= 0.76 Cox and Snell, p<0.001).

3.3.5.2. The slow-wave activity, spindle incidence and spindle o-Quality increase within NREM episodes

Previous EEG human (Gottesmann, 1996; Dijk, 2009) and rodent (Vyazovskiy, Achermann, Borbély, & Tobler, 2004), studies have shown that the slow-wave activity increases within uninterrupted episodes of NREM sleep and that this increase slightly reduces towards the end of the episodes. We proceeded, therefore, to investigate whether the *o-Quality* of LFP (S1) spindles would increase as well. To do this, we detected episodes of uninterrupted NREM sleep from 12-h baseline sleep recordings. These NREM episodes consisted of at least 45 4-s epochs of NREM sleep. Brief

awakenings (also called micro-arousals here) of up to 12-s were not considered as changes of state. The average duration of uninterrupted NREM episodes across mice was 7.74 minutes ± 0.4 (mean ± SEM across mice). As done in previous studies (Himanen *et al.*, 2002; Alfonsi *et al.*, 2019), we divided NREM episodes into five equally sized bins, and calculated how the slow-wave activity and spindle parameters varied as a function of NREM bin in the LFP (S1) channel that showed the highest density of spindles per mouse (i.e. overall these are channels located in layer 4 of S1).

A repeated measures ANOVA indicated that slow-wave activity increased significantly across NREM bins **(**

Figure 16.A) ($F_{4,28}$=63.20, p<0.0001, ***Table 17***). Pairwise comparisons (using Sidak correction) show that this increase occurs during the first quarter of the NREM episode (p<0.0001 first NREM bin vs all the other bins), after which the slow-wave activity plateaus (p<0.05 for all other contrasts, ***Table 17***). Interestingly, similar to the slow-wave activity, both the spindle incidence ($F_{4,28}$=33.68, p<0.0001, ***Table 18***) and spindle *o-Quality* showed a significant increase ($F_{4,28}$=9.5, p<0.0001, ***Table 18***) as a function of NREM bin **(**

Figure 16.B). This increase appears progressive for spindle incidence, while the spindle *o-Quality* only appears to significantly increase from the first to the second NREM episode bin, after which there is no significant change (p<0.0001 first NREM bin vs all the other bins, ***Table 18***).

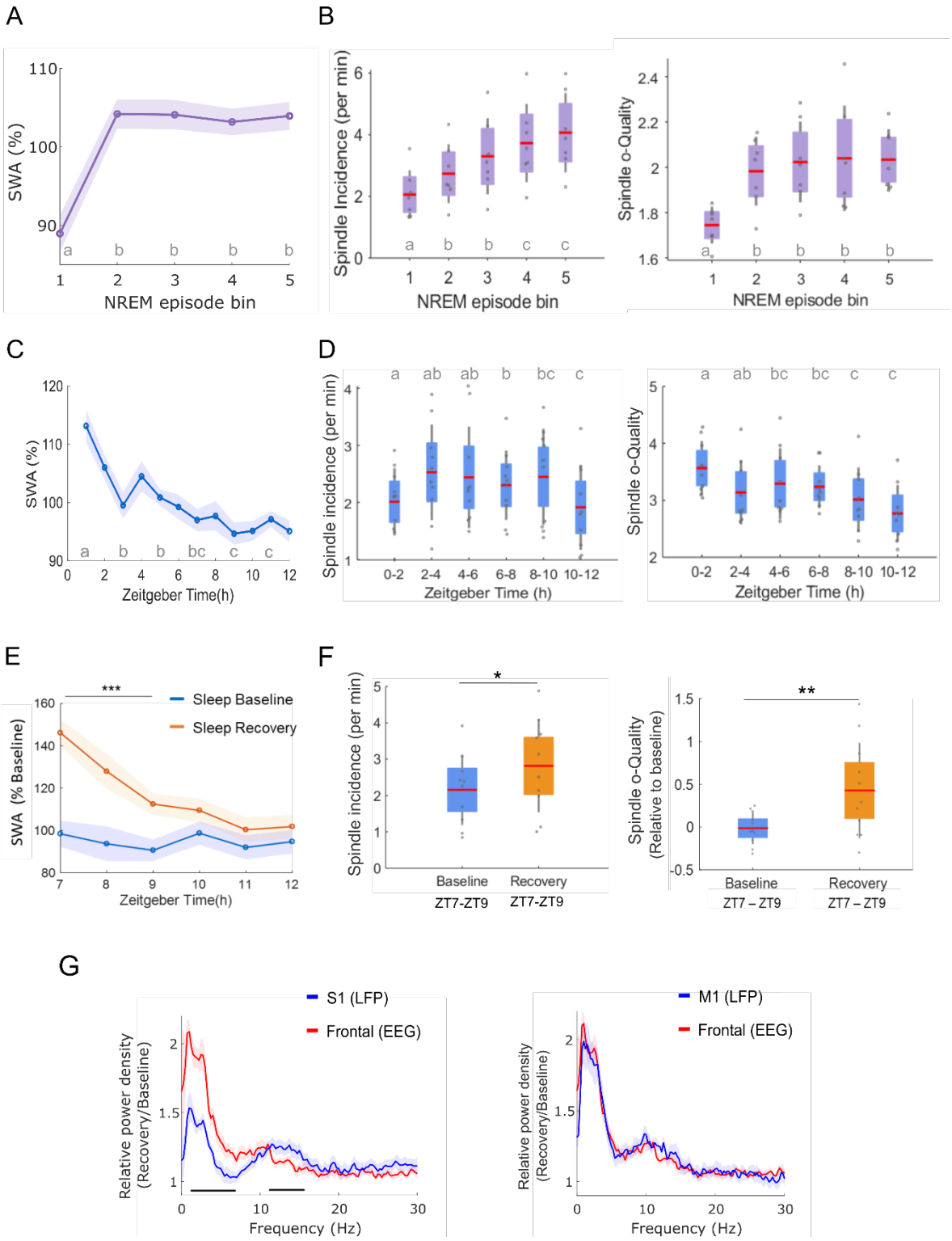


Figure 16. Both slow-wave activity and spindle o-Quality show an increase in different contexts of elevated sleep pressure. (A) *Time-course of slow-wave activity (0.5-4 Hz) in the S1 LFP signal across non-interrupted NREM episodes (divided into five equally sized bins) throughout 12h light periods. SWA values are expressed as % of mean 12-h NREM sleep value during light*

period. n= 7 mice implanted in S1. ***(B)*** *Spindle incidence (left) and o-Quality (right) measured within un-interrupted NREM episodes (plotted across five equally sized NREM episode bins) throughout a 12h light period.* n= 7 mice implanted in S1. ***(C)*** *Time-course of slow-wave activity (0.5-4 Hz) in the S1 LFP signal across a 12-h light period. SWA values are expressed as % of mean 12-h NREM sleep value. n= 10 mice implanted in S1*. ***(D)*** *Spindle incidence (left) and o-Quality (right) measured across a 12-h light period.* n= 10 mice implanted in S1. ***(E)*** *Time-course of slow-wave activity (0.5-4 Hz) in the S1 LFP signal during sleep recovery after 6 hours of sleep deprivation (orange) and corresponding sleep baseline time period (blue). SWA values are expressed as % of mean 6-h (ZT7-ZT11) baseline value. ZT= Zeitgeber time (i.e. time from light onset). n= 10 mice implanted in S1.* ***(F)*** *Spindle incidence (left) and o-Quality (right) measured during the first two hours of sleep recovery after sleep deprivation (ZT7-ZT9) and corresponding sleep baseline time-period. Note: Analyses in A-F were performed on one LFP (S1) channel per mouse, i.e. the channel that showed highest spindle density. n= 10 mice implanted in S1.* ***(G)*** *Change in EEG and LFP power density during the first two hours of sleep recovery relative to baseline. S1 n=7; M1 n=7; Frontal n=7. NOTE: Means denoted by a different letter (i.e. a,b,c) indicate significant differences between treatments. *p<0.05, **p<0.001, ***p<0.0001. (Box-plots: red lines= mean across mice; blue boxes= SEM; grey bars= 95% confidence intervals; dots= individual values for each mouse).*

3.3.5.3. Slow-wave activity, spindle incidence, and spindle o-Quality decrease within 12-h sleep (light) periods

Different studies performed in humans (Himanen et al., 2002; Andrillon et al., 2011) and rodents (Trachsel et al., 1988; Vyazovskiy et al., 2004) have found that slow-wave activity shows a progressive decrease across the 12-h light period (i.e. inactive period), and we proceeded to investigate whether the spindle *o-Quality* and incidence would show a related decrease as well. Again, we focused this analysis on the LFP channel with highest density of spindles per mouse (Layer 4). Indeed, we found that both the slow-wave activity (

Figure 16.C) ($F_{11,77}$=6.14, p<0.0001, ***Table 19***) and the spindle *o-Quality* (

Figure 16.D) ($F_{5,25}$=2.4*, p*<0.0001, ***Table 20***) progressively decreased across the light period. The incidence of spindles, however, only showed a subtle decrease towards the last two hours (ZT10-ZT12) of the light period **(**

Figure 16.D) ($F_{5,35}$=2.9, p<0.05, ***Table 20***). Interestingly, these results suggest that the density and *o-Quality* of spindles are dissociable, and therefore, may be regulated separately.

These results are contrary to previous studies, which report a progressive increase in slow-wave activity and a progressive decrease in sigma power across the 12h light period both in humans (Andrillon et al., 2011; Himanen, Virkkala, Huhtala, & Hasan, 2002; Trachsel, Tobler, & Borbely, 1988) and rodents (Vyazovskiy et al., 2004). The majority of these studies have been based on EEG recordings (except from some studies like Andrillon et al. (2011), where intra-cranial depth EEG was recorded during human sleep). Our divergent results could reflect, therefore, differences between species, recording spatial scales (EEG vs LFP), or recorded brain region. Indeed, previous results suggest that the association between slow-wave activity and spindles varies substantially between brain regions (Andrillon et al., 2011). These divergences will be further studied in future work.

3.3.5.4. Slow-wave activity, spindle incidence, and spindle o-Quality increase after sleep deprivation

Slow-wave activity (0.5-4 Hz) during NREM sleep is known to increase with wake duration, peak during early sleep and progressively decline in late sleep. As such,

slow-wave activity has been proposed to be an index of sleep/wake homeostasis, and reflect the levels of sleep need (Borbely, 1982; Borbély et al., 2016). We therefore performed 6-hours of sleep deprivation followed by sleep recovery in order to investigate the relationship between slow-wave activity and spindle *o-Quality* in a context of increased slow-wave activity power and sleep need. As expected, a mixed ANOVA revealed a significant interaction between the time since light onset (Zeitgeber time) and the sleep conditions (sleep baseline vs recovery) (ZT-time*sleep condition: $F_{5,40}$=7.9, p<0.0001, ***Table 21***). Specifically, in accordance with previous studies (Dijk et al., 1993; Vera Knoblauch et al., 2003; Vyazovskiy et al., 2004), a robust and significant increase in slow-wave activity (0.5-4 Hz) was found during the first two hours of sleep recovery (ZT7 to ZT9) relative to sleep baseline (*p*<0.0001, see post-hoc tests in ***Table 21***) (

Figure 16.E).

Interestingly, similar to the slow-wave activity, both the incidence ($F_{1,9}$=7.9, p<0.05, ***Table 22***) and *o-Quality* ($F_{1,9}$=8.1, p<0.01, ***Table 22***) of spindles in the LFP (S1) showed a significant increase in the first two hours of sleep recovery (

Figure 16.F). Intriguingly, this increase was not present in the case of spindles detected in the EEG (Incidence $F_{1,9}$=0.49, p=0.5; *o-Quality* $F_{1,9}$=0.88, *p*=0.37, ***Table 24***). In contrast to our results, previous human (Dijk, Hayes and Czeisler, 1993; Knoblauch *et al.*, 2003) and rodent (Vyazovskiy et al., 2004) studies have found that sleep deprivation affects the density of spindles in the EEG, mainly leading to a reduction during the first hours of sleep recovery relative to baseline. Our divergent results could reflect differences between species, recording spatial scales (EEG vs LFP), or recorded brain region.

Additionally, previous studies have predominantly used spectral approaches to detect and analyse spindles. Therefore, we proceeded to run spectral analyses (FFT for 4-s epochs, Hanning window: 0.25Hz resolution) to examine the impact of sleep deprivation on the power density in both the LFP (S1 and M1) and frontal EEG derivations.

Figure 16.G shows the relative change in power density in the EEG and LFP during the first two hours of sleep after sleep deprivation relative to baseline. A multivariate ANOVA followed-up with multivariate tests, indicates that the frontal EEG shows a significantly higher increase in relative power density at frequencies between 0.5 Hz and 7 Hz compared to the S1 LFP (p<0.05 for all these comparisons, ***Table 23***). This increase progressively decays across increasing frequencies until reaching almost baseline levels at 20Hz. In contrast to the frontal EEG, the S1 LFP power density shows significant increases during sleep after sleep deprivation (relative to baseline), at frequencies between 0.5 Hz and 7 Hz, as well as between 9 Hz and 16 Hz (p<0.05 for all these comparisons, ***Table 23***).

Interestingly, no significant difference was found between the M1 LFP and frontal EEG in terms of relative change in power density in the first two hours of recovery sleep relative to baseline. Overall, our results suggest that sigma power (10-15 Hz) is increased in recovery sleep relative to baseline in both EEG and LFP. However, while this seems to reflect an overall increase in power density in the EEG, in the LFP this increase is specific to slow and spindle-like frequencies and, therefore, is likely to reflect genuine spindle oscillations. Previous human studies have reported opposing results, showing that sigma power decreases after sleep deprivation (Dijk et al., 1993). To

reconcile these results, it would be informative to investigate the association between slow-wave dynamics and spindle activity across different regions in the brain. Indeed, our results suggest that the effect of sleep deprivation (i.e. increase in homeostatic sleep need) on sigma power may show topographical differences.

Additional analyses on 4-s epochs were performed to better understand the association between slow-wave and sigma activity after sleep deprivation relative to baseline sleep. We calculated the spectral power of the LFP (S1) signals across mice using FFT on 4-s epochs. We chose the LFP channel that showed the highest incidence of spindles for each mouse, which in all cases was located in Layer 4. We calculated the association between relative spectral power densities in frequencies between 0.5-4Hz (slow-wave activity) and 10-15Hz (sigma activity) by grouping all 4-s epochs during NREM into thirty bins based on their slow-wave activity (for recovery sleep and baseline sleep respectively).

In line with previous literature (Ang *et al.*, 2018), we found that slow-wave activity and sigma activity (recorded throughout 12h of rest, i.e. light period) were positively associated (R^2=0.75 Cox and Snell, p<0.0001) when slow-wave activity (normalised to mean slow-wave activity during NREM) was below 88%. Above 88%, however, the relationship inverted and we observed a negative association between slow-wave activity and sigma activity (R^2=-0.77 Cox and Snell, p<0.0001) **(Figure 15.C)**. We found, however, a pronounced negative association between slow-wave activity and spindles during sleep recovery after sleep deprivation (R^2=-0.97 Cox and Snell, p<0.0001). This suggests that although there is a positive relationship between slow-wave activity and

sigma activity (as well as spindle *o-Quality*), which is most prominent when sleep pressure is slow, at a short scale (4-s) slow-waves and spindles are incompatible.

3.3.5.5. Interim summary

Taken together, the results from this section show that high *o-Quality* spindles (which show increased oscillatory strength, power, and reflect a more synchronised state of the oscillatory network than low *o-Quality* spindles) are more likely to be preceded by slow-waves. This effect is present both at local (LFP) and global (EEG) levels, however EEG spindles and local spindles in areas like M1 are not likely to reach very high *o-Quality*, as compared to S1. Moreover, these results further demonstrate that the *o-Quality* of spindles is a metric of synchrony within cortical networks and is sensitive to the levels of homeostatic sleep need.

3.3.6. The o-Quality of spindles varies as a function of the infra-slow oscillation

Brain activity follows patterns at different timescales, which range from milliseconds up to hours and days (Buzsáki and Draguhn, 2004). As done in the previous section, spindle dynamics have predominantly been analysed at time scales of seconds and beyond. In addition to these timescales, however, spindles have been found to exhibit an infra-slow oscillation (Achermann and Borbély, 1997; Lecci et al., 2017; Lázár et al., 2019) defined by frequencies in the 0.01 to 0.02 Hz range. This infra-slow oscillation

has been reported to predominate in the posterior cortex, in both mice and humans (Lecci, 2018; Lazar, 2019). It is uncertain, however, whether the oscillatory strength of spindles varies as a function of the infra-slow oscillation. We proceeded, therefore, to investigate this.

3.3.6.1. Evidence of infra-slow oscillation in spindle activity

First, we examined whether the sigma power in the LFP and EEG signals recorded from our mice showed signs of periodic variability. **Figure 17.A-C**, show eight-minute segments of LFP and EEG signals during NREM sleep, filtered at the sigma frequency range (10-15 Hz). Bursts of high amplitude sigma activity (i.e. putative spindles) clearly occur in the S1 signal, while in M1 and the frontal EEG the occurrence of putative spindles seems to be more sporadic. To quantify the periodicity of putative spindle events we extracted uninterrupted NREM episodes (minimum duration 45 4-s epochs) from LFP (S1 and M1) signals recorded during the light period. The average duration of uninterrupted NREM episodes across mice was 7.74 minutes ± 0.4 (mean ± SEM). We then band-pass filtered (i.e. Butterworth filter) the signal in the sigma band (10-15 Hz) and calculated the signal envelope by means of a Hilbert transform. The periodicity of this "spindle envelope" was then assessed by Welch's power spectral density estimate.

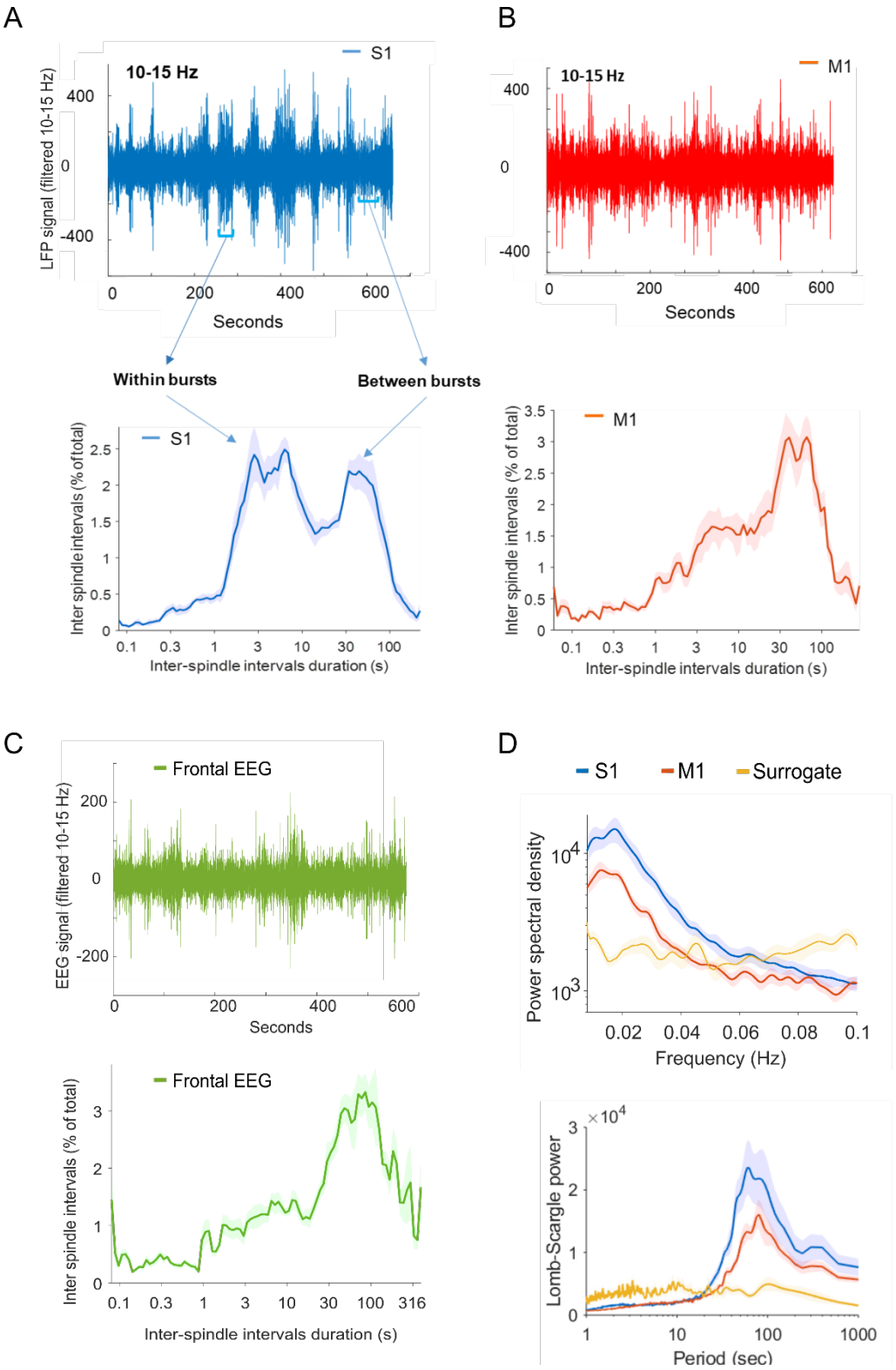


Figure 17. Infra-slow oscillation of spindle activity. (A,B,C) *Top panels show eight-minute segments of S1 LFP, M1 LFP, and frontal EEG signals, respectively, during NREM sleep, filtered at the spindle frequency range (10-15 Hz). Bursts of putative spindles are mainly evident in S1. The bottom panels show inter-spindle intervals (i.e. time difference between the onset of consecutive*

spindle events) within uninterrupted NREM episodes recorded throughout 12-h light periods in S1, M1 and the frontal EEG (mean and SEM across mice). In the case of S1 (panel A) there is a bimodal distribution. The first peak indicates ISI between spindles within bursts, the second peak indicates the time interval between bursts (i.e. last spindle of a burst to the first spindle of next burst). This bimodal distribution is not evident in M1 or the frontal EEG where the occurrence of individual or couples of spindles occurs more sporadically but still with a cycle length of ~60-80s. ***(D)*** *Top panel shows the power spectral density of the envelope of filtered LFP signals (10-15 Hz) recorded from S1 and M1, and respective filtered (10-15 Hz) surrogates (n=19 per derivation). Bottom panel shows the Lomb-Scargle periodogram of the LFP (S1 and M1) and surrogate time series. (Figures show mean and SEM across mice). S1 (n=7 laminar); M1 (n=7 laminar).*

In line with previous findings, this analysis revealed a predominant frequency of 0.02 ± 0.001 Hz in S1 and 0.017 ± 0.001 Hz in M1, which corresponds to cycle lengths of around 60-s for S1 and 80-s for M1 **(Figure 17.D)**. We confirmed the periodicity of the infra-slow oscillation by computing a Lomb-Scargle Periodogram, which is optimal for handling this type of unevenly distributed data (VanderPlas, 2018). Indeed, this analysis showed peaks indicating cycle lengths of around 60-s in S1 and 80-s in M1 **(Figure 17.D)**. The width of the periodogram peaks span up to ~150-s, suggesting that a high variability exists in the cycle lengths corresponding to the infra-slow oscillation. Notably, no predominant frequency or periodicity was found in the 19 LFP surrogate signals (see Methods. *Surrogate signal generation*). This confirms that the infra-slow oscillation identified in the LFP signals reflect a physiological process rather than variations resulting from chance.

We then examined whether spindles detected with the AR-model in the LFP and EEG signals would exhibit an infra-slow (~0.02 Hz) oscillation. To do this, we calculated the time difference between the onset of consecutive spindle events (i.e. inter-spindle intervals) within uninterrupted NREM episodes in S1, M1 and the frontal EEG. This

analysis confirmed that in S1 LFP spindles occur in bursts, which last on average 14.4 ± 0.2 s (mean ± SEM), and are comprised of one spindle every ~2.38 ± 0.005 s **(Figure 17.A)**. Moreover, it confirms that these spindle bursts exhibit a cycle length of ~50s in the LFP recorded from S1. These analyses also confirmed that spindles in M1 **(Figure 17.B)** and the frontal EEG **(Figure 17.C)**, spindles do not occur in bursts but rather individual or couples of spindles show inter-spindle intervals of around 85.3 ± 0.3 s (M1, mean ± SEM) and 92.4 ± 0.2 s (EEG, mean ± SEM).

To further explore how the dynamics of spindles varied as a functions of their phase within the infra-slow oscillation and their phase within the sleep stage, we detected spindle bursts within NREM episodes of the LFP S1 signals (selecting the LFP channel that showed the highest density of spindles per mouse). Based on our previous results, we considered 'spindle bursts' as trains of at least four consecutive spindles with a maximum inter-spindle interval duration of 10-s. We divided NREM episodes into five equally sized bins and calculated the variability in spindle-burst incidence and duration across NREM episodes **(Figure 18.A)**. First, we found that the incidence of spindles per burst increases progressively across NREM episode bins **(Figure 18.B)** ($F_{4,40}$=26.78, p<0.0001, ***Table 25***). Similarly, the incidence ($F_{4,40}$=21.0, p<0.0001, ***Table 26***) and duration ($F_{4,40}$=4.8, p<0.01, ***Table 26***) of spindle-bursts increase progressively across NREM episode bins **(Figure 18.C,D)**.

3.3.6.2. Dynamics of spindle o-Quality as a function of the infra-slow oscillation

Having confirmed that spindles in S1 and M1 follow an infra-slow oscillation, we proceeded to investigate the relationship between this rhythm and the *o-Quality* of

spindles. To do this, we divided each spindle burst time segment into six equally sized bins **(Figure 18.A)**. We investigated whether the *o-Quality* of spindles increased within spindle bursts, and whether this variability changed as a function of time spent in NREM sleep. Interestingly, we found a significant interaction between spindle-burst bin and time spent in NREM sleep ($F_{5,20}$=2.5, p<0.05, ***Table 27***). Specifically, the *o-Quality* of spindles significantly increased across spindle-burst bins (i.e. within a cycle of the infra-slow oscillation) when the bursts occurred during the first NREM episode bin ($F_{5,20}$=5.2, p<0.01), but not in the last (fifth) ($F_{5,20}$=1.6, p=0.2) or middle (third) ($F_{5,20}$=1.2, p=0.3) NREM episode bin **(Figure 18.E)**. (***Table 27*** contains all contrasts). Finally, to calculate the level of increase in *o-Quality* of spindles per spindle-burst (infra-slow oscillation cycle) across NREM episodes, we subtracted the mean spindle *o-Quality* in the first spindle-burst bin from the mean spindle *o-Quality* in the last (6^{th}) spindle-burst bin and plotted these differential values across NREM episode bins **(Figure 18.F)**. This analysis showed a significant increase in spindle *o-Quality* within spindle-bursts across NREM episodes ($F_{4,28}$=4.4, p<0.001, ***Table 28***).

3.3.6.3. Interim summary

Overall, the results in this chapter suggest that, in agreement with previous studies (Lecci et al., 2017; Lázár et al., 2019), spindles in S1 and M1 follow an infra-slow oscillation. Moreover, these results suggest that in S1 the *o-Quality* of spindles varies within the cycles of the infra-slow oscillation across NREM sleep episodes. As illustrated in **(Figure 18.G)**, the *o-Quality* of spindles is low and constant within infra-slow cycles that occur in the first quarter of NREM episodes, while it increases within the infra-slow cycles that occur in the last quarter of NREM episodes.

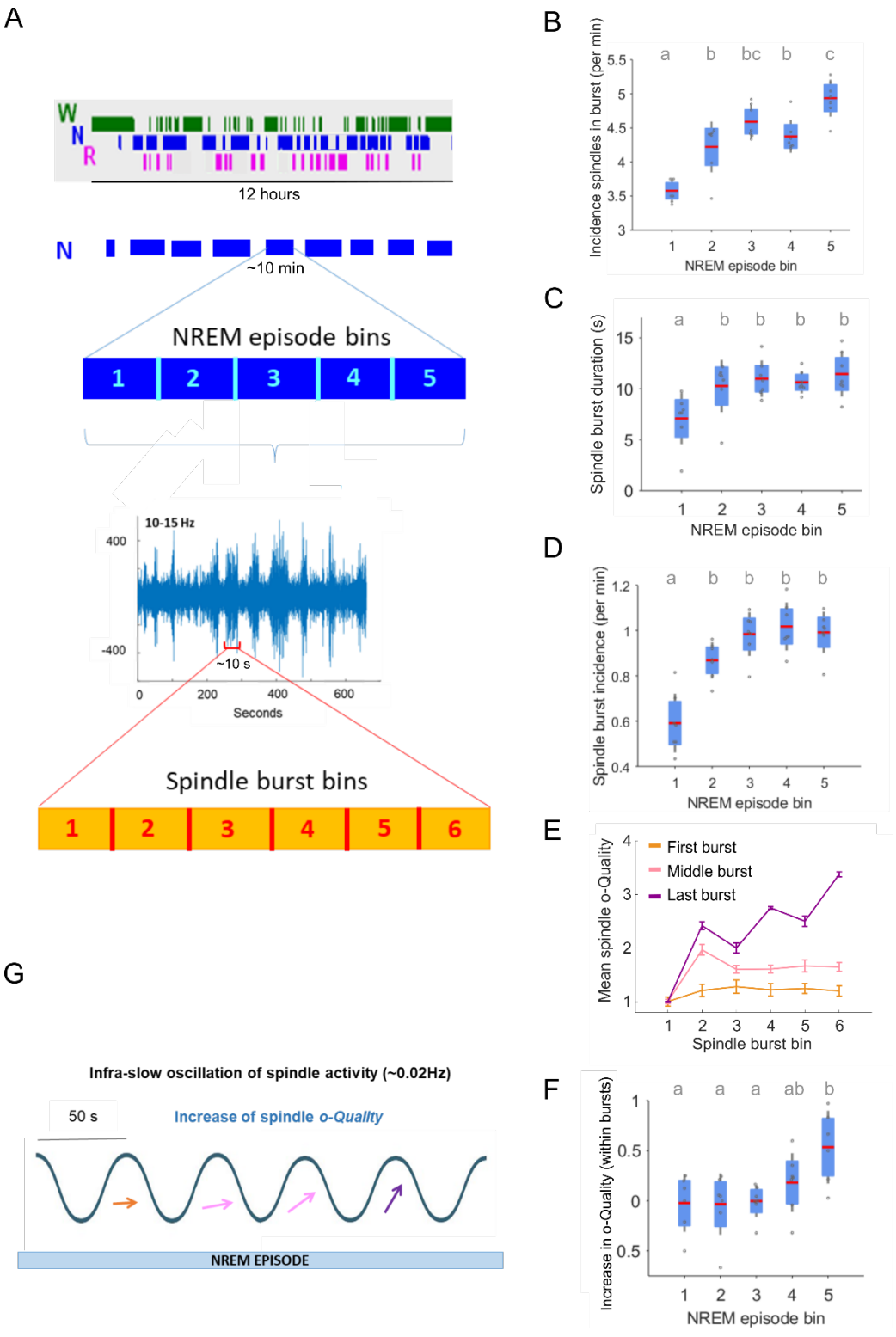


Figure 18. The o-Quality of spindles varies as a function of the infra-slow oscillation in spindle activity. (A) *Diagram illustrating the analysis pipeline. NREM episodes consisted of at least 50 seconds continuous of NREM sleep. Brief awakenings of up to 12-s were not considered as changes of state. These episodes were divided into five equally sized bins for further analysis.*

Additionally, spindle bursts were detected within NREM episodes. These bursts consisted of at least four continuous spindles separated by 10-s maximum. Spindle bursts were divided into six equally sized bins for further analysis. ***(B)*** *Incidence of spindles per spindle burst as a function of NREM episode bin.* ***(C)*** *Mean spindle burst duration and* ***(D)*** *incidence per minute as a function of NREM episode.* ***(E)*** *Mean spindle o-Quality of spindle bursts occurring during the first (yellow), third (light pink), and fifth (magenta) NREM bin.* ***(F)*** *Increase of spindle o-Quality within spindle bursts (i.e. within cycles of the infra-slow oscillation), as a function of NREM episode bin. The level of spindle o-Quality increase within spindle bursts was calculated by subtracting the mean o-Quality during the first spindle-burst bin, from the mean spindle o-Quality during the last (6th) spindle-burst bin.* ***NOTE:*** *Means denoted by a different letter indicate significant differences between treatments. (Box plots: red lines= mean across mice; blue boxes= SEM; grey bars= 95% confidence intervals; dots= individual values for each mouse). *p<0.05, **p<0.001, ***p<0.0001. n= 7 mice implanted with laminar probe in S1.*

3.4. DISCUSSION

3.4.1. Spindles are not all-or-none phenomena but there is high variability in their properties such as oscillatory-Quality

The present results demonstrate that, contrary to the assumption widely used in the field, sleep spindles form a continuum rather than representing all-or-none phenomena. Properties such as their amplitude show lognormal distributions, as has been found for several brain physiological parameters (Buzsáki and Mizuseki, 2014). Based on these distributions, it is not possible to define a single meaningful threshold that separates fully-fledged spindle events from background variations in sigma frequency amplitude. Several studies have previously highlighted that spindles show a substantial variability in terms of density, frequency and amplitude across different

spatiotemporal dimension (Andrillon et al., 2011; Nir et al., 2011; Piantoni et al., 2017; Vyazovskiy et al., 2004). Our results show that this variability is captured in their *o-Quality*, a fundamental property of oscillations that reflects their stability, strength, duration and power.

In spite of this pronounced variability, the detection and characterization of spindles has predominantly relied on single fixed thresholds, which bias the focus towards a subset of events for further careful scrutiny, whilst rejecting the remaining putative events and ignoring their existence. Our results show that this type of binary classification of spindles based on single fixed thresholds is arbitrary and cannot be justified physiologically or mathematically. Most importantly, this constitutes not merely a methodological issue that can be satisfactorily addressed with the advent of more sophisticated approaches for threshold optimisation. It highlights instead the likely possibility that the variability in spindle characteristics has an important meaning beyond what the scrutiny of arbitrarily defined events can provide.

To address this important methodological issue, we propose the novel concept of *oscillatory-Quality (o-Quality)*, which reflects the oscillatory strength of rhythmic oscillations, and is particularly useful for investigating the properties of sleep spindles. Spindles with high oscillatory strength (i.e. weak damping) received a high *o-Quality* score, while spindles with low oscillatory strength (i.e. strong damping) received a high *o-Quality* score. Taking into account the *o-Quality* of spindles opens up a new avenue to understand their spatiotemporal dynamic and physiological relevance.

3.4.2. The Oscillatory-Quality gives an index of the local and global synchrony of the spindle generating network

Overall, our results support the view that spindles are mostly local phenomena (Andrillon et al., 2011; Nir et al., 2011; Piantoni et al., 2017; Fernandez et al., 2018), but global spindles can also occur across large cortical regions (Contreras et al., 1997a; Achermann and Borbély, 1998; Sejnowski and Destexhe, 2000; Steriade, 2003; Bonjean et al., 2011). Spindles with low *o-Quality* are local and transient, while high *o-Quality* spindles are longer and encompass larger cortical regions. This indicates that the *o-Quality* is a direct measure of the local and global synchrony of the spindle-generating network. Additionally, the finding that slow-waves are more likely to precede high *o-Quality* spindles than low *o-Quality* spindles further supports this. It further suggests that, like previously proposed (Contreras and Steriade, 1996; Buzsáki and Draguhn, 2004; Staresina *et al.*, 2015), slow-waves provide spatiotemporal synchrony to spindles across widespread cortical regions. However, it is also possible that the co-occurrence of high amplitude slow waves and high *o-Quality* sleep spindles reflect a synchronised state of cortical networks.

Notably, our results show that the majority (~91.7%) of local LFP spindles remain undetected at the global EEG level. This suggests that studies of spindle dynamics based on "global" EEG recordings only should be viewed with caution as these include only a small proportion of high *o-Quality* and synchronous events, while the majority of local spindles and their dynamics are omitted. At present, it is not feasible to obtain intracranial recordings in humans outside of clinical contexts. Nonetheless, we have

demonstrated here that the *o-Quality* of oscillations like spindles is a direct measure of the synchrony and dynamics of spindles within complex local and global networks.

3.4.3. The Oscillatory-Quality reveals a more complete picture of the topography of spindles

The present study supports previous findings, which suggest that the properties of spindles are strongly influenced by their underlying topography (Finelli et al., 2001; Andrillon et al., 2011; Piantoni et al., 2017; Hagler et al., 2018; Krishnan et al., 2018). Our results further suggest that the *o-Quality* varies substantially between macroscopic regions, being higher in posterior (somatosensory) relative to more anterior (motor) brain regions. Moreover, our results suggest that properties such as their prominence and oscillatory strength and stability (i.e. *o-Quality*) do not only vary between macroscopic regions, but can also show substantial variability within microscopic regions separated by just a few hundred micrometres in the cortex (within and across cortical layers). In line with previous studies (Kandel and Buzséki, 1997; Hagler et al., 2018), we found that the incidence and *o-Quality* of spindles is higher in layers 3 and 4 of the somatosensory cortex. Additionally, we demonstrate that the laminar profile of spindles varies across macroscopic areas of the cortex. This is consistent with previous findings showing that the density of thalamo-cortical projections to different layers varies across cortical areas (Hunnicutt et al., 2014). For instance, in the motor cortex, where thalamo-cortical projections form the majority of synapses in layer 5, spindles showed highest incidence and *o-Quality* in layers 4 and 5a.

At this point, it is highly relevant to highlight that taking into account the *o-Quality* of spindles is crucial for having a complete understanding of their topography and network dynamics. Given the substantial variability that spindles show in terms of their *o-Quality* and amplitude across different macroscopic, mesoscopic and microscopic areas, basing their detection on a single fixed threshold will inevitably bias the picture we acquire of their topography. Moving forward, it will be important for future analyses, which are focused on understanding the network dynamics of spindles, to take into consideration the variability that these oscillations possess in terms of *o-Quality,* and explore spindle properties (i.e. density, duration, frequency) in the light of such variability.

3.4.4. The o-Quality of spindles is directly related to the occurrence of slow waves and is sensitive to the levels of homeostatic sleep need

Overall, taking into account the variability of spindles, in terms of their *o-Quality,* allowed us to have a more complete understanding of their interactions with the slow-wave activity. High *o-Quality* spindles (which show increased oscillatory strength, power, and reflect a synchronised state of the oscillatory network) are more likely to be preceded by slow waves than low *o-Quality* spindles. This effect is present both at local (LFP) and global (EEG) levels, however EEG spindles and local spindles in areas like M1 are not likely to reach very high *o-Quality* as is the case for S1. Taken together, these results support the findings suggesting that slow waves provide spatiotemporal synchrony to spindles (Contreras and Steriade, 1996; Buzsáki and Draguhn, 2004; Staresina et al., 2015; Niethard et al., 2018). The increase in slow-wave activity and

spindle *o-Quality* after sleep deprivation also support the idea that sleep need reinforces the recruitment of large neuronal populations (Vyazovskiy et al., 2009b). Moreover, our results further demonstrate that the *o-Quality* of spindles is a metric of synchrony within cortical networks and is sensitive to the levels of homeostatic sleep need.

Our results also showed that the *o-Quality* of spindles consistently showed a positive relationship with slow-waves activity, across different contexts where the levels of slow-wave activity (i.e. sleep pressure) substantially varied. In some contexts (specifically after sleep deprivation and towards the end of NREM episodes), we also found that the incidence of spindles showed a positive association with slow-wave activity. Previous studies have found an inverted-U shaped relationship between slow-wave and spindle activity within NREM episodes (AESCHBACH and BORBÉLY, 1993; Himanen et al., 2002; Alfonsi et al., 2019). Other studies have also shown that while slow-wave activity shows a progressive decrease across the light period (12-h), sigma power shows an opposite trend (Trachsel et al., 1988; Vyazovskiy et al., 2004a). Moreover, it has also been found that the density of spindles in the EEG decreases during the first hours of sleep recovery after sleep deprivation (Dijk et al., 1993; Knoblauch et al., 2003; Vyazovskiy et al., 2004).

The divergence between previous studies and the present results could reflect differences between different species and recording measures. However, a possible explanation for this divergence is that, these previous studies made use of spectral-based methods, which are not optimal for distinguishing between neuronal oscillation and stochastic variability in the EEG background. As a result, overall increases in power

density that affect the sigma-band activity (as we found in the EEG signal during the first two hours after sleep deprivation), could lead to the detection of false positive putative spindles. The AR-model we used to detect spindles (Achermann & Olbrich, 2004; Olbrich & Achermann, 2005) addresses this shortcoming, and is therefore more likely to discriminate between the stochastic EEG (or LFP) background and genuine spindle oscillations.

3.4.5. The quality of spindles varies as a function of the infra-slow oscillation

Our results support previous findings indicating that both sigma activity and spindles follow an infra-slow oscillation, which is predominant in posterior areas of the brain (Achermann and Borbély, 1997; Lecci et al., 2017; Lázár et al., 2019). Our results showed, however, that the cycles of this oscillatory activity are not strictly periodic, but rather show a substantial variability in their length. More research is needed to better understand how the infra-slow oscillation varies across different time-scales (i.e. within hours and days). Our results also show that the number of spindles per cycle increases progressively within NREM episodes. This result is consistent with previous findings showing that the incidence of spindles increases within NREM episodes and is prominent prior to NREM to REM transitions (Gottesmann, 1996; Vyazovskiy et al., 2004a).

Moreover, our results suggest that (at least in the somatosensory cortex) the *o-Quality* of spindles varies within the cycles of the infra-slow oscillation, showing marked increase only within cycles that occur towards the end of NREM episodes. The infra-slow oscillation has been proposed to divide NREM sleep into phases of high and low

susceptibility to sensory stimulation and memory processing (Lecci et al., 2017), and it is possible that the *o-Quality* of spindles could play a role in this process. On the other hand, the infra-slow oscillation has been reported to occur in neuronal firings rate across different cortical and subcortical areas (Lüthi and McCormick, 1998), in the gamma activity (Nir et al., 2008), and in the hippocampal ripple activity (Lecci et al., 2017). It has also been reported in the BOLD brain response (Picchioni et al., 2011) and, during sleep, the heart rate seems to fluctuate following this rhythm as well. It is possible, therefore, that the *o-Quality* variability that spindles show within the infra-slow cycles is related to a widespread system process.



CHAPTER 4 – Investigating spindle-related deficits in GRIA1$^{-/-}$ mice, a mouse model relevant for schizophrenia

4.1. INTRODUCTION

Schizophrenia is a neurodevelopmental disorder characterised by a complex array of positive (i.e. hallucinations, delusions, and motor hyperactivity), negative (i.e. anhedonia and impaired goal-directed behaviour), and cognitive symptoms (i.e. executive dysfunction). Sleep disturbance is often experienced by patients with schizophrenia (Hudson et al., 1993; Wulff et al., 2010), and is associated with poorer prognosis and diminished quality of life (Hofstetter et al., 2005). Polysomnography studies have reported abnormalities in the sleep architecture of patients with schizophrenia. Overall, these have reported decreased total sleep time, decreased NREM sleep, increased sleep latency, and increased REM sleep density (Benca et al., 1992; Yang and Winkelman, 2006; Göder et al., 2015).

The aforementioned results, however, have been highly inconsistent and previous

meta-analyses have failed to identify a consistent significant difference in any specific sleep architecture parameter between patients with schizophrenia and control groups (Benca et al., 1992). Additionally, the sleep profile in patients can also be affected by their history of medication (Cohrs, 2008), however several studies do not differentiate between drug-naive unmedicated and medicated patients. Recently, increasing efforts have been made to go beyond sleep architecture and investigate spectral properties of sleep in this clinical population, including prominent EEG oscillations like sleep spindles.

In this line of research, mounting evidence suggests that EEG sleep spindles (10-16 Hz) are significantly reduced in patients with schizophrenia relative to healthy control subjects (Ferrarelli *et al.*, 2007; Manoach and Stickgold, 2019). Based on EEG recordings, different studies have found that patients with schizophrenia show a reduction in different spindle parameters such as density, duration and amplitude (Ferrarelli, 2007; Ferrarelli and Tononi, 2016). These deficits have been associated with both slow (11-14 Hz) and fast (14 -16 Hz) spindles, and do not seem to be related to the medication status of patients (Ferrarelli et al., 2010).

These deficits in EEG spindles have been found to be associated with the positive symptoms presented by patients with schizophrenia. Specifically, an inverse correlation has been found between spindle density and the severity of psychosis (i.e. hallucinations and delusions) (Ferrarelli et al., 2010; Wamsley et al., 2012; Tesler et al., 2015). Additionally, reduced spindle density correlates with scores of psychotic symptom proneness in first degree healthy relatives of patients with schizophrenia (Lustenberger et al., 2015; D'Agostino et al., 2018). As a result, deficits in EEG sleep

spindles have been proposed to be a potential biomarker or endo-phenotype for schizophrenia (D'Agostino et al., 2018; Manoach and Stickgold, 2019). The problem, however, is that evidence of spindle deficits in patients with schizophrenia is based mainly on correlational rather than causational studies, and does not seem to be specific to this disease. Deficits in spindles have also been reported in patients with Williams syndrome, Alzheimer's disease, and children with developmental disorders (Bódizs et al., 2012; Gorgoni et al., 2016; Farmer et al., 2018)..

Additionally, spindles are believed to play a crucial role in the consolidation of memory during sleep (Stickgold, 2005; Rasch and Born, 2013). Consequently, increasing efforts have been made to investigate the association between spindle and memory deficits in patients with schizophrenia (Demanuele et al., 2017; Manoach and Stickgold, 2019). Different studies have reported that deficits in spindles correlate with impairments in tests assessing declarative (Göder et al., 2015) and procedural memory (Wamsley et al., 2012) in patients with schizophrenia. Several studies, however, have failed to find these correlations (Manoach et al., 2010; Genzel et al., 2015). Moreover, the evidence supporting a role of spindles in memory consolidation is based on correlational studies and direct causational proof is still lacking.

A few studies have attempted to establish a direct non-correlative association between spindles and memory consolidation. Specifically, enhancing spindle-like activity through optogenetic stimulation of the reticular nucleus of the thalamus (Latchoumane et al., 2017) or auditory stimulation presented at the spindle frequency range (Antony et al., 2018), has been found to improve hippocampal-related memory consolidation in humans and rodents. This effect is reported to happen only when putative spindles are

phase-locked with the up-state of cortical slow-waves (0.5-4 Hz) (Antony et al., 2018) and with hippocampal sharp-wave ripples (150-250 Hz) (Latchoumane et al., 2017). However, a limitation of these studies is that, although they report inducing 'spindle-like activity' with their stimulation protocols, they do not verify that the characteristics of the induced oscillations are representative of natural spindles and, for instance, they report 8 Hz oscillations as spindle events. Additionally, other studies have failed to replicate these results (Ngo et al., 2019).

In spite of these limitations, a common assumption in the field is that the coupling between slow-waves, spindles, and sharp-wave ripples facilitates a hippocampal-cortical dialogue during sleep, which leads to the transfer of information from temporary storage in the hippocampus to long-term storage in distributed cortical regions (Wilson and McNaughton, 1994; Rasch and Born, 2013; Staresina et al., 2015). Conclusions like these have led researchers to attempt to improve memory performance and overall cognition in schizophrenia by manipulating sleep spindles (i.e. using transcranial stimulation or GABAa agonists) (Wamsley et al., 2013; Göder et al., 2015; Mylonas et al., 2020). The majority of these attempts, however, have failed to improve cognitive performance in patients or healthy control subjects. These negative results highlight the need for a better understanding of the role of spindles in the normal healthy brain and the mechanisms underlying spindle dysfunction in schizophrenia. Additionally, these negative results highlight that caution is required when interpreting the cognitive and behavioural effects of such dysfunction.

A useful tool for gaining insight into the biological underpinnings of sleep deficits in schizophrenia is the study of mice with genetic modifications relevant for this disorder.

Mice lacking the GluA1 subunit of the glutamate AMPA receptor (GRIA1$^{-/-}$ mice) constitute one of these genetic lines. Several lines of evidence suggest that the glutamatergic and dopaminergic systems play a crucial role in neuropsychiatric disorders like schizophrenia (Coyle, 2006; Stone et al., 2007). Although an emphasis has been placed on dopamine and NMDA glutamate receptors, recent genome wide association studies (GWAS) have linked the GRIA1 gene with schizophrenia (Kirov et al., 2012; Lips et al., 2012; Ripke et al., 2014)

The GRIA1 gene encodes the GluA1 subunit of the glutamate AMPA receptor (McNamara et al., 1992). AMPA receptors are ion channels composed of four subunits, namely GluA1-4 (Shepherd and Huganir, 2007). The dynamics of AMPA receptors within the postsynaptic membrane have been found to play a crucial role in long and short-term plasticity processes (Malinow and Malenka, 2002), and the GluA1 subunit has been found to be a primary mechanism for synaptic plasticity (Diering et al., 2014). Mice lacking the GluA1 AMPA receptor subunit seem to show deficits in long-term potentiation (Zamanillo et al., 1999; Hoffman et al., 2002). However, different studies have also shown that long-term potentiation can be preserved in the absence of GluA1 (Romberg et al., 2009; Granger et al., 2013).

Deficits in synaptic plasticity are thought to be of crucial importance in schizophrenia (Crabtree and Gogos, 2014), which is highly relevant since risk genes for schizophrenia, like GRIA1 (Barkus *et al.*, 2014; Ripke *et al.*, 2014), encode synaptic proteins that are important mechanisms for synaptic plasticity. Additionally, post-mortem studies have shown that the expression of GluA1 (Kerwin et al., 1990; Eastwood et al., 1997) and GluA1 mRNA (Harrison et al., 1991; Eastwood et al., 1995; Sokolov, 1998) are markedly

reduced in the brains of patients with schizophrenia. Notably, these results do not appear to be secondary to antipsychotic medication (Harrison et al., 1991; Eastwood et al., 1997). This further suggests an important role of GluA1 in this disease.

Of notable importance, GRIA1$^{-/-}$ mice also show striatal hyper-dopaminergia and a behavioural phenotype relevant for the positive, negative, and cognitive symptoms of schizophrenia (Wiedholz et al., 2008; Barkus et al., 2012, 2014). Modelling aspects of the positive symptoms, these mice show novelty-induced locomotor hyperactivity, deficits in pre-pulse inhibition, and increased impulsive choice (Bannerman et al., 2004; Wiedholz et al., 2008; Barkus et al., 2012). Regarding negative symptoms, these mice show reduced social interaction in novel environments and, although they can exhibit goal-directed behaviour, they tend to transition to habitual responses faster than wild-type mice (Johnson et al., 2005). GRIA1$^{-/-}$ mice also show a cognitive profile that includes deficits in short-term habituation (Sanderson et al., 2010), which manifests in secondary deficits on working memory (Bannerman et al., 2003) and increased sensitization to recently presented stimuli (Sanderson et al., 2011; Barkus et al., 2014). Interestingly, despite showing working memory deficits, their spatial reference memory performance is intact (Bannerman et al., 2003, 2014; Schmitt et al., 2003), and long-term memory can be even enhanced relative to wild-type mice (Sanderson et al., 2009).

Notably, a recent study showed that GRIA1$^{-/-}$ mice show sleep and EEG spindle deficits that closely resemble the EEG deficits presented by patients with schizophrenia (Ang et al., 2018). Specifically, GRIA1$^{-/-}$ mice show a marked reduction in EEG spindles (10-15 Hz) relative to control littermates. Additionally, GRIA1$^{-/-}$ mice show longer REM

episodes and a reduced rate of decline of slow-wave activity during sleep recovery after 6-hours of sleep deprivation. These parameters are also affected in some psychiatric disorders (Gottesmann and Gottesman, 2007) and support previous evidence suggesting that GluA1 is implicated in the homeostatic regulation of sleep (Vyazovskiy et al., 2008). Given the link that is thought to exist between spindles and memory, it is interesting that despite showing a substantial reduction in EEG spindle incidence, the performance of GRIA1$^{-/-}$ mice in long-term memory tasks is preserved or even enhanced (Zamanillo et al., 1999; Reisel et al., 2002; Schmitt et al., 2003; Sanderson et al., 2009; Bannerman et al., 2014).

In the previous chapter, we presented evidence that the majority of sleep spindles are local and remain undetected by surface EEG recordings. This raises the question of whether local spindles are also affected in GRIA1$^{-/-}$ mice. Additionally, in the previous chapter we demonstrated that the spatiotemporal dynamics of spindles beyond the EEG level is quite complex. Therefore, we introduced the concept of *oscillatory-Quality (o-Quality),* which reflects the level of synchrony within cortical networks, and demonstrated that taking into account this parameter, as well as the interaction between spindles and other sleep-related oscillations like slow-waves, allows us to obtain a more thorough understanding of the network spindle dynamics. We, therefore, proceeded to investigate the effect of knocking-out GRIA1 in mice on local and global spindle dynamics, their *o-Quality*, their coupling with slow-waves (0.5-4 Hz), and the resulting network dynamics.

4.2. METHODS

4.2.1. Animals

Experiments were performed on adult male GRIA1$^{-/-}$ and littermate WT mice, aged 18-22 weeks old, and bred at the Biomedical Sciences Building, University of Oxford. These mice were generated as previously described (Zamanillo et al., 1999) and maintained on a C57BL/6J x CBA/J background. Specifically, heterozygote parents were bred, resulting in ~25% GRIA1$^{-/-}$ mice that lacked both copies of the GluA1 allele, ~25% WT mice that had both copies of this allele, and ~50% heterozygote mice that were not used here. At the end of all experiments, the genotype of mice was confirmed by genotyping. This was carried out by TransnetYX, US using ear notch samples and PCR-mediated amplification methods.

Specifically, fourteen mice (GRIA1$^{-/-}$ n=7; WT littermates n=7) underwent electrophysiological recordings. Another fourteen mice (GRIA1$^{-/-}$ n=7; WT littermates n=7), four of which had been used for electrophysiological recordings (GRIA1$^{-/-}$ n=2; WT$^{-/-}$ n=2), underwent a spatial reference memory task. Finally, a separate cohort of fourteen un-implanted mice (GRIA1$^{-/-}$ n=7; WT littermates n=7) underwent a recognition memory-task.

Experimental procedures were performed in accordance with the Animal (Scientific Procedures) Act 1986 under a UK Home Office Project Licence and were in accordance with institutional guidelines.

4.2.2. Surgical Procedure

Surgical procedures were performed under isoflurane anaesthesia. All mice were implanted: 1) epidural screws to record EEG signals, 2) intra-cortical probes to record LFP and MUA signals, and 3) tungsten wires in the nuchal muscle to record the EMG. See Chapter 2 - *Surgical Procedure*, for details on the EEG and EMG implants. Mice were implanted with a polymide-insulated tungsten microwire array (Tucker-Davis Technologies Inc (TDT), USA) into deep layers (target: layer V-IV) of the primary somatosensory cortex (S1). The recording area was chosen based on the results we obtained in Chapter 3, and previous studies that have identified well-defined spindles in the mouse S1 area (Kim et al., 2015; Fernandez et al., 2018). The array consisted of 16-channels with properties as follows: two rows of eight wires, wire diameter 33µm, electrode spacing 250µm, row separation L-R: 375µm and tip angle 45 degrees. Arrays were customised so the left row was 250µm longer. A craniotomy of approximately 1x2mm was made and the midpoint of the craniotomy was located relative to bregma: -1mm anteroposterior (AP) and −3.25mm mediolateral (ML).

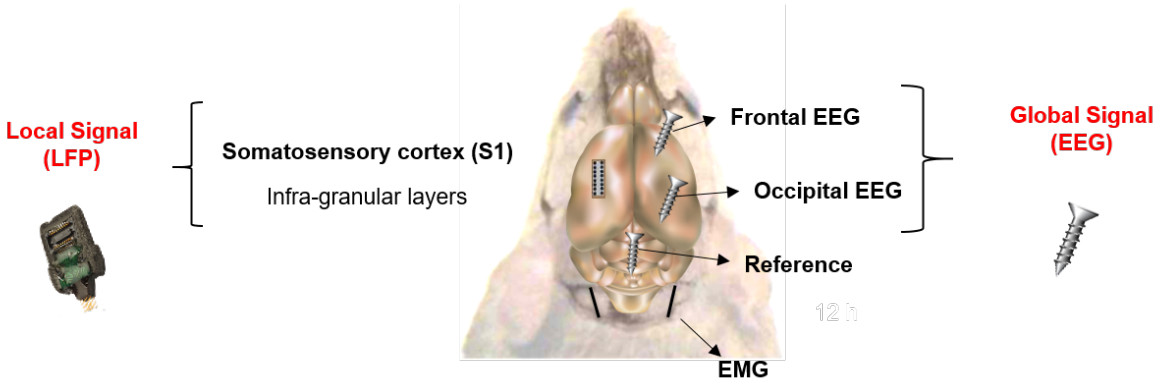


Figure 17. Schematic of implantation sites. *EEG screws were implanted epidurally over frontal and occipital regions. A reference screw was implanted over the cerebellum. EMG was recorded*

from the two stainless steel wires inserted on both sides of the nuchal muscle. LFP and MUA were recorded from micro-wire arrays implanted into infra-granular cortical layers of S1.

A schematic of implantation locations is shown in **Figure 17**. Mice were given a minimum two weeks to recover and were habituated to the recording cage and cables for a minimum of four days prior to recording.

4.2.3. Histological verification of recording sites

For details on the histological verification of recording sites, see Chapter 2 – *Histological verification of recording sites*. In brief, after completing all recordings, mice were deeply anesthetised, electrolytic micro-lesions were performed (10μm, 20s) (NanoZ, Neuralynx), and mice perfused (0.9% saline, 4% paraformaldehyde). Brains were sliced to obtain 50μm coronal slices, using a Vibratome (Leica VT1000 S, Germany). The brain slices were stained with DAPI, mounted on slides, and imaged with a fluorescence microscope (Olympus Bx51, Japan), using 1.6, 2.5, and 5x magnifications. The electrode locations were mapped using the Dil stain and microlesion traces, and the actual rostro-caudal and medio-lateral recording coordinates were identified using the Allen mouse brain atlas (Lein et al., 2007), as shown in **Figure 18**.

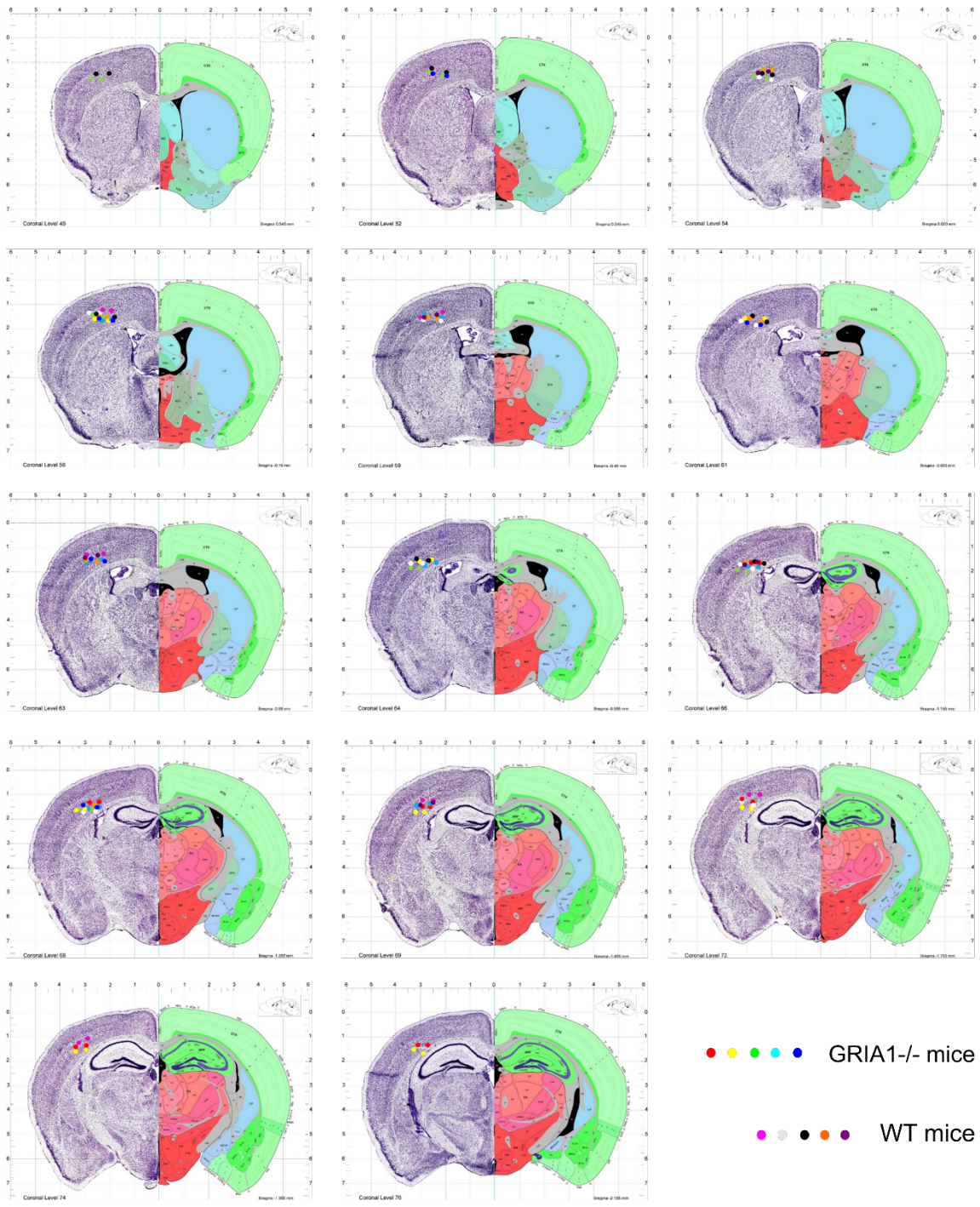


Figure 18. Location of recording electrodes. *Sixteen channel micro-wire arrays were implanted into infra-granular layers (layers 5 and 6) of the primary somatosensory cortex to record LFP and MUA signals. The circles indicate the locations of individual microwires (i.e. electrodes), with the different colours representing their location in each mouse. The electrode locations were mapped using the Dil stain and microlesion traces, and the actual rostro-caudal and medio-lateral recording coordinates were identified using the Allen mouse brain atlas (Allen, 2007).*

4.2.4. Behavioural tasks

The potential role of spindles in memory processing during sleep is a topic of intensive debate. While it is widely believed that spindles support the consolidation of hippocampal-based memories during sleep (Wilson and McNaughton, 1994; Ngo *et al.*, 2013; Rasch and Born, 2013; Staresina *et al.*, 2015a; Latchoumane *et al.*, 2017), several studies do not support this view (Ang et al., 2018; Henin et al., 2019; Ngo et al., 2019). Interestingly, GRIA1$^{-/-}$ mice have been found to show EEG spindle deficits, but their long-term memory has been found to be preserved (Bannerman et al., 2003, 2014; Schmitt et al., 2003). To investigate whether spindles are indeed necessary for hippocampal-based learning, we proceeded to assess the performance of GRIA1$^{-/-}$ mice in two behavioural tasks that depend on the hippocampus activity.

4.2.4.1. Reference memory task

Spatial long-term reference memory was assessed in GRIA1$^{-/-}$ (n=7) and WT (n=7) mice using a four arm plus-shaped maze (**Figure 19**). This task assesses the capacity of mice to learn the spatial location of a fixed positioned reward, despite their start-arm location, a process dependent on hippocampal activity (O'Keefe and Nadel, 1979; Buzsáki and Moser, 2013). In fact, this specific task has been previously found to depend on hippocampal activity, and be impaired after hippocampal lesions (Bannerman et al., 2003).

Each arm of the plus-shaped maze measured 60 cm in length and 10 cm in width. The walls of the maze were grey and 10 cm in height. Metal food wells were located at the

end of two arms of the maze, which were considered the goal arms (east and west arms). The other two arms (north and south) were considered starting arms. Prior to the onset of training, mice were food restricted to limit their weight to 85% - 90% of their normal weight.

The experiment was composed of four phases: *handling, habituation, training* and *test*. First, during the *handling* phase, mice were handled by the experimenter for two minutes, once a day for five days. Subsequently, during the *habituation* phase, mice were habituated to the reward (condensed milk) in their home-cage first and subsequently in the maze. Mice were also habituated to the plus-shaped maze for six days (two five-minute sessions per day). Initially, mice were exposed to the maze in groups (i.e. together with their littermates) and subsequently habituation was performed individually.

During the *training* phase, mice were trained for six days to learn the location of a fixed-positioned reward (placed in either the east or west goal arms of the plus-shaped maze) regardless of their start arm location. The start arm would be either the north or south arm, and the opposite arm (south or north) was blocked so mice could only choose between east and west arms on every trial. The allocation of the rewarded arm was counterbalanced across mice for both genotypes. Each training session was composed of 20 trials, with an inter-trial interval of 60s. The maze was rotated 180% every other day to prevent association of the reward with subtle intra-maze cues. Training was performed at noon (Zeitgeber time from light onset: 3h).

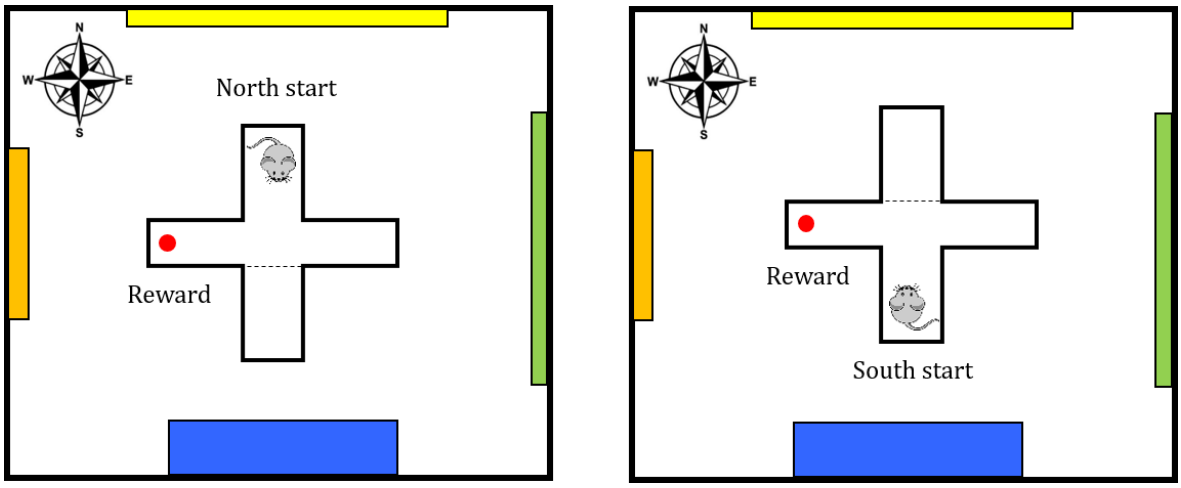


Figure 19. Schematic of the reference-memory task. *Mice were trained to learn the location of a fixed-positioned reward regardless of their start arm location in the plus-maze. The two panels represent two different trials during a training session where mice would start from the north or south arm of the plus-maze. Note that in the training room (outer black square) fixed landmarks (represented here as coloured boxes) were present and were kept constant across trials and training days. The dashed line inside the maze represents the blockade of the arm opposite the start arm (start arm can be either the north or south arm).*

Finally, the *test* session was performed 24 hr after the sixth day of training. The same procedure was followed as during the training day, however, mice were given the reward only after they had ran into the correct goal arm, in order to confirm that mice were not solving the task merely based on olfactory cues associated with the milk reward itself (i.e. they were not smelling the reward). Overall, performance was calculated based on the percent of correct choices (choices of the correct rewarded goal arm selected for each mouse). Note that continuous 24h electrophysiological recordings were performed in six mice (GRIA1$^{-/-}$ n=3) prior to training in this task, while the other eight mice (GRIA1$^{-/-}$ n=4) only performed the behavioural task.

4.2.4.2. Object displacement task

The object displacement task (Vogel-Ciernia and Wood, 2014) was used to assess spatial memory in GRIA1$^{-/-}$ mice (n=7) and littermate controls (n=7). Overall, this task measures spatial memory by assessing the natural, spontaneous preference of mice to explore a familiar object displaced in space over another familiar object that remains in its original location. Previous studies have shown that hippocampal lesions, and hippocampal inactivation impair the performance of mice in this task (Broadbent et al., 2004; Oliveira et al., 2010). Testing chambers consisted of a white square open field (23 x 23 x 23 cm). Light was adjusted so it would reach ~47 LUX at the bottom of the testing chambers. Polarising cues were placed respectively on the north, east and west walls of the chamber to serve as spatial landmarks. The experiment consisted of four stages: *handling, habituation, exposure*, and *test*. Sessions for each stage were performed at around noon (Zeitgeber time from light onset: 3h).

First, mice were *handled* by the experimenter for two minutes, once a day for five days. Second, mice were allowed to *habituate* to the testing chamber for three minutes in the absence of any objects. Habituation was repeated once daily for six days. The third step was the *exposure* session. Two identical objects were placed over predefined marks inside the testing chamber. Each mouse was placed inside the chambers as far away from the objects as possible. Mice were allowed to explore the chamber and objects for ~10 minutes. GRIA1$^{-/-}$ mice are known to show novelty induced locomotor hyperactivity and increased exploratory activity towards cues of all types (Bannerman et al., 2004; Wiedholz et al., 2008), which could provide more opportunity to learn about the spatial location of the cues (Barkus *et al.*, 2014). To control for this, the time that GRIA1$^{-/-}$ mice spent exploring the objects during this exposure phase was yoked to

that of WT mice. This ensured that both groups were matched in terms of object exposure time.

Finally, 24 hours after the exposure session, a test session was performed. This allows us to asses long-term memory in mice (Vogel-Ciernia and Wood, 2014). The same two identical objects were placed inside the chamber but this time one of these objects was displaced to a novel location, while the other one was left in the familiar location. The specific object that was displaced to a novel location was counter-balanced across mice. Mice were placed inside the chamber as far away from the objects as possible, and were allowed to explore the objects for 5 minutes (**Figure 20**).

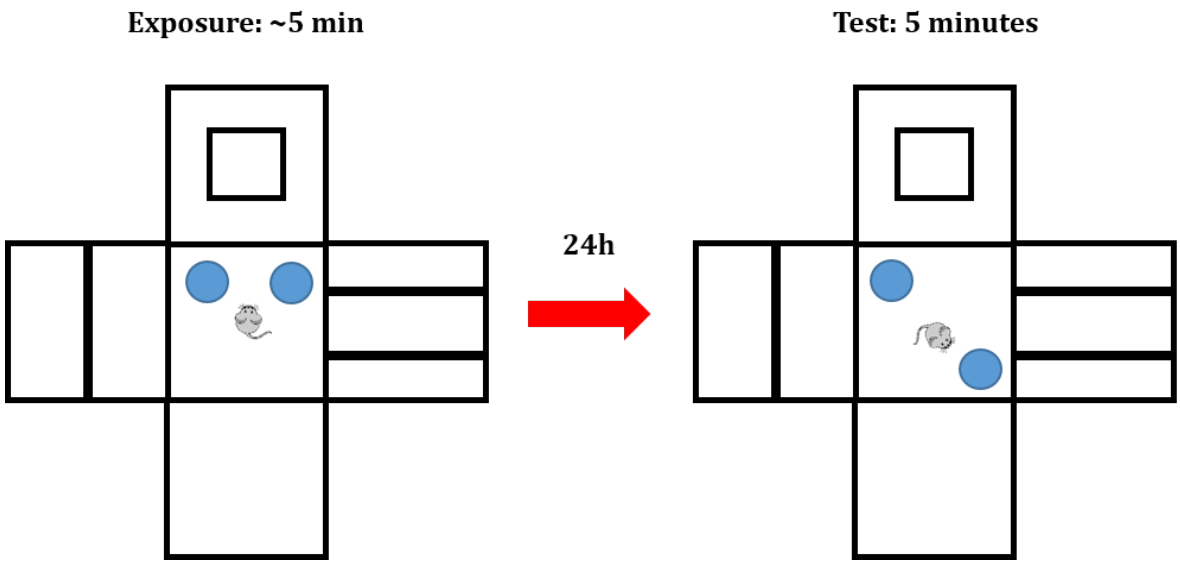


Figure 20. Schematic of the object displacement task *showing an example of the exposure and testing sessions. Note that the walls of the testing chamber had landmarks that were kept constant across sessions.*

Videos were recorded during the habituation, exposure and test phases, and automated tracking was subsequently performed with the ANY-maze software (version 4.5;

Stoelting, Wood Dale, IL). Data analysis was performed off-line using a custom-made MATLAB code. The object exploration times for displaced and non-displaced objects during the test session were compared between genotypes. Exploration was set in ANY-maze as interaction between the mouse and the object, where the mouse's nose is pointed directly at the object, and located within a 1cm distance of the object. A discrimination index was calculated as follows: (Time exploring novel object – Time exploring the familiar object) / (Time exploring novel + familiar) * 100.

4.2.5. Spindle detection

Oscillatory events were detected with an algorithm developed by Olbrich and Achermann (2005), and adapted by us to detect spindle events with varying damping. This algorithm treats electrophysiological brain signals as a superposition of stochastically-driven harmonic oscillators with damping and frequency varying in time. Briefly, an autoregressive model of order 8 was fitted to overlapping (shifted by 1 sample interval) 1-s segments of LFP and EEG signal. Oscillatory events were detected whenever the damping at one or more frequencies exceeded one of five r_b thresholds (r_b = 0.92, 0.93, 0.94, 0.95, 0.96). Detected oscillatory events that had a frequency of around 10 to 15 Hz were selected as 'putative spindles'. This algorithm is explained in detail in Chapter 3 (Methods, section *3.2.7. Spindle detection*).

As explained in Chapter 3, we used the damping strength of detected spindle events, as a measure of their *Oscillatory-Quality* (*o-Quality*). Specifically, we classified all the spindles detected in the LFP and EEG signals into one of five *o-Quality* levels (i.e. oQ1

oQ2, oQ3, oQ4, oQ5), based on the highest r_b threshold they reached (i.e. based on their oscillatory strength). Spindles with low oscillatory strength received a low *o-Quality* index, while spindles with high oscillatory strength received a high *o-Quality* index (section 3.3.2. in Chapter 3 gives a detailed explanation of the *oQuality* index).

4.3. RESULTS

In order to investigate the dynamics of spindles at a global and local level, we performed in-vivo chronic EEG, LFP, MUA and EMG recordings during spontaneous sleep in GRIA1$^{-/-}$ (n=7) and WT (n=7) mice (**Figure 21.A**). Intra-cortical LFP and MUA signals were recorded from infra-granular layers of S1 (**Figure 21.C**). Both genotypes showed expected electrophysiological signatures of waking, NREM sleep and REM sleep (**Figure 21.B**). The overall sleep architecture was similar between genotypes although, as previously reported, GRIA1$^{-/-}$ mice show longer latency from light onset until the first consolidated period of NREM sleep (Ang et al., 2018). Additionally, in both genotypes, waking and REM sleep were characterised by the usual low voltage, high frequency oscillations, while NREM sleep was characterised by high voltage slow-waves (0.5-4Hz) (**Figure 21.D**).

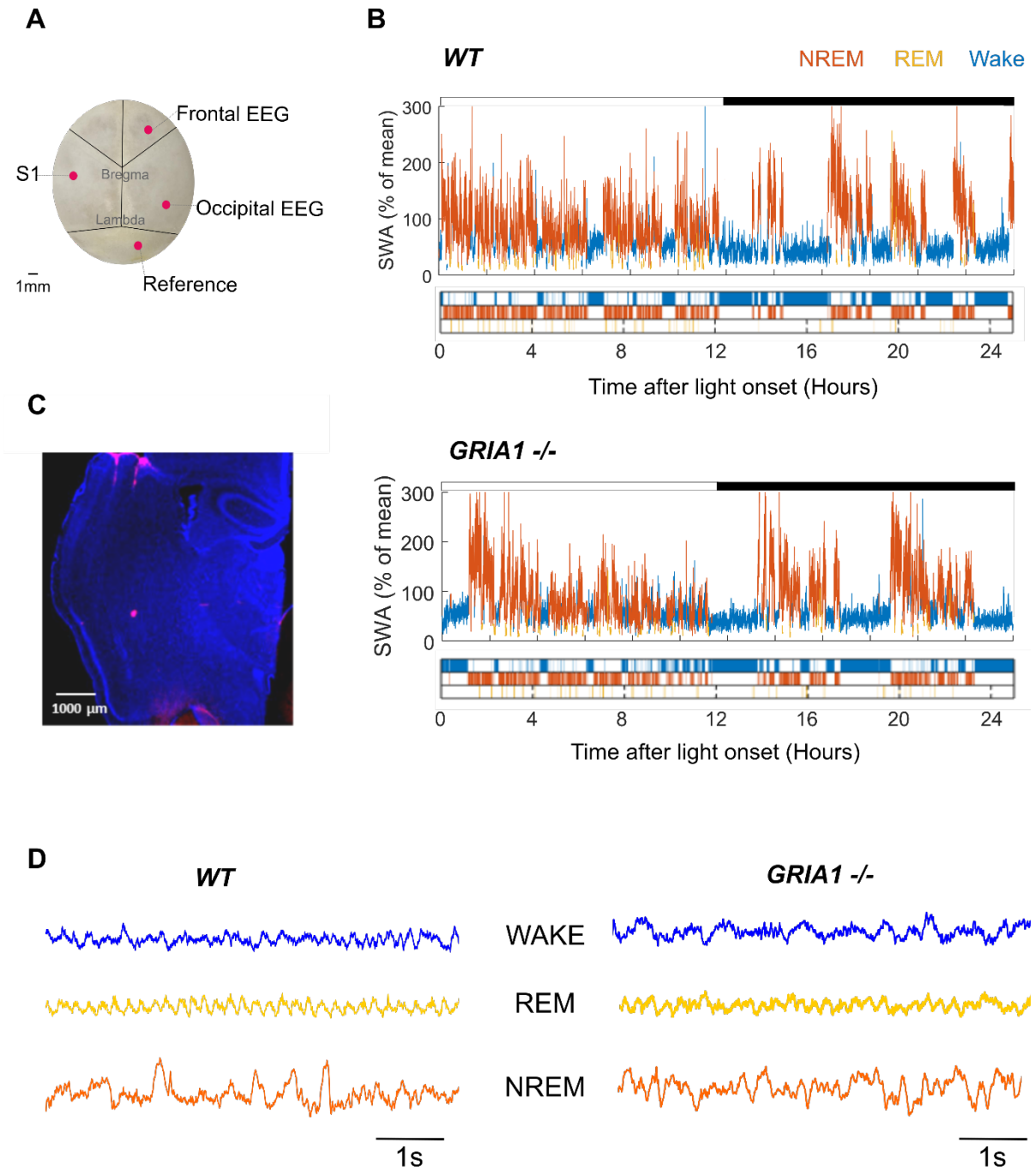


Figure 21. Recording sites and cortical activity during wake and sleep in GRIA1$^{-/-}$ and WT mice. ***(A)*** *Locations where the EEG screws (frontal, occipital, and cerebellar reference) and microwire arrays (S1 infra-granular layer) were implanted.* ***(B)*** *Representative spectrogram and respective hypnogram for one WT mouse (top) and one GRIA1$^{-/-}$ mouse (bottom) during an undisturbed 24h period (12h light/12h dark cycle represented by the white/black frame on top).* ***(C)*** *The location of the electrodes across or within S1 cortical layers was verified with histological evidence of electrolytic microlesions and Dil stain electrode traces (magenta) on brain slices stained with DAPI (blue).* ***(D)*** *A 5-s representative example for frontal EEG recordings in one WT*

mouse (left) and one GRIA1$^{-/-}$ mouse (right) during wake, REM (high theta activity 6-9 Hz), and NREM (0.5 – 4 Hz).

4.3.1. GRIA1$^{-/-}$ mice show a profound reduction in EEG spindle activity

In a previous study, we reported that EEG spindles are absent in GRIA1$^{-/-}$ mice (Ang et al., 2018). In line with this previous study, spectral analysis of the frontal EEG signal during NREM sleep revealed a significant reduction in the frequency above 10 Hz in GRIA1$^{-/-}$ relative to WT mice ($F_{80,960}$= 8.97, p<0.0001; p<0.05 for frequencies 11.5 to 19.5, ***Table 29***) (**Figure 22.A**). Spectral-based analyses, are not optimal for discriminating between stochastic background and oscillations like spindles in electrophysiological signals (Wen and Liu, 2016). As a result, apparent reductions in the spindle frequency range (10-15 Hz) in GRIA1$^{-/-}$ mice could represent overall lower EEG power in high frequencies (including 10-15 Hz). To confirm that this was not the case, we investigated the occurrence of spindle events detected with an AR-model (Achermann and Olbrich, 2004; Olbrich and Achermann, 2005).

Additionally, previous evidence suggesting an absence of EEG spindles in GRIA1$^{-/-}$ mice (Ang et al., 2018), is based on a spindle detection approach which makes use of a single amplitude-based threshold. As we demonstrated in Chapter 3, spindles are not all-or-none phenomena but rather show a substantial variability in their *o-Quality* (i.e. their oscillatory stability and strength). Here we detected spindles with the AR-model using several r_b (damping-based) thresholds. This allowed us to detect spindles with varying

o-Quality and gain a more thorough understanding of the potential EEG spindle deficits in GRIA1$^{-/-}$ mice.

Our results confirmed that the mean incidence of EEG spindles (including spindles at all *o-Quality* levels) is indeed profoundly reduced in GRIA1$^{-/-}$ relative to WT mice ($F_{1,12}$= 17.62, p<0.0001, ***Table 30***) (**Figure 22.B**). We found, however, that EEG spindle events are not completely absent in GRIA1$^{-/-}$ mice. Specifically, while GRIA1$^{-/-}$ mice lacked high *o-Quality* (oQ4 and oQ5) spindles, they still expressed low *o-Quality* (oQ1, oQ2 and oQ3) spindles. The incidence of even these low *o-Quality* spindles showed, however, a significant reduction in GRIA1$^{-/-}$ mice relative to WT mice (see ***Table 31*** for specific contrasts) (**Figure 22.C**). Indeed, overall GRIA1$^{-/-}$ mice showed a significant reduction in mean EEG spindle *o-Quality* relative to WT mice ($F_{1,11}$= 15.21, p<0.05, ***Table 30***) (**Figure 22.D**). Moreover, in line with the results reported in Chapter 3, we found that in both genotypes the incidence of those low *o-Quality* spindles (oQ1, oQ2 and oQ3) progressively increased as their *o-Quality* decreased (WT: $F_{1,4}$= 11.23, p<0.05; KO: $F_{1,4}$= 17.15, p<0.001, ***Table 31***) (**Figure 22.C**).

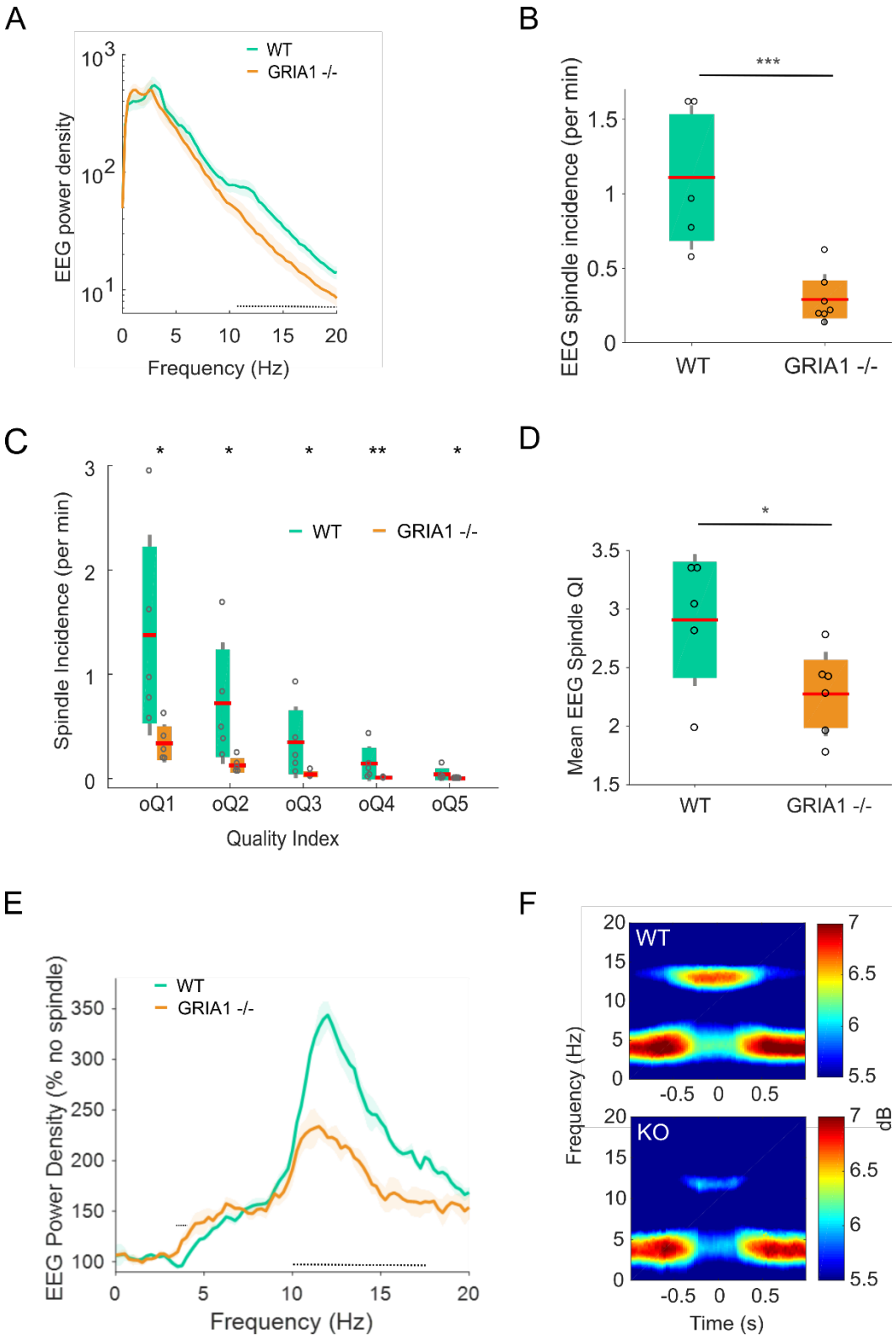


Figure 22. EEG spindle dynamics in GRIA1$^{-/-}$ and WT mice. (A) *Mean EEG power density during NREM sleep in the frontal derivation in GRIA1$^{-/-}$ (n=7) and WT mice (n=5). The shaded areas represent the SEM.* ***(B)*** *Mean EEG spindle incidence per minute of NREM sleep for both genotypes. GRIA1$^{-/-}$ (n=7) and WT mice (n=5).* ***(C)*** *Spindle incidence per minute of NREM sleep as a function*

of the o-Quality of spindles detected in the frontal EEG in both genotypes. Higher oQ index indicates higher o-Quality (i.e. oscillatory strength). GRIA1$^{-/-}$ (n=7) and WT mice (n=5). ***(D)*** *Mean spindle o-Quality for NREM sleep spindles detected in the frontal EEG in both genotypes. GRIA1$^{-/-}$ (n=6, the oQ of one mouse is still being processed) and WT mice (n=5)* ***(E)*** *Mean EEG power density in the frontal EEG channel during epochs with automatically detected spindle events. Mean (lines) and SEM (shaded area) are shown for each frequency bin expressed as a percentage of mean power density during NREM sleep epochs without detected spindles ('% no spindle'). GRIA1$^{-/-}$ (n=7) and WT mice (n=5).* ***(F)*** *Distribution of spectral power <20Hz around the midpoint of individual spindle events in the frontal EEG channel recorded from WT (top) and GRIA1$^{-/-}$ ('KO' bottom) mice. EEG spectral power represents mean across mice. GRIA1$^{-/-}$ (n=7) and WT mice (n=5). NOTE:* ***(A,E)*** *The dotted line depicts bins where EEG spectra differed significantly between genotypes.* ***(B,C,D)*** *Box-plots: red lines= mean across mice; blue boxes= SEM; grey bars= 95% confidence intervals; dots= individual values for each mouse. *p<0.05, **p<0.001, ***p<0.0001.*

We then proceeded by calculating EEG spectra separately for 4-s epochs where spindle events were detected with the AR-model and epochs where no spindles were detected. As expected, in both genotypes, the EEG power density in spindle epochs was enhanced around the spindle frequency range (10-18.5 Hz) relative to no-spindle epochs (WT: $F_{3.4,13.7}$=36.57, p<0.0001; KO: $F_{1.3,4.1=}$14.79, p<0.01, ***Table 32***). However, this increase was significantly higher in WT compared to GRIA1$^{-/-}$ mice (see ***Table 32*** for specific comparisons) (**Figure 22.E**). Indeed, spectrograms centred at the midpoint of spindle events detected with the AR-model, show a prominent increase in EEG power at the spindle frequency range (10-15 Hz) in WT mice that is substantially reduced in GRIA1$^{-/-}$ mice (**Figure 22.F**). In both genotypes, the detection of a spindle event was associated with a suppression of power in the slow-wave frequency range (0.5-4 Hz). This is in line with previous evidence suggesting that, during sleep, thalamo-cortical and cortical neurons undergo transitions between spindle-dominated to slow-wave-dominated

EEG patterns based on their level of hyperpolarization (Steriade et al., 1991; Dijk, 1995).

Overall, in line with our previous study (Ang et al., 2018), these results show that both the incidence and *o-Quality* of EEG spindles during NREM sleep are reduced in GRIA1$^{-/-}$ mice relative to littermate WT mice. In Chapter 3 we found, however, that the majority of sleep spindles are local and remain undetected by surface EEG recordings. Therefore, next we investigated whether the local dynamics of spindles are affected in GluA1 deficient mice.

4.3.2. Despite the reduction in EEG spindles, local LFP spindles are preserved in GRIA1$^{-/-}$ mice

Despite the striking reduction of EEG spindles during NREM sleep in GRIA1$^{-/-}$ mice, visual inspection of the S1 LFP signals during NREM sleep revealed well-defined bursts of activity between 10-15 Hz in both genotypes (**Figure 23.A**). As expected from the results we reported in Chapter 3, LFP spindles in both genotypes were predominantly local. Specifically, visual inspection of the LFP signals and histological results suggested that LFP spindles were predominantly present in recording channels located in layer 5 with no visually detectable spindles in neighbouring channels located only a few hundred micrometres away in layer 6. To compare the incidence and *o-Quality* of local spindles between genotypes we started by focusing our analyses on the channel that showed highest incidence of spindles per mouse, which in every case was located in layer 5 of S1.

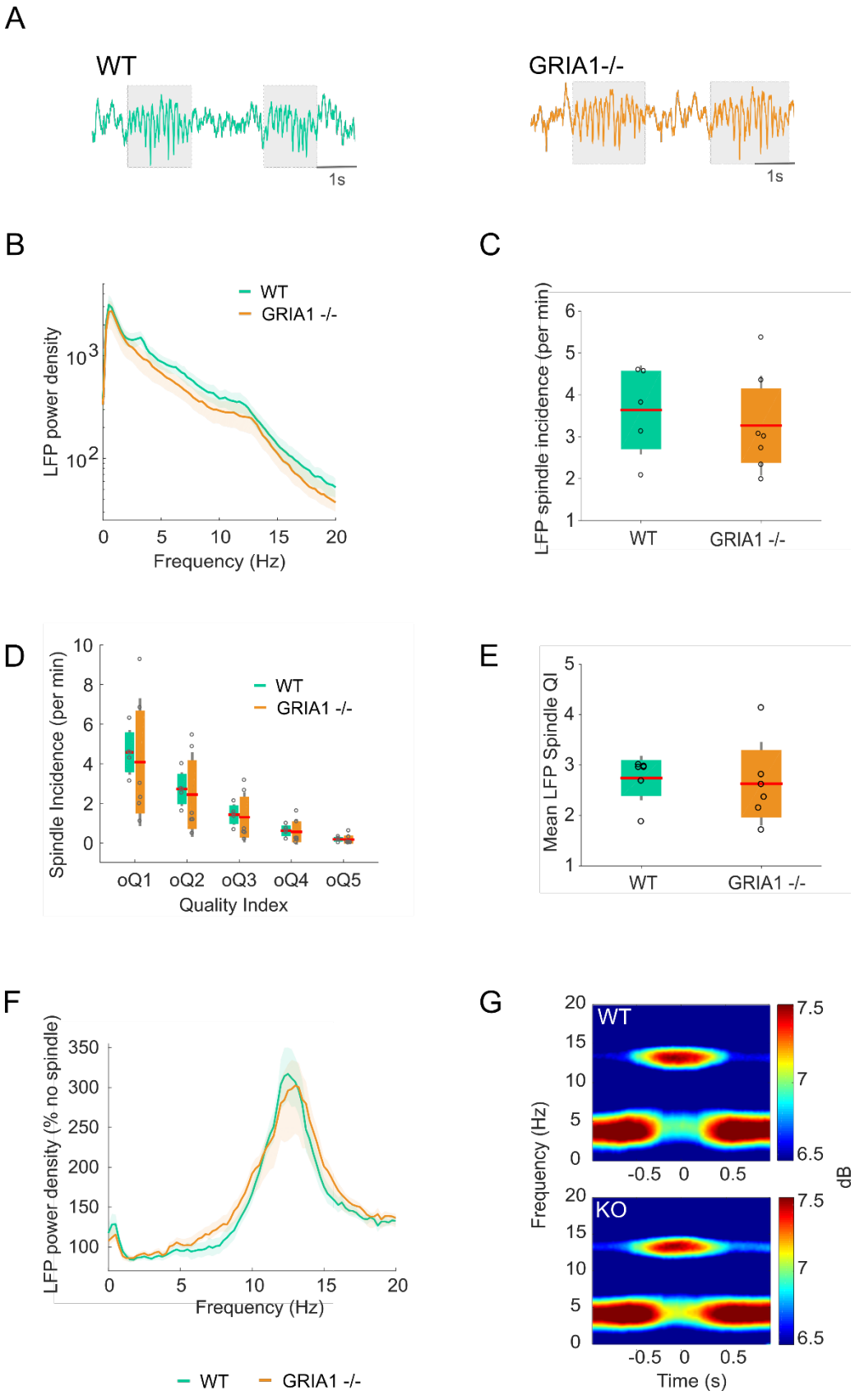


Figure 23. LFP spindle dynamics in GRIA1$^{-/-}$ and WT mice. (A) *Six second segments of LFP signal (500µV amplitude range) recorded from layer 5 of S1 from one WT and one GRIA1$^{-/-}$ mouse,*

showing illustrative examples of LFP spindle events in both genotypes. Spindles are highlighted with grey shading. ***(B)*** *Mean LFP power density during NREM sleep in the LFP signal recorded from layer 5 of the S1 cortex in both GRIA1$^{-/-}$ and WT mice. The shaded areas represent the SEM. GRIA1$^{-/-}$ (n=7) and WT mice (n=5).* ***(C)*** *Mean LFP spindle incidence per minute for both genotypes. GRIA1$^{-/-}$ (n=7) and WT mice (n=5).* ***(D)*** *Spindle incidence per minute as a function of the o-Quality of spindles detected in an LFP signal recorded from layer 5 of the S1 cortex in both genotypes. Higher oQ index indicates higher o-Quality (i.e. oscillatory strength). GRIA1$^{-/-}$ (n=7) and WT mice (n=5).* ***(E)*** *Mean LFP spindle o-Quality in both genotypes. GRIA1$^{-/-}$ (n=6, the oQ of one mouse is still being processed) and WT mice (n=5).* ***(F)*** *Mean LFP power density in Layer 5 S1 LFP channels during epochs with automatically detected spindle events. Mean (lines) SEM (shaded area) are shown for each frequency bin expressed as a percentage of mean power density during NREM sleep epochs without detected spindles. GRIA1$^{-/-}$ (n=7) and WT mice (n=5).* ***(G)*** *Distribution of spectral power <20Hz around the midpoint of individual spindle events in an LFP signal recorded from layer 5 of the S1 cortex in WT (top) and GRIA1$^{-/-}$ (bottom) mice. LFP spectral power represents mean across mice. NOTE:* ***(C,D,E)*** *Box-plots: red lines= mean across mice; blue boxes= SEM; grey bars= 95% confidence intervals; dots= individual values for each mouse.*

Spectral analysis revealed no significant interaction between frequency and genotype ($F_{80,960}$= 0.23, *p*=0.77, ***Table 33***) or difference between genotypes in terms of absolute LFP power density during NREM sleep ($F_{1,11}$=1.35, p=0.27, ***Table 33***) (**Figure 23.B**). As for the EEG, we detected spindles in all LFP signals with the AR-model using several r_b (damping-based) thresholds. There was no significant difference in the mean incidence of LFP spindles (including spindles at all *o-Quality* levels) between genotypes ($F_{1,11}$= 0.314, p=0.59, ***Table 34***) (**Figure 23.C**). Similarly, there was no difference between genotypes in the mean LFP spindle *o-Quality* (including all *o-Quality* levels, **Figure 23.E**) ($F_{1,10}$=0.85, p=0.77, ***Table 34***) or in the spindle incidence distribution across *o-Quality* levels ($F_{1,10}$= 0.07, *p*=0.79, ***Table 35*****)** (**Figure 23.D**). Moreover, in line with the findings reported in Chapter 3, the incidence of spindles progressively increased as their *o-Quality* decreased ($F_{4,36}$= 32.8, *p*<0.0001, *Table 35*).

We calculated LFP spectra separately for 4-s epochs where spindle events were detected with the AR-model and epochs where no spindles were detected. This revealed enhanced relative LFP power density in the spindle frequency range (10 – 15 Hz) in both GRIA1$^{-/-}$ and WT mice ($F_{80,960}$=22.6, p<0.0001, ***Table 36***) (**Figure 23.F**). Notably, no significant difference was evident between genotypes ($F_{1,11}$=0.16, p=0.70**,** ***Table 36***) and there was no significant interaction between frequency and genotype ($F_{80,960}$=0.26, p=0.74, ***Table 36***). Indeed spectrograms centred at the midpoint of spindle events detected with the AR-model, show a prominent increase in LFP power at the spindle frequency range (10-15 Hz) in both GRIA1$^{-/-}$ and WT mice (**Figure 23.G**). In both genotypes, the detection of LFP spindle events was associated with a suppression of power in the slow-wave frequency range (0.5-4 Hz), although this suppression seems to be more prominent and last longer in WT relative to GRIA1$^{-/-}$ mice.

It is worth noting that although the average incidence and *o-Quality* of spindles, as well as the LFP power density at the sigma frequency range (10-15Hz), do not vary between genotypes, GRIA1$^{-/-}$ mice show higher intra-group variability in these parameters. This suggests that the deletion of GluA1 could potentially have a slight impact on the expression of LFP spindles. Nonetheless, given that the specific local underlying area being recorded from has an important effect on the parameters of LFP spindles (as we demonstrated in Chapter 3), a bigger sample size would be required to investigate this between-subject variability.

Overall, these results show that local (LFP) spindles occur in GRIA1$^{-/-}$ mice but remain undetected at the global EEG level. These results suggest that the deletion of GluA1 does not affect the generation of spindles within the reticular-nucleus of the thalamus, but

rather generates an impairment at the thalamo-cortical network level. Results from Chapter 3 indicate that in WT mice the large-scale network synchronization of spindles is a prerequisite for the expression of spindles at the global EEG level. We proceeded, therefore, to investigate whether the deletion of GluA1 in any way affected the network synchronization of spindles.

4.3.3. The deletion of GluA1 affects the large scale synchronization of spindles

We started by investigating whether the deletion of GluA1 affected the synchrony of spindles within local cortical networks. To do this, we compared the spatial extent of LFP spindles recorded from S1 in both genotypes. The spatial extent of spindles was calculated based on the number of local recording electrodes that detected a spindle event and the spacing between these electrodes (250μm inter-electrode spacing). In line with the findings presented in Chapter 3 we found that, in both genotypes, the spatial extent of LFP spindles progressively increased as their *o-Quality* increased ($F_{4,40}$=57.3, p<0.0001, ***Table 37***) (**Figure 24.A**). Moreover, although the spatial extent of LFP spindles across *o-Quality* levels appeared to be slightly reduced in GRIA1$^{-/-}$ relative to WT mice, there was no significant difference between groups in this respect ($F_{4,40}$=1.9, p=0.19, *Table 37*). This suggests that the synchrony of spindles at a local LFP level seems to be preserved in GRIA1$^{-/-}$ mice.

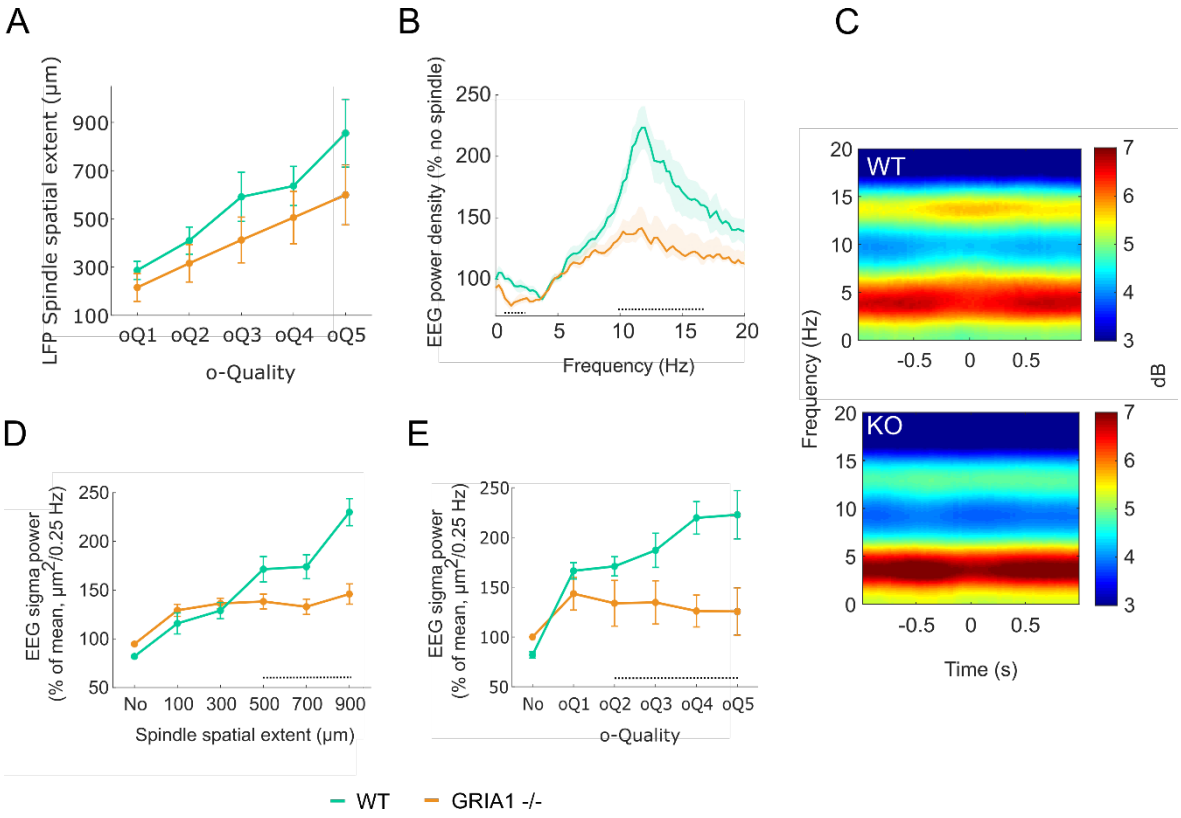


Figure 24. Synchrony within local and global cortical networks in GRIA1$^{-/-}$ and WT mice. (A) *Mean spatial extent of LFP spindles recorded from 16-channel micro-wire arrays from S1 in WT and GRIA1$^{-/-}$ mice, as a function of o-Quality. The spatial extent of a spindle is calculated from the number of LFP electrodes involved in each spindle event. Higher oQ index indicates higher o-Quality (i.e. oscillatory strength).* ***(B)*** *Mean power density in the frontal EEG during epochs where spindle events were automatically detected in LFP channels (located in Layer 5 of S1). Mean (lines) and SEM (shaded area) are shown for each frequency bin expressed as a percentage of mean power density during NREM sleep epochs without detected spindles.* ***(C)*** *Distribution of frontal EEG spectral power <20Hz aligned to the midpoint of spindle events detected in LFP signals recorded from layer 5 of the S1 cortex in WT (top) and GRIA1$^{-/-}$ (bottom) mice. The EEG spectral power represents mean across mice.* ***(D,E)*** *Mean EEG sigma power in the frontal derivation during epochs with detected spindles as a function of spindle spatial extent (D) and o-Quality of local LFP spindles (E) detected in S1 layer 5 in both genotypes. Higher oQ index indicates higher o-Quality (i.e. oscillatory strength). NOTE: figures show mean and SEM across mice. Dotted lines depict bins where values differed significantly between genotypes.*

Results presented in Chapter 3 suggest that the *o-Quality* and local synchrony of LFP spindles give an index of the global synchrony of spindles within widespread cortical EEG networks. It is intriguing, therefore, that the synchrony of spindles within local networks does not differ (statistically) between genotypes, yet GRIA1$^{-/-}$ mice show substantially reduced EEG spindles. To further investigate the association between local and global spindle dynamics in both genotypes, we proceeded by calculating the mean frontal EEG power spectra during 4-s epochs in which LFP spindles were detected with the AR-model (including all *o-Quality* levels in the channel with highest incidence of spindles per mouse) and during epochs where no LFP spindles were detected.

As expected, a mixed ANOVA revealed a significant interaction between genotype and frequency ($F_{80,800}$=11.53, p<0.0001, ***Table 38***). Follow-up repeated measures ANOVAS performed for each genotype showed in both of them, the EEG power density during epochs where LFP spindles were detected was enhanced around the spindle frequency range (10-18.5 Hz) relative to epochs were no spindles were detected (WT: $F_{1.9,5.9}$=29.52, p<0.0001; KO: $F_{2.8,14.3}$=21.4, *p*<0.001, ***Table 38***). However, t-tests performed with Sidak correction showed that this increase was significantly higher in WT compared to GRIA1$^{-/-}$ mice (p<0.05 for frequencies between 9.5 and 17.5, see *Table 38* for specific comparisons) (**Figure 24.B**). Furthermore, spectrograms centred at the midpoint of spindle events detected in the LFP signal with the AR-model, show a prominent increase in EEG power at the spindle frequency range (10-15 Hz) in WT mice that is substantially reduced in GRIA1$^{-/-}$ mice (**Figure 24.C**).

Additionally, we measured how the relative EEG sigma power (i.e. during epochs where LFP spindles were detected relative to epochs were no spindles were detected) varied

based on the spatial extent and *o-Quality* of spindles. We found that WT mice showed an expected increase in relative EEG sigma power as both the spatial extent ($F_{1,4}$= 44.9, p<0.0001, ***Table 39***) and the *o-Quality* ($F_{1,4}$= 14.57, p<0.0001, *Table 40*) of local LFP spindles increased (**Figure 24.D-E**). Interestingly, however, this increase was absent in GRIA1$^{-/-}$ mice, which showed reduced levels of relative EEG sigma power even when the spatial extent ($F_{1,5}$= 0.94, *p*=0.44, *Table 39*) and the *o-Quality* ($F1_{,5}$= 0.82, *p*=0.56, *Table 40*) of local LFP spindles increased and was matched to that of the wild-type mice. Overall, these results suggest that deletion of GluA1 does not significantly affect the synchrony of spindles within local cortical networks, but rather causes an impairment in large network synchronization, which is a prerequisite for the expression of spindles at the global EEG level.

4.3.4. GluA1 deletion affects the association between *spindle o-Quality and both the incidence of slow-waves and the levels of homeostatic sleep need*

4.3.4.1. GRIA1$^{-/-}$ mice exhibit preserved coupling between spindles and slow-waves

Cortical slow-waves have been proposed to play a role in the synchronization of spindle activity across widespread cortical and thalamic regions (Contreras and Steriade, 1996; Buzsáki and Draguhn, 2004; Staresina et al., 2015; Klinzing et al., 2016; Niethard et al., 2018). In line with this, the results we reported in Chapter 3 suggest that high *o-Quality* spindles (which show increased oscillatory strength, increased power, and reflect a synchronised state of the oscillatory network) are more likely to be preceded by slow-waves relative to low *o-Quality* spindles. Given the impairment we found in large

network synchronization of spindles in GRIA1$^{-/-}$ mice, it is possible that the coupling between slow-waves and spindles is in some way affected by the deletion of GluA1. We proceeded, therefore, to investigate the relationship between slow-wave and spindle activity in both genotypes.

First, we explored whether the incidence and amplitude of slow-waves differed between genotypes. To do this, we detected slow-waves in band-pass filtered (0.5-4 Hz) EEG and LFP signals, as positive deflections between two consecutive negative deflections below the zero-crossing (separated by at least 0.1-s). The amplitude of slow-waves was calculated as the distance between the zero-crossing and the maximal positive peak. No significant differences were found between genotypes in the incidence of slow-waves detected in the LFP (t_{11}=0.79, p=0.44, ***Table 41***) and EEG signals (t_{11}=0.95, p=0.36, ***Table 42***) (

***Figure 25*.A**). Furthermore, there were no significant differences between genotypes in the distribution of the amplitude of slow-waves detected in the LFP (Z-statistic=0.002) and EEG (Z-statistic=0.075) signals (

Figure *25*.B*).*

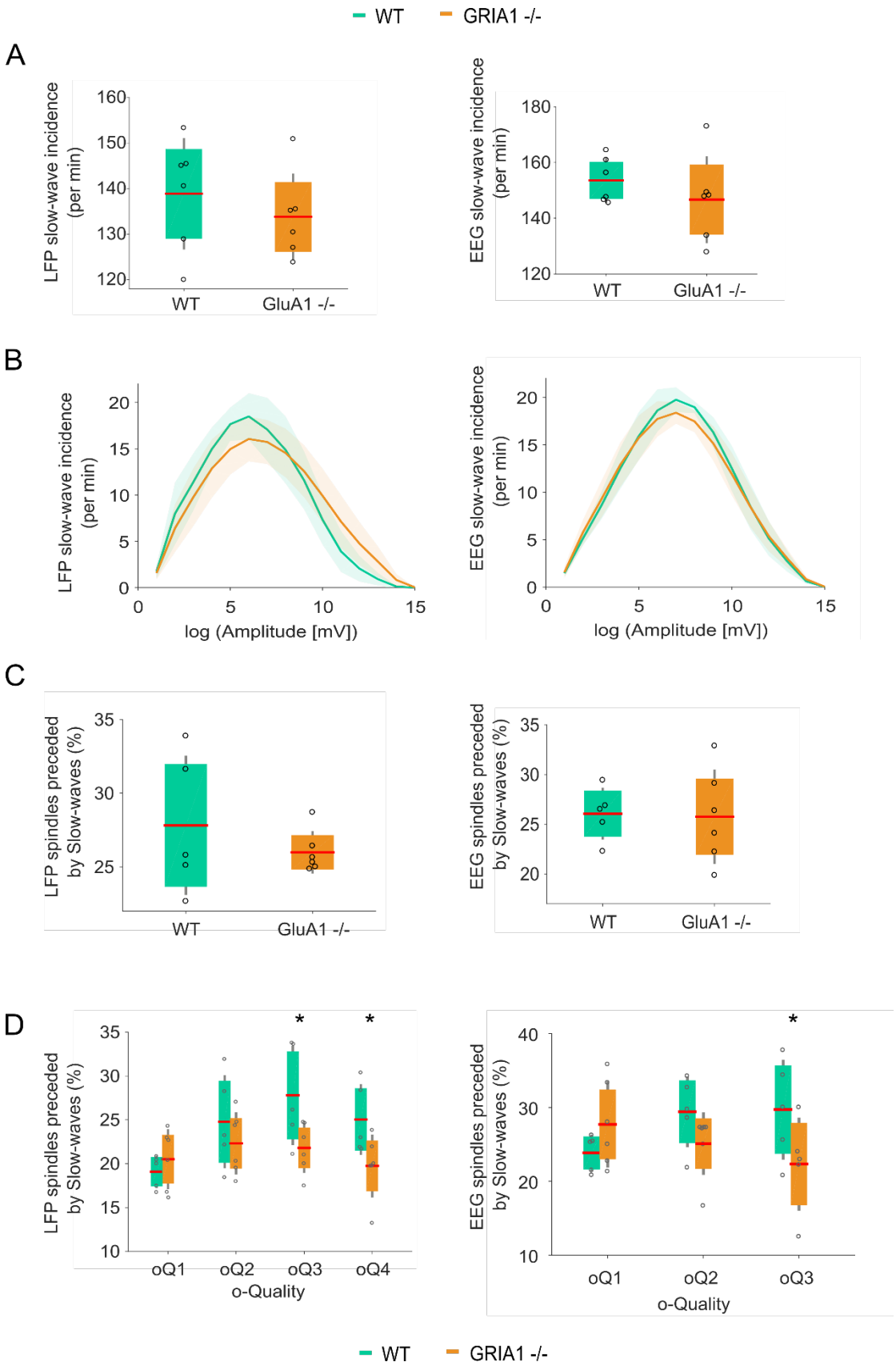


Figure 25. Dynamics of slow-wave activity and coupling between slow-waves and spindles in WT and GRIA1$^{-/-}$ mice. (A) *Incidence of slow-waves per minute of NREM sleep in LFP (left) and*

frontal EEG (right) signals in both genotypes. ***(B)*** *Distribution of slow-wave peak amplitude incidence per minute for both genotypes in LFP (left) and frontal EEG (right) signals. The lines represent the mean and the shaded areas represent SEM across mice.* ***(C)*** *Percentage of spindles preceded by slow-waves in LFP (left) and frontal EEG (right) signals.* ***(D)*** *Incidence of spindles preceded by slow-waves in LFP (left) and frontal EEG (right) derivations as a function of the o-Quality of spindles detected in these derivations. Note that only three o-Quality levels were included for the EEG because spindles generally show low o-Quality in this derivation and not enough high o-Quality spindles (i.e. oQ4) were detected to run these analyses. *p<0.05, **p<0.001, ***p<0.0001. NOTE:* ***(A,C,D)*** *Box-plots: red lines= mean across mice; blue boxes= SEM; grey bars= 95% confidence intervals; dots= individual values for each mouse. GRIA1$^{-/-}$ n=6; WT n=5.*

4.3.4.2. GRIA1 $^{-/-}$ mice do not show a direct relationship between spindle o-Quality and the incidence of slow-waves

We then proceeded to assess the relationship between slow-waves and spindles in the EEG and in the LFP channels where more spindles were detected in each mouse. Spindles were considered to co-occur with slow-waves if their onset occurred within a window of 0.5-s after the slow-wave onset. Contrary to our hypothesis, there was no significant difference between genotypes in the percent of LFP spindles (t_{11}=0.83, p=0.45, ***Table 43***) or EEG spindles (t_{11}=0.13, p=0.90, ***Table 44***) preceded by a slow-wave (

Figure 25*.C**). Interestingly, however, the percent of spindles preceded by slow-waves changed as a function of the *o-Quality* of spindles, and this change was different between genotypes (interaction effect -genotype*oQ- on LFP spindles: $F_{3,27}$=39.46, p<0.05, Table 45; interaction effect -genotype*oQ- on EEG spindles $F_{2,18}$=4.07, p<0.05, ***Table 46) (

Figure *25*.D). Specifically, the percent of LFP spindles and EEG spindles preceded by slow-waves increased as the *o-Quality* of spindles increased in WT mice (Effect on LFP spindles: $F_{3,12}$=11.68, p<0.001, ***Table 45***; Effect on EEG spindles: $F_{2,8}$=4.43, p<0.05, ***Table 46***). However, this effect was not present in GRIA1 $^{-/-}$ mice (effect on LFP spindles: $F_{3,15}$=0.97, p=0.44, ***Table 45***; effect on EEG spindles: $F_{2,10}$=1.07, p=0.38, ***Table 46***).

Overall, these results suggest that when GluA1 is deleted, the direct relationship between slow-waves and spindle *o-Quality* (that is evident in WT mice), is no longer apparent. The results we reported in Chapter 3 suggested that the incidence and *o-Quality* increase as the levels of homeostatic sleep need increase as well. Therefore, we were interested in assessing whether the association between slow-wave activity and spindle *o-Quality* would still be affected in GRIA1$^{-/-}$ mice in a context of increased slow-wave activity power.

4.3.4.3. GRIA1 $^{-/-}$ mice exhibit an increase in o-Quality in the context of high homeostatic sleep need for spindles detected in Layer 6 of S1 but not for spindles detected in other areas

Slow-wave activity is thought to reflect the levels of homeostatic sleep need (Borbely, 1982; Borbély et al., 2016). It increases with wake duration and shows a homeostatic decrease during sleep (Trachsel et al., 1988; Vyazovskiy et al., 2004a). We compared the incidence and *o-Quality* of spindles between genotypes in two contexts of increased slow-wave activity.

First, we performed this comparison during the first few hours of sleep after sleep onset, when slow-wave activity has been reported to be elevated (Trachsel et al., 1988; Vyazovskiy et al., 2004a). As expected, we found that the levels of SWA were highest during the first hours of sleep after sleep onset and decreased across the light period ($F_{11,99}$=6.24, p<0.0001, ***Table 47***) (**Figure 26.A**). The dynamics of SWA across the light period were similar between genotypes ($F_{1,10}$=2.04, *p*=0.19, ***Table 47***). In line with the results presented in Chapter 3, we found that in WT mice the spindle *o-Quality* showed a direct association with the levels of SWA. Specifically, similar to the dynamics of SWA, the *o-Quality* of spindles was highest during the first hours of sleep after sleep onset and then decreased across the light period ($F_{1,10}$=4.26, *p*<0.01, ***Table 48***) (**Figure 26.A**). In contrast, this direct relationship was not evident in GRIA1 $^{-/-}$ mice ($F_{1,10}$=0.97, *p*=0.43, ***Table 48***), which showed higher intra-group variance in terms of spindle *o-Quality* but no decline across the light period (**Figure 26.A**).

Second, we compared the incidence and *o-Quality* of spindles between genotypes during the first hours of sleep recovery after six hours of sleep deprivation (see Chapter 2, *General Methods, Sleep deprivation*), when the levels of SWA have been reported to increase (Dijk et al., 1993; Vyazovskiy et al., 2004a). Interestingly, we found that the effect of sleep deprivation on the levels of SWA and the *o-Quality* of spindles varied depending on the cortical layer.

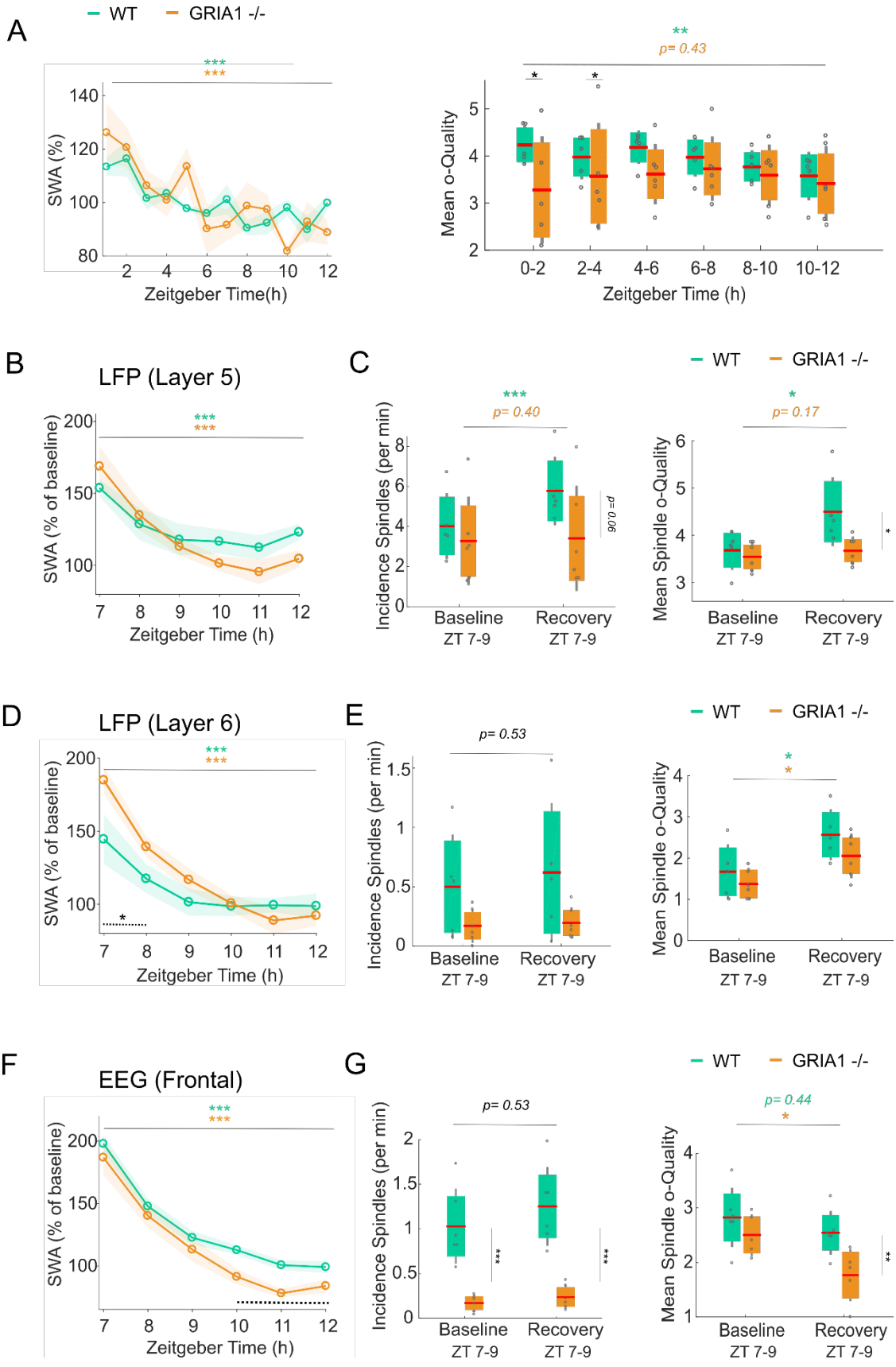

A
WT
GRIA1 -/-
SWA (%)
Zeitgeber Time(h)
Mean o-Quality
Zeitgeber Time (h)
p= 0.43
B
LFP (Layer 5)
SWA (% of baseline)
Zeitgeber Time (h)
C
Incidence Spindles (per min)
Mean Spindle o-Quality
p= 0.40
p= 0.17
p= 0.06
Baseline ZT 7-9
Recovery ZT 7-9
D
LFP (Layer 6)
E
p= 0.53
F
EEG (Frontal)
G
p= 0.44

Figure 26. Slow-wave activity and spindle dynamics in the context of increased sleep pressure. (A-left) *Time-course of slow-wave activity (0.5-4 Hz) in S1 (layer 5) LFP signals recorded from GRIA1$^{-/-}$ and WT mice across a 12-h light period. SWA values are expressed as % of mean 12-h NREM sleep value.* ***(A-right)*** *Spindle o-Quality measured across a 12-h light period in both genotypes.* ***(B,D,F)*** *Time-course of slow-wave activity (0.5-4 Hz) in S1 (layer 5) LFP (B), S1 (layer 6) LFP (D), and frontal EEG (F) signals during sleep recovery after 6 hours of sleep deprivation in GRIA1$^{-/-}$ and WT mice. SWA values are expressed as % of mean 12-h baseline value.* ***(C,E,G)*** *Spindle incidence (left) and o-Quality (right) measured during the first two hours of sleep recovery after sleep deprivation (ZT7-ZT9) and corresponding sleep baseline time-period in S1 (layer 5) LFP (C), S1 (layer 6) LFP (E), and frontal EEG (G) signals recorded from both genotypes. NOTE: Line plots show the mean (line) and standard deviation (shaded area) across mice. For the box-plots, red lines represent mean across mice, blue boxes represent SEM, grey bars represent 95% confidence intervals, and dots represent individual values for each mouse. Significance values presented on top of each figure indicates within-subject effects, while dotted lines or side-bars depict bins where values differed significantly between genotypes. *p<0.05, **p<0.001, ***p<0.0001. GRIA1$^{-/-}$ n=6; WT n=5.*

We proceeded then to analyse the SWA and spindle dynamics in channels located in layer 5 of S1. Specifically, we selected the channel in layer 5 that showed highest density of spindles per mouse. A robust and significant increase in slow-wave activity (0.5-4 Hz) was found during the first two hours of sleep recovery (ZT7 to ZT9) relative to sleep baseline in both genotypes ($F_{5,45}$=23.56, p<0.0001, ***Table 49***) (**Figure 26.B**). This homeostatic rebound did not significantly differ between genotypes (interaction ZT * genotype: $F_{5,45}$=2.52, *p*=0.06; main effect of genotype: $F_{1,9}$=4.03, *p*=0.08, ***Table 49***), although the SWA shows a strong trend towards a reduction in GRIA1 $^{-/-}$ mice relative to WT mice at ZT10 to ZT12.

Regarding the spindle dynamics in layer 5, we found a significant interaction between genotypes in the incidence and *o-Quality* of spindles presented during the different

sleep conditions, i.e. sleep baseline vs recovery (incidence: $F_{1,9}$=47.29, p<0.0001 ***Table 50***; *o-Quality:* $F_{1,9}$=6.35, p<0.05 ***Table 51***). In line with the results reported in Chapter 3, showed that in WT mice the spindle incidence and *o-Quality* showed a direct association with the levels of SWA. Specifically, based on a repeated-measures ANOVA the incidence ($F_{1,4}$=86.98, p<0.0001, ***Table 50***) and *o-Quality* ($F_{1,4}$=10.78*, p*<0.05, ***Table 51***) of spindles detected in layer 5 showed a significant increase during recovery sleep (ZT7 to ZT9) relative to baseline sleep (ZT7 to ZT9) in WT mice. This increase, however, was not apparent in GRIA1$^{-/-}$ mice (incidence $F_{1,5}$=0.85, p=0.4, ***Table 50***; *o–Quality* $F_{1,5}$=2.61, p=0.17, ***Table 51***) (**Figure 26.C**). A follow-up ANOVA further showed that there was no significant difference between genotypes in spindle incidence ($F_{1,10}$=0.39, p=0.55, ***Table 50***) and *o-Quality* ($F_{1,10}$=0.4, p=0.54, ***Table 51***) during baseline sleep. During sleep recovery, however, WT mice showed increased spindle *o-Quality* ($F_{1,10}$=6.49, p<0.05, ***Table 51***) and a tend towards an increase in spindle incidence ($F_{1,10}$=4.41, p=0.06, ***Table 50***), relative to GRIA1$^{-/-}$.

Next, we analysed the SWA and spindle dynamics in channels located in layer 6 of S1. We selected the channel in layer 6 that showed the highest density of spindles per mouse. A mixed ANOVA revealed a significant interaction between genotype (WT vs GRIA1$^{-/-}$) and the Zeitgeber time (i.e. time from light onset) across a 12h light period ($F_{5,45}$=4.99, p<0.001, ***Table 52***). Specifically, repeated measures ANOVA follow-ups showed a robust and significant increase in slow-wave activity (0.5-4 Hz), during the first two hours of recovery sleep (ZT7 to ZT9) relative to baseline sleep, both in WT ($F_{1,4}$=7.09, p<0.05, ***Table 52***) and GRIA1$^{-/-}$ mice ($F_{1,5}$=50.48, p<0.0001, ***Table 52***) (**Figure 26.D**). A follow-up ANOVA showed that this homeostatic rebound was

significantly higher in GRIA1$^{-/-}$ mice relative to WT mice (ZT7 $F_{1,10=}$4.95, p<0.05 and ZT8 $F_{1,10}$=5.54, p<0.05, ***Table 52***).

Regarding the spindle dynamics, in both genotypes the incidence of spindles in layer 6 was low and remained unchanged after sleep deprivation (interaction genotype * sleep condition [baseline vs recovery]: $F_{1,10}$=0.18, p=0.68; main effect of sleep condition $F_{1,10}$=0.42, p=0.53, ***Table 53***). Interestingly, however, in both genotypes the *o-Quality* of spindles detected in layer 6 showed a significant increase during recovery sleep (ZT7 to ZT9) relative to baseline sleep (ZT7 to ZT9) (interaction genotype * sleep condition [baseline vs recovery]: $F_{1,9}$=0.15, p=0.47; main effect of ZT time: $F_{1,9}$=9.75, p<0.05, ***Table 54***) (**Figure 26.E**). This result was surprising (given that the *o-Quality* of spindle in GRIA1$^{-/-}$ appears consistently low) and could potentially suggest that the *o-Quality* of spindles in GRIA1$^{-/-}$ can increase in layer 6 of S1, or in local regions where the SWA is significantly increased.

Finally, we analysed the SWA and spindle dynamics in the frontal EEG channel. This homeostatic rebound did not significantly differ between genotypes across the 12h light period (interaction ZT * genotype: $F_{5,45}$=0.98, p=0.39, ***Table 55***). A significant increase in slow-wave activity (0.5-4 Hz) was found during the first two hours of recovery sleep (ZT7 to ZT9) relative to baseline sleep both in WT ($F_{5,25}$=127.83, p<0.0001, ***Table 55***) and GRIA1$^{-/-}$ mice ($F_{5,30}$=58.15, p<0.0001, ***Table 55***) (**Figure 26.F**).

Regarding the spindle dynamics in the frontal EEG, no increase was evident in their incidence in either genotype (interaction: $F_{1,10}$=0.9, p=0.36; main effect of genotype:

$F_{1,10}$=3.22, *p*=0.10, ***Table 56***). As expected, GRIA1$^{-/-}$ showed reduced incidence of frontal EEG spindles relative to WT both during baseline and recovery sleep ($F_{1,10}$=33.1, p<0.0001, ***Table 56*)**. Regarding spindle *o-Quality,* we found a significant interaction between genotypes and sleep condition, i.e. sleep baseline vs recovery ($F_{1,9}$=5.15, p<0.05, ***Table 57***). Specifically, in WT mice the *o-Quality* of EEG spindles remained unchanged after sleep deprivation ($F_{1,5}$=0.71, p=0.44, ***Table 57***), while in GRIA1$^{-/-}$ it showed a significant reduction ($F_{1,4}$=11.3, p<0.05, ***Table 57*)** during sleep recovery (ZT7 to ZT9) relative to baseline sleep (ZT7 to ZT9) (**Figure 26.G**).

While inconclusive at this stage, these results tentatively suggest that the association between spindle *o-Quality* and homeostatic sleep need varies according to the underlying cortical layer. Specifically, when GluA1 is deleted, the direct association between spindle *o-Quality* and the levels of homeostatic sleep need is no longer apparent in global EEG networks and middle-superficial layers of the S1 cortex (i.e. Layer 5), where the incidence of spindles is high. It remains unclear why the homeostatic rebound of SWA in layer 6 was higher in GRIA1$^{-/-}$ mice relative to WT mice. However, our results tentatively suggest that the *o-Quality* of spindles in GRIA1$^{-/-}$ mice can indeed increase (at least in layer 6 of S1) in a context of high sleep need and highly increased SWA. It is important to note however, that the incidence of spindles in Layer 6 is low, which reduces the statistical power of these results.

4.3.5. The infra-slow oscillation of spindle activity is preserved in GRIA1$^{-/-}$ mice but the infra-slow dynamics of the spindle o-Quality differs between genotypes

Sigma activity has been found to exhibit an infra-slow oscillation defined by frequencies in the 0.01 to 0.02 Hz range (Achermann and Borbély, 1997; Lecci et al., 2017; Lázár et al., 2019). In agreement with previous literature (Lecci, 2018; Lazar, 2019), in Chapter 3 we found that this infra-slow oscillation (~0.02 Hz) in spindle activity occurs in WT (C57/BL6) mice and is predominant in the posterior cortex. Additionally, we found that the *o-Quality* of spindles increases within cycles of the infra-slow oscillation across uninterrupted NREM episodes. Therefore, we next investigated whether the deletion of GluA1 in any way alters the infra-slow oscillation of spindle activity or the dynamics of the spindle *o-Quality* within the cycles of this oscillation.

4.3.5.1. The infra-slow oscillation of LFP spindles is preserved in GRIA1$^{-/-}$ mice

Figure 27.A shows eight-minute segments of S1 LFP signals during NREM sleep, filtered at the sigma frequency range (10-15 Hz). Bursts of high amplitude sigma activity (i.e. putative spindles) clearly occur in the S1 LFP signals of both GRIA1$^{-/-}$ and WT littermates. We proceeded then to detect NREM episodes (minimum duration 45-s) from the LFP signals recorded from 12-h baseline sleep recordings during the light period. We selected the LFP signal that showed the highest incidence of spindles per mouse, which in all cases was located in layer 5 of S1. We band-pass filtered (10-15 Hz) and calculated the envelope of all these LFP signal segments, using a Butterworth filter

followed by a Hilbert transform of the filtered signal. The power spectral density of these envelopes was calculated using the Welch's power spectral density estimate. This analysis revealed a predominant frequency of 0.02 ± 0.001 Hz for the sigma activity in both genotypes, which corresponds to cycle lengths of around 60-s (**Figure 27.C**).

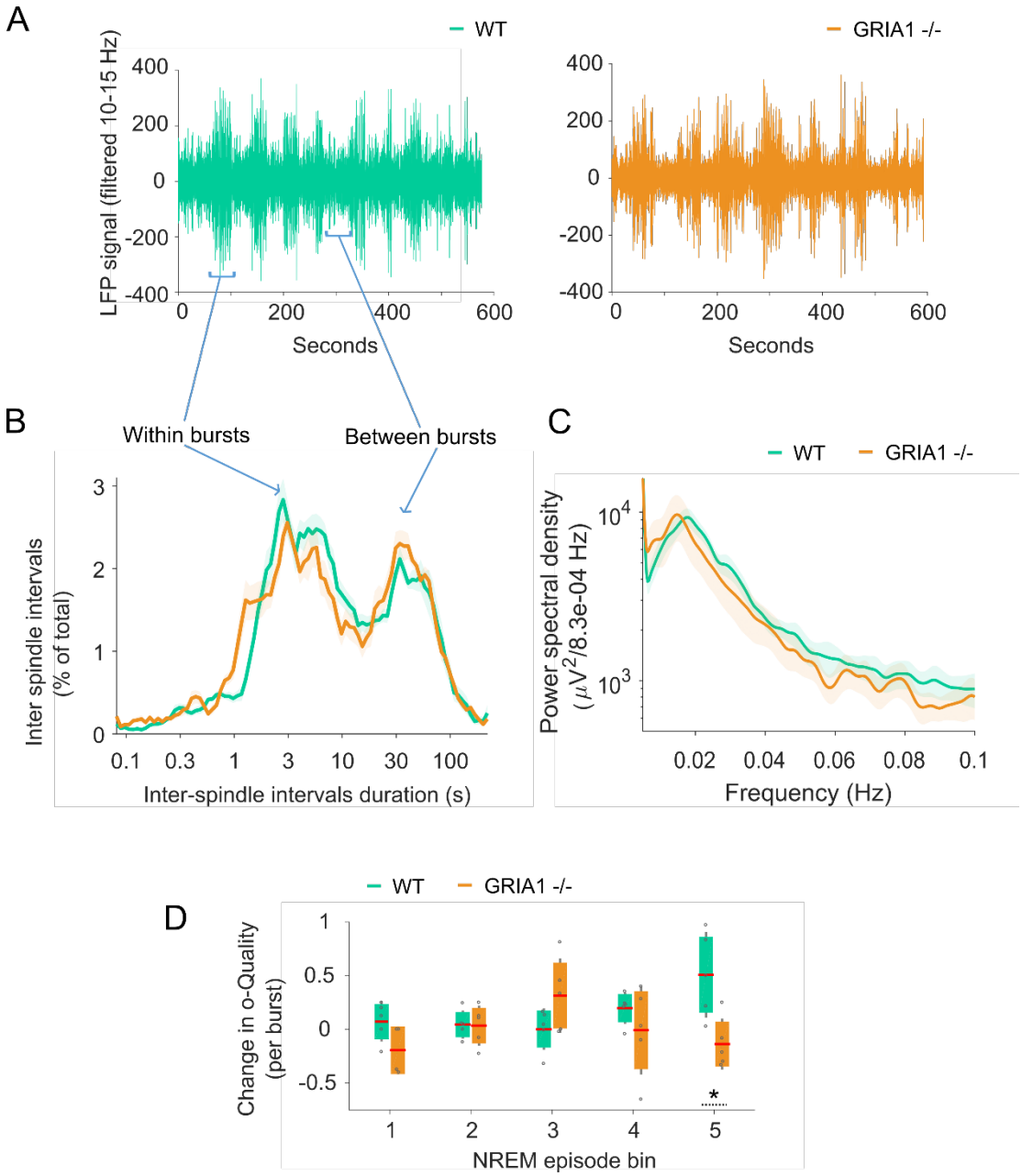


Figure 27. Infra-slow oscillation of LFP spindle activity in GRIA1$^{-/-}$ and WT mice. (A) *Eight-minute segments of S1 (layer 5) LFP signals recorded during NREM sleep in GRIA1$^{-/-}$ and WT mice,*

filtered at the spindle frequency range (10-15 Hz). Bursts of putative spindles are evident in both genotypes. ***(B)*** *Inter-spindle intervals (ISI, i.e. time difference between the onset of consecutive spindle events) within uninterrupted NREM episodes recorded throughout 12-h light periods in S1 layer 5 LFP signals in both GRIA1$^{-/-}$ and WT mice (mean and SEM across mice). There is a bimodal distribution for both WT and GRIA1$^{-/-}$ mice. The first peak indicates ISI between spindles within bursts, the second peak indicates the time interval between bursts (i.e. last spindle of a burst to the first spindle of next burst).* ***(C)*** *Power spectral density of the envelope of filtered LFP signals (10-15 Hz) recorded from layer 5 of S1. A predominant frequency of ~0.02Hz is evident in both genotypes (mean and SEM across mice).* ***(D)*** *Change in spindle o-Quality within spindle bursts, as a function of NREM episode bin. The amount of spindle o-Quality increase within spindle bursts was calculated by subtracting the mean o-Quality during the first spindle-burst bin, from the mean spindle o-Quality during the last (6th) spindle-burst bin****. NOTE:*** *(Box plots: red lines= mean across mice; blue boxes= SEM; grey bars= 95% confidence intervals; dots= individual values for each mouse). *p<0.05.*

We then examined whether spindles detected with the AR-model in the LFP signals would exhibit an infra-slow (~0.02 Hz) oscillation. To do this, we calculated the time difference between the onsets of consecutive spindle events (i.e. inter-spindle intervals) within uninterrupted NREM episodes in the LFP signals. This analysis confirmed that in both genotypes, LFP spindles recorded from S1 occur in bursts, which last on average 14.1 ± 0.3 s (mean ± SEM), and are comprised of one spindle every ~2.36 ± 0.004 s (**Figure 27.B**).

4.3.5.2. The variation in spindle o-Quality as a function of the infra-slow oscillation differs between GRIA1$^{-/-}$ and WT mice

Having confirmed that spindles in S1 follow an infra-slow oscillation in both genotypes, we proceeded to investigate the relationship between this rhythm and the *o-Quality* of spindles. To do this, we followed the same procedure as Chapter 3, section 3.4.5, which is schematized in **Figure 18.A**. Specifically, we detected spindle bursts within NREM episodes of the LFP S1 signals (selecting the LFP channel that showed the highest density of spindles per mouse). Based on our previous results, we considered 'spindle bursts' as trains of at least four consecutive spindles, with a maximum inter-spindle interval duration of 10-s. We then calculated the change in *o-Quality* of spindles per cycle of the infra-slow oscillation across NREM episodes. To do this, we subtracted the mean spindle *o-Quality* in the first sixth of each infra-slow oscillation cycle from the mean spindle *o-Quality* in the last sixth. We plotted this differential values across five NREM episode bins (**Figure 27.D**).

We found that the dynamics of the *o-Quality* of spindles per cycle of the infra-slow oscillation across NREM episodes varied between genotypes (interaction term: $F_{4,32}$=4.62, p<0.0001, ***Table 58***). In line with the results presented in Chapter 3, we found that WT mice show a significant linear increase in spindle *o-Quality* within cycles of the infra-slow oscillation across NREM episodes (Repeated measures ANOVA, $F_{4,16}$=3.36, p<0.05, Linear effect $F_{1,4}$=8.85, p<0.05, ***Table 58***). Specifically, WT mice show the highest increases in mean *o-Quality* within cycles of the infra-slow oscillation during the last fifth of NREM episodes (i.e. last bin). On the other hand, the spindle *o-Quality* across cycles of the infra-slow oscillation show a quadratic trend in GRIA1$^{-/-}$

mice ($F_{1,4}$=19.54, p<0.05, ***Table 58***). Specifically, these mice show a significant increase in spindle *o-Quality* within cycles of the infra-slow oscillation across the first half of a NREM episode ($F_{4,16}$=13.6, p<0.05, ***Table 58***), which reach the highest increases during the third bin of NREM episodes (out of five NREM bins). However, this increase statistically diminishes during the last NREM episode bin relative to WT mice ($F_{1,9}$=9.69, p<0.05, ***Table 58***) (**Figure 27.D**).

Taken together, these results suggests that LFP spindles in GRIA1$^{-/-}$ mice follow an infra-slow oscillation, as in WT mice (Lecci et al., 2017) and human EEG spindles (Achermann and Borbély, 1997; Lázár et al., 2019). However, the dynamics of the spindle *o-Quality* within cycles of the infra-slow oscillation vary between genotypes. While in WT mice, the *o-Quality* of spindles seems to show a marked increase only within cycles that occur towards the end of NREM episodes, in GRIA1$^{-/-}$ mice this increase occurs towards the middle of NREM episodes after which it declines. Further analyses, however, are needed to better understand this process and its physiological and biological relevance.

4.3.6. Despite showing deficits in spindle dynamics, long-term memory is preserved in GRIA1$^{-/-}$ mice

Spindles are believed to play a crucial role in the consolidation of hippocampus-dependent memory during sleep. As previously reported in this chapter, GRIA1$^{-/-}$ mice show deficits in the dynamics of spindle activity. Specifically, they exhibit a striking reduction of EEG spindles, deficits in the large scale synchronization of spindles, and

changes in the spindle *o-Quality* dynamics across slow-wave and infra-slow rhythms. If the occurrence of spindles, as well as their timing and coupling with other oscillations, are crucial for the storage of long-term memories during sleep, it might be expected that GRIA1$^{-/-}$ mice will show some long-term memory deficits. However, previous studies suggest that this might not be the case (Zamanillo et al., 1999; Reisel et al., 2002; Schmitt et al., 2003; Sanderson et al., 2009; Bannerman et al., 2014). We proceeded here to assess the performance of GRIA1$^{-/-}$ in two long-term memory tasks known to rely on hippocampal activity (Bannerman et al., 2003; Vogel-Ciernia and Wood, 2014; Vorhees and Williams, 2014).

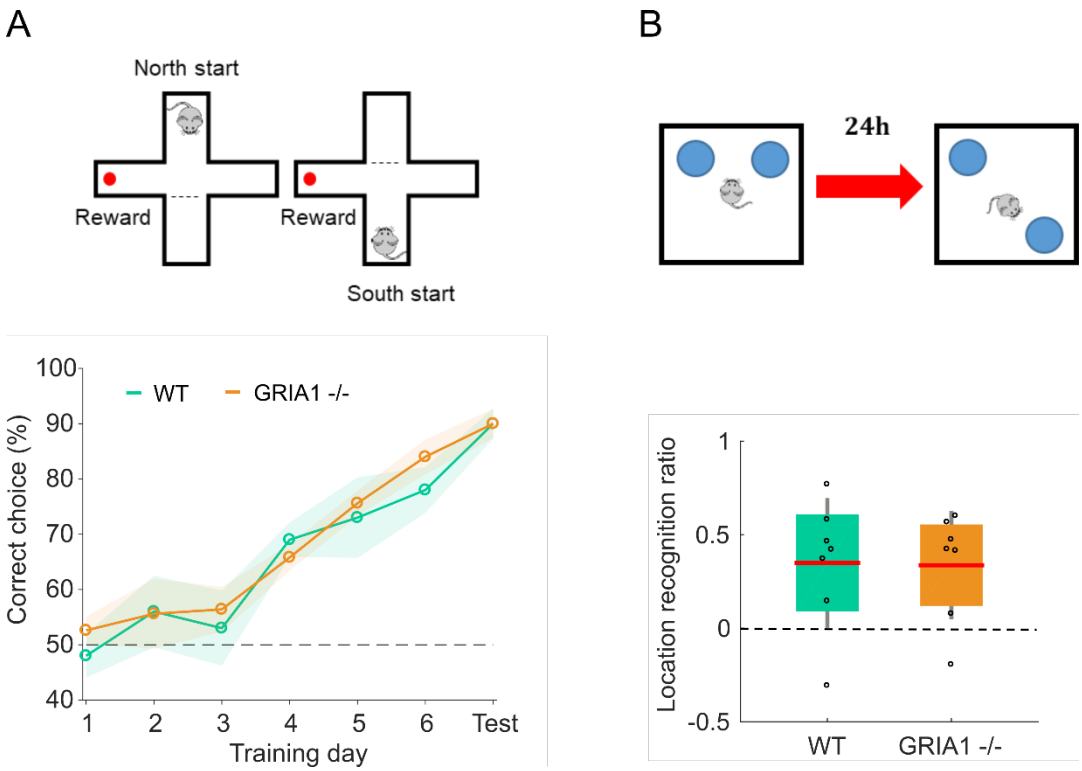


Figure 28. Normal spatial reference memory in GRIA1$^{-/-}$ mice. (A) *Plus-maze setup for spatial reference learning (top). Percentage of correct choices for GRIA1$^{-/-}$ and WT mice during the training and test sessions. Dashed line indicates chance level performance.* ***(B)*** *Setup for the object displacement test (top). The bottom panel shows the location recognition ratio for both GRIA1$^{-/-}$ and WT mice. This is calculated as follows: Time exploring displaced object – Time exploring the*

*non-displaced object) / (Time exploring displaced + not-displaced) * 100. Box plots: red lines= mean across mice; blue boxes= SEM; grey bars= 95% confidence intervals; dots= individual values for each mouse).*

First, we assessed the performance of GRIA1$^{-/-}$ mice (n=7) relative to WT littermates (n=7) in a plus-maze task that measures hippocampus-dependent, long-term spatial reference memory (Bannerman et al., 2003). Specifically, we tested the capacity of mice to learn the location of a fixed-positioned reward regardless of their start arm location in the plus maze. Successful performance in this task could reflect the capacity to build an allocentric representation of an environment, and form a long-term association between an outcome and a spatial location (within this allocentric frame). These processes rely on structures including the hippocampus (O'keefe and Nadel, 1979; Bannerman et al., 2003; Buzsáki and Moser, 2013). We found that both Gria1$^{-/-}$ and WT mice managed to learn the location of the fixed-positioned reward, and reached 90% correct choices on the test session after 6 days of training ($F_{6,72}$=22.94, p<0.0001 and significant linear contrast, ***Table 59***). There was no significant difference between genotypes in memory performance across training days or the test session ($F_{1,12}$=0.15, p=0.71, ***Table 59***), and no significant genotype by training day interaction ($F_{6,72}$=0.26, p=0.95, , ***Table 59***) (**Figure 28.A**).

Second, we performed an object displacement task to assess spatial memory in both genotypes. This task measures spatial memory as the natural preference of mice to explore a familiar object displaced in space relative to initial exposure, over another familiar object that remains in its original location. These processes are known to rely on the hippocampus (Moser and Moser, 1998), and hippocampal inactivation has been

found to impair the performance of mice in this task (Broadbent et al., 2004; Oliveira et al., 2010).

Mice were exposed to a training context with two identical objects. During the exposure phase, exploration times of GRIA1$^{-/-}$ mice were yoked the exploration times of WT mice. On average GRIA1$^{-/-}$ took 1.2 ± 0.74 minutes less than WT mice to reach the yoked time. Upon re-exposure to the same context 24 hours later with one of the familiar objects now displaced to a new location, both WT and GRIA1$^{-/-}$ mice performed significantly above chance ($F_{2,26}$=4.03, p<0.05, ***Table 60**, i.e.* spent significantly longer exploring the displaced object versus the non-displaced object). Moreover, we did not find any difference between genotypes in the time they spent exploring the displaced versus the non-displaced object (t_{13}=0.69, p=0.95, ***Table 60***) (**Figure 28.B**).

In line with previous findings (Sanderson et al., 2009; Bannerman et al., 2014), these results suggest that despite their spindle deficits, long-term spatial memory is preserved in GRIA1$^{-/-}$ mice.

4.4. DISCUSSION

We assessed the dynamics of sleep spindles in mice lacking the GluA1 AMPA receptor subunit, which have a genotype and behavioural phenotype relevant for schizophrenia. Our results show that GRIA1$^{-/-}$ mice exhibit a profound reduction in the incidence and *o-Quality* of EEG spindles while local cortical spindles in S1 are preserved. Additionally, our results suggest that the deletion of GluA1 generates an impairment in the large network synchronization of spindle-related activity which, as we demonstrated in

Chapter 3, is a prerequisite for the expression of spindles at the global EEG level. These results have several important implications.

4.4.1. Potential neural mechanisms underlying spindle dynamics and deficits

First, our results suggest that an important link exists between glutamatergic neurotransmission and the network mechanisms implicated in the generation of spindles. In fact, AMPA and NMDA receptors are known to play an important role in the generation of thalamo-cortical oscillations (Jones, 2009; Deleuze and Huguenard, 2016). Our results further suggest that the GluA1 subunit of the AMPA receptor specifically plays an important role. Specifically, the pattern of preserved local spindles and the reduced presence of global spindles in GRIA1$^{-/-}$ mice, suggests that the deletion of GluA1 might not affect the initiation of spindles within the reticular-nucleus of the thalamus, but rather lead to an impairment at the thalamo-cortical network level.

This possibility is further supported by our results showing a dissociation between both the *o-Quality* and local synchrony of LFP spindles, and the expression of global EEG spindles in GRIA1$^{-/-}$ mice. While these metrics are directly associated in WT littermates and WT C57/BL6 mice (reported in Chapter 3), their association is absent in GRIA1$^{-/-}$ mice. In the case of GRIA1$^{-/-}$ mice, high *o-Quality* spindles that show high synchrony at the local LFP level fail to express within widespread cortical EEG networks. These results reinforce the hypothesis that the deletion of the GluA1 AMPA receptor subunit generates an impairment in large network synchronization, while sparing the initiation of spindles within the reticular nucleus of the thalamus (at least somatosensory-related TRN areas) and the synchrony of spindles within local cortical networks.

In line with this hypothesis, electron microscopy reports indicate that although thalamo-cortical and corticothalamic synapses in the reticular nucleus of the thalamus express high levels of AMPA receptors, these contain mainly GluA4 and some GluA2/3 subunits, but GluA1 is barely detectable in this brain region (Mineff and Weinberg, 2000). In contrast, GluA1-rich AMPA receptors are expressed in high levels in synapses between thalamo-cortical projecting cells and fast-spiking interneurons in the cortex. The GLuA1 subunit has been proposed to play a role in the precise spike timing of fast-spiking cells and to affect the power expression of gamma oscillations, at least in hippocampal slices (Fuchs et al., 2007). In the case of the thalamo-cortical network, it has been suggested that among other mechanisms, these GluA1-rich AMPA receptors could provide rapid activation kinetics capable of recruiting feedforward inhibitory circuits that could propagate spindles across cortical circuits (Fernandez and Lüthi, 2020). In fact, there is evidence suggesting that spindle network synchrony is regulated by intracortical connectivity and cortico-thalamic feedback control (Contreras and Steriade, 1996; Kandel and Buzséki, 1997; Bonjean et al., 2011; Timofeev and Chauvette, 2013). It is possibly that the recruitment of feedforward inhibitory circuits, is impaired in GRIA1$^{-/-}$ mice, and this could relate to the spindle profile observed in our results.

Laminar recordings of cortical activity combined with recordings or manipulations of the reticular nucleus of the thalamus, would be relevant for further understanding of the association between GluA1, cortico-thalamic feedback control, and spindle network synchrony. Furthermore, although the current results suggest that the spindle deficits caused by the deletion of the GluA1 AMPA receptor subunit reflect a large-scale

network synchronisation deficit, it remains to be directly assessed whether the reticular nucleus of the thalamus remains unaffected in these mice.

4.4.2. Potential neural mechanisms underlying local and global sleep spindles

Our results are also consistent with previous studies (Andrillon et al., 2011; Piantoni et al., 2017; Fernandez et al., 2018), and the results we reported in Chapter 3, indicating that spindles express as both local and global phenomena. In addition, the present results demonstrate that local spindles can still occur even when global EEG spindles are substantially reduced. Different processes could explain this pattern of spindle expression.

On the one hand, the pattern of preserved local spindles in the absence of global spindles in GRIA1$^{-/-}$ mice could suggest that, to a certain level, different mechanisms support the generation of local and global spindles. In fact, it has been previously suggested that two different pathways might give rise to local and global spindles. Specifically, focal thalamic projections from core relay cells to cortical layers-IV/V have been proposed to generate localized spindles, while diffuse thalamic projections from matrix relay cells to superficial cortical layers are thought to generate more synchronous and spatially coherent spindle activity (Bonjean et al., 2012; Krishnan et al., 2018). Assuming this hypothesis, it is possible that the deletion of GluA1 preferentially affects the thalamo-cortical matrix pathway, which would restrict the capacity of the network to give rise to synchronized and widespread EEG spindles.

On the other hand, the ability of synaptic weights to adapt to the timing of oscillatory activity is a crucial process for the convergence of synchronous states in the brain (Karbowski and Ermentrout, 2002; Takahashi et al., 2009). The GluA1 AMPA receptor subunit is known to underlie a primary mechanism for synaptic plasticity (Diering, Gustina and Huganir, 2014). Long-term (Zamanillo et al., 1999; Andrásfalvy et al., 2003) and short-term (Romberg et al., 2009; Erickson et al., 2010) forms of synaptic plasticity have been found to be reduced in GRIA1$^{-/-}$ mice. It is possible, therefore, that the spindle deficits in GRIA1$^{-/-}$ mice reflect deficits of synaptic weights to adjust to widespread oscillatory dynamics in the brain. Having said this, it also important to be cautious when interpreting the current results. The GRIA1$^{-/-}$ mouse line used here, is a constitutive knockout and compensation mechanisms can affect the observed results. Of particular importance in this respect, are previous studies highlighting that long-term potentiation can be supported by a variety of glutamate receptor subtypes (Romberg et al., 2009; Granger et al., 2013). Overall, further research is needed to test these hypotheses and to investigate the potential origin and differential mechanisms of local and global spindles.

4.4.3. Potential effects of the deletion of GluA1 on the association between slow waves and spindles

Aside from having a potential direct effect on spindle network synchrony, the deletion of GluA1 could also affect other brain processes that affect the large-scale synchrony of spindle activity. For instance, cortico-thalamic feedback and more specifically, the coupling with slow waves is thought to provide synchronization and spatial coherence

to spindles across widespread thalamic and cortical areas (Contreras and Steriade, 1996; Buzsáki and Draguhn, 2004; Staresina et al., 2015a). We found that slow-wave activity (i.e. incidence, amplitude and amplitude of slow-waves) and the coupling between slow-waves and spindles is preserved overall in GRIA1$^{-/-}$ mice. Interestingly, however, the direct relationship between slow-wave activity and spindle *o-Quality,* which was confirmed in different contexts in WT mice, is impaired in the frontal derivation and the cortical layer 5 (i.e. one of the layers that shows highest spindle density) in GRIA1$^{-/-}$ mice.

These results could have different potential implications. On the one hand, they could suggest that although slow-waves may be implicated in the synchronization of local LFP spindles, they are not strictly necessary. As shown in the case of GRIA1$^{-/-}$ mice, spindles can be highly synchronous in local areas (i.e. show high *o-Quality*), without having a strong relationship with the occurrence of slow waves. On the other hand, our results could suggest as well, that slow wave/spindle coupling is relevant for large-scale network synchronization of spindles, which is a prerequisite for their expression at the global EEG level. In this context, the deletion of GluA1 may alter the coupling between slow-waves and high *o-Quality* LFP spindles (which is present in WT but not GRIA1-/- mice), or even disrupt the process through which slow waves entrain and synchronise spindles and, therefore, result in the reduced expression of spindles at the global EEG level.

An interesting observation that arose from our results is that the effect of sleep pressure on SWA varied dramatically between different cortical layers and between genotypes.

In contrast to the frontal derivation and layer 5 of the cortex, sleep deprivation led to a SWA rebound in layer 6 that was significantly higher in GRIA1$^{-/-}$ than WT mice. Intriguingly, the direct association between slow-waves and the *o-Quality* and incidence of spindles, was preserved in LFP signals recorded from this cortical layer. Thus, only in this context of increased SWA in layer 6, is the direct association between slow-wave and spindle activity evident in GRIA1$^{-/-}$ mice. This finding could suggest that GluA1 plays a role in the potential slow-wave induced modulation of spindles. However, further research should be undertaken to investigate this hypothesis.

It remains unclear why the homeostatic rebound of SWA in layer 6 was higher in GRIA1$^{-/-}$ mice relative to WT mice during the first two hours of recovery sleep after sleep deprivation, while it was similar to WT mice in layer 5 and the frontal EEG. On the one hand, previous evidence suggests that the levels and phosphorylation states of GluA1 are consistent with synaptic potentiation during wakefulness, and a homeostatic drive to reduce these levels during sleep (Vyazovskiy et al., 2008). Based on such dynamic, one could expect SWA rebound to be overall decreased in GRIA1$^{-/-}$. Being a constitutive knockout, however, can result in genetic compensation (El-Brolosy and Stainier, 2017) affecting the structure of AMPA receptors and/or expression of other subunits (Granger et al., 2013) as well as a cascade of related cellular processes that could be related with the SWA changes.

On the other hand, sleep deprivation was performed in the home cages of mice, where they were presented with novel stimuli to elicit exploratory behaviour. GRIA1$^{-/-}$ mice have been previously found to show novelty-induced locomotor hyperactivity, including prolonged investigation times and increased attention to novel objects

(Bannerman et al., 2004; Wiedholz et al., 2008; Barkus et al., 2012; Sanderson *et al.*, 2011). These mice also show increased hippocampal-prefrontal theta coherence during exposure to novelty (Bygrave et al., 2019). It is possible that increased exploratory behaviour in GluA1 KO mice during the 6 hours of sleep deprivation could have induced increased sleep pressure and thus increased local SWA during sleep recovery in GRIA1$^{-/-}$ mice. These possibilities remain to be tested and the reason why SWA was increased only in layer 6 remains to be understood.

A more detailed analysis of the dynamics of slow-waves and spindles across cortical layers could serve to address some of the remaining open questions. Laminar recordings were performed from two GRIA1$^{-/-}$ mice and one WT littermate. Further recordings and analyses will be done to address these issues in the future. Additionally, electrophysiological recordings and motion detection (using passive infrared sensors) were collected during sleep deprivation. Future work will be done to better understand the association between behavioural activity during wake and the subsequent changes in slow-wave and spindle activity.

4.4.4. Potential effects of the deletion of GluA1 on the association between the infra-slow oscillation and the spindle o-Quality

Apart from the coupling dynamics between slow-waves and the spindle *o-Quality,* the dynamics of the latter in relation to the infra-slow oscillation of spindle activity was also affected in GRIA1$^{-/-}$ mice. While WT mice showed a progressive increase in spindle *o-Quality* within cycles of the infra-slow oscillation across NREM episodes, in GRIA1$^{-/-}$

mice this type of dynamic was evident only during the first half of a NREM episode. This suggests that although the infra-slow oscillation of spindle activity is preserved in GRIA1$^{-/-}$ mice, the way cortico-thalamic networks are recruited across the cycles of this oscillation is altered. The infra-slow oscillation has been proposed to divide NREM sleep into periods of fragility and continuity of sleep consolidation (Lecci et al., 2017). GRIA1$^{-/-}$ mice have in fact been found to show more fragmented NREM sleep than WT mice (Ang et al., 2018). The association between the dynamics of spindle *o-Quality* across cycles of the infra-slow oscillation, and sleep consolidation is an important issue for future analyses.

4.4.5. Clinical significance of the pattern of spindle deficits in GRIA1$^{-/-}$ mice

Additionally, our results have potential clinical implications given the link between GluA1 and neuropsychiatric disorders like schizophrenia. Several studies have reported that EEG spindles are reduced in patients with schizophrenia (Ferrarelli, 2007; Ferrarelli et al., 2010; Ferrarelli and Tononi, 2016; Manoach et al., 2016; Manoach and Stickgold, 2019), and they further suggest that this reflects deficits in the thalamic reticular nucleus and thalamo-reticular circuits in this disease (Ferrarelli et al., 2010; Ferrarelli and Tononi, 2017). Our results show, however, that local spindles can still be preserved even when EEG global spindles are substantially reduced. This suggests that the deletion of GluA1 might not affect the initiation of spindles within the reticular-nucleus of the thalamus, but rather lead to an impairment at the thalamo-cortical network level. Furthermore, our results suggest the intriguing possibility that large-scale synchronization deficits, resulting from glutamatergic disruption, could alter the

expression of spindles at the global EEG level in schizophrenia, even when (at least some) spindle initiation mechanisms are preserved.

Overall, our results highlight that finding methods to better understand the local and global dynamics of spindles in schizophrenia is an important issue for future research. It is practically unfeasible on a large scale to obtain intracranial recordings from patients with schizophrenia. However, the study of mice with genetic modifications relevant for this disorder, like the study of GRIA1$^{-/-}$ mice, might offer a promising tool to gain mechanistic insights into this disease. In this respect, a relevant question for future research is to understand whether these deficits are also present in other mouse models of schizophrenia (i.e. glutamate and non-glutamate based).

4.4.6. Functional significance of the spindle deficits in GRIA1$^{-/-}$ mice

Spindles are believed to play a crucial role in the consolidation of hippocampal-based memories (Stickgold, 2005; Rasch and Born, 2013). The infra-slow oscillation in the spindle activity is believed to divide NREM sleep into periods of increased and reduced responsiveness to stimulation from the environment (Lecci et al., 2017). During offline periods, it is believed that the coupling between slow-waves, spindles, and sharp-wave ripples facilitates the transfer of information from temporary storage in the hippocampus to long-term storage in the neocortex (Wilson and McNaughton, 1994; Rasch and Born, 2013; Staresina et al., 2015; Latchoumane et al., 2017). Hypotheses like these, have led researchers to attempt to improve memory performance and overall

cognition in schizophrenia by manipulating global EEG sleep spindles (Wamsley et al., 2013; Göder et al., 2015; Mylonas et al., 2020).

The present results suggest, however, that global EEG spindles do not seem necessary for the maintenance of long-term spatial memories (at least over 24 hours). Even when the large-scale synchrony of spindles and their expression at the global EEG level is substantially reduced in GRIA1$^{-/-}$ mice, they show normal performance in hippocampal-based memory tests. This suggests that despite the spindle deficits, these mice manage to build allocentric representations of different environments, and form a long-term association between outcomes and spatial locations. Similar results have been previously shown in other memory tasks, including the water-maze and the reference memory version of the radial maze (Zamanillo et al., 1999; Reisel et al., 2002; Bannerman et al., 2003, 2014; Schmitt et al., 2003; Sanderson et al., 2009). These results argue against a necessary role of global EEG spindles in memory consolidation during sleep, although a role for local LFP spindles or a more nuanced role of spindles in other aspects of memory consolidation cannot be excluded.

It is possible, for instance, that the behavioural tasks performed are not complex enough to reveal a potential role of global EEG spindles in memory processing. For instance, GRIA1$^{-/-}$ mice show reduced goal-directed behaviour and an increased propensity to exhibit habit-like behaviours (Johnson et al., 2005, 2007). It is possible, therefore, that these mice have difficulties integrating new long-term memories into their existing cognitive models of the world (Vyazovskiy et al., 2017), a process that may only be assessed using behavioural tasks with higher complexity. Additionally, GRIA1$^{-/-}$ mice have been found to show deficits in short-term habituation (Bannerman

et al., 2003; Sanderson et al., 2010), and increased sensitization to recently presented stimuli (Sanderson et al., 2011)(Barkus *et al.*, 2014). It is possible, therefore, that EEG spindles play a role in dishabituation during sleep and in restoring attentional capacity to engage in complex goal-directed behaviours during wake (Vyazovskiy et al., 2017). A potential role of spindles in regulating the susceptibility of the brain to external stimuli during sleep (Dang-Vu et al., 2011; Lecci et al., 2017) will be the main topic of the next chapter.



CHAPTER 5 - Insights into the dynamics and function of spindles using auditory stimulation during sleep

5.1. INTRODUCTION

Sleep poses something of an evolutionary paradox. On one hand, organisms are vulnerable to external threat while asleep, yet it seems to be essential to fundamental processes in the brain and body (Siegel, 2005; Cirelli and Tononi, 2008; Anafi et al., 2019). Reduced mobility and an increased threshold to respond to external stimuli are some of the main behavioural criteria defining sleep (Rechtschaffen et al., 1966; Campbell and Tobler, 1984; Carskadon and Dement, 2010). Nonetheless, relevant sensory stimuli still seem to be processed during sleep (Kouider et al., 2014; Blume et al., 2017), or at least can interrupt this state. It appears, therefore, that two opposing needs have to be balanced during sleep to ensure survival: to promote offline periods during which the brain and body can recover while maintaining a certain degree of sensory reactivity to the environment. Mounting evidence suggests that sleep

oscillations, like spindles, are part of a network that plays a crucial role in the way that the brain balances these two needs (Lecci et al., 2017; Fernandez and Lüthi, 2020).

Sleep spindles were first described by Alfred Loomis, E. Newton Harvey and Garret Hobart in 1935, who identified them as brain responses to auditory stimulation. Performing brain potential recordings in sleeping humans during the presentation of auditory stimuli, they noted that: "when asleep, sounds of a certain character [...] will quite regularly initiate a train of waves which may last for from 5 to 8 seconds (frequency 9 to 10/seconds) and then die out" (Loomis et al., 1935). **Figure 29** shows an example of these recordings. Since then the association between auditory stimulation and spindle activity has been widely studied, and has revealed important insights into some of the potential functional roles of sleep oscillations. Overall, the most widely accepted hypothesis is that spindles are both protective and reactive to external stimulation. They protect sleep from sensory disruption (Yamadori, 1971; Steriade, 1991; Elton et al., 1997; Cote et al., 2000; Lecci et al., 2017), but they can also be induced by auditory stimuli (Antony and Paller, 2017; Lustenberger et al., 2018), as discussed below.

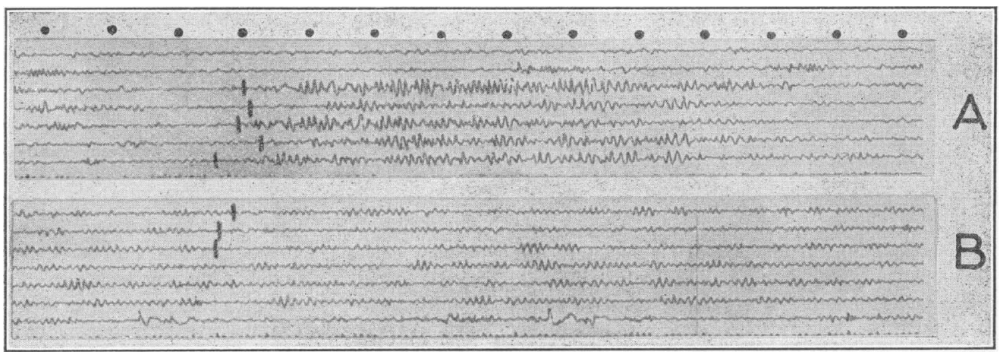


Figure 29. First evidence of spindle-like activity. *Brain potential recordings taken from a human subject during wake (A) and sleep (B) published by* Loomis, Harvey and Hobart (1935).

They *show the first examples of spindle-like activity. The vertical marks represent time point when sensory stimuli were delivered.*

5.1.1. A potential role of spindles in the protection of sleep from sensory disruption

One of the most popular views regarding the functional role of spindles is that they support the maintenance of sleep by disrupting the transfer of sensory stimuli to the cortex. Supporting this hypothesis, human studies have shown that sensory stimuli (i.e. auditory or somatosensory) fail to generate evoked responses in the cortex and need to have increased intensity to waken subjects, when stimulation occurs in phase with spindle events detected in the thalamus or cortex (Yamadori, 1971; Elton et al., 1997; Dang-Vu et al., 2010; Lecci et al., 2017). Additionally, the density of EEG spindles during spontaneous sleep positively correlates with the tolerance shown by subjects to environmental noise during sleep (Dang-Vu et al., 2010). Combined EEG and fMRI studies in humans, have also shown that pure tones (e.g.400Hz, 100ms) elicit activation in the thalamus and primary auditory cortex, which is similar during NREM sleep and wake, but is reduced or absent when the sounds are paired with spindles or the down-states of the slow oscillation (Dang-Vu et al., 2011; Schabus et al., 2012).

The potential role of spindles in protecting sleep from environmental disruption has been attributed to the thalamic origin of these oscillations. The thalamus is an important station for the relay of sensory information to the cortex (McCormick and Bal, 1994) and an important control centre that shapes sensation and action (Halassa and Acsády, 2016). These operations require precise inhibition control, which is largely

driven by innervation from structures like the reticular nucleus of the thalamus (Steriade et al., 1987; McCormick and Feeser, 1990; Pinault, 2004). Specifically, both thalamo-cortical neurons and neurons in the reticular nucleus can display tonic and bursting firing modes (Steriade et al., 1986), which were described in Chapter 1 *General introduction*. While these two firing modes seem to relay sensory information to the cortex, it has been found that burst firing generated during spindles can distort these sensory inputs (McCormick and Feeser, 1990; Murray Sherman, 2001). Specifically, this burst firing seems to reduce the action potential output that TC neurons generate relative to their excitatory input. This has been proposed as one of the mechanisms through which burst firing in thalamo-cortical networks, which gives rise to oscillations like spindles, could disrupt the transfer of sensory stimuli to the cortex during sleep (Astori et al., 2013). In line with these hypotheses, mice over-expressing Ca^{2+}-dependent small-conductance-type 2 potassium (SK2) channels (which have been found to support spindle generation), show enhanced thalamic spindle activity together with decreased responsiveness to noise exposure during sleep (Wimmer et al., 2012).

Contrary to these previous results arising from non-invasive recordings, recent studies measuring neuronal activity during natural sleep more directly do not seem to support the sensory-gating hypothesis of spindle function. Intra-cortical recordings of neuronal activity and local field potentials (LFP) in rodents show that the response of neurons in the primary auditory cortex to short sounds (100ms) presented at a variety of frequencies and intensities (8-45 kHz, 30–80dB), is preserved regardless of the presence of spindles in this area (Sela et al., 2016). Moreover, in this study it was reported that auditory stimuli led to an early termination of a subset of spindles (evident ~150ms after stimulus onset), when sounds with high intensity were

presented. Specifically, 4% and 11% of spindles detected in the auditory cortex showed and early termination when sounds were presented at 60dB and 80dB, respectively.

These results might suggest that spindles do not interrupt the transmission of sensory information to primary sensory areas, like the primary auditory cortex, during sleep. It is also possibly that the capacity of spindles to protect sleep depends on the intensity of the presented stimuli. On the other hand, in Chapter 3 of this thesis we demonstrated that spindles show a substantial variability in properties such as their *o-Quality,* amplitude and duration. It is possible, therefore, that the potential effect of spindles on sensory processing during sleep depends on the *o-Quality* (i.e. strength) of each specific spindle event. This is an open question, which is outside of the scope of the present thesis, but will be addressed in the future, using the data collected here.

5.1.2. The effect of auditory stimulation on spindle activity

Following the logic that spindles play a role in sensory gating, it has been hypothesised that external stimulation could induce spindle activity. The first anecdotal evidence supporting this came from the aforementioned observations of Loomis, Harvey and Hobart (1935), who reported ~10Hz waves arising in brain potential recordings from environmental sounds. More recent studies have attempted to induce synchronized sleep-oscillations using external open-loop stimulation in the forms of electrical, transcranial magnetic, and auditory modalities. These studies have managed to induce cortical slow-oscillations in humans (Massimini et al., 2007; Tononi et al., 2010; Ngo et al., 2013a) and rodents (Vyazovskiy et al., 2009a; Maingret et al., 2016), which are reported to be followed by an increase in spindle amplitude and sigma power. This is

consistent with previous reports, suggesting that spindle activity can be driven by the depolarised up state of the slow-oscillation (Steriade, 1993; Niethard et al., 2018).

In addition, a few studies have reported inducing immediate spindle-like EEG activity in the parietal and frontal cortex of sleeping humans using open-loop oscillatory sounds (i.e. white noise) mimicking the rhythm of spindles (Antony and Paller, 2017; Lustenberger et al., 2018). Interestingly, these studies report to induce a frequency-specific effect such that slow spindles (10-13 Hz) were predominantly enhanced by white noise oscillating at 12Hz, while fast spindles (14-15 Hz) were predominantly enhanced by white noise modulated at 15Hz. Control conditions using white noise modulated outside the spindle frequency-range (i.e. 40 or 50 Hz) have resulted in inconsistent results. Specifically, they appear to disrupt spindles in some cases (Antony and Paller, 2017), and promote spindles in some others (Lustenberger et al., 2018) .

Different studies have demonstrated that the brain state and precise timing at which sensory stimuli is presented during sleep, substantially determines the type and intensity of the evoked response. For instance, auditory stimulation (i.e. pairs of white noise clicks) presented during stable bouts of NREM sleep (Ngo et al., 2013a), and specifically in phase with the slow-oscillation up state, has been reported to be particularly effective in enhancing the amplitude of slow-oscillations and related spindle activity (Ngo et al., 2013b; Navarrete et al., 2020). Additionally, a refractory period of 2-3s after spindle termination has been reported, during which the probability that another spindle can be evoked is diminished (Antony et al., 2018).

As a result, closed-loop auditory stimulation[1] during NREM sleep has started to be widely used to modulate the activity of sleep oscillations and study their functional role. Different studies report enhancing slow-wave and spindle activity in parietal and temporal regions during NREM sleep, by presenting auditory stimuli (i.e. white noise single pulse, paired-pulse or click trains) both: in phase with the up-state of the slow oscillation (Ngo et al., 2013b; Ong et al., 2016; Leminen et al., 2017), and outside the 2-3s post-spindle refractory period (Antony et al., 2018). These studies claim enhancing declarative memory consolidation with their intervention.

Other studies, however, have replicated the enhancement of slow-oscillation and spindle activity, but have not found an improvement in declarative or spatial memory with such intervention (Miller et al., 2013; Henin et al., 2019). This null result persisted even when trying to replicate previous methodologies that had reported a positive effect on memory consolidation (Henin et al., 2019). Additionally, some studies have failed to evoke spindle activity using closed-loop auditory stimulation in phase with the slow-oscillation up-state (Ngo et al., 2019).

Several factors could explain the inconsistencies found in this field of research. In the first place, the potential mechanisms by which auditory processing affects the dynamics of sleep oscillations have not been systematically studied. Similarly, the mechanisms by which sleep oscillations might support memory consolidation remain a matter of debate (Rasch and Born, 2013; Tononi and Cirelli, 2014). Furthermore, the

[1] In the neuroscience literature the term 'closed-loop system' has been typically defined as a setup where a brain oscillation (or event) is detected on real time and triggers a stimulus. Technically, a closed-loop system is one that automatically regulates itself towards a desired set point (Mayr and Johnson, 1976). The feedback systems discussed in this thesis are, therefore, not strictly closed-loop systems, but the term will be kept to remain consistent with the literature.

aforementioned studies report the effect that auditory stimulation has on the slow oscillation, spindle activity and memory performance, without taking into consideration how the exerted manipulation affects sleep architecture as a whole and the dynamics of sleep-related oscillations.

Previous work, however, suggests that sleep is regulated by two main mechanisms, namely homeostatic and circadian processes, which ensure a balance between wake and sleep by modulating the duration, timing and intensity of these states (Borbely, 1982; Borbély et al., 2016). Although the exact nature of the homestatic sleep drive is unknown, the dynamic of the slow-wave activity has been found to be a reliable marker of sleep homeostasis across mammals (Borbely, 1982; Tobler, 2010; Borbély et al., 2016). Given this type of regulation, it is possible that the acute manipulation of sleep oscillations using sensory stimulation has an impact on their overall dynamics that is not taken into account when interpreting the effects of such manipulations. It has been proposed that slow-wave activity and sigma power are regulated in an opposite manner and spindles are suppressed when sleep pressure is high (Dijk, Hayes and Czeisler, 1993; Knoblauch et al., 2003; Vyazovskiy et al., 2004). However, to date, whether the sleep spindle activity is regulated in a homeostatic fashion, has not been extensively studied.

To address some of these issues, here we investigated the effect of presenting long (8-s) and short (i.e. 500ms) pure tones to mice during sleep, on the dynamics of LFP spindle, slow-wave, theta activity, as well as multi-unit activity, simultaneously recorded from somatosensory and auditory, as well as EEG signals recorded from frontal regions, across 12-hour light periods. In this chapter, we focus on the results

arising from the S1 and frontal recordings but future work will incorporate results from A1.

For the LFP and MUA recordings, we were interested in S1, as this is one of the cortical regions that shows the highest incidence of spindle activity, as shown in Chapter 3 and reported by different studies (Lüthi, 2014; Kim et al., 2015; Fernandez and Lüthi, 2020). Moreover, different of human studies using auditory stimulation during sleep have reported changes in spindle activity in the parietal lobe (including somatosensory cortex), amongst other brain areas (Antony and Paller, 2017; Lustenberger et al., 2018). Additionally, auditory stimuli are known to generate robust evoked-responses in S1 arising from a variety of sources like the thalamic nuclei (i.e. auditory, somatosensory or multisensory), cortico-cortical A1 to S1 connections, or inputs from higher association areas to S1 (Zhou and Fuster, 2004; Lemus et al., 2010; Maruyama and Komai, 2018). Although its relevant to mention that sounds can also induce whisker vibrations or twitches in rodents even under anaesthesia (Neimark et al., 2003). These potential mechanisms are further discussed in the context of our results below.

We were also interested in exploring the hypothesis that spindles protect sleep from sensory disruption. To do this, we developed for the first time a real-time auditory stimulation system to detect spindles and deliver sounds at the time of these spindle events in real time (typically referred to as "closed-loop auditory stimulation system" within the neuroscience field). Previous studies have used these "closed-loop" approaches to deliver sounds based on the slow-oscillation phase but not based on spindle activity directly. The main principles of this real-time stimulation system will

be presented, as well as some preliminary results addressing the potential role of spindles in protecting sleep from sensory disruption.

The overall aim of this chapter is, therefore, to use auditory stimulation to investigate the effects of modulating sleep oscillations on the architecture and dynamics of sleep, and test the hypothesis that spindles protect sleep from sensory disruption. Overall, the results of this chapter suggest that spindles are regulated in a homeostatic manner. Additionally, our results seem to be in line with the hypothesis that spindles protect sleep from sensory disruption, however, they also suggest that the interaction of spindles and auditory processing is very complex and highly depends on the timing and characteristics of the presented sound.

5.2. METHODS

5.2.1. Animals

Experiments (included in this thesis) were performed in adult male C57BL/6 mice (n=12, Harlan UK Ltd, Bicester, United Kingdom) and GRIA1$^{-/-}$ mice (n=7 KO; n=7 WT littermates). Mice were aged 3 months old. During the experiments, mice were individually housed in plexiglass cages (20.3 x 32 x 35cm) under a 12:12 light-dark cycle (lights on at 9am). Cages were housed in sound-attenuated, ventilated Faraday chambers. Five mice underwent electrophysiological recordings from S1 (LFP and MUA) and frontal (EEG) areas during baseline sleep and the presentation of sounds following a semi-periodic stimulation paradigm (i.e. sounds presented every 45s or 10s with a jitter of 5s, as described below). Seven mice underwent electrophysiological

recordings from S1 and A1 (LFP and MUA) as well as frontal (EEG) areas during baseline sleep and during the presentation of sounds following a closed-loop stimulation paradigm.

The C57BL/6 mouse strain used here is the strain most widely used in laboratories and the most common genetic background for genetically modified mouse strains. As such, it is a useful model to use in neuroscience research. C57BL/6 mice, however, are known to present age-related progressive hearing loss, which results from a mutation in the Cdh23 locus (Noben-Trauth et al., 1997). This hearing loss starts approximately at 2 months of age, affecting initially the highest spectral frequencies (~100 kHz in mice) and progressively affecting lower frequencies over the next 12 months (Ison et al., 2007). We, therefore, performed the present experiments in 3-month old mice and used sound stimulation with frequencies (i.e. 5-16 KHz) known to be preserved in mice of this age.

Moreover, we replicated all the experiments carried out with C57BL/6 mice, on a novel C57BL/6 strain (C57BL/6NTac.Cdh23$^{753A>G}$), in which the Cdh23ahl allele that predisposes these mice to age-related high frequency hearing loss was corrected (Mianné et al., 2016). These experiments were performed on three of the auditory function rescued mice and results were consistent with those obtained using C57BL/6 mice. Detailed analyses of the results from the C57BL/6NTac.Cdh23$^{753A>G}$ mice will be presented in future work, when more mice are included, but are beyond the scope of this thesis.

5.2.2. Surgical Procedure

Recordings of EEG, LFP and EMG signals, as well as multi-unit activity (MUA), were performed on the fifteen mice during the 12-h light period of baseline sleep and auditory stimulation. Details on the surgery procedures undertaken to record EEG and EMG signals can be found on Chapter 2. Surgical Procedure. To obtain LFP and MUA recordings during the experiments using semi-periodic auditory stimulation, five of these mice were implanted with 16-channel laminar probes (NeuroNexus, A1x16-3mm-100-703, 100µm spacing) in S1 (-0.5mm AP, −3.25mm ML, and 32° inclination). This electrode configuration allowed us to record signals across layers of the S1 cortex. **Figure 30** shows a schematic of these implants.

In addition to this, for the experiments using closed-loop auditory stimulation, seven mice were implanted with intra-cortical recording electrodes both in S1 and in the primary auditory cortex (A1). Specifically, 16-channel laminar probes (NeuroNexus, A1x16-3mm-100-703, 100µm spacing) were implanted in S1 (+0.26mm AP, −3.25mm ML) using an inclination of 32° to record in parallel to laminar layers (

Figure *30*.A).

Regarding A1, 16-channel 4x4 probes (NeuroNexus, A4x4-3mm-100-125-703, 100µm spacing) were implanted (-2.46mm AP, −2.75 to -3.55mm ML) with an inclination of 27° in order to achieve recordings from Layers 2/3, 4, and 5, where (as reported in Chapter 3) the incidence and *o-Quality* of spindles in S1 is high (**Figure 30.B**). Histological evidence suggests that the implants were located in Layers 4, 5 and 6.

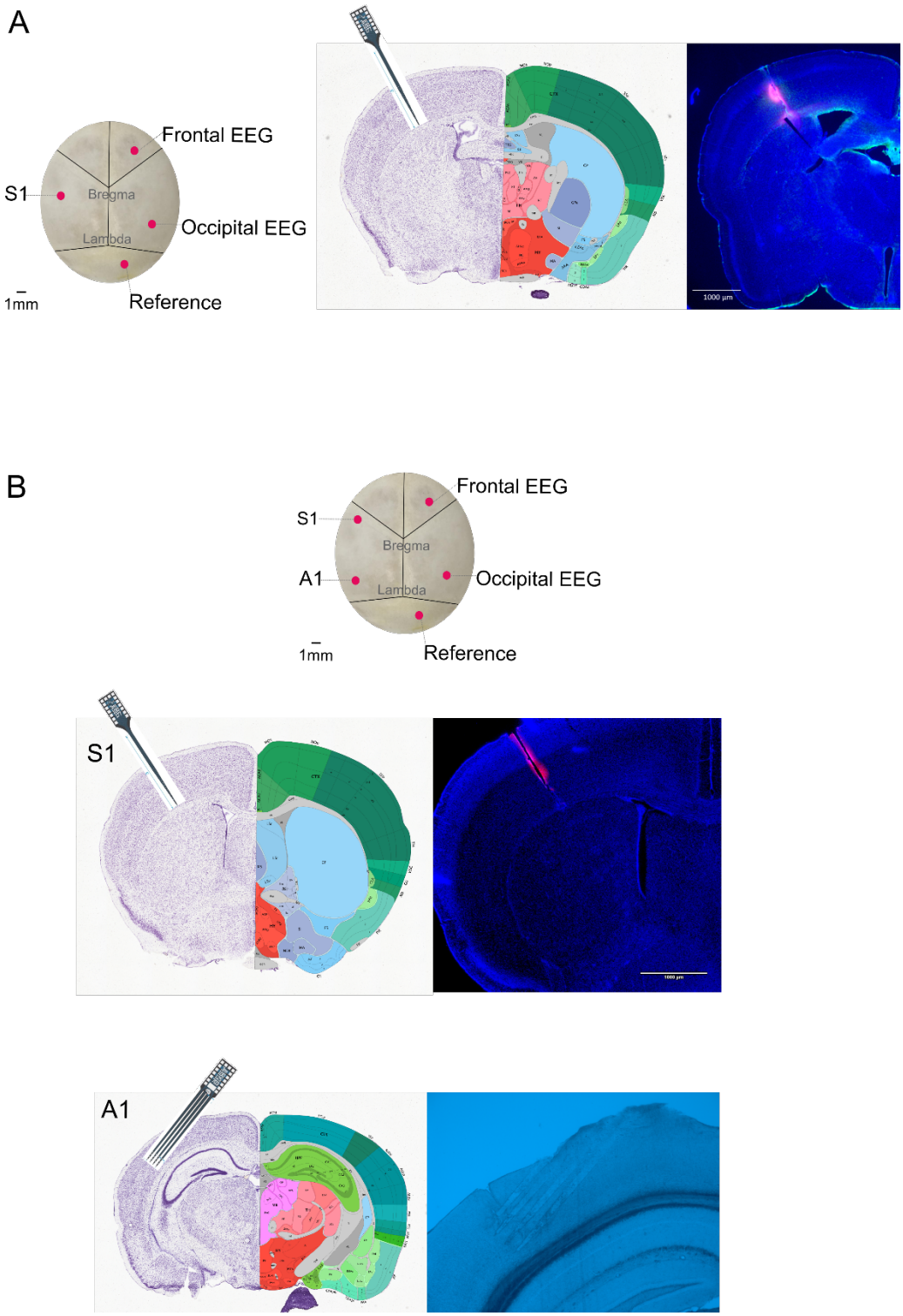


Figure 30. Schematic of implantation sites and histology. (A) *Implantation locations for the first set of experiments using semi-periodic auditory stimulation. Mice were simultaneously*

*implanted with EEG screws (frontal and occipital) and a 16-channel laminar probe in S1. (**B**) Implantation locations for the second set of experiments using closed-loop stimulation. Mice were simultaneously implanted with EEG screws (frontal and occipital), one 16-channel laminar probe in S1, and one 16-channel (4x4) probe in A1. **(A,B)** Right – The laminar location of the electrodes was verified with histological evidence of electrolytic microlesions made at the end of recordings and DiI stained electrode traces (magenta) on brain slices stained with DAPI (blue). The recording coordinates for each implant type were identified using the Allen mouse brain atlas (Allen, 2007). Different colours and boundaries highlight different brain areas.*

Previous studies have detected spindles in the rat auditory cortex (Sela et al., 2016). Studies performed in mice, however, have shown that both sigma power and the incidence of spindles are substantially reduced in the auditory cortex relative to S1 (where spindles are prominent) (Fernandez et al., 2018). Careful visual inspection of the signals recorded from A1 did not reveal spindle events in any of the animals or recording channels. This does not suggest that spindles are not present in A1, but rather they were not easily discernible in our data. (Further work is required to determine whether spindles are present in A1). This result will be further discussed in the context of our results. Following on from this, the response of A1 neurons to the sound presentation in these experiments is outside the scope of this thesis, but is an interesting avenue that will be pursued in future work.

5.2.3. Auditory Stimulation

Open-field auditory stimulation was performed in the mice's home cage (sound-attenuated Faraday chambers, where mice were single-housed). Sounds were played through magnetic speakers (MF1 Multi-Field Magnetic Speakers, Tucker-Davis

Technologies) mounted on the chamber ceilings. A pilot auditory-stimulation session during sleep was performed on three mice to identify sound parameters that generated an evoked response in S1 without keeping mice in a constant state of arousal. Fifty (n=50) different sounds, which ranged in frequency (between 4KHz–16kHz) and intensity (between 60dB–90 dB) were used. We found that sounds ranging between 5KHz to 12KHz at an intensity of 80 dB gave the best compromise, and therefore we used these parameters for the following experiments. In all experiments, the sound intensity was calibrated using a sound level meter, with the help of Dr. Fernando Nodal from the University of Oxford. Note that for all experiments the order in which different sound types were presented, was counterbalanced across mice.

5.2.3.1. Semi-periodic auditory stimulation

For the first set of experiments, addressing the question of how auditory stimulation affects sleep architecture, we presented auditory stimuli to mice (n=5 C57BL/6) in a semi-periodic fashion during 12h light periods. One day before starting the experiments, mice were habituated to the sounds by repeated exposure at varying times of the day. On the days when experiments were carried out, two 2-hour auditory stimulation sessions were presented during each 12h light period. The first session was presented 45 minutes after light onset (zeitgeber time ZT 0.75 – ZT 2.75) when sleep pressure is highest (Borbély et al., 2016). The second session was presented eight hours after light onset (ZT8-ZT10), when sleep pressure is lower and REM sleep is more pronounced (Jouvet, 1967; Borbély et al., 2016). **Figure 31.A** provides a schematic representation of the stimulation paradigm across 12h light periods.

Following the aforementioned paradigm, two different experiments were performed on different days. In the first one, the auditory stimulation sessions were composed of sounds played every ~10s (jitter: 5s) for a duration of 500ms **Figure 31.B**. In the second experiment, the auditory stimulation sessions were composed of sounds played every ~45s (jitter: 5s) for a duration of 8-s **Figure 31.C**. In both cases, these sounds were either a 5 KHz pure tone played with an intensity of 80 dB (stimulation condition) or 0 dB (sham condition, i.e. silence). The stimulation and sham conditions were applied on two different days (separated by at least 48 hours) and the presentation order was counter-balanced across mice. EEG, EMG, LFP and MUA recordings were continuously performed during the days of stimulation.

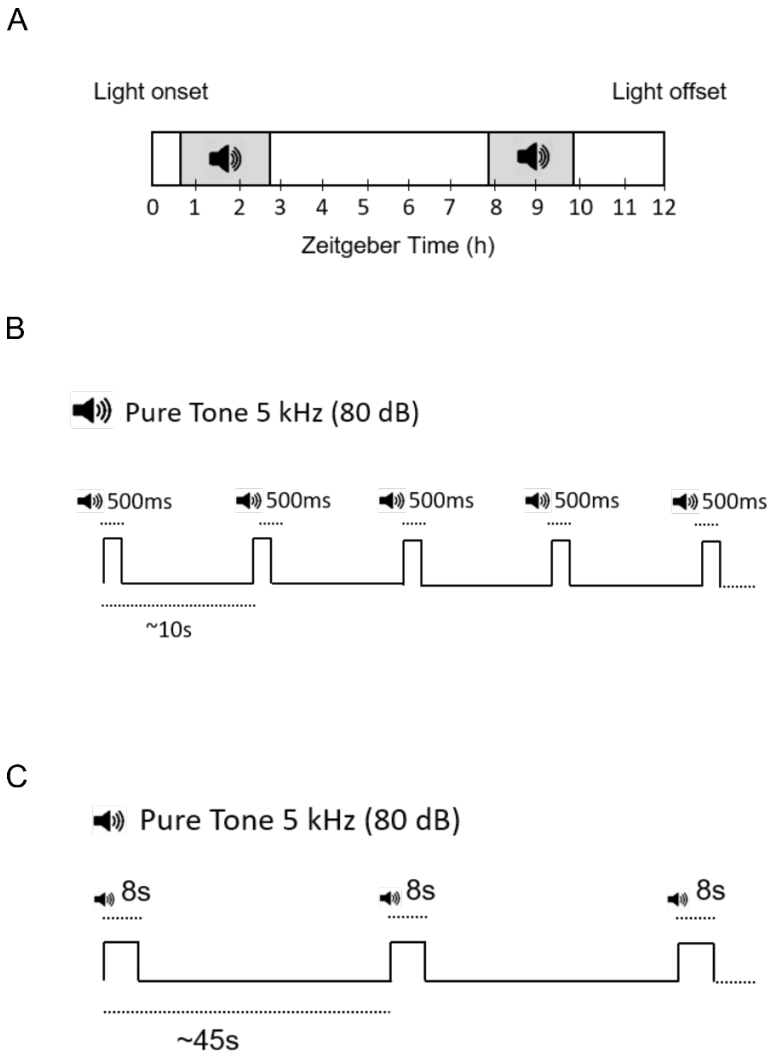


Figure 31. Schematic of the semi-periodic auditory stimulation paradigm. (A) *Schematic of the structure of the semi-periodic auditory stimulation paradigm across 12h light periods (white bar). Zeitgeber time indicates the time from light onset (lights on at 9am; lights off at 9pm). The shaded boxes indicate the times during which the auditory stimulation paradigms were carried out.* ***(B)*** *Pattern of stimulation presented during the first set of experiments, which consisted of 500ms sounds played every ~10s for two hours.* ***(C)*** *Pattern of stimulation presented during the second set of experiments, which consisted of 8-s sounds played every ~45s for two hours.*

5.2.3.2. Closed-loop auditory stimulation

Another set of experiments, were performed to study both the protective effect of spindles on sleep, and their reactive behaviour upon sound presentation. During these set of experiments, auditory closed-loop stimulation was performed to play sounds at the time of spindle occurrence. Auditory stimulation was presented 3.5 and 9.5 hours after light onset during the light period (i.e. ZT 3.5- ZT 9.5) and electrophysiological recording were performed during the whole 12h light period **Figure 32.C**. Two type of experiments were performed:

First, to investigate whether spindles in S1 can be modulated by sounds mimicking spindle activity, click trains with frequencies of 12Hz (i.e. within spindle frequency range) and 40Hz (i.e. control) were presented upon detection of spindles in S1, on two different days. Sham stimulation was also presented on different days by presenting these train clicks using an intensity of 0 dB (i.e. silence) (**Figure 32.D**). For these experiments, mice were habituated to the sounds by repeated exposure at varying times of the day, one day before experiments started.

Second, to investigate the hypothesis that spindles protect sleep from sensory disruption, brief (100ms) sounds were presented at 70dB (sound condition) or 0dB (sham, i.e. silence) during and in the absence of spindle events (**Figure 32.E**). The effect on the EMG activity (i.e. movement) was assessed here, although future analyses will include a detailed analysis of the neuronal responses in S1 and A1 upon sound presentation.

For these experiments, an auditory closed-loop stimulation algorithm was developed using the electrophysiological software Synapse (Tucker-Davis Technologies Inc., Alachua, FL, USA). The delivery of auditory stimuli was timed by the real-time detection of putative spindle events detected in LFP signals recorded from the S1. Specifically, for each mouse, the recording channel showing highest incidence of spindles (typically layer IV) was chosen for real-time detection. The following steps were taken for real-time detection and stimulation: (These processing steps and examples of real-time spindle detection are illustrated in **Figure 32.A-B**).

A. *Signal filtering:* The selected LFP signals were first filtered with a high-pass filter at 0.1 Hz and low-pass filter at 100 Hz, and stored at a sampling rate of 305 Hz. A second order parametric filter was then applied to filter the signal between 10-15 Hz. Parametric filters offer control of parameters such as the centre frequency and bandwidth of the filtering process. Therefore, they are efficient for boosting the signal band of interest and filtering out content outside that band (Van Waterschoot and Moonen, 2007). In our case, we chose a centre frequency (Fc-1) at 12.5 Hz and a fractional bandwidth (Bw-1) of 0.4. Additionally, second order filtering makes the attenuation of signals outside the selected band sharper, so their roll off (i.e. in our case: letting 9 Hz or 16Hz signal pass) is low (Van Waterschoot and Moonen, 2007).

B. *Power proxy calculation:* Next, we calculated a proxy for the power of the filtered (10-15 Hz) signal. The power of a signal is the sum of its absolute squares divided by its timespan. Real-time detection of spindles (which last around 0.5 to 3s) requires such a calculation to be fast. Therefore, we used

the square of the signal as an approximation of its power. Note that we also tried using the root mean square (RMS) of the signal as the proxy. However, this was not fast enough to detect spindles in real-time.

C. *Smoothing:* To further remove the chance of spurious detections resulting from noise in the data, we performed smoothing of the power signal. We used an exponential smoothing function, which applies an exponentially decreasing weight to the data as a function of time. In this way, the calculation is front-loaded such that the further back in time the power is calculated, the less of an effect it had on the real-time power signal.

D. Threshold-based detection: The smoothed power signal was amplified and a threshold constant value was set to detect spindles based on the power proxy of the signal at 10-15 Hz. This threshold was varied between different experiments, depending on the aim of each one of them, but was kept constant within experiments. Based on a performance comparison with the AR spindle detection algorithm (described in detail in Chapter 3), the threshold for real-time detection was set at a range of 3.5 to 4.5 times the mean of the smoothed power signal. We ran a pilot session for each mouse to confirm the accuracy of the real-time spindle detection by visual inspection and exploring the spectral density of the signal around each detection. As mentioned in Chapter 3, using a single constant threshold is arbitrary and was chosen here as an initial approach that was sufficiently fast to detect spindles. Future work can include varying this threshold to detect spindles with varying *o-Quality.* For the current work, the *o-Quality* of spindles was characterised offline.

E. *Restricting stimulation to NREM sleep:* In order to restrict the detection and stimulation of spindles to NREM sleep (i.e. avoiding REM sleep and movement), we set two condition that had to be met for the algorithm to deliver an output. First, we calculated the proxy power of the EMG signal (recorded from two stainless steel wires inserted on the nuchal muscle). During the pilot session, one threshold was set for each mouse to distinguish between movement and immobility. Second, following the procedure explained above, we filtered the occipital EEG signal between 4 and 7 Hz (i.e. theta frequency range, which is prominent during REM sleep) and calculated a power proxy for this filtered signal. During the pilot session, a corresponding threshold was set for each mouse to identify REM sleep. If either of these two conditions were met (i.e. mobility or high theta power in the occipital derivation) no auditory stimulation would be delivered.

F. *Output:* Auditory stimuli were designed with Synapse software. The algorithm was set to deliver these stimuli only when a spindle was detected AND no movement or REM sleep were present. Three different sounds were designed for different experiments: 2-second 12 Hz clicks, 2-second 40 Hz clicks, and 100ms 12KHz pure tones. These sounds were played at 80dB. Sham versions of each sound were created by replicating them but playing them at 0dB (i.e. silence).

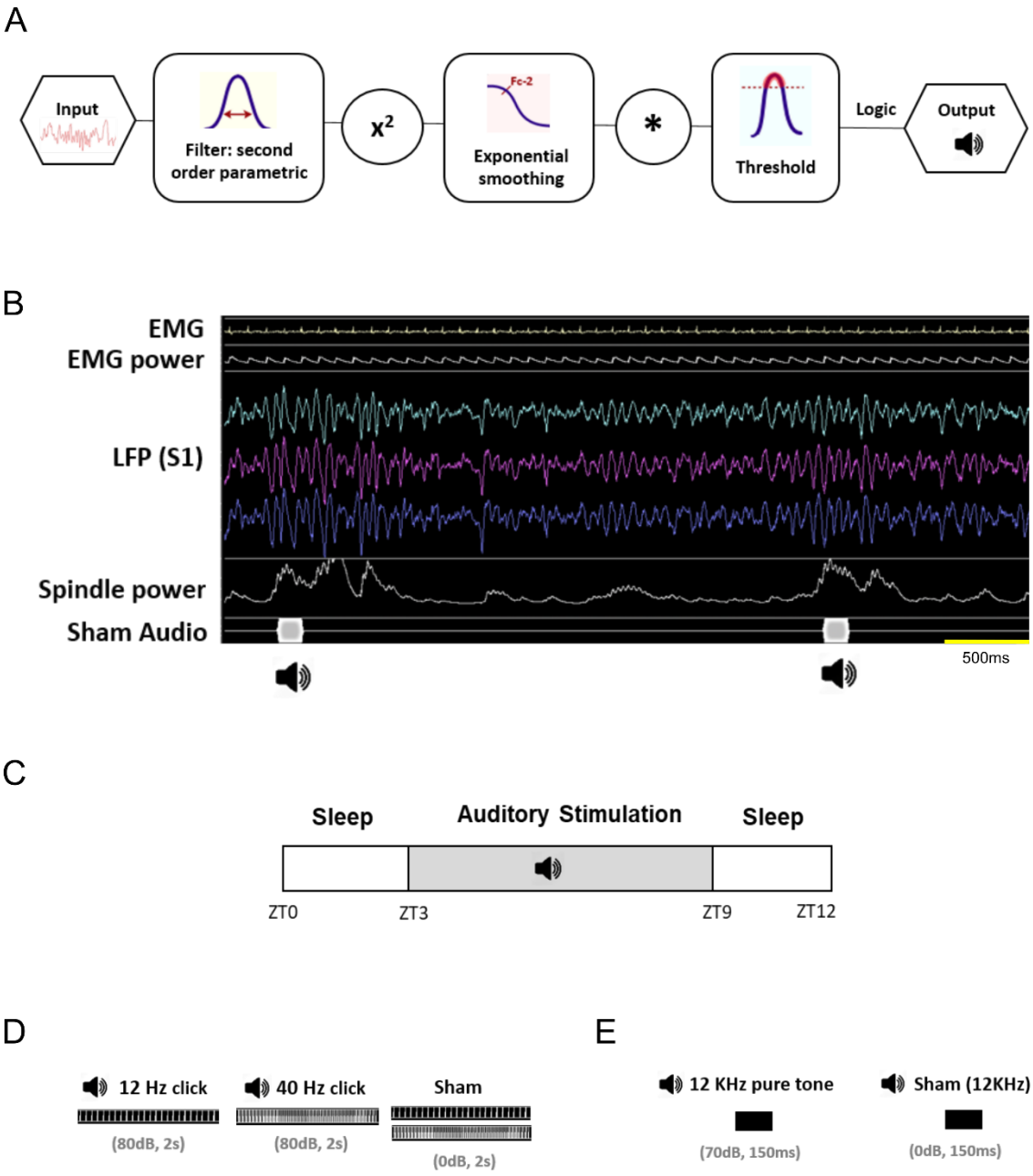


Figure 32. Principles and schematic of the auditory closed-loop stimulation paradigm. (A) *Processing steps followed by the system to detect spindles (10-15Hz) in real time and deliver sounds times-based on these detections.* ***(B)*** *Examples of real-time spindle detection in a sham (0dB sound) condition. Spindles were detected when the power of S1 LFP signals increased and reached a set threshold. Sounds were delivered only if the EMG and theta power in the occipital EEG were low.* ***(C)*** *Schematic of the structure of the auditory-stimulation paradigm performed using the closed-loop system, across 12h light periods (white bar). Zeitgeber Time indicates the time from light onset (lights on at 9am; lights off at 9pm). The shaded boxes indicate the times during which the auditory stimulation paradigms were carried out.* ***(D)*** *Auditory stimuli used*

during a first set of experiment exploring the effect of delivering sounds mimicking spindles on the spindle dynamics. ***(E)*** *Auditory stimuli used during a second set of experiments exploring the hypothesis that spindles protect sleep from sensory disruption. These sounds were played in the presence or absence of spindles.*

5.2.4. Spindle detection

Oscillatory events were detected offline with an algorithm developed by Olbrich and Achermann (2005), and adapted by us to detect spindles with varying damping. This algorithm treats electrophysiological brain signals as a superposition of stochastically-driven harmonic oscillators with damping and frequency varying in time. Briefly, an autoregressive model of order 8 was fitted to overlapping (shifted by 1 sample interval) 1-s segments of LFP and EEG signals. Oscillatory events were detected whenever the damping at one or more frequencies exceeded one of five r_b thresholds (r_b = 0.92, 0.93, 0.94, 0.95, 0.96). Detected oscillatory events that had a frequency of around 10 to 15 Hz were selected as 'putative spindles'. This algorithm is explained in detail in Chapter 3 (Methods, section *3.2.7. Spindle detection*).

As explained in Chapter 3, we used the damping strength of detected spindle events, as a measure of their *Oscillatory-Quality* (*o-Quality*). Specifically, we classified all the spindles detected in the LFP and EEG signals into one of five *o-Quality* levels (i.e. oQ1 oQ2, oQ3, oQ4, oQ5), based on the highest r_b threshold they reached (i.e. based on their oscillatory strength). Spindles with low oscillatory strength received a low *o-Quality* index, while spindles with high oscillatory strength received a high *o-Quality* index (section 3.3.2. in Chapter 3 gives a detailed explanation of the *o-Quality* index).

5.3. RESULTS

We collected EEG, EMG, and intra-cortical multi-electrode LFP and MUA recordings in freely moving mice during the presentation of auditory stimuli at different times of 12h light periods. Semi-periodic and closed-loop auditory stimulation paradigms were designed to investigate the effects of auditory stimulation on sleep architecture and the role of spindles in sleep maintenance. We will start by presenting results for the semi-periodic auditory stimulation paradigm. The main aim of these experiments was to address the question of how auditory stimulation affects sleep architecture.

5.3.1. Evidence of a homeostatic regulation of spindles in granular layers of S1 and in the frontal cortex after disruption caused by auditory stimulation

5.3.1.1. Evidence of spindle homeostasis following disruption related to 5KHz pure-tones played for 500ms every 10s

During the first set of semi-periodic auditory stimulation, 5KHz pure tones were played at 80dB for 500ms approximately every 10 seconds. We chose these sounds parameters because previous studies have shown that similar sounds, i.e. 250ms pure tones presented at 80dB, can modulate spindle activity in rodents (Sela et al., 2016). Such stimulation was performed in two 2-hour blocks presented at ~ZT 0.75 – ZT 2.75 and ZT 8 – ZT 10. During each 2-hour block, therefore, 720 sounds were played (i.e. 1440 sounds in total within a 12h light period). Auditory stimulation was performed on two

different days (12h light periods), where sounds were presented at 80dB ('stimulation') on one day and 0dB ('sham') on the other. The order in which different sound types were presented, was counterbalanced across mice.

We found that, on average across mice (n=5) and conditions, 65.32% ± 1.24 (mean ± SEM across mice) (n=941) of sounds were played during NREM sleep, 9.64% ± 2.35 (n=139) of sounds were played during REM sleep, and 25.05% ± 2.74 (n=360) of sounds were played during wake. There was no significant difference between conditions (stimulation vs sham) in the percent of sounds played per sleep/wake state (NREM, REM, wake) ($F_{11,44}$=0.085, p=0.92, ***Table 61***).

First, we analysed sleep/wake architecture during these 12h light periods. During both, the stimulation and sham conditions, mice showed a sleep-wake distribution typical for nocturnal mice. There was no significant difference between the stimulation and sham conditions in total time spent in NREM ($F_{1,4}$=0.009, p=0.93, ***Table 62***) or REM ($F_{1,4}$=0.001, p=0.98, ***Table 63***) sleep. The time spent in NREM and REM per hour was calculated across 12h light periods and no significant interaction was found between time of day and condition (stimulation vs sham) in the case of NREM ($F_{11,44}$=0.74, p=0.69, ***Table 62***) (**Figure 33.C**) and REM sleep ($F_{11,44}$=1.04, p=0.42, ***Table 63***) (**Figure 33.D**). Additionally, we detected brief awakenings, as periods of low voltage, high frequency oscillations in the EEG and LFP signals accompanied by movement, lasting ≤16 seconds. There was no significant difference between the stimulation and sham conditions in the incidence of brief awakenings per minute identified across 12h light periods ($F_{11,44}$=1.42, p=0.24**,** ***Table 64***) (**Figure 33.E**). These results indicate that the

auditory stimulation paradigm did not induce arousals in the mice and did not have a significant impact on the overall sleep/wake architecture.

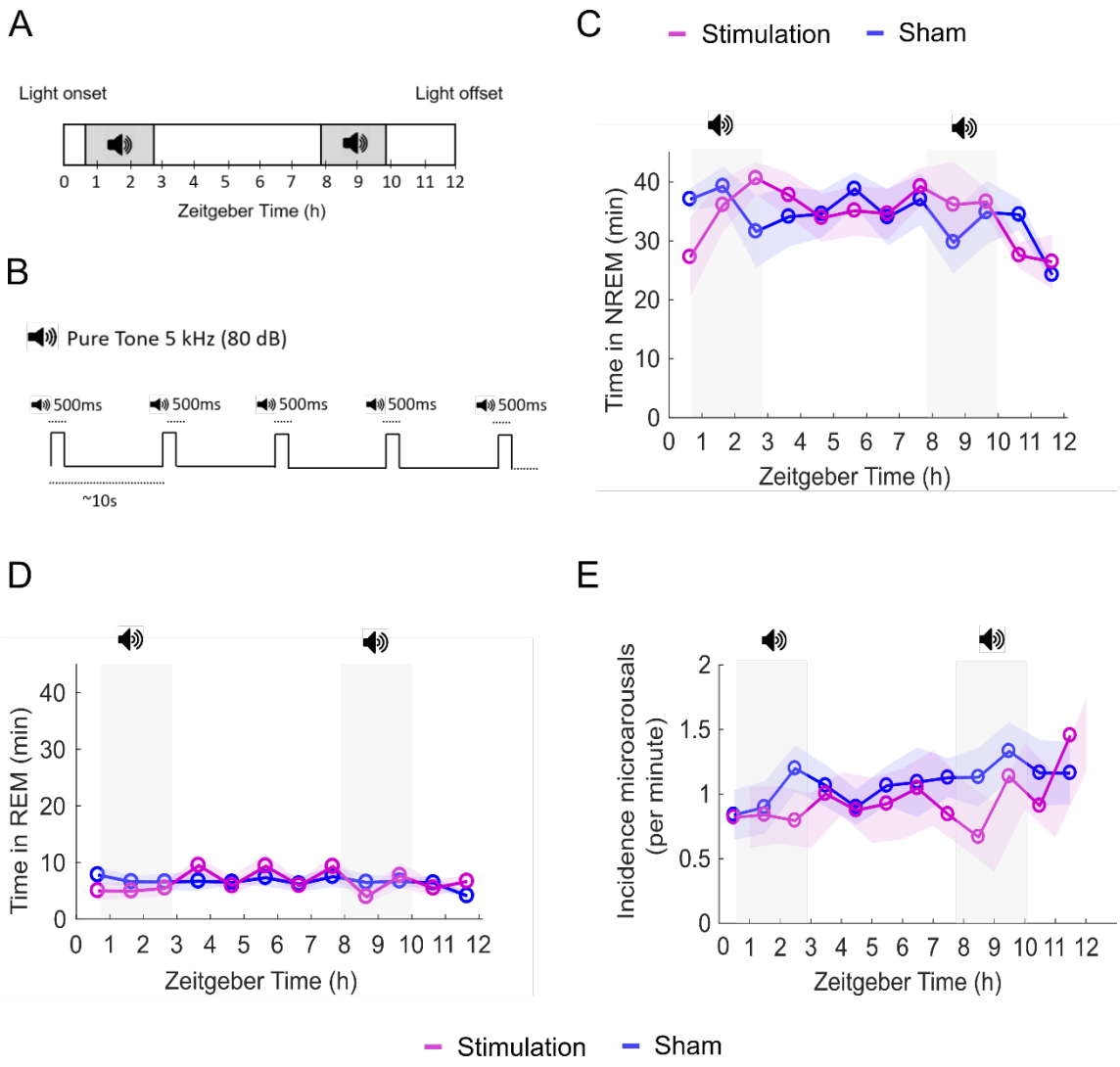


Figure 33. Effects of the semi-periodic auditory stimulation paradigm using 500ms pure-tones (every ~10s) on the sleep/wake architecture. (A) *Structure of the auditory stimulation paradigm across the 12h light period. Zeitgeber time represent time from light onset (9am). The shaded areas represent the time-periods during which auditory stimulation was performed (stimulation blocks).* ***(B)*** *During each stimulation block, the pattern of stimulation consisted of 500ms sounds played every ~10s for two hours.* ***(C,D)*** *Time (minutes) spent in NREM (C) and REM (D) sleep per hour across 12h light periods.* ***(E)*** *Incidence of micro-arousals per minute, averaged*

per hour, across 12h light periods. ***NOTE****: Open circles= mean across mice; coloured shaded areas= SEM of the mean; grey shaded boxes= time-intervals during which auditory stimulation was presented. Zeitgeber time= time from light onset.*

Visual inspection of the signals during the 12h light periods showed that spindle activity in the S1 LFP and frontal EEG signals was substantially reduced during the 2 hours where auditory stimulation was performed. In contrast, spindle activity appeared increased and prominent for a few hours (i.e. ~ 3 hours) following the 2h sound stimulation periods. These results were somewhat surprising, given that previous human studies have reported that sound stimulation (i.e. pure tones or white noise modulated at the spindle frequency range) can induce spindle activity (Ngo et al., 2013a; Antony and Paller, 2017; Antony et al., 2018; Lustenberger et al., 2018). Moreover, if spindles protect sleep from sensory disruption, an increase in spindle activity could potentially be expected at the time of external sensory events. However, it has also been reported in the literature that sound stimulation presented at 80dB can disrupt up to 10% of spindles in the rat auditory cortex (Sela et al., 2016).

We proceeded, therefore, to investigate how the auditory stimulation affected spindle activity across the 12h light periods. We performed these analyses on the S1 LFP channel that showed highest incidence of spindles per mouse (which in all cases was located in Layer 4), and on the frontal EEG. Note that for the results presented in this section, we used one-hour bins to analyse the data. The auditory stimulation starts at ZT0.75 (i.e. at the last quarter of the first 1-hour bin), which means that the first bin contains information from both before and during auditory stimulation. All analyses

were repeated using different duration time bins and the results are consistent with those presented here.

First, we calculated the mean sigma (10-15 Hz) power per hour, and found that the dynamics of sigma power across time differed between conditions (interaction: $F_{11,44}$=3.8, p<0.01, ***Table 65***) (**Figure 34.A**). In the sham condition, as expected, the LFP sigma power showed a linear increase across the 12h light period ($F_{11,44}$=6.92, p<0.001, ***Table 65***). In contrast, in the stimulation condition the LFP sigma power increased across the light period ($F_{11,44}$=8.96, p<0.01, ***Table 65***) but did not follow a linear trend. Interestingly, instead of this, the sigma power was significantly reduced during the periods where auditory stimulation occurred (*ZT1-2*: $F_{1,4}$=11.02, p<0.05; *ZT9-10*: $F_{1,4}$=15.06, p<0.05, ***Table 65***). Moreover, after these periods of reduced sigma activity, a rebound in sigma activity seems to emerge. Specifically, the sigma power increased significantly in the stimulation condition relative to sham (*ZT4-5*: $F_{1,4}$=14.9, p<0.05; *ZT5-6*: $F_{1,4}$=7.62, p<0.05; *ZT10-11*: $F_{1,4}$=31.87, p<0.01, ***Table 65***). Note that similar results, although less pronounced, were obtained for the EEG signal recorded from the frontal derivation.

Next, we sought to confirm whether the changes in sigma power resulting from the auditory stimulation corresponded to changes in spindles properties, such as their incidence, *o-Quality* and duration. All the analyses assessing spindle incidence and duration included all spindles of any *o-Quality*. We found that during the auditory stimulation block taking place at ZT 0.75 to ZT 2.75 (i.e. a time of high sleep pressure), the incidence (ZT1-2: $F_{1,4}$=13.39, p<0.05, ***Table 66***), *o-Quality* (ZT1-2: $F_{1,4}$=6.30, p<0.05, ***Table 67***) and duration (ZT1-2: $F_{1,4}$=6.6, p<0.05, ***Table 68***) of spindle events, detected

with the AR-detection algorithm, were reduced in the stimulation condition relative to sham (**Figure 34.B-D**).

During the second block (ZT 8 to ZT 10), however, the incidence of spindles did not significantly change ($F_{1,4}$=10.61, p=0.07, although showed a strong trend towards a reduction, ***Table 66***) while the *o-Quality* ($F_{1,4}$=10.79, *p*<0.05, ***Table 67***) and duration ($F_{1,4}$=63.24, p<0.001, ***Table 68***) of spindles were again significantly reduced in the stimulation condition relative to sham. This reduction in spindle *o-Quality* and duration, combined with the strong trend to reduced spindle incidence, might explain the decrease in sigma power at this time point. This highlights the relevance of taking parameters like the *o-Quality* of spindles into account, as they provide additional information to understand their dynamics.

In line with the sigma power results, after the periods of reduced spindle activity, the incidence of spindles increased in the stimulation condition relative to sham (ZT4-5: $F_{1,4}$=17.69, p<0.05; ZT5-6: $F_{1,4}$=15.16, p<0.05, ***Table 66***) (**Figure 34.B**). This increase was not significantly expressed, however, in other spindle parameters such as their *o-Quality* ($F_{1,4}$=5.16, p=0.08, ***Table 67***) and duration ($F_{1,4}$=5.71, p=0.05, ***Table 68*****)**, although a trend towards a relative increase was evident at ZT4 to ZT5 in both cases (**Figure 34.C-D**).

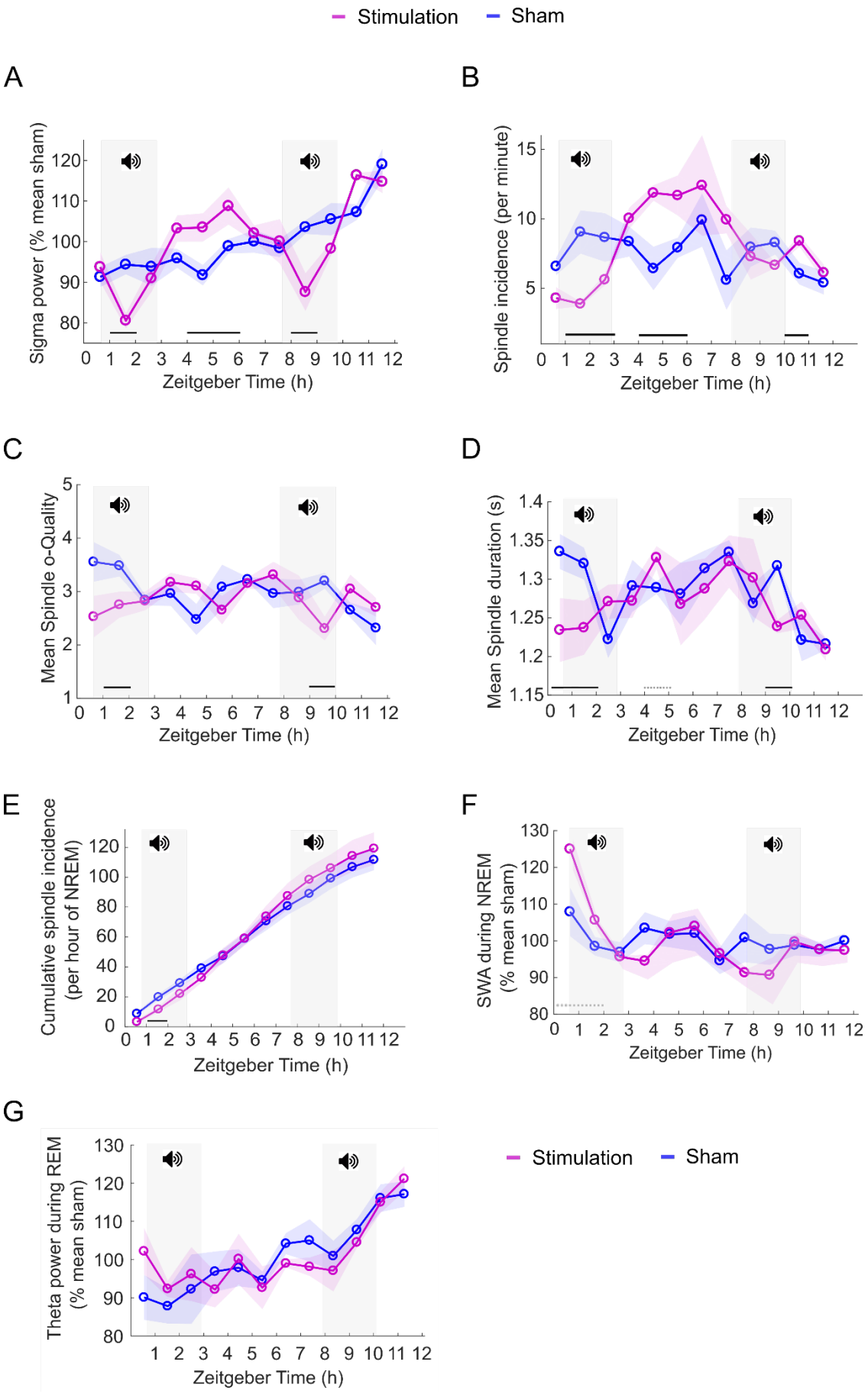

Stimulation
Sham
A
Sigma power (% mean sham)
Zeitgeber Time (h)
B
Spindle incidence (per minute)
Zeitgeber Time (h)
C
Mean Spindle o-Quality
Zeitgeber Time (h)
D
Mean Spindle duration (s)
Zeitgeber Time (h)
E
Cumulative spindle incidence (per hour of NREM)
Zeitgeber Time (h)
F
SWA during NREM (% mean sham)
Zeitgeber Time (h)
G
Theta power during REM (% mean sham)
Zeitgeber Time (h)
Stimulation
Sham

Figure 34. Effects of the semi-periodic auditory stimulation paradigm using 500ms pure-tones (every ~10s) on the dynamics of sleep oscillations in the S1 granular layer. *All graphs show values averaged within each mouse and then averaged per hour and across mice, during 12h light periods where 'stimulation' or 'sham' stimuli were presented. All analyses were performed on one S1 LFP channel per mouse, located in cortical layer 4.* ***(A)*** *Power density at the spindle frequency range (sigma: 10-15Hz) across 12h light periods. Open circles show the average across mice, per hour, expressed as the percentage of the mean sigma power during the sham condition.* ***(B,C,D,E)*** *Mean spindle incidence per minute (B), mean spindle o-Quality (C), mean spindle duration in seconds (D), and cumulative spindle incidence per hour averaged across mice (E). Analyses were performed on spindle events detected with the AR-based detection algorithm from one S1 LFP channel per mouse.* ***(F)*** *Slow-wave power density (μV^2/0.25Hz) between 0.5-4Hz during NREM sleep. Values are expressed as the percentage of the mean slow-wave power in NREM sleep during the sham condition.* ***(G)*** *Power density in the theta frequency band (4-8Hz) during REM sleep. Values are expressed as the percentage of the mean theta power in REM sleep during the sham condition.* ***NOTE:*** *Black lines above x-axis represent statistical significant difference. Dotted grey lines above x-axis represent p-values that were not significant but were very below 0.07, indicating a strong trend. Open circles= mean across mice and hour; coloured shaded areas= SEM; grey shaded boxes= two-hour time-intervals during which auditory stimulation was presented. Zeitgeber time= time from light onset.*

Taken together, these results suggest that 5KHz pure-tones presented at 80dB for a duration of 500ms disrupt LFP spindles in S1. Interestingly, spindle activity seems to be homeostatically regulated such that its disruption is followed by a rebound increase in spindle incidence and power. To confirm that the sound-related reduction in spindle activity was indeed being compensated by the subsequent increases in incidence, we calculated the cumulative spindle incidence across the 12h light periods. As expected, we found that the slope of spindle events accumulation per hour differed between conditions ($F_{11,44}$=4.71, p<0.001, ***Table 69***) (**Figure 34.E**). Specifically, the cumulative incidence of spindles was lower during in the stimulation condition relative to sham during the stimulation period (i.e. ZT1-2) ($F_{1,4}$=10.6, p<0.05, ***Table 69***). Upon the

termination of auditory stimulation (i.e. at ZT 2.75), the slope of spindle events accumulation was steeper in the stimulation condition relative to sham (i.e. steeper trend between ZT3 and ZT8: the time-period following the spindle reduction caused by the first stimulation block, $F_{1,4}$=10.6, p<0.05, ***Table 69***). As a result, the cumulative spindle incidence did not differ between conditions by the end of the light period ($F_{1,4}$=1.33, p=0.31, ***Table 69***).

The slow-wave activity is considered to be a marker of, and be functionally implicated in, sleep-wake homeostasis (Daan et al., 1984; Tobler and Borbély, 1986; Tononi and Cirelli, 2003, 2006; Bartram et al., 2017; González-Rueda et al., 2018). Therefore, there is a question as to whether the sound presentation affected other sleep-related oscillations, like slow-wave activity, and thereby caused a subsequent overall increase in sleep intensity. To address this, we compared the slow-wave activity during NREM sleep and theta dynamics during REM sleep in both conditions (i.e. stimulation vs sham). Interestingly, we did not find a significant difference in slow-wave activity during NREM (interaction: $F_{11,44}$=1.19, p=0.32, ***Table 70***) or theta power during REM (interaction: $F_{11,44}$=1.43, p=0.20, ***Table 71***) across the light period between conditions (**Figure 34.F-G**).

In the case of the slow-wave activity, there was a trend towards an increase during the first auditory stimulation block in the stimulation condition relative to sham (ZT0-1: $F_{11,44}$=4.71, p=0.06; ZT1-2: $F_{11,44}$=5.33, p=0.05, ***Table 70***). This trend is in line with previous studies suggesting that auditory stimulation is effective for inducing slow-wave activity during sleep (Tononi et al., 2010; Ngo et al., 2013a; Ong et al., 2016; Henin et al., 2019; Navarrete et al., 2020). In the case of the present experiment, however, this

trend was strong but not statistically significant (ZT0-1: p=0.06 and ZT 1-2= 0.05), although increasing the sample size could be informative.

Overall, these results suggest that the resulting increase in spindle incidence following a period of spindle reduction related to the presentation of sounds during sleep, is not secondary to an overall increase in sleep-related oscillations or intensity, but rather suggests a homeostatic regulation of spindle activity.

5.3.1.2. Evidence of spindle homeostasis following disruption related to *5KHz pure-tones* played for 8-s

Previous human and rodent studies have predominantly studied the relationship between spindles and auditory stimulation using sounds lasting a few hundred milliseconds or less (e.g. 50ms – 500ms) (Sela et al., 2016; Antony and Paller, 2017; Lecci et al., 2017; Lustenberger et al., 2018; Sela et al., 2020). We were also interested in investigating the effect that longer sounds (i.e. 8s) would have on the dynamic of sleep oscillations. We, therefore, performed a second set of semi-periodic auditory stimulation, where 5KHz pure tones were played for 8-s approximately every 45 seconds (**Figure 35.B**).

Such stimulation was performed in two 2-hour blocks presented at ~ZT 0.75 – ZT 2.75 and ZT 8 – ZT 10 (**Figure 35.A**). During each 2-hour block, therefore, 160 sounds were played (i.e. 320 sounds in total within a 12h light period). Auditory stimulation was performed on two different days (12h light periods), where sounds were presented at

80dB ('stimulation') on one day and 0dB ('sham') on the other. We found that, on average across mice (n=5) and conditions, 61.59% ± 2.29 (mean ± SEM across mice) (n=197) of sounds were played during NREM sleep, 15.08% ± 2.14 (n=48) of sounds were played during REM sleep, and 23.31% ± 2.89 (n=75) of sounds were played during wake. There was no significant difference between conditions (stimulation vs sham) in the percent of sounds played per sleep/wake state (NREM, REM, wake) ($F_{2,8}$=0.072, p=0.97, ***Table 72***).

To investigate the effect of auditory stimulation during NREM sleep on sleep-related oscillations, we selected only auditory stimuli played during NREM sleep that did not induce movement. This selection was done by visually inspecting the effect of each stimulus on the EEG, LFP and EMG signals. This resulted in 135 ± 10.4 (mean ± SEM across mice) sounds played during NREM, being included in the analyses. Interestingly, visual inspection also suggested that auditory stimuli disrupt LFP spindle activity in S1 channel located in granular and infra-granular during NREM sleep (**Figure 35.C**).

Note that we ran all analyses on signals recorded from granular and infra-granular layers of S1, as well as the frontal EEG. We will focus here on the effects of auditory stimulation during NREM on the granular layer of S1, where the incidence of spindles is highest, although we will also briefly highlight the most relevant results acquired from infra-granular and frontal areas.

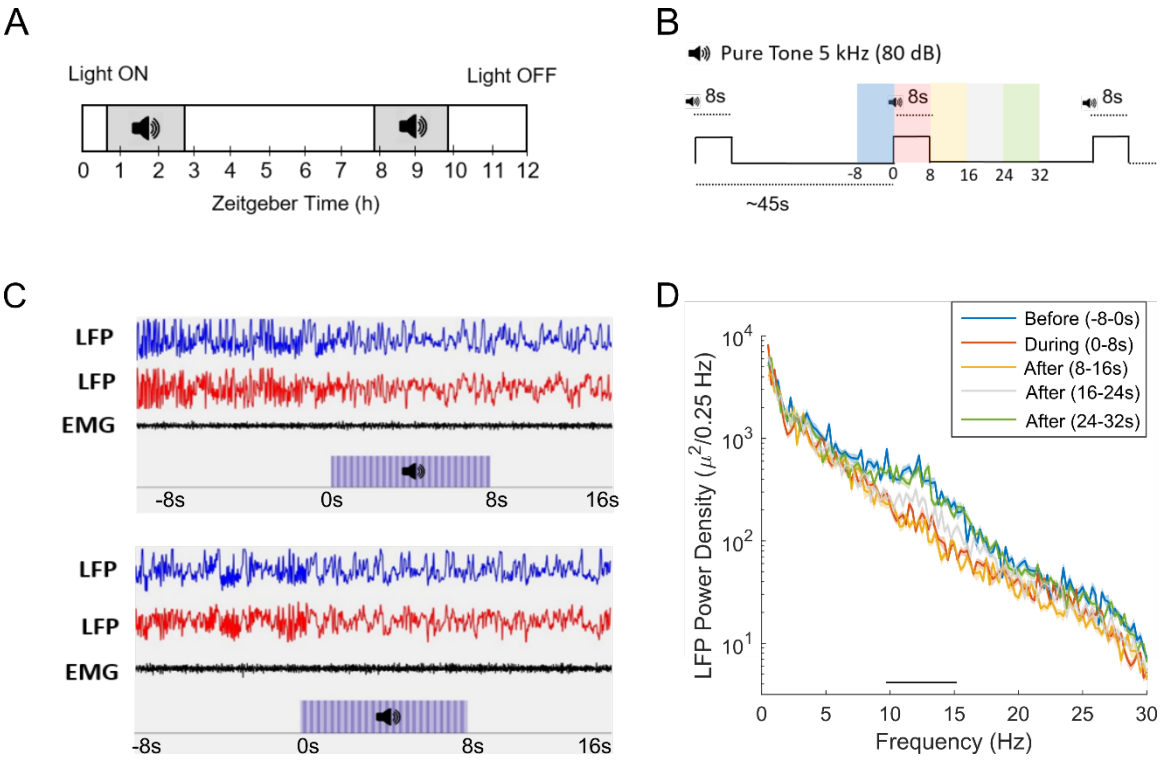


Figure 35. Effects of the semi-periodic auditory stimulation paradigm using 8-s pure-tones (every ~45s) on the LFP power density and putative spindles in the S1 granular layer. (A) *Structure of the auditory stimulation paradigm across the 12h light period. Zeitgeber time represent time from light onset (9am). The shaded areas represent the time-periods during which auditory stimulation was performed (stimulation blocks).* ***(B)*** *Auditory stimulation consisted of 8-s sounds played every ~45s for two hours. Coloured boxed indicate 8s intervals relative to sound onset, with the colours representing individual time intervals in panel D.* ***(C)*** *Examples of 24-s segments of two LFP signals recorded from the S1 granular layer and the EMG signal during a sound-stimulation trial (80dB sounds). The blue bar at the bottom represents the 8s-long sound.* ***(D)*** *Mean LFP power density (across mice) during NREM sleep in the LFP channel showing highest incidence of spindle activity in each mouse. Line colours represent 8-s time intervals relative to sound onset, as indicated in panel B. The shaded areas represent the SEM. Black lines above x-axis represent statistical significant difference obtained by running t-tests with Sidak correction.*

Effects of auditory stimulation on Layer 4 of S1

To analyse this quantitatively, first we investigated the effect of auditory stimulation on the overall LFP power spectra. For each mouse, we chose the LFP signal with highest spindle density, which in all cases consisted of a recording channel located in layer 4 of S1. Next, we calculated the absolute power spectra for 8s-long LFP segments around the time of sound presentation. The timing of these segments relative to sound onset is explained in detail in **Figure 35.B**.

As expected, spectral analyses revealed that the difference in terms of averaged LFP power density between these time-segments was frequency-specific (0-30 Hz) (Interaction: $F_{11, 44}$=9.17, p<0.001, ***Table 73***). Specifically, t-tests using Sidak correction (see ***Table 73***) indicate that the LFP power density in the spindle frequency range (9.75 – 15.25 Hz) was relatively enhanced in the 8-s segments before (-8-0s) and after (24-32s) sound stimulation, relative to the 8-s segments during and immediately after the sound offset (8-16s and 16-24s) (**Figure 35.D**). This suggests that sound stimulation leads to a reduction in LFP power density at the spindle frequency range, which lasts at least 24s. Interestingly, the sigma power seems to be restored in a progressive manner (i.e. as suggested by the progression in LFP power density, between 8-32 s. See yellow-grey-green lines in **Figure 35.B**, which corresponds to the line colours in **Figure 35.D**).

In contrasts, the LFP power density did not differ between time-segments at frequencies outside the spindle frequency range (see ***Table 73*** for specific contrasts) **Figure 35.D**. This suggests that 5KHz sounds, played for a duration of 8-s during NREM sleep, induce a specific disruption of sigma activity without significantly affecting other frequency bands.

To further investigate this, we next assessed the effects of these 5KHz pure tones on the LFP sigma power, as well as the incidence of spindle events (including all *o-Quality* levels) detected with the AR-detection algorithm. We calculated the average sigma power of the LFP signals and the incidence of spindles within 8-s time-segments across 48-s intervals surrounding each stimulus presentation. As expected, we found that the sigma power (interaction: $F_{5,20}$=31.43, p<0.001, ***Table 75***) (**Figure 36.B**) and the number of spindle events (interaction: $F_{5,20}$=11.36, p<0.001, ***Table 74***) (**Figure 36.A**) across these time segments differed between conditions. Specifically, there was a substantial reduction of both sigma power and spindle number during the sound presentation and during the ~8-s segment immediately following sound offset (See ***Table 74*** and ***Table 75*** for specific contrasts). Interestingly, in line with the results reported in the previous set of experiments, this suppression of spindle activity was followed by an increase in sigma power and spindle incidence, which started around 16-s after sound offset and lasted for at least 24s, when the next sound was played (see ***Table 74*** and ***Table 75*** for specific contrasts) (**Figure 36.A-B**).

Note that the sigma power and spindle incidence are increased in the stimulation condition (relative to sham) during the 8-s segments prior to the sound onset. This could be explained by the fact that auditory stimuli were played every ~45 and, therefore, sounds in the stimulation condition were likely to be played when spindle activity was increased following the presentation of the previous sound. In order to better understand the effect that these sounds have at longer time-frames, future experiments should set the inter-stimulus interval at a time span greater than 45s.

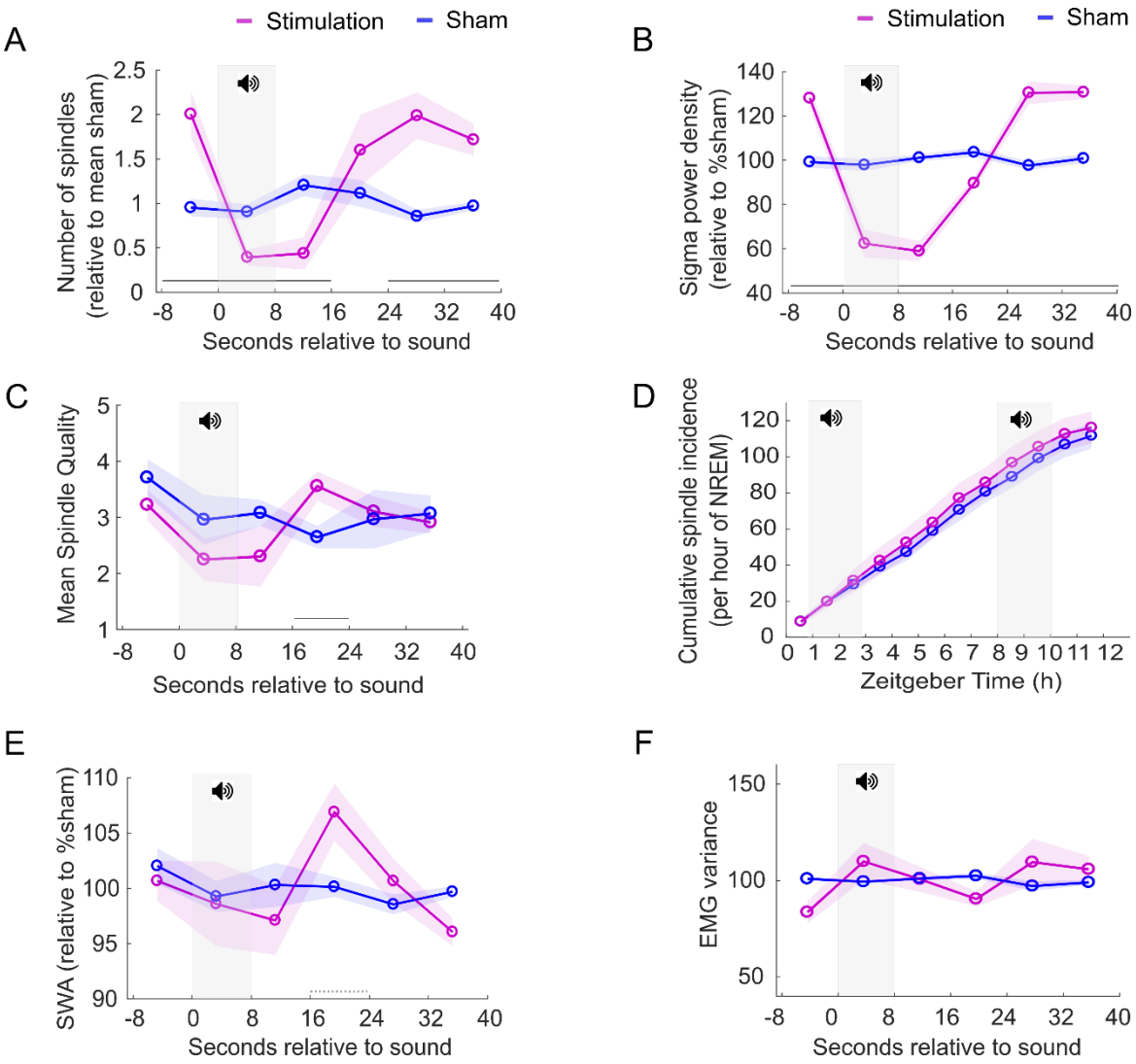


Figure 36. Effects of the semi-periodic auditory stimulation paradigm using 8-s pure-tones (every ~45s) on spindle and slow-wave activity in the S1 granular layer. *All graphs show values averaged within each mouse and then averaged across mice and within 8-s time-segments across 48-s surrounding each stimulus presentation ('stimulation' or 'sham'). All analyses were performed on one S1 LFP channel per mouse, located in cortical layer 4.* ***(A,C,D)*** *Mean spindle incidence (A) and mean spindle o-Quality (C) around the onset of stimulation. Analyses were performed on spindle events detected with the AR-based detection algorithm from one S1 granular LFP channel per mouse.* ***(B)*** *Sigma power density in granular LFP signals around the onset of stimulation, expressed as the percentage of the mean sigma power during the sham condition.* ***(D)*** *Cumulative spindle incidence per hour, averaged across mice, during 12h light periods where 'stimulation' or 'sham' stimuli were presented.* ***(E)*** *Slow-wave power density between 0.5-4Hz during NREM sleep, around the onset of stimulation. Values are expressed as the percentage of the mean slow-wave power in NREM sleep during the sham condition.* ***(F)*** *EMG*

variance around the onset of stimulation, expressed as the percentage of the mean EMG variance during NREM sleep during the sham condition. ***NOTE:*** *Black lines above x-axis represent statistical significant difference. Dotted grey lines above x-axis represent p=~0.05. Open circles= mean across mice; coloured shaded areas= SEM; grey shaded boxes= time-intervals during which auditory stimulation was presented. Zeitgeber time= time from light onset.*

On the other hand, the mean *o-Quality* of spindles does not seem to be significantly affected here by the sound presentation (ZT0 - ZT8: $F_{1,5}$=1.47, *p*=0.26, ***Table 76***) (**Figure 36.C**). However, caution should be taken when interpreting these results, as the number of spindles during sound presentation is substantially reduced, which reduces the statistical power of these analyses. Interestingly, however, the spindle *o-Quality* does increase significantly in the stimulation condition relative to sham (ZT16 - ZT24: $F_{1,5}$=7.76, *p*<0.05, ***Table 76***) during the 8-s segment starting around 8-s after sound offset (i.e. following the reduction in spindle incidence and power).

In line with the results presented in the previous section, the present results suggest that 5KHz pure-tones presented for a duration of 8-s disrupt LFP spindles in S1. Moreover, spindle activity seems to be homeostatically regulated such that the aforementioned reduction is followed by an increase in spindle incidence and power. In the present experiment, such an increase initiates ~8-s after sound offset. To confirm that the sound-related reduction in spindle activity was indeed being compensated by the subsequent increases in incidence, we calculated the cumulative spindle incidence across the 12h light periods. As expected, we found that the cumulative spindles incidence per hour across time, did not differ between conditions (interaction: $F_{11,55}$=1.09, p=0.39, ***Table 77***) (**Figure 36.D**).

To double-check that the sound-related changes in spindle activity were not explained by an overall change in sleep depth, we investigated how the sound presentation affected the slow-wave activity and the EMG signal (i.e. which reflects motor activity) during the trials selected for analysis. We found that the sound presentation did not significantly change the slow-wave activity ($F_{5,20}$=1.48, p=0.24, ***Table 78***) (**Figure 36.E**) or the EMG variance (i.e. did not induce a movement) ($F_{5,20}$=1.64, p=0.21, ***Table 79***) (**Figure 36.F**) across time segments surrounding the sound onset, in the stimulation condition relative to sham. Interestingly, however, there was trend towards an increase in slow-wave activity during the 8-s segment starting 8-s after the sound offset ($F_{1,5}$=4.83, p<0.06, ***Table 78***) (**Figure 36.E**). This non-significant effect coincides in time with the increase in spindle activity, although a larger sample size would be required to determine its meaning and relevance.

Effects of auditory stimulation on the frontal EEG and infra-granular layers of S1

Based on visual inspection, it appears that spindles in deeper layer of S1 are not substantially disrupted by the sound presentation. We were interested, therefore, in analysing the effects of the sound presentation beyond the LFP signals recorded from layer 4 in S1 (the layer we initially studied given the high incidence of spindles presented there). We proceed, therefore, to analyse the effect of the presentation of the 8-s pure tones on the spindle activity in frontal EEG signals and LFP signals recorded from infra-granular layers (specifically from layers 5b and 6). Interestingly, the effect of the auditory stimulation on the frontal EEG signal was similar to the effect observed in layer 4 of S1 (**Figure 37.A**). Specifically, there was a decrease in spindle incidence (including all *o-Quality levels*) during sound stimulation (T(0): $F_{1,5}$=7.12, p<0.05, ***Table***

80) and the 8-s segment following (T(8): $F_{1,5}$=23.2, p<0.001, ***Table 80***) the sound offset in the stimulation condition relative to sham. Moreover, this decrease was followed by an increase in spindle incidence evident ~24s after the sound offset in the stimulation condition relative to sham.

In contrast to the effect of auditory stimulation on layer 4 of S1 and the frontal EEG, the sounds did not seem to significantly affect the incidence of spindles in infra-granular layers (i.e results shown for layer 5b) ($F_{5,20}$=0.99, p=0.31, ***Table 81***) (**Figure 37.B**). The incidence of spindles in these layers is generally very low so caution should be taken when interpreting these results. Nevertheless, these results may suggest that the effect of auditory stimuli on spindles differs across layers of S1.

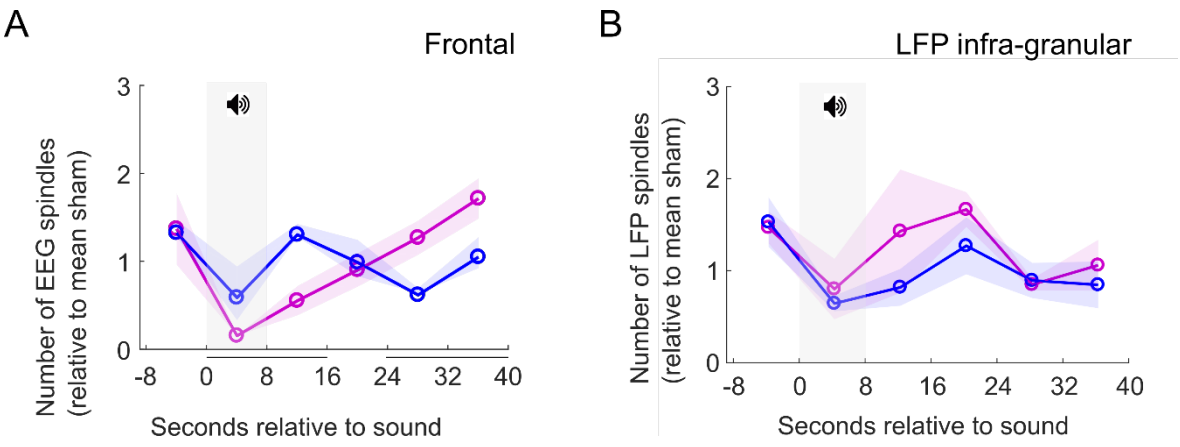


Figure 37. Effects of the semi-periodic auditory stimulation paradigm using 8-s pure-tones (every ~45s) on spindle activity in the frontal EEG and S1 infra-granular layers. *Mean spindle incidence in the frontal EEG* ***(A)****, and in one S1 infra-granular recording channel per mouse* ***(B)****. Graphs show values averaged across mice and within 8-s time-segments across 48-s surrounding each stimulus presentation ('stimulation' or 'sham'). Analyses were performed on spindle events detected with the AR-based detection algorithm from the respective channels. Black lines below the x-axis represent statistically significant differences. Open circles= mean across*

mice; coloured shaded areas= SEM; grey shaded boxes= time-intervals during which auditory stimulation was presented.

Taken together, the results generated by the semi-periodic auditory stimulation paradigm, suggest that 5KHz pure-tones played at 80dB for 0.5 or 8 seconds disrupt spindle activity in layer 4 of S1 in mice. Spindle activity, however, seems to be homeostatically regulated and reductions in spindle activity are followed by a rebound increase in spindle incidence and power. This homeostatic compensation can start occurring ~8-s after the sound offset in cases where there is an opportunity for recovery (i.e. when another sound was not played within the next ~35s) (**Figure 36.A-B**). However, this homeostatic compensation can also occur hours after the spindle reduction initiated, in cases where there is no immediate opportunity for recovery (i.e. when sounds were played every 10s) (**Figure 34.A-B**).

It is relevant to note that, as shown in Chapter 3, the infra-slow oscillation of spindle activity has a cycle length of ~50s in S1 (i.e. bursts of spindles recur with a period of around 50s). This cycle length is similar to the inter-stimulus interval length that we used in our second semi-periodic auditory stimulation (i.e. 45s), and it could be argued that it might have influenced our results. In fact, a slight infra-slow modulation of spindle activity can be appreciated in our sham condition. However, the modulation of spindle activity generated by the auditory stimuli is substantially different from the sham condition and our results are constant across different experiments (using different stimulation patterns). Therefore, it is not likely that the modulation of spindle activity that we see in this experiment arises from the natural infra-slow modulation of spindle activity.

Previous studies have reported that sounds modulated at the spindle frequency range, and played in phase with the slow-oscillation up state, induce spindle activity in parietal and frontal regions of the brain (Antony and Paller, 2017; Lustenberger et al., 2018). Other studies have failed to replicate these results (Ngo et al., 2019), and the present results further suggest that the semi-periodic presentation of pure-tones during sleep can disrupt spindles in mice. This suggests that the precise parameters and pattern of stimulation (e.g. tone type, timing, duration, intensity, and length of the inter-stimulus interval), are important variables determining the effect this stimulation will exert on spindle activity throughout the light period. Further work will be needed to elucidate how and why auditory stimulation appears to be effective in modulating sleep-oscillations like spindles or slow waves. Our data suggest that this effect appears to vary across cortical layers of S1. Therefore, we proceeded to investigate how the auditory stimulation affected the population spiking activity recorded across layers of S1.

5.3.2. Auditory stimulation induces a reduction in multi-unit activity in granular layers of S1

We next investigated how the 5KHz pure tones played at 80dB for 8-s, affected the multi-unit activity recorded with 16-channel laminar probes across layers of S1. As done for the previous analyses, we selected only auditory stimuli played during NREM sleep that did not induce arousal. This resulted in 135 ± 10.4 (mean ± SEM across mice) trials per mouse (n=5) being included in the analyses. To analyse the multiunit activity, the timing of extracellular neuronal activity occurring before, during and after the sound presentation was calculated and the number of spikes were averaged into 500ms

bins. Note that bin lengths of 50, 100 and 250ms were also tested and consistent results were obtained.

Figure 38.A shows multi-unit activity averaged across trials in different recording channels, which are normalised to the mean number of spikes in the 8-s segment immediately preceding the sound stimulation. We found that the sound presentation was associated with an initial increase in multi-unit activity (10% ± 3.2 increase from baseline, mean ± SEM across mice) lasting a few milliseconds, followed by reduction of multi-unit activity in channels located in or around the granular layer of S1. This reduction ranged from 10% to 65% (mean across mice) relative to mean spiking during the 8-s period before sound onset, and was most prominent in the granular layer. As the recording channels distanced from the granular layer, the sound-induced reduction in multi-unit activity was less pronounced (e.g. **Figure 38.A** LFP1 and LFP2 located in supra-granular layers, and LFP6 and LFP7 located in infra-granular layers). Additionally, in channels located in deeper layers (i.e. layer 5b, see LFP8 in **Figure 38.A**), the initial evoked-increase in multi-unit activity was more pronounced (21.36% ± 1.8 increase from baseline, mean ± SEM across mice), and was followed by an increase in multi-unit activity.

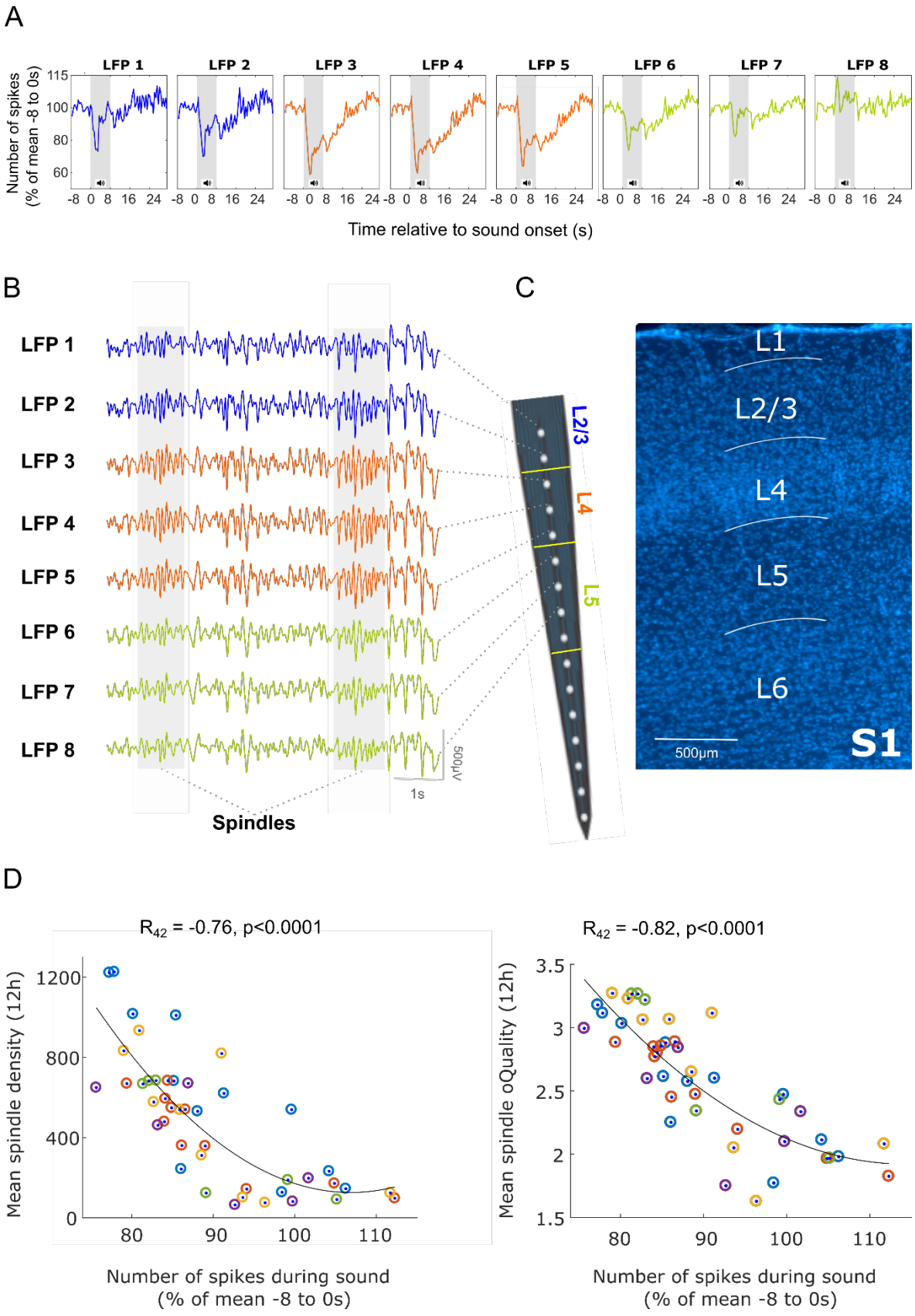


Figure 38. Effects of the semi-periodic auditory stimulation paradigm using 8-s pure-tones (every ~45s) on the multi-unit activity across layers of S1. (A) *Multi-unit activity (MUA)*

averaged across trials (in one mouse) in different recording channels of a 16-channel laminar probe implanted in S1. The values are normalised to the mean number of spikes in the 8-s segment preceding the sound stimulation. The different line colours represent different cortical layers, (blue=L2/3; orange=L4; green=L5). ***(B)*** *10s segments of LFP signals recorded across layers of S1 in one mouse. The line colours represent different cortical layers (blue=L2/3; orange=L4; green=L5). These signals show examples of spindle events occurring during undisturbed sleep across layers of S1.* ***(C) Right -*** *Histological image (using DAPI staining) showing the identification of different cortical layers.* ***Left -*** *The illustration of a laminar probe indicates the approximate location of different recording electrodes (white dots) across cortical layers in this example.* ***(D)*** *Correlation between the average spindle density (within a 12h light period) and the number of spikes during the 8-s sound presentation. The black line represent the best fit provided by second order polynomial, R^2_{41}=-0.71 (**D-left**). Correlation between the average spindle o-Quality (within a 12h light period) and the number of spikes during the 8-s sound presentation. The black line represent the best fit provided by second order polynomial, R^2_{41}=-0.79 (**D-right**). The number of spikes are expressed as a percentage of the mean spiking during the 8s interval before sound stimulation (i.e. -8s to 0s). The different colours represent different mice and the different circles represent different channels.*

In-vivo whole-cell recording from neurons in the barrel cortex (S1) in mice, suggest that auditory stimuli presented during anaesthesia, trigger robust "up-states", which reach ~60% of the response amplitude generated by somatosensory stimulation (Maruyama and Komai, 2018). Additionally, it has been reported that high neuronal activity during sleep can to be followed by periods of diminished oscillatory and population neuronal activity across cortical and subcortical regions, which lasts a few seconds (Miyawaki et al., 2017). Such a phenomenon could potentially be related to the diminished spiking activity we observe in some layers of S1. It is interesting, however, that this response differs across layers of S1.

Visual inspection of the evoked-responses across layers of S1 reveals an interesting observation: the magnitude of the evoked response seems to be related to the overall

magnitude of spindle activity in each recording channel. **Figure 38.B**, shows examples of spindle events occurring during undisturbed sleep, across layers of S1 (specified by histology, **Figure 38.C**). Visual inspection of **Figure 38.A-B** suggests that the magnitude of the multi-unit activity reduction, resulting from sound presentation, is associated with the *o-Quality* (i.e. oscillatory strength) of spindles in each local region (i.e. channel).

To investigate this quantitatively, we calculated the correlation between the average spindle density (within a 12h light period) and the mean spiking during the 8-s sound presentation across mice and recording channels (R_{42}=-0.76, p<0.0001) (**Figure 38.D**). We also calculated the correlation between the mean spindle *o-Quality* (within a 12h light period) and the mean spiking during the 8-s sound presentation (R_{42}=-0.82, p<0.0001) (**Figure 38.D**). In both cases, we found a negative correlation. This confirms our previous observation suggesting that the more pronounced the spindle activity is, in a certain local region, the greater the sound-related reduction in multi-unit activity will be. Note that only the MUA was assessed here and the sounds can be generating effects on slow oscillation dynamics and K-complexes that are not being captured here. This possibility is outside the scope of the current work but will be analysed in the future.

The aforementioned observation could merely reflect differences in the properties or network connectivity of neurons across layers of S1, which could result in spindles and spiking reductions being more prominent in certain local regions. It is also possible, however, that this association reflects functional properties of the spindle-generating network. To investigate further this possibility, approaches for detecting spindles in real time and delivering stimulation in phase with these oscillations would be highly

informative. We, therefore, developed a closed-loop system to detect spindles in real time and designed different auditory stimulation protocols. Preliminary results from the application of this system will be presented next.

5.3.3. Preliminary insights based on auditory closed-loop stimulation targeting spindle events

We developed an auditory close-loop system, which detects spindle-like activity based on the power of filtered (10-15Hz) electrophysiological signals and delivers stimulation during spindles in real time. Twenty-four hour recordings of EEG, EMG, LFP signals as well as MUA were performed throughout the experimental days. LFP and MUA signals were recorded from S1 and auditory cortices. For our experiments, we initially envisioned to trigger the stimulation based on spindles detected in the primary auditory cortex. Unexpectedly, however, we could not visually detect clear-cut spindle activity in any of the LFP signals recorded from this region in any of the seven mice (**Figure 39**).

Previous studies have detected spindles in the rat auditory cortex (Sela et al., 2016). Studies performed in mice, however, have shown that both sigma power and the incidence of spindles are substantially reduced in the auditory cortex relative to S1 (where spindles are prominent) (Fernandez et al., 2018). Histological images indicate that the recording electrodes were implanted in middle and deep cortical layers of the primary auditory cortex, which may not express spindles of a high *o-Quality* (as is the case for S1). A better characterization of the laminar profile of sleep-oscillations within the primary auditory cortex may be informative for interpreting these results. We

proceeded, therefore, to base the auditory closed-loop stimulation on the detection of LFP spindles recorded from the granular layer of S1 only (where they are highly prominent).

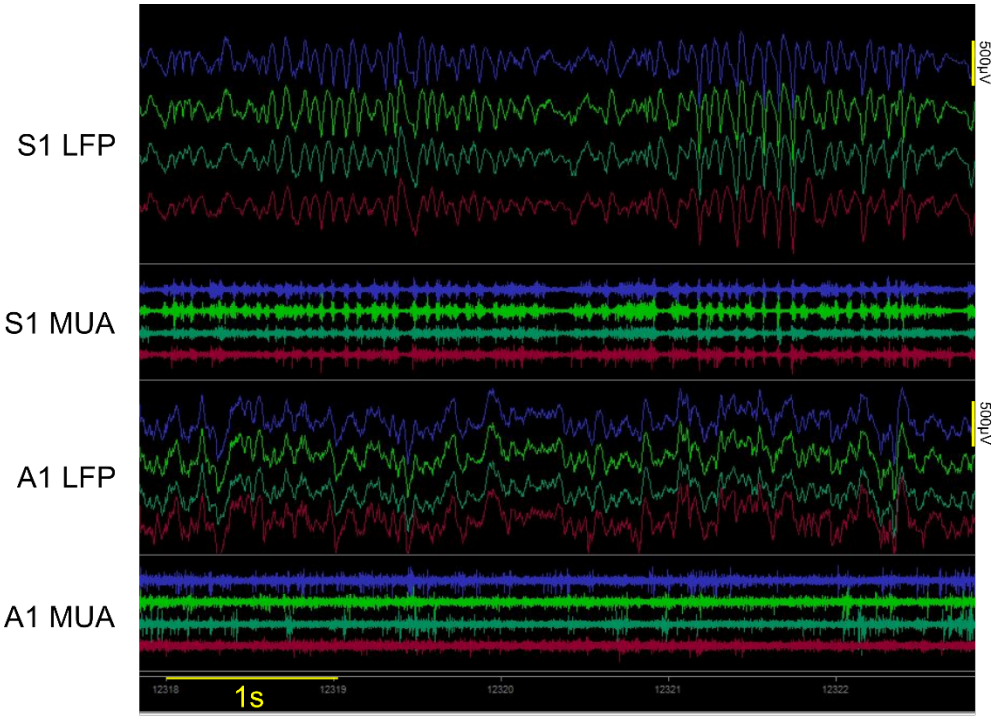


Figure 39. Segments of LFP and MUA recordings in both S1 and A1. *Five-second segments of LFP signals and MUA, recorded simultaneously from one mouse. Note that spindle activity can be clearly observed in the S1 LFP and MUA recordings, while simultaneous LFP and MUA recordings from A1 do not show corresponding spindle activity.*

In order to evaluate the performance of detection algorithms, previous studies have compared the automated spindle detection with the visual identification by trained experts and other automated algorithms (Warby et al., 2014). As we discussed in Chapter 3, spindles are not all-or-none phenomena and therefore such evaluation is subjective. We compared the spindle detections achieved with our real-time spindle detector with the detections achieved with the lowest thresholds (r_b= 0.92) AR spindle

detection algorithm (discussed in detail in Chapter 3). We found that when the power threshold used to detect spindles in real time was set at 3 times the mean of the smoothed power signal, the comparative sensitivity (comparative true positive rate) reached a level of 71.4% ± 1.96 (mean ± SEM across mice). When the power threshold used to detect spindles in real time was set at 4.5 times the mean of the smoothed power signal, the comparative sensitivity reached a level of 82.6% ± 2.11 (mean ± SEM across mice). As discussed in previous chapters, the choice of any fixed thresholds would be arbitrary and was used here as a first approach to facilitate rapid detection. Future work is required to develop online systems that do not rely on signal filtering and that used adaptable thresholds.

To inspect the performance of the real-time detection further, we explored the spectra within frequencies between 0-20 Hz in the S1 LFP signal used for spindle detection. Indeed, spectrograms centred at the time of real time detection, show a prominent increase in LFP power at the spindle frequency range in S1, which as expected from visual inspection, was not present in the primary auditory cortex (**Figure 40**). Interestingly, the system seemed to detect predominantly fast spindles (~12-15 Hz). This may have occurred because the real-time detector was set detect spindles only when theta activity (4-7 Hz) was low. There may be some overlap between fast theta and slow spindles, which caused low frequency spindles to be missed by the real-time detector. This possibility will be further analysed in future work. We performed different types of auditory closed-loop stimulation paradigms, and will present the preliminary results for two of them next.

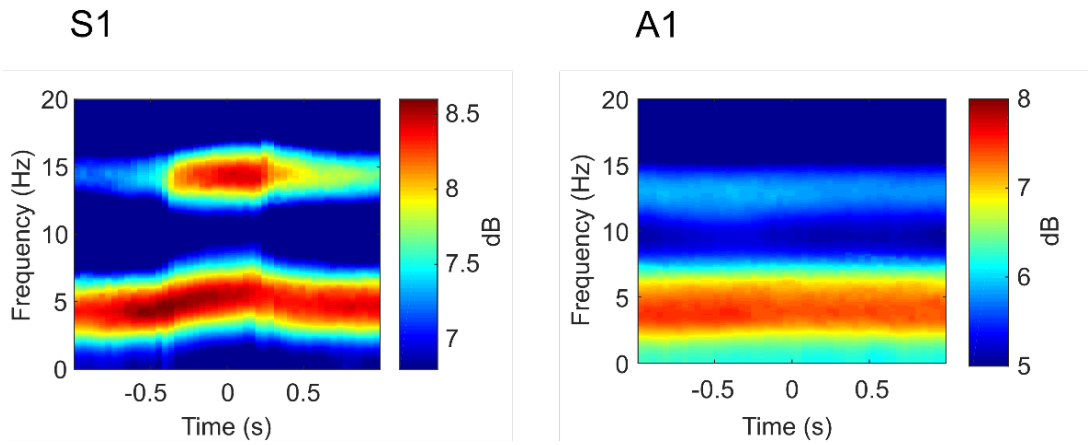


Figure 40. Spectrograms centred at the time of real-time spindle detections. *Average spectrogram of 1-s segments of LFP signal recorded from S1 and A1. Spectrograms are aligned to the time-stamp where spindles were detected with the real-time detection algorithm.*

5.3.3.1. Clicks train played at the time of spindle occurrence seems to increase the duration and o-Quality of these oscillations but this effect seems to be layer-specific

Previous evidence suggests that the amplitude of the slow-oscillation during NREM sleep can be increased by presenting sounds in phase with their up-sate (Ngo et al., 2013b, 2013a; Ong et al., 2016; Navarrete et al., 2020). Additionally, a couple of studies suggest that presenting sounds, modulated at the spindle frequency range, can induce an increase in spindle-like activity in parietal and frontal brain regions in humans (Antony and Paller, 2017; Lustenberger et al., 2018). Interestingly, these studies report to induce a frequency-specific effect such that slow spindles (10-13 Hz) were predominantly enhanced by white noise oscillating at 12Hz, while fast spindles (14-15 Hz) were predominantly enhanced by white noise modulated at 15Hz. Control conditions using white noise modulated outside the spindle frequency-range (i.e. 40 or

50 Hz) have resulted in inconsistent results. Specifically, they appear to disrupt spindles in some cases (Antony and Paller, 2017), and promote spindles in some others (Lustenberger et al., 2018) . Based on the previous literature, we wanted to investigate whether presenting 12Hz and 40Hz click trains, at the time of spindle occurrence (using threshold 4.5x mean sigma power), could modulate the properties of these oscillations.

Auditory stimulation was performed for six hours during the light period, specifically between ZT3.5 and ZT9.5 (i.e. 3.5 hours to 9.5 hours after the light onset). Click trains were played for 2-s at 80dB, upon detection of a spindle event, with an inter-stimulus interval of minimum 12-s. Four types of auditory stimuli were presented on four different days (12h light periods separated by at least 48 hours) and the presentation order was counter-balanced across mice. These stimuli consisted of 12Hz and 40Hz clicks presented at 80dB, and their respective sham conditions (i.e. the same click trains played at 0dB). The 40Hz clicks were introduced as a non-spindle control frequency. Approximately 550 ± 30 stimuli were played during the 6 hours of auditory stimulation. **Figure 41** shows examples where 12Hz, 40 Hz and sham clicks were played.

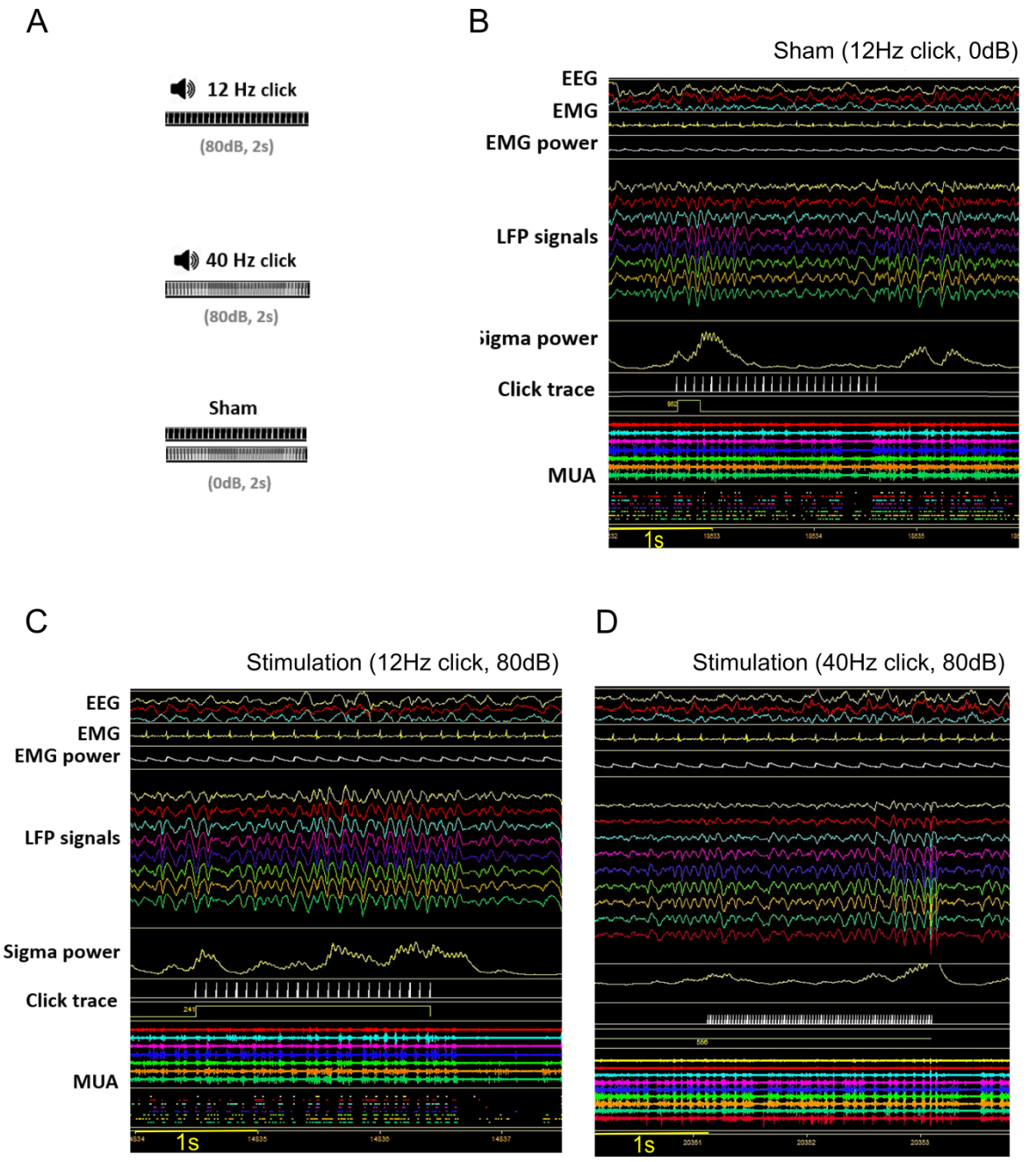


Figure 41. Examples of auditory closed-loop stimulation trials playing 12Hz and 40Hz clicks at the time of spindle occurrence. (A) *Illustration of the sounds played in this paradigm.* ***(B)*** *Example of a 'sham' trial where a 12Hz sham click was played at 0dB upon the detection of a spindle event.* ***(C)*** *Example of a 'stimulation' trial where a 12Hz click was played at 80dB upon the detection of a spindle event.* ***(D)*** *Example of a 'stimulation' trial where a 40Hz click was played at 80dB upon the detection of a spindle event.*

In line with previous studies (Antony and Paller, 2017; Lustenberger et al., 2018), our preliminary results suggest that the 12Hz clicks significantly increased the average duration ($F_{2,16}$=5.86, p<0.05, ***Table 82***) and *o-Quality* ($F_{2,16}$=6.2, p<0.001, ***Table 83***) of stimulated LFP spindles in the granular layer of S1, relative to the 12Hz sham stimulation (**Figure 42**.C). However, this 12Hz click-related increase was not generalised to spindles occurring in infra-granular layers of S1 (**Figure 42.D**) or the in frontal EEG (**Figure 42**.**E**) (Contrasts in ***Table 85*** to ***Table 90***).

Notably, the 40Hz clicks seemed to induce a significant increase in the average duration ($F_{2,16}$=5.86, p<0.05, ***Table 82***) of stimulated LFP spindles in the granular layer of S1, relative to the 40Hz sham stimulation (**Figure 42**.**C**). A trend towards an increase in the average duration of spindles ($F_{2,16}$=3.6, p=0.05, ***Table 85***) was also apparent in the infra-granular layers of S1 (**Figure 42**.**D**), however, this effect was not statistically significant. Unexpectedly, the 40Hz clicks seemed to increase the *o-Quality* of the stimulated spindles in infra-granular layers of S1 ($F_{2,16}$=7.94, p<0.0001, ***Table 86***) (**Figure 42**.**D**), but not in granular S1 layers (**Figure 42**.**C**) or in the frontal EEG (**Figure 42**.**E**) (Contrasts in ***Table 86*** and ***Table 89***).

Despite the effect that the auditory stimulation had on the duration and *o-Quality* of LFP spindles, there was no significant change in the incidence of spindles (including all *o-Quality* levels) in the frontal EEG ($F_{2,16}$=1.99, *p*=0.18, ***Table 90***), or in the granular ($F_{2,16}$=0.88, *p*=0.44, ***Table 84***) and infra-granular ($F_{2,16}$=3.36, p=0.11, ***Table 87***) layers

of S1 (**Figure 42.C-E**). The incidence in this case was measured during the six hours when auditory stimulation was being performed (i.e. ZT3.5 to ZT9.5).

Overall, the results from this experiment support our aforementioned conclusion that the precise pattern and parameters used for sound stimulation, determine the effects that stimulation exerts on spindle activity. While long-lasting (0.5 or 8s) pure tones seem to disrupt spindles in granular and infra-granular layers of S1, 12Hz click trains played at the time of spindles seem to increase their duration and *o-Quality.* Additionally, based on previous work (Antony and Paller, 2017) we expected the 40Hz clicks to disrupt spindle activity in S1. Other studies, however, have found that sounds modulated at 40Hz can induce spindles during NREM sleep (Lustenberger et al., 2018). Our results are partially consistent with this, and further suggest that the effect could depend on the cortical layer being recorded. Future studies are needed to investigate this hypothesis and possible underlying mechanisms. Additional work will be done to further analyse the present dataset and investigate the effect that the different auditory stimulation paradigms had on the dynamics of spindles throughout the 24h light/dark period.

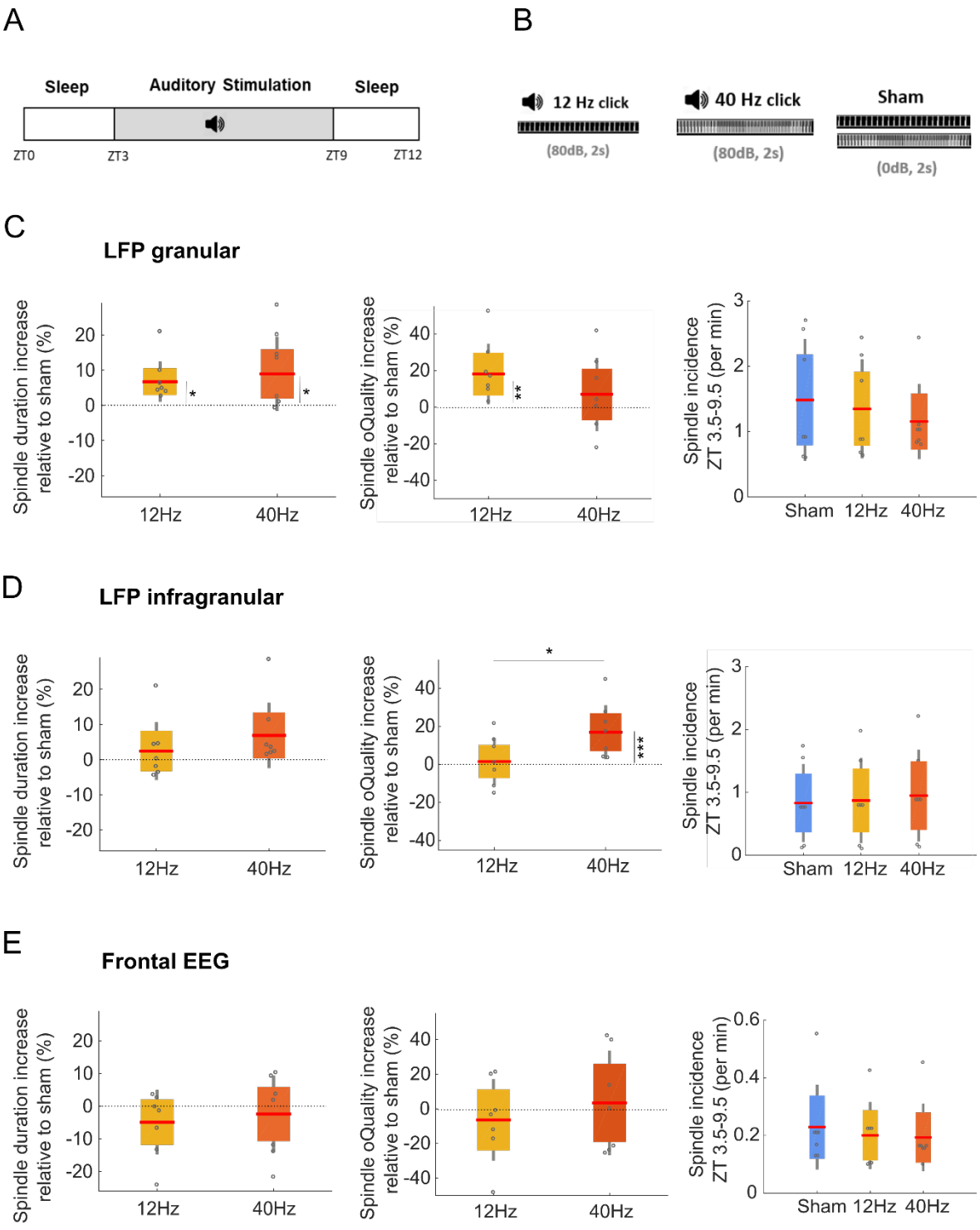


Figure 42.Effect of auditory click trains played at 12Hz and 40Hz on spindle properties. (A) *Structure of the auditory stimulation paradigm across the 12h light period. Zeitgeber time (ZT) represents time from light onset (9am). The shaded areas represent the time-periods during which auditory stimulation was performed (stimulation blocks).* ***(B)*** *Illustration of the auditory click trains that were played.* ***(C, D, E) Left and middle panels -*** *show the percentage change in spindle duration and o-Quality, when 12Hz and 40Hz clicks were played, relative to mean sham. These*

results are shown for S1 granular layers (C), S1 infra-granular layers (D), and for the frontal EEG (E). ***(C, D, E) Right panel –*** *Spindle incidence per minute during the time-period in which the different auditory stimulation paradigms (12Hz, 40Hz, sham) were performed. Box-plots: red lines= mean across mice; blue boxes= SEM; grey bars= 95% confidence intervals; dots= individual values for each mouse. *p<0.05, **p<0.001, ***p<0.0001.*

5.3.3.2. Preliminary evidence associating spindle activity with reduced arousability

Accumulating evidence suggests that spindles protect sleep from sensory disruption (Dang-Vu et al., 2011; Schabus et al., 2012; Lecci et al., 2017) . We sought to assess this hypothesis by using the auditory closed-loop stimulation system to deliver sounds to sleeping mice during the presence and absence of spindle events detected in S1. We set the detection threshold at 3.5 times the mean sigma power. EEG and EMG signals, as well as LFP and MUA recordings from S1 and the primary auditory cortex were collected during 24h periods (including the auditory stimulation sessions). In the present section, we analysed the EMG response to sound stimulation across conditions.

Auditory stimuli consisted of 12KHz pure tones played for 150ms at 70dB. This sound frequency was selected based on studies suggesting that 12kHz optimally induces evoked responses, is affected late in development by hearing loss in C57BL/6 mice (Ison et al., 2007), and is behaviourally relevant for mice (Grimsley et al., 2016). As in the previous paradigm, auditory stimulation was performed for six hours during the light period, specifically between ZT3.5 and ZT9.5. Sounds were delivered during ('spindle' condition) or in the absence of spindles ('no-spindle' condition) in a pseudo-random order. A minimum inter-stimulus interval of 3-s was allowed. Approximately

550 ± 30 stimuli were played during the 6 hours of auditory stimulation. **Figure 43** shows examples of 'spindle' and 'no-spindle' trials.

Our preliminary results suggest that the variance of the EMG signal (recorded from the nuchal muscle) shows a trend towards an increase ($F_{1,6}$=3.44, p=0.062, ***Table 91***) during the 200ms of sound stimulation, when sounds are not paired with spindles ('no-spindle' condition) compared to trials where they are ('spindle' condition). Similar results were achieved when analysing the power of the EMG signal. Decreased movement during the 'spindle' condition relative to 'no-spindle', could suggest that mice may show a lower reactivity to sensory stimulation presented during spindle events. This would possibly support the hypothesis that spindles protect sleep from sensory disruption.

In the present preliminary analysis, however, we do not control the timing of the 'no-spindle' condition. Specifically, sounds in this condition are triggered when no 'spindle' event is detected and the EMG power does not exceed a predefined threshold suggesting 'wakefulness'. However, it is still possible that microarousal-related EMG activity is biasing these results. Additionally, the phase of the slow oscillations at which these sounds are played may also contribute to the observed results. Further experiments were performed where pure tones and clicks were paired with both NREM ON or OFF states, detected from the S1 multi-unit activity. Finally, it would be relevant to analyse whether the *o-Quality* of spindles is related to their potential capacity to protect sleep from sensory disruption. Future work will investigate these possibilities.

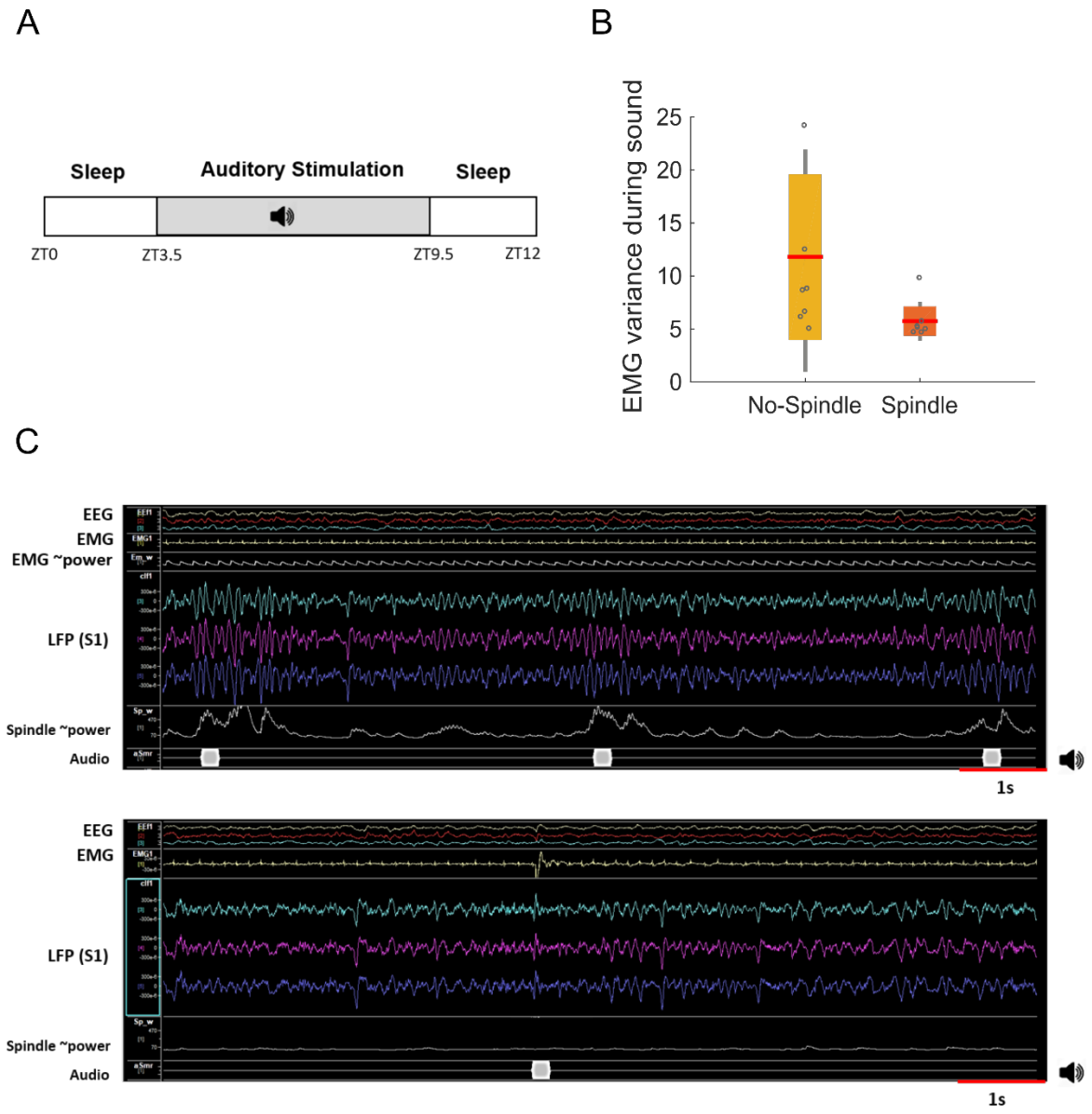
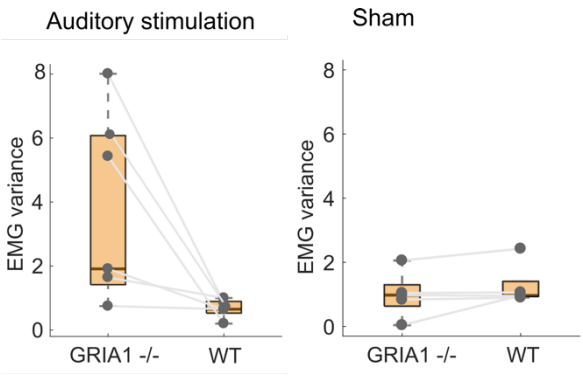


Figure 43. Effects of playing low-intensity 12KHz pure-tune during the presence or absence of spindles. (A) *Structure of the auditory stimulation paradigm across the 12h light period. ZT= Zeitgeber Time (i.e. time from light onset). The grey shaded area represents the time-period during which auditory stimulation (12KHz pure tones presented for 150ms at 70dB) occurred.* ***(B)*** *EMG variance in micro-volts during the 150ms of sound presentation, normalised by the mean EMG variance during NREM, in conditions where sounds were played in the presence of spindles ('Spindle' trials) or in their absence ('No-spindle' trials).* ***(C)*** *Examples where sounds were played in the presence of spindles (**Top panel** - 'Spindle' trials) or in their absence (**Bottom panel** - 'No-spindle' trials).*

5.3.3.3. Preliminary results: Preliminary results: GRIA1$^{-/-}$ mice seem to show increased responsiveness to auditory stimulation during sleep relative to WT littermates

If spindles do protect sleep from sensory disruption, it could be expected that lower spindle density would be associated with an increased responsiveness to sensory stimulation during sleep. We proceeded to investigate, therefore, whether GRIA1$^{-/-}$ mice (which show reduced EEG spindle activity and reduced synchrony of LFP spindles across wide-range cortical networks) showed increased responsiveness to auditory stimulation presented during sleep.

To address this, we performed a third set of semi-periodic auditory stimulation, where 5KHz pure tones were played for 8-s approximately every 45 seconds to GRIA1$^{-/-}$ mice and WT littermates. Such stimulation was performed in two 2-hour blocks presented at ~ZT 0.75 – ZT 2.75 and ZT 8 – ZT 10. During each 2-hour block, therefore, 160 sounds were played (i.e. 320 sounds in total within a 12h light period). Auditory stimulation was performed on two different days (12h light periods), where sounds were presented at 80dB ('stimulation') on one day and 0dB ('sham') on the other. Preliminary results suggest that the variance of the EMG signal (recorded from the nuchal muscle) was increased in GRIA1$^{-/-}$ mice relative to WT mice during the 8s of sound stimulation, when sounds were played during sleep. No difference between genotypes was found for the sham condition, where a sound with 0dB (no intensity) was played. These preliminary results seem to support the hypothesis that spindles protect sleep from sensory disruption. These results, however, are preliminary and further work is needed to check them and extract solid conclusions.



Supplementary Figure 44. EMG variance during auditory stimulation in GRIA1-/- and WT littermates.

5.4. DISCUSSION

Results in this chapter show that the interactions between spindle activity and auditory-related processing during sleep is complex, and highly dependent on the precise properties of both the auditory stimuli and the spindles themselves. On the one hand, parameters such as the duration, intensity, and frequency of sounds, determine the effect that these will have on spindle activity. We found, for instance that long sounds (0.5s and 8s pure-tones at 80dB) can disrupt S1 and frontal spindles, while shorter sounds with lower intensity (150ms pure-tones at 70dB) or click trains (12Hz or 40Hz at 80dB) do not have a major effect and, in the case of the latter, can even increase their *o-Quality* and duration.

On the other hand, characteristics of spindles, such as the precise region where they are recorded, substantially determine the effect that auditory stimuli will have on their properties and dynamics. For instance, spindles generated in granular and supra-granular layers of S1 seem to be more likely to be disrupted or enhanced by certain types of auditory stimuli (i.e. pure tones or 12Hz clicks) than spindles generated in

infra-granular layers. Such observations rise important questions about the mechanisms mediating the effects of auditory stimulation on sleep oscillatory dynamics.

5.4.1. Potential mechanisms implicated in the association between spindle activity and auditory stimulation

5.4.1.1. Insights from the semi-periodic presentation of pure tones

Our results suggest that long pure tones (0.5s – 8s) presented during NREM sleep, induce an initial brief increase followed by a substantial, and long-lasting (~24s), reduction in the population spiking activity of neurons in S1 layers where spindles are most prominent (i.e. granular and supra-granular layers). Interestingly, spindles recorded from these layers also seem to be disrupted by these sounds, and show a homeostatic rebound after ~16s of undisrupted sleep. As mentioned before, it has been reported that high neuronal activity during sleep can be followed by periods of diminished oscillatory (Bergmann et al., 1987) and population neuronal activity across different regions of the brain (Miyawaki et al., 2017). The periods of reduced spiking and spindle activity during sound presentation, and the subsequent post-stimulus increase in spindle activity observed in our experiments, could be potentially associated with such phenomena.

In fact, in line with our results, the periods of "low activity", described before (Miyawaki et al., 2017), have been found to last several seconds and to be followed by a transient

increase in sleep-related oscillations (i.e. sharp-wave ripples and slow-waves). Furthermore, periods of "low activity" have been reported to occur during natural sleep in response to REM sleep, UP slow-wave states, and sharp-wave ripples. It has been suggested that coordinated reductions in neuronal spiking during sleep may favour cellular rest and restoration (Vyazovskiy and Harris, 2013). It is possible, that in our experiments and elsewhere, these periods of reduced population spiking reflect a need for cellular restoration in response to increased levels of activity initially triggered by the long-duration and high-intensity sounds. Along this line of thought, it is possible that short sounds played at low intensity did not induce substantial reductions in multi-unit or spindle activity because their initial evoked response was smaller than the response to long high intensity sounds.

The interaction between sounds and spindles is also likely to be modulated by subcortical neuromodulatory centers. These nuclei, such as the noradrenergic Locus Coeruleus or the cholinergic basal forebrain react strongly to salient stimuli (Bouret and Richmond, 2015) and have a profound influence on sleep and arousal (Carter et al., 2010; Naganuma et al., 2019). Indeed, it has recently been shown that Locus Coeruleus reacts to sounds during sleep and is involved in determining whether such sounds result in an arousal or not (Hayat et al., 2020). Hence, it is certainly possible that the results in this chapter involve sound-induced activity of subcortical neuromodulators. For instance, the transient suppression of spindle activity in response to constant tones could be due to increased arousal promoting signalling from locus coeruleus and/or nucleus basalis.

5.4.1.2. Insights from the closed-loop presentation of click trains

Given that long (0.5 and 8-s) sounds temporarily reduced neuronal and oscillatory activity in S1, it is interesting that the click trains (12Hz or 40Hz) did not disturb but rather (in some cases) amplified spindle oscillations. Previous studies suggest that optogenetic stimulation of parvalbumin-expressing inhibitory neurons in the reticular nucleus of the thalamus can induce spindle-like activity in the EEG and LFP (Halassa et al., 2011; Latchoumane et al., 2017). These studies report inducing spindles in the cortex by stimulating TRN with 8Hz 6.25ms (Latchoumane et al., 2017) pulses or a single 20ms pulse (Halassa and Acsády, 2016). It is possible that, similar to those studies, click trains induce repetitive burst firing in thalamic-projecting areas (e.g. TRN) and thereby enhance spindle activity. Moreover, these results could potentially suggest that stimulation outside the spindle frequency range may positively modulate spindles in the cortex as long as they induce burst firing of TRN.

The reason why the sounds we presented, affected the neuronal and oscillatory activity differentially across layers of S1 is uncertain. Auditory stimuli are known to generate robust evoked-responses in S1 arising from a variety of sources like the thalamic nuclei (i.e. auditory, somatosensory or multisensory), cortico-cortical A1 to S1 connections, or inputs from higher association areas to S1 (Zhou and Fuster, 2004; Lemus et al., 2010; Maruyama and Komai, 2018). The different sets of thalamocortical and corticocortical connections in S1 could possibly explain the different effects of sounds across S1. For instance, cortico-cortical inputs from A1 to S1 have been reported to be of feedback nature and terminate mainly in upper supra granular and lower infra-granular layers (Henschke et al., 2015; Massé et al., 2019).

On the other hand, thalamo-cortical projections to S1 mainly terminate in the granular layer and also layer 6 (Lee and Imaizumi, 2013). Such divergent sources of input could explain why the long 5 kHz pure tones induced an increase in neuronal activity in infra-granular layers and a reduction in the granular layer, specifically in areas where thalamo-cortical oscillations (i.e. spindles) were most pronounced. It is possible, for instance, that the sound presentation at a spindle frequency range had a specific effect on spindles in the granular layer, if this sound type had an effect on the firing frequency of thalamo-cortical cells. Future studies recording simultaneously from thalamic nuclei and S1 could help to elucidate some of these possibilities.

5.4.2. The spindle activity seems to show a homeostatic regulation

The results from our different semi-periodic auditory stimulation paradigms, consistently suggest that spindles are regulated in a homeostatic fashion. This is a novel finding, which had not been reported previously. In our different experiments, spindle activity showed a rebound increase after the disruption induced by the auditory stimulation (long pure-tones presented at 80dB). This homeostatic rebound initiated ~8-s after the sound offset in cases where there was an opportunity for recovery (i.e. when stimuli were presented at ~45s intervals). Moreover, this rebound increase lasted as long as ~2 to 3 hours, after spindle activity was reduced for ~2 hours (during the auditory paradigm where sounds were repeated at ~10-s intervals). Sleep/wake homeostasis balances these two processes by regulating the intensity and duration of these states. Interestingly, during the rebound period we observed here, the main

increase was in the incidence of spindles, while their *o-Quality* (strength) and duration only showed minor increases.

These results have several important implications. On the one hand, due to their hypothesised relevance in different cognitive processes and in brain disorders, spindles have become an attractive target for neuro-modulation. Several approaches have been developed to enhance or inhibit these oscillations in attempts to study their functional role (Latchoumane et al., 2017; Lustenberger et al., 2018), improve memory performance (Antony and Paller, 2017; Antony et al., 2018; Henin et al., 2019; Ngo et al., 2019) or treat disorders like schizophrenia (Manoach et al., 2020). These approaches have achieved inconsistent results, which may arise in part by the fact that the effect of the sleep-oscillation manipulation in the architecture of sleep and the long-term dynamics of these oscillations is often not taken into consideration.

Based on our present results, it is still not clear whether a stimulation-related increase in spindle activity could cause a resulting homeostatic decrease. Further analyses on the data acquired from these experiments may shed light onto this phenomenon. Nonetheless, it would be relevant if future approaches attempting to manipulate spindle activity take into consideration that such interventions can have an impact in the dynamics of spindle incidence over long time-periods.

5.4.3. Potential role of spindles protecting sleep from sensory disruption

One of the most popular views regarding the functional role of spindles is that they support the maintenance of sleep by disrupting the transfer of sensory stimuli to the

cortex (Dang-Vu et al., 2011; Schabus et al., 2012; Lecci et al., 2017). Although some of our results seem to be in line with this hypothesis, further work needs to be done to interpret them fully. Specifically, the fact that mice showed reduced motor responses (i.e. lower EMG variance and power) when sounds were paired withS1 spindles than in the absence of these oscillations, is a first preliminary result pointing in this direction. Similarly, the fact that neuronal silencing in response to auditory stimulation is stronger in local areas showing the highest density and *o-Quality* of spindles in S1, might also suggest a potential role of spindles in the protection of sleep from sensory disruption (although it could reflect a coincidental phenomenon).

Following this line of thought, it is therefore somewhat surprising that click trains, played exactly at the time of spindles occurrence, actually increased the duration and *o-Quality* of granular spindles. This preliminary result could potentially suggests that not all sounds are disrupted by the thalamo-cortical burst activity, or that the spindle-generating system respond to spindles in different ways. Overall, the process by which the brain maintains sensory reactivity to the environment, while allowing a level of sensory disconnection, is fundamental for survival and, therefore, is an important matter to investigate further.

Overall, our results are still too preliminary to draw strong conclusions about the potential role of spindles in the protection of sleep from sensory disruption, which has been suggested before (Yamadori, 1971; McCormick and Feeser, 1990; Elton et al., 1997; Murray Sherman, 2001; Dang-Vu et al., 2010; Lecci et al., 2017). However, our results hint that spindles can be both protective and reactive to sensory stimulation. Additionally, our current work was mainly based on spindles detected in the

somatosensory cortex and the EMG activity. To further investigate this hypothesis, future work will be done on the collected dataset to analyse the neuronal and oscillatory (EEG and LFP) dynamics in both S1 and the primary auditory cortex in response to the different auditory stimulation paradigms that we performed.



CHAPTER 6 - General Discussion and Future Directions

Due to their purported biological relevance, over the last decades spindles have become one of the most widely studied sleep oscillations and emerged as an attractive target for neuromodulation technologies. Within this context, the overarching aim of this thesis was to investigate the spatiotemporal dynamics and functional role of spindles, taking into account the fact that they emerge within highly complex and multidimensional networks. Naturally, our first step was to evaluate critically how sleep spindles have been traditionally defined and analysed. Then, we made an effort to propose and develop a novel conceptual and methodological framework that take into account their complex dynamics. Our work led to a series of methodological, conceptual, and practical advances, which are discussed below.

6.1. Methodological advances

Traditionally, neural oscillations like spindles have been considered all-or-none phenomena and, hence, have been detected using single fixed thresholds (Schimicek et

al., 1994; Huupponen et al., 2000, 2007; Achermann and Olbrich, 2004; Olbrich and Achermann, 2005; Devuyst et al., 2006; Ray et al., 2010; Wamsley et al., 2012). Our results show that this type of binary classification of spindles based on single fixed thresholds is arbitrary and cannot be justified physiologically or mathematically. We therefore developed a quantitative metric of the strength of oscillatory activity, which we termed *oscillatory-Quality* (*o-Quality*). This parameter reflects a fundamental property of oscillations, and therefore, together with other parameters such as their frequency, offers a more complete picture of their behaviour. We applied this metric to detect spindles across a range of brain areas and spatial scales, for the first time, in mice. Combining the *o-Quality* metric with spatial information (spanning local MUA up to more "global" EEG levels), we obtained new insights into the spatiotemporal dynamics of spindles and their interaction with other sleep oscillations.

Building on this, we then developed an experimental approach to detect and stimulate spindles in real time. To the best of our knowledge, this is the first time that a "closed loop-system" has been successfully applied to the detection and manipulation of sleep spindles, which relies exclusively on the detection of actual spindles instead of slow-waves. It therefore constitutes an important step towards more precise and targeted manipulations, potentially useful for future applications. The next steps will be to utilise our newly established *o-Quality* metric for online spindle detection, as well as to adapt this approach for other sleep oscillations, including slow waves and theta-activity. Since *o-Quality* provides a more complete picture of the spatio-temporal dynamics of neural oscillations, we argue that this represents an important refinement for the existing technologies, and will benefit numerous applications for basic and clinically relevant research. Additionally, the present approach uses discrete *o-Quality* levels, which we

used as an initial approach to understand the spatio-temporal dynamics of spindles. In future steps, we will analyse the *o-Quality* as a continuous function in order to better understand the potential continuity in spindle dynamics.

Note that the incidence of spindles detected with the AR-model presented and expanded in this thesis does not relate directly with the power in the sigma activity as calculated with spectral analyses (FFT). This divergence was expected given that spectral analyses are not optimal for differentiating fractal and oscillatory activity in electrophysiological signals (Wen and Liu, 2016), while the AR-model can differentiate oscillatory events from background activity (Olbrich and Achermann, 2005). As the sigma activity is traditionally used in the literature as a proxy for spindle-like activity future work will be performed to understand and characterise the divergence between the oscillatory activity detected with the AR-model and the sigma activity characterised with spectral analyses.

6.2. Insights into the spatio-temporal dynamics of spindles

6.2.1. The progressive occurrence of spindles in space and time

One of the central findings in this thesis is that spindles are not all-or-none phenomena. Instead, we demonstrate that their properties such as *o-Quality* and incidence show a progressive change across different spatial and temporal scales. First, in terms of their spatial dynamics, these parameters vary substantially from one brain region to another, as well as over small distances (few hundred micrometers) within the cortex. Specifically, we found that LFP spindles show higher incidence and *o-Quality* in primary

somatosensory (S1) relative to primary motor cortex (M1), while no strong evidence of spindle activity was found in the primary auditory cortex (A1). Additionally, spindles show higher incidence and *o-Quality* in layers 4 and 3 in S1, and layers 4 and 5 in M1, which is in agreement with previous evidence (Kandel and Buzséki, 1997; Fernandez et al., 2018; Hagler et al., 2018) and the architecture of thalamo-cortical connectivity (Killackey, 1973; Jensen and Killackey, 1987; Lee and Imaizumi, 2013; Hunnicutt et al., 2014). It remains to be investigated whether the prominence of spindles in sensory areas is specific to laboratory rodents, or whether it generalises to other animals including humans.

Second, the *o-Quality* and incidence of spindles can also vary over different temporal scales. For instance, they can vary within seconds, from one event to another, and possibly in direct relationship with the slow wave activity. Furthermore, spindle activity can also progressively increase within infra-slow oscillation cycles across NREM episodes, which typically last a few minutes, or decrease across hour time-scales within light periods.

6.2.2. Spindle o-Quality and network synchrony

Our results further indicate that the *o-Quality* reflects the level of synchrony within the networks involved in the expression of spindles, and can be a useful metric to understand conditions in which the network synchrony is affected. On the one hand, while spindles with low *o-Quality* tend to show a localised expression and are transient, high *o-Quality* spindles are longer and encompass larger cortical regions. Additionally, these is a positive relationship between spindle *o-Quality* and slow wave activity, which

has been previously shown to reflect the level of synchrony across neuronal populations (Vyazovskiy et al., 2009b; Nir et al., 2011) and provide network synchronization to higher frequency oscillations, such as spindles (Contreras and Steriade, 1996; Buzsáki and Draguhn, 2004; Staresina et al., 2015).

On the other hand, our results suggest that a relevant link exists between glutamatergic neurotransmission and the network mechanisms implicated in the generation and/or synchronization of spindles. Specifically, deficits related to the deletion of the GluA1 subunit of the AMPA receptors can result in network states in which spindles are preserved within local circuits but do not synchronize and express in the EEG. AMPA receptors have been found to play an important role in the propagation of thalamo-cortical rhythms within the cortex (Fernandez et al., 2018), and future work is needed to further our understanding of *o-Quality* dynamics in models where AMPA receptors in general, or specific receptor subunits in particular, are targeted.

In this regard, it should be highlighted that while our results suggest that the variability of spindles in terms of their *o-Quality* is progressive, it is important to further investigate the potential source of this variability, i.e. are spindles with different *o-Quality* generated from the same, or different, origins and sources? Current source density analyses could be applied to our data to give an initial indication. Additionally, it has been proposed that matrix and core regions of first order and second order thalamic nuclei may give rise to global and local spindles, respectively (Bonjean et al., 2011, 2012; Hagler et al., 2018; Krishnan et al., 2018). Future studies that, for example, simultaneously record from the thalamus and cortex would be informative to address this question.

6.2.3. Characterising spindles: from global, to local, to dynamic

For decades after their discovery, spindles were considered global phenomena that extended wide thalamo-cortical areas (Contreras et al., 1997a; Achermann and Borbély, 1998; Sejnowski and Destexhe, 2000; Steriade, 2003). Technological developments allowing LFP measurements within local neuronal populations have promoted the idea that, although sleep appears behaviourally as a global state, sleep related neuronal activity is predominantly local (i.e. can show substantial changes within micro-meter distances) (Andrillon et al., 2011; Nir et al., 2011; Bonjean et al., 2012; Piantoni et al., 2017; Fernandez et al., 2018). It is widely accepted, therefore, that sleep oscillations manifest as mixture of local activity and synchronous activity across wide-spread brain areas. Our results extend these ideas by suggesting that, although sleep oscillations, like spindles, can show substantial divergence at different spatial and temporal scales, these changes lie on a continuum. As such, sleep-related activities, at least in the case of spindles, should not be classified as simply 'local' or 'global' as they are typically portrayed, but there is rather a gradual progression in their dynamics.

Interpreting this in a wider picture, neuronal networks in the mammalian brain have an intrinsic capacity to generate and sustain a wide range of rhythmic activity patterns, which are intimately related (Buzsáki and Draguhn, 2004). A relevant question therefore arises based on our results: if spindles exhibit progressive change in their properties across different spatial and temporal scales, would this progressive behaviour also characterise other sleep oscillations or even sleep/wake states? A binary system balancing sleep/wake states has been proposed, wherein two mutually inhibitory circuits act to switch the body between wake and sleep states (commonly

referred as the flip-flop model) (Saper et al., 2001, 2010). Other approaches, however, have suggested that the sleep/wake dynamics can be more accurately modelled when considered on a continuous scale rather than using pre-defined stages (Pardey et al., 1996). Our results support the idea that at least some events during sleep vary in a gradual or even continuous manner. Investigating whether other sleep oscillations display this type of dynamic behaviour would be a relevant avenue for future research.

6.3. Insights into the homeostatic regulation of spindles

Another fundamental finding is that spindles are homeostatically regulated. Specifically, we found for the first time, that decreases in spindle activity resulting from extended wakefulness or auditory stimulation are followed by a compensatory increase in spindle activity. In other words, the total amount of spindle activity was preserved but, interestingly, the compensatory processes could be either instantaneous or delayed, depending on the specific experimental paradigm. Therefore, our results suggest that the specific parameters used for spindle manipulation, as well as the time scale considered, might be crucial for determining the resulting effect.

The homeostatic control of sleep/wake states has long been considered a basic principle of sleep regulation (Borbely, 1980, 1982; Daan et al., 1984), and EEG slow wave activity has traditionally served as the main indicator of this principle (Tobler et al., 1983; Feinberg et al., 1985; Dijk et al., 1987; Achermann et al., 1993; Werth et al., 1997). The biological mechanisms behind this process remain unknown, although fundamental developments have suggested that sleep homeostasis reflects a process whereby sleep counterbalances, for instance, net synaptic strengthening (Tononi and

Cirelli, 2003, 2006) or the accumulation of metabolites, like adenosine (Porkka-Heiskanen and Kalinchuk, 2011), which occur during wakefulness. These hypotheses have stimulated extensive research and discussion within the field, which has been crucial for our growing understanding of sleep dynamics and function. In this context, our results further suggest that sleep spindles are homeostatically regulated, and not only in response to the dynamics of the slow wave activity, as it has been previously reported (Knoblauch et al., 2002). This raises another important question as to whether the mechanisms implicated in the homeostatic regulation of spindles are the same, or at least linked to, those regulating sleep/wake states or slow wave activity. Additionally, if they happen to be different mechanisms, it would be relevant to understand how they might interact.

There are several biological mechanisms that could potentially be implicated in the homeostatic regulation of spindles. On the one hand, it has been reported that spindles have the capacity to modulate synaptic plasticity by facilitating (Contreras et al., 1997b; Niethard et al., 2018; Dickey et al., 2020) or inducing long-term potentiation (Rosanova and Ulrich, 2005), although depression can also be induced depending on the type of stimulation (Crochet et al., 2006). Their homeostatic regulation could therefore reflect a process through which net synaptic weights are being regulated. On the other hand, subcortical neuromodulatory centres react strongly to salient stimuli (Bouret and Richmond, 2015) and have a profound influence on sleep and arousal (Carter et al., 2010; Xu et al., 2015). Spindle changes, induced through extended wakefulness our auditory stimulation, could be an epiphenomenon of a wider modulation of neuromodulatory activity. At any rate, while the biological relevance of spindle

homeostasis remains to be determined, our findings provide novel perspectives for understanding their functional role.

6.4. Insights into the functional role of sleep spindles

The functional role of spindles remains debated. One of the most popular hypotheses is that spindles are part of a network that protects sleep from sensory disruption to facilitate recovery and memory consolidation (Gais et al., 2002; Bergmann et al., 2012; Born and Feld, 2012; Ngo et al., 2013b; Rasch and Born, 2013; Latchoumane et al., 2017; Lecci et al., 2017). In this regard, our results that long-term memory is preserved in GRIA1$^{-/-}$ mice, suggest that at least highly synchronous spindles (i.e. those detected at the EEG level) are not strictly necessary for long-term memory consolidation. Specifically, we found that GRIA1$^{-/-}$ mice showed comparable memory performance to WT mice in hippocampal-based memory tasks, even when the large-scale synchrony of spindles, and their expression at the EEG level, is significantly reduced in these mice. These results are consistent with extensive literature, where a significant variety of memory tests have been performed (which has previously been extensively studied, e.g. Zamanillo et al., 1999; Reisel et al., 2002; Schmitt et al., 2003; Sanderson et al., 2009; Bannerman et al., 2014). It is important to highlight that GRIA1$^{-/-}$ mice is a constitutive knockout and resulting genetic compensation in related genes are possible (El-Brolosy and Stainier, 2017). Nonetheless, regardless of the specific molecular mechanism, there is a network alteration of spindle activity in these mice, which does not necessarily lead to deficits in several hippocampal-based learning tasks.

To date, several studies in the literature, which support the role of spindles in the consolidation of memory during sleep, have focused on correlations and comparisons between sleep and wake, taking the latter as a constant state. Our results highlight, however, that it is important to reassess whether spindles are actually necessary, or simply epiphenomena reflecting other processes that may support memory processing during sleep. Moreover, the continuous nature of sleep oscillations, like spindle-activity, invites us to interpret comparisons between sleep and wake processes from a different angle, taking into account the possibility that they are highly dynamic and heterogeneous states.

Finally, our results are still too preliminary to draw strong conclusions about the potential role of spindles in the protection of sleep from sensory disruption, which has been suggested before (Yamadori, 1971; McCormick and Feeser, 1990; Elton et al., 1997; Murray Sherman, 2001; Dang-Vu et al., 2010; Lecci et al., 2017). However, what these results highlight is that the interaction between spindles and auditory processing is highly complex. Our results hint that spindles can be both protective and reactive to sensory stimulation, and that their particular behaviour strongly depends on the specific parameters of the presented sound, the topography of the spindle activity, and likely other factors. Our current work, however, was mainly based on spindles detected in the somatosensory cortex, and different interactions might be evident in the auditory cortex. To further investigate this hypothesis, future work will be done on the collected dataset to analyse the neuronal and oscillatory dynamics in both S1 and the primary auditory cortex in response to the different auditory stimulation paradigms that we performed.

6.5. Practical and clinical implications of these advances

Advances in the physiological understanding of sleep oscillations, combined with the evolving progress of technologies for modulating spindles (Halassa et al., 2011; Lustenberger et al., 2016, 2018; Antony and Paller, 2017; Latchoumane et al., 2017), have opened new avenues to further understand their functional role and biological relevance in both health and disease (Astori et al., 2013; Geiser et al., 2020; Manoach et al., 2020). It should be emphasised that sleep is a strictly regulated process, and our results show that spindles, in addition to slow waves, which together comprise two fundamental hallmarks of NREM sleep, are homeostatically regulated. Building on this, future approaches attempting to manipulate spindle activity should take into consideration the likelihood that such interventions can have an impact in the dynamics of spindle incidence over long time-periods.

Additionally, our results show that the EEG, which is typically used to study spindles in humans and is one of the most widespread techniques used in clinical environments to record neuronal electrical activity (Freeman, 2006), does not capture the dynamical complexity of spindle activity. Studies of spindle dynamics and manipulations based on scalp EEG recordings only, should be viewed, at most, with caution. While such recordings are sensitive to the strongest and most synchronous spindle oscillations (which are only a small proportion of the whole spindle population), the method is effectively blind to the majority of spindles occurring at finer spatial scales.

APPENDIX CHAPTER 3: STATISTIC TABLES

Abbreviations and notes:

- **WS**: within-subject factor.
- **BS**: between-subject factor.
- **GG**: Greenhouse-Geisser test used sphericity is not assumed (Mauchly's Test, p<0.05).
- *p<0.05, **p<0.001, ***p<0.0001.
- Note: tables are coloured to facilitate the discrimination of different analysis steps.

Variables	Multivariate ANOVA Pillai's Trace (mouse as covariate)	Follow-up Repeated measures ANOVA	Pair-wise comparisons (Sidak)
Dependent variable1: Spindle incidence (per min) **Dependent variable2:** Spindle duration (s) **Dependent variable3:** Spindle Frequency **WS Factor:** r_b thresholds (0.92, 0.93, 0.94, 0.95, 0.96)	Effect of *o-Quality* on spindle incidence, duration and frequency. $F_{4,49}$=83.1, p<0.0001	Effect of r_b thresholds on **incidence** $F_{4,40}$=98.6, p<*** (GG)	p<*** for all contrasts
		Effect of r_b thresholds on **duration** $F_{4,40}$=237.9, p<*** (GG)	p<*** for all contrasts
		Effect of r_b thresholds on **frequency** $F_{4,40}$=8.5, p<* (GG)	oQ1= a,e oQ2= b,e oQ3= c,e oQ4= d,e oQ5= e

Table 1. Statistical analyses for **Figure 8.E**

Variables	Mixed ANOVA	Pair-wise comparisons
Dependent variable: Spindle spatial extent (µm) **WS Factor:** spindle oQuality (oQ1 to 5) **BS Factor:** Electrode configuration (S1 horizontal, S1 laminar, M1 laminar)	**WS effect** *o-Quality* $F_{4,72}$=132.4, p<*** (GG) **BS Effect** electrode configuration $F_{4,17}$=27.5, p<*** (GG) **oQuality * electrode configuration** $F_{4,72}$=1.6, p=0.15 (GG)	**WS: (Sidak)** p<*** for all comparisons (oQ1 to 5). **BS: (Games-Howell)** S1 horizontal=a S1 laminar= a M1 laminar= b

Table 2. Statistical analyses for **Figure 11.A**

Variables	Mixed ANOVA	Post-Hoc (Games-Howell)	Follow-up repeated-measures ANOVA (spindle extent [µm])	Pairwise comparison (Sidak)
Dependent variable: EEG sigma power. **WS Factor:** Spindle spatial extent (µm) **BS Factor:** Electrode configuration (S1 horizontal, S1 laminar, M1 laminar).	**Spindle extent * electrode configuration** $F_{4,72}$=3.1, *p*<* (GG)	S1 horizo.=a S1 lamin.= a M1 lamin.= b	Effect of **spindle extent (µm)** in **S1 horizontal** $F_{4,72}$= 20.5, *p*<*** (GG)	100µm= a 300µm= a 500µm= a, b 700µm= b 900µm= c
			Effect of **spindle spatial extent (µm)** in **S1 laminar** $F_{4,72}$=11.6, *p*<*** (GG)	100µm= a 300µm= a,b 500µm= b,c 700µm= c 900µm= d
			Effect of **spindle spatial extent (µm)** in **M1** $F_{4,72}$=2.7 *p*<* (GG)	100 vs 900µm, *p*<** 100 vs 500µm, *p*<* All other contrasts *p*>*

Table 3. Statistical analyses for **Figure 11.B**

Variables	Mixed ANOVA	Follow-up repeated-measures ANOVA (oQuality)	Pairwise-comparison (Sidak)
Dependent variable: EEG sigma power. **WS Factor:** Spindle oQuality (oQ1 to 5) **BS Factor:** Electrode configuration (S1 horizontal, S1 laminar, M1 laminar)	**WS effect** *o-Quality* $F_{4,72}$=2.97, *p*<* **BS effect** electrode configuration $F_{4,17}$=1.12, *p*=0.36 **oQuality * electrode configuration** $F_{4,72}$=0.3, *p*=0.97	Effect of ***o-Quality*** in S1 horizontal $F_{4,72}$=24.4, *p*<*** (GG)	oQ1= a oQ2= a oQ3= b oQ4= b oQ5= c
		Effect of ***o-Quality*** in S1 laminar $F_{4,72}$=8.0, *p*<* (GG)	oQ1= a oQ2= a oQ3= a oQ4= b oQ5= a,b
		Effect of ***o-Quality*** in M1 laminar $F_{4,72}$=1.11, *p*=0.06 (GG)	

Table 4. Statistical analyses for **Figure 11.B**

Variables	Multinomial logistic regression	B-values (intercept / B)	Confidence intervals (95%)
Dependent variable1: Spindle o Quality **Factor:** Spindle spatial extent (µm) (Including spindles detected in S1 laminar, S1 micro-wire arrays, and M1)	X^2_4=109.1 *p*<***	REF oQ5 oQ1= 4.7 / 4.9 oQ2= 5.3 / 7.1 oQ3= 4.7 / 8.6 oQ4= 2.7 / 10.6	 5.5 – 38 33 – 452 129 – 2400 719 - 22055
Dependent variable2: Spindle spatial extent (µm) **Factor:** EEG sigma power (Including spindles detected in S1 laminar, S1 micro-wire arrays, and M1)	X^2_4=163.3, *p*<***	REF oQ5 oQ1= 1.27 /.19 oQ2= 1.19 / .30 oQ3= .84 / .39 oQ4= .78 / .54	 1.06-1.38 1.19-1.56 1.29-1.69 1.51-1.97
Dependent variable2: *o-Quality* **Factor:** EEG sigma power (Including spindles detected in S1 laminar, S1 micro-wire arrays, and M1)	X^2_4=163.3, *p*<**	REF oQ5 oQ1= .08 / .18 oQ2= .18 / .66 oQ3= .15 / 1.11 oQ4= -.04 / 1.5	 .48 - .29 .72 – 5.14 1.11 – 8.4 1.6-13.0

Table 5. Statistical analyses for **Figure 11**. **A - B**

Variables	Mixed ANOVA	Follow-up univariate ANOVA (derivation)	Post-Hoc (Games-Howell)	Follow-up repeated-measures ANOVA (Spindle incidence)	Post-Hoc (Sidak)
Dependent variable: Spindle incidence **WS Factor:** Spindle oQuality (oQ1 to 5) **BS Factor:** Derivation	**derivation * oQuality** $F_{4,128}$=22.11, *p*<*** (GG)	Effect of **derivation** in **oQ1.** $F_{3,33}$=21.9, *p*<***	S1= a M1= b Fro= b Occ= b	Effect of **oQuality** in **S1** $F_{2,10}$= 28.8, *p*<*** (GG)	*P*<*** for all contrasts but 0Q4vsoQ5, *p*<*
		Effect of **derivation** in **oQ2.** $F_{3,33}$=17.2, *p*<***	S1= a M1= b Fro= b Occ= b	Effect of **oQuality** in **M1** $F_{1,6}$= 18.03, *p*<*** (GG)	oQ1= a oQ2= b oQ3= b oQ4= b oQ5= b
		Effect of **derivation** in **oQ3.** $F_{3,33}$=13.3, *p*<***	S1= a M1= b Fro= b Occ= b	Effect of **oQuality** in **Frontal**	oQ1= a oQ2= b

(S1 LFP, M1 LFP, Frontal EEG, Occipital EEG		Effect of **derivation** in **oQ4.** $F_{3, 33}$=9.22, *p*<***	S1= a M1= b Fro= b Occ= b	$F_{1,10}$= 33.5, *p*<*** (GG)	oQ3= c oQ4= d oQ5= d
				Effect of **oQuality** in **Occipital** $F_{1,10}$= 24.8, *p*<*** (GG)	*P*<*** for all contrasts but 0Q4vsoQ5, *p*<*
		Effect of **derivation** in **oQ4.** $F_{3, 33}$=5.05, *p*<**	S1= a M1= b Fro= b Occ= b		

Table 6. Statistical analyses for **Figure 12.A (top panel)**

Variables	**Mixed ANOVA**	**Follow-up univariate ANOVA (derivation)**	**Post-Hoc (Games-Howell)**	**Follow-up Repeated measures ANOVA (Spindle duration)**	**Post-Hoc (Games-Howell)**
Dependent variable: Spindle duration **WS Factor:** Spindle oQuality (oQ1 to 5) **BS Factor:** Derivation (S1 LFP, M1 LFP, Frontal EEG, Occipital EEG)	**derivation * oQuality** $F_{4,128}$=1.89, *p*<* (GG)	Effect of **derivation** in **oQ1.** $F_{3,33}$=7.88, *p*<***	S1= a M1= b Fro= b Occ= b	Effect of **oQuality** in **S1** $F_{1,10}$= 94.7, *p*<*** (GG)	oQ1= a oQ2= b oQ3= c oQ4= d oQ5= d
		Effect of **derivation** in **oQ2.** $F_{3,33}$=8.2, *p*<***	S1= a M1= b Fro= b Occ= b	Effect of **oQuality** in **M1** $F_{1,6}$= 72.2, *p*<** (GG)	oQ1= a oQ2= b oQ3= c oQ4= c oQ5= d
		Effect of **derivation** in **oQ3.** $F_{3,33}$=13.6, *p*<***	S1= a M1= b Fro= b Occ= b	Effect of **oQuality** in **Frontal** $F_{1,10}$= 75.3, *p*<*** (GG)	oQ1= a oQ2= b oQ3= c oQ4= c, d oQ5= d
		Effect of **derivation** in **oQ4.** $F_{3,33}$=4.3, *p*<*	S1= a, M1= b Fro= a,b Occ= a,b		
		Effect of **derivation** in **oQ5.** $F_{3,33}$=4.5, *p*<*	S1= a M1= b Fro= b Occ= a,b	Effect of **oQuality** in **Occipital** $F_{1,10}$= 76.0, *p*<*** (GG)	oQ1= a oQ2= b oQ3= c oQ4= d oQ5= d

Table 7. Statistical analyses for **Figure 12.A (bottom panel)**

Variables	Univariate ANOVA (Spindle duration)	Post-Hoc (Games-Howell)
Dependent variable: Spindle oQuality **Factor1:** Derivation (S1 LFP, M1 LFP, Frontal EEG, Occipital EEG)	Effect of **oQuality** in **S1** $F_{3,33}$= 10.12, *p*<*** (GG)	S1= a M1= b Frontal= b Occipital= b

Table 8. Statistical analyses for **Figure 12.B**

Variables	Mixed ANOVA	Follow-up univariate ANOVA (Layer)	Post-Hoc (Tukey)	Follow-up univariate ANOVA (deriv.)	Follow-up *t*-test (Derivation - Sidak)
Dependent variable: Spindle Incidence **WS Factor:** Cortical layer (L2,L3, L4, L5a, L5b, L6) **BS Factor:** Derivation (S1 LFP, M1 LFP)	**Layer * Derivation** $F_{4,48}$=19.58, *p*<***	Effect of **Layer** in **S1.** $F_{5,60}$=19.9, *p*<***	L2= a L3= b L4= b L5a= b,c L5b= a,c L6= a	**BS effect** derivation $F_{5,60}$=14.5, *p*<***	Effect of **derivation** in **L2** T_9= 2.5, *p*<*
					Effect of **derivation** in **L3** T_8= 5.5, *p*<**
					Effect of **derivation** in **L4** t_{10}= 6.2, *p*<***
					Effect of **derivation** in **L5a** t_{10}= 3.9, *p*<**
		Effect of **Layer** in **M1.** $F_{5,60}$=2.8, *p*<*	L3 vs L5b, *p*<* *p*>* for all other contrasts		Effect of **derivation** in **L5b** t_{10} = 1.47, *p*=0.17
					Effect of **derivation** in **L6b** t_{12}= -0.5, *p*=0.59

Table 9. Statistical analyses for **Figure14*.B (left)***

Variables	Mixed ANOVA	Follow-up Repeated-measures ANOVA (Layer)	Pair-wise comparison	Follow-up univariate ANOVA (deriv.)	Follow-up *t*-test (Derivation - Sidak)
Dependent variable: spindle oQuality **WS Factor:** Cortical layer	**WS effect** Layer $F_{5,45}$=10.55, *p*<*** **BS effect** Derivation	Effect of **layer** in **S1** $F_{5,60}$=27.88, *p*<***	L2= a,b L3= c,d L4= c L5a= c,e L5b= a,d,e L6= b	Effect of **derivation** on spindle oQuality. $F_{5,60}$=14.5, *p*<**	Effect of **derivation** in **L2** t_{11}= 1.2, *p*=0.26
					Effect of **derivation** in **L3** t_{10}= 5.0, *p*<**

(L2/3, L4, L5a, L5b, L6) **BS Factor** Derivation (S1 LFP, M1 LFP)	$F_{1,9}$=28.24, *p*<*** **Layer * Derivation** $F_{5,60}$=2.9, *p*<*	Effect of **layer** in **M1** $F_{5,60}$=2.68, *p*<*	L2 vs L4, *p*<* L2 vs L5a, *p*<* *p*>* for all other contrasts		Effect of **derivation** in **L4** t_{12}= 3.4, *p*<* Effect of **derivation** in **L5a** t_{12}= 2.7, *p*<* Effect of **derivation** in **L5b** t_{12} = 2.5, *p*=0.05 Effect of **derivation** in **L6b** t_{12}= -0.5, *p=0.6*

Table 10. Statistical analyses for **Figure14.B *(right)***

Variables	Multivariate ANOVA Pillai's Test (mouse as covariate)	Follow-up univariate ANOVA (Layer)	Post-Hoc (Games-Howell)
Dependent variable: Spindle Incidence (percent of total) by oQuality in S1 **Factor1:** Cortical layer (L2,L3, L4, L5a, L5b, L6)	Effect of **layer** on spindle Incidence. $F_{20,80}$=2.8, *p*<*	Effect of **Layer** in **oQ1.** $F_{5,27}$=0.6, *p*=0.6	
		Effect of **Layer** in **oQ2.** $F_{5,27}$=0.4, *p*=0.8	
		Effect of **Layer** in **oQ3.** $F_{5,27}$=0.8, *p*=0.5	
		Effect of **Layer** in **oQ4.** $F_{5,27}$=1.9, *p*=0.04	L2= a L3= b L4= b L5a= b L5b= a L6= a
		Effect of **Layer** in **oQ5.** $F_{5,27}$=2.8, *p*<*	L2= a L3= b L4= b L5a= b L5b= a L6= a

Table 11. Statistical analyses for **Figure14.C *(left)***

Variables	MANOVA

	(Pillai's Test)
Dependent variable: Spindle Incidence (percent of total) by oQuality in M1 **Factor1:** Cortical layer (L2/3, L4, L5a, L5b, L6)	Effect of **layer** on spindle Incidence. $F_{20,80}$=1.6, p=0.18

Table 12. Statistical analyses for **Figure14.C (*right)***

Variables	Repeated-measures ANOVA (Spindle duration)	Pair-wise comparison (Sidak)
Dependent variable: Normalised probability of slow waves occurring. **WS Factor1:** LFP (S1) spindle oQuality (oQ 1 to 5)	Effect of **slow wave occurrence** on **oQuality** $F_{4,28}$= 5.64, p<***	oQ1= a oQ2= a oQ3= a oQ4= a,b oQ5= b

Table 13. Statistical analyses for **Figure 15.B**

Variables	Repeated-measures ANOVA (Spindle duration)	Pair-wise comparison (Sidak)
Dependent variable: Normalised probability of slow waves occurring. **WS Factor1:** LFP (M1) spindle oQuality (oQ 1 to 5)	Effect of **slow wave occurrence** on **oQuality** $F_{4,28}$= 3.28, p<*	oQ1= a oQ2= a oQ3= a oQ4= a,b oQ5= b

Table 14. Statistical analyses for **Figure 15.B**

Variables	Repeated-measures ANOVA (Spindle duration)	Pair-wise comparison (Sidak)
Dependent variable: Normalised probability of slow waves occurring. **WS Factor1:** EEG frontal spindle oQuality (oQ 1 to 5)	Effect of **slow wave occurrence** on **oQuality** $F_{3,21}$= 8.97, p<** Only oQ1-oQ4 included!	oQ1= a oQ2= a,b oQ3= a,b oQ4= b oQ5= excluded due to lack of oQ5 spindles

Table 15. Statistical analyses for **Figure 15.B**

Variables	Repeated-measures ANOVA (Spindle duration)	Pair-wise comparison (Sidak)
Dependent variable: Normalised probability of slow waves occurring. **WS Factor1:** EEG occipital spindle oQuality (oQ 1 to 5)	Effect of **slow wave occurrence** on **oQuality** $F_{3,21}$=37.6, p<*** Only oQ1-oQ3 included!	oQ1= a oQ2= a oQ3= b oQ4 and oQ5 excluded due to lack of oQ5 spindles

Table 16. Statistical analyses for **Figure 15.B**

Variables	Repeated-measures ANOVA	Pair-wise comparison (Sidak)
Dependent variable-1: SWA activity (%) **WS Factor:** NREM episode bin (1 to 5)	Effect of **NREM episode bin** $F_{4,28}$=63.20, p<***	NRb1= a NRb2= b NRb3= b NRb4= b NRb5= b

Table 17. Statistical analyses for

Figure *16*.A

Variables	MANOVA Pillai's Test (mouse as covariate)	Repeated-measures ANOVA (Spindle duration)	Pair-wise comparison (Sidak)	Repeated-measures ANOVA (oQuality)	Pair-wise comparison (Sidak)
Dependent variable-1: Spindle Incidence **Dependent variable-2:** Spindle mean oQuality **WS Factor:** NREM episode bin (1 to 5)	Effect of **NREM episode bin** $F_{4,28}$=4.5, p<***	**WS effect** of NREMbin (NRb) on spindle **incidence.** $F_{4,28}$=33.68, p<***	NRb1= a NRb2= b NRb3= b NRb4= c NRb5= c	Effect of **NREMbin** on spindle **mean oQuality.** $F_{4,28}$=9.5, p<***	NRb1= a NRb2= b NRb3= b NRb4= b NRb5= b

Table 18. Statistical analyses for

Figure *16*.B

Variables	Repeated-measures ANOVA	Pair-wise comparison (Sidak)
Dependent variable-1: SWA activity (%) **WS Factor:** Zeitgeber Time	Effect of **Zeitgeber Time** $F_{11,77}$=6.14, p<***	ZT0= a ZT1= a,b ZT2= b ZT3= a,b ZT4= b ZT5= b,c ZT6= b,c ZT7= b,c ZT8= b,c ZT9= c ZT10= b,c ZT11= c

Table 19. Statistical analyses for

Figure *16*.C

Variables	MANOVA (Pillai's Test)	Follow-up repeated-measures ANOVA (Spindle incidence)	Pair-wise comparison (Sidak)	Follow-up repeated-measures ANOVA (oQuality)	Pair-wise comparison (Sidak)
Dependent variable-1: Spindle Incidence **Dependent variable-2:** Spindle mean oQuality **WS Factor:** Zeitgeber Time	Effect of **Zeitgeber time** $F_{5,35}$=2.9, p<*	Effect of **Zeitgeber Time** on spindle **incidence.** $F_{5,35}$=5.66, p<**	ZT0-2= a,b ZT2-4= a ZT4-6= a ZT6-8= a,c ZT8-10= a ZT10-12= b,c	Effect of **Zeitgeber Time** on spindle **mean oQuality.** $F_{5,25}$=2.4, p<*** (GG)	ZT0-2= a ZT2-4= a,b ZT4-6= a,b ZT6-8= b ZT8-10= b,c ZT10-12= c

Table 20. Statistical analyses for

Figure *16*.D

Variables	Mixed ANOVA	Follow-up univariate ANOVA (Sleep condition)	Follow-up repeated-measures ANOVA (Z-Time)	Post-Hoc (Sidak)
Dependent variable: Slow wave activity (%) **WS Factor:** Zeitgeber Time **BS factor:** Sleep condition (Baseline vs recovery)	**Zeitgeber Time * Sleep Condition** $F_{5,40}$=7.9, *p*<***	Effect of **sleep condition** at **ZT7** $F_{1,14}$=37.8, *p*<***	Effect of **Zeigeber Time** on Slow wave activity at **baseline** $F_{5,42}$=1.9, *p*=0.1	
		Effect of **sleep condition** at **ZT8** $F_{1,14}$=17.8, *p*<***		
		Effect of **sleep condition** at **ZT9** $F_{1,14}$=23.4, *p*<***		
		Effect of **sleep condition** at **ZT10** $F_{1,14}$=1.9, *p*=0.2	Effect of **Zeitgeber Time** on Slow wave activity at **recovery** $F_{5,42}$=12.5, *p*<***	ZT7= a ZT8= a,b ZT9= b,c ZT10= b,c ZT11= c ZT12= c
		Effect of **sleep condition** at **ZT11** $F_{1,14}$=0.9, *p*=0.4		
		Effect of **sleep condition** at **ZT12** $F_{1,14}$=0.4, *p*=0.5		

Table 21. Statistical analyses for

Figure *16*.E

Variables	Mixed ANOVA	Follow-up repeated-measures ANOVA (Spindle incidence)	Follow-up repeated-measures ANOVA (oQuality)

Dependent variable-1: LFP Spindle Incidence **Dependent variable-2:** LFP Spindle mean oQuality **WS Factor:** Sleep condition (Sleep baseline, Sleep recovery).	Effect of **Sleep condition** $F_{2,18}$=4.6, p<*	Effect of **Sleep condition** on spindle **incidence.** $F_{1,9}$=7.9, p<*	Effect of **Sleep condition** on spindle **mean oQuality.** $F_{1,9}$=8.1, p<**

Table 22. Statistical analyses for

Figure *16*.F

Variables	Mixed ANOVA	Follow-up univariate ANOVA
Dependent variable-1: LFP power density **WS factor:** Frequency (Hz) **BS factor:** Sleep condition (Sleep baseline, Sleep recovery).	Frequency* Condition $F_{79,1422}$=10.03, p<***	p<0.05 All contrasts between: 2.5Hz to 7Hz 11Hz to 15Hz

Table 23. Statistical analyses for

Figure *16*.G

Variables	Multivariate ANOVA	Follow-up repeated-measures ANOVA (Spindle incidence)	Follow-up repeated-measures ANOVA (oQuality)
Dependent variable-1: EEG Spindle Incidence **Dependent variable-2:** EEG Spindle mean oQuality **Factor:** Sleep condition (Sleep baseline, Sleep recovery).	Effect of **Sleep condition** $F_{2,18}$=0.34, p=0.71 (GG)	Effect of **Sleep condition** on spindle **incidence.** $F_{1,9}$=0.49, p=0.5 (GG)	Effect of **Sleep condition** on spindle **mean oQuality.** $F_{1,9}$=0.88, p=0.37 (GG)

Table 24. Statistical analyses for

Figure 16.F

Variables	Repeated-measures ANOVA	Pair-wise comparison (Sidak)
Dependent variable-1: Incidence of spindles per burst **WS factor:** NREM episode bin (1-5)	Effect of **NREM episode bin (NRb)** $F_{4,28}$=26.78, p<***	NRb1= a NRb2= b NRb3= b,c NRb4= b NRb5= c

Table 25. Statistical analyses for **Figure 18.B**

Variables	Multivariate ANOVA (Pillai's Test)	Follow-up repeated-measures ANOVA (spindle burst duration)	Pair-wise comparison (Sidak)	Follow-up repeated-measures ANOVA (spindle burst incidence)	Pair-wise comparison (Sidak)
Dependent variable-1: Spindle burst duration **Dependent variable-2:** Spindle burst incidence **Factor:** NREM episode bin (1-5)	Effect of **NREM episode bin** $F_{8,60}$=5.4, p<***	Effect of **NREM episode bin** on **spindle burst duration** $F_{4,40}$=4.8, p<**	NRb1= a NRb2= a,b NRb3= b NRb4= b NRb5= b	Effect of **NREM episode bin** on **spindle burst incidence.** $F_{4,40}$=21.0, p<***	NRb1= a NRb2= b NRb3= b NRb4= b NRb5= b

Table 26. Statistical analyses for **Figure 18.C**

Variables	Mixed ANOVA (Sphericity assumed)	Follow-up repeated measures ANOVA (Spin.burst position)	Pair-wise comparison (Sidak)	Follow-up repeated measures ANOVA (BurstBin)	Pair-wise comparison (Sidak)
Dependent variable: Mean spindle oQuality **WS Factor:** Spindle burst bin (1-6)	**Spindle burst bin * Spin.burst position** $F_{5,20}$=2.5, p<*	Effect of **spin.burst position** at **BurstBin1** Mean=1 (all other bins normalised to first bin)		Effect of spindle **burst bin** on spindle oQuality during **first spindle burst** $F_{5,20}$=1.6, p=0.2	

BS factor: Spindle burst position within NREM episodes (first burst, middle burst, last burts)		Effect of **spin.burst position** at **BurstBin2** $F_{2,9}$=5.5, p<*	Early= a Mid= a,b Late= b		
		Effect of **spin.burst position** at **BurstBin3** $F_{2,9}$=6.2, p<*	Early= a Mid= a,b Late= b	Effect of spindle **burst bin** on spindle oQuality during **first middle burst** $F_{5,20}$=1.2, p=0.3	
		Effect of **spin.burst position** at **BurstBin4** $F_{2,9}$=3.12, p=0.05	Early= a Mid= a Late= a		
		Effect of **spin.burst position** at **BurstBin5** $F_{2,9}$=6.6, p<*	Early= a Mid= a,b Late= b	Effect of spindle **burst bin** on spindle oQuality during **first last burst** $F_{5,20}$=5.2, p<**	BBin1= a BBin2= b BBin3= c BBin4= a,b,c BBin5= a,b,c BBin6= b,c
		Effect of **spin.burst position** at **BurstBin6** $F_{2,9}$=19.1, p<***	Early= a Mid= a Late= b		

Table 27. Statistical analyses for **Figure 18.C**

Variables	**Repeated-measures ANOVA**	**Pair-wise comparison (Sidak)**
Dependent variable-1: Increase in spindle oQ within spindle burst **WS Factor:** NREM episode bin (1-5)	Effect of **NREM episode bin (NRb)** $F_{4,28}$=4.4, p<**	NRb1= a NRb2= a NRb3= a NRb4= a,b NRb5= b

Table 28. Statistical analyses for **Figure 18.D**

APPENDIX CHAPTER 4: STATISTIC TABLES

Abbreviations and notes:

- **WS**: within-subject factor.
- **BS**: between-subject factor.
- **GG**: Greenhouse-Geisser test used sphericity is not assumed (Mauchly's Test, p<0.05).
- **WT**: Wild-type mice
- **KO**: GRIA1 -/- mice
- *p<0.05, **p<0.001, ***p<0.0001.
- Note: tables are coloured to facilitate the discrimination of different analysis steps.

Variables	Mixed ANOVA	Follow-up T-test (Sidak) (BS Factor)
Dependent variables: Log transformed EEG absolute power density (for each frequency bin (Freq=0:0.25:20) **BS factor:** Genotype (WT,KO) **WS factor:** Frequency	**Genotype*Frequency** $F_{80,960}$= 8.97, *p*<*** (GG)	*p*<* for frequencies 11.5 to 19.5 All other T-tests *p*>*

Table 29. Statistical analyses for **Figure 22.A**

Variables	Multivariate ANOVA	Follow-up ANOVAS
Dependent variable1: Mean EEG spindle incidence	Effect **Genotype** $F_{2,20}$= 7.82, *p*<**	Effect **Genotype** on incidence $F_{1,12}$= 17.62, *p*<***

Dependent variable2: Mean EEG spindle *o-Quality* **Independent variable:** Genotype (WT,KO)		Effect **Genotype** on *o-Quality* $F_{1,11}$= 15.21, *p*<*

Table 30. Statistical analyses for **Figure 22.B**

Variables	Mixed ANOVA	Follow-up Repeated Measure (WS factor)	Pair-wise comparison	Follow-up Kruskal-Wallis Test (BS factor)
Dependent variable1: EEG spindle incidence **BS factor:** Genotype (WT,KO) **WS factor:** EEG spindle *o-Quality* (oQ1 to 5)	Effect **Genotype* oQuality** $F_{4,40}$= 5.97, *p*<*	Effect of **spindle oQuality** in **WT** $F_{1,4}$= 11.23, *p*<* (GG)	**WT:** Effect of *O-Quality* on incidence oQ1= a oQ2= b oQ3= c oQ4= c oQ5= c	**oQ1:** WT vs KO X^2_1=5.77, *p*<*
				oQ2: WT vs KO X^2_1=5.77, *p*<*
				oQ3: WT vs KO X^2_1=5.77, *p*<*
		Effect of **spindle oQuality** in **KO** $F_{1,4}$= 17.15, *p*<** (GG)	**KO:** Effect of *O-Quality* on incidence oQ1= a oQ2= b oQ3= c oQ4= c oQ5= d	**oQ4:** WT vs KO X^2_1=6.81, *p*<**
				oQ5: WT vs KO X^2_1=6.14, *p*<*

Table 31. Statistical analyses for **Figure 22.C**

Variables	Mixed ANOVA	Follow-up T-test (Sidak) (BS Factor)	Repeated Measures ANOVA (WS Factor)
Dependent variables: EEG power density (for each frequency bin (Freq=0.25:20) during epochs with detected spindles in the EEG **BS factor:** Genotype (WT,KO) **WS factor:** frequency	**Genotype*Frequency** $F_{80,560}$=6.47, *p*<** (GG)	**BS Effect** *P*<* for: 3.25 to 4.5 Hz 11.75 to 18.5 All other T-tests *p*>*	**Effect of frequency in WT** $F_{3.4,13.7}$=36.57, p<*** (GG)
			Effect of frequency in KO $F_{1.3,4.1}$=14.79, *p*<** (GG)

Table 32. Statistical analyses for **Figure 22.E**

Variables	Mixed ANOVA
Dependent variables: Log transformed LFP power density (for each frequency bin (Freq=0:0.25:20) **BS factor:** Genotype (WT,KO) **WS factor:** frequency	**WS effect** (Frequency) $F_{80,960}$=170.2, p<*** (GG) **BS effect** (Genotype) $F_{1,11}$=1.35, p=0.27 **Genotype*Frequency** $F_{80,960}$= 0.23, p=0.77 (GG)

Table 33. Statistical analyses for **Figure 23.B**

Variables	Multivariate ANOVA	Follow-up ANOVAS
Dependent variable1: Mean LFP spindle incidence **Dependent variable2:** Mean LFP spindle *o-Quality* **Independent variable:** Genotype (WT,KO)	Effect **Genotype** $F_{2,9}$=1.73, p=0.23	Effect **Genotype** on incidence $F_{1,11}$= 0.314, p=0.59 Effect **Genotype** on *o-Quality* $F_{1,10}$=0.85, p=0.77

Table 34. Statistical analyses for **Figure 23.C,E**

Variables	Mixed ANOVA
Dependent variable1: LFP spindle incidence **BS factor:** Genotype (WT,KO) **WS factor:** LFP spindle *o-Quality* (oQ1 to 5)	**WS Effect** (*o-Quality*) $F_{4,36}$= 32.8, p<*** (GG) **BS Effect** (Genotype) $F_{1,10}$= 0.07, p=0.79 (GG) Effect **Genotype*oQuality** $F_{4,36}$= 0.41, p=0.75 (GG)

Table 35. Statistical analyses for **Figure 23.D**

Variables	Repeated measures ANOVA
Dependent variables: LFP power density (for each frequency bin (Freq=0.25:20) during epochs with detected spindles in the LFP **BS factor:** Genotype (WT,KO) **WS factor:** Frequency	**WS effect** (Frequency) $F_{80,960}$=22.6, p<*** (GG) **BS effect** (Genotype) $F_{1,11}$=0.16, p=0.70

	Genotype*Frequency $F_{80,960}$=0.26, *p*=0.74 (GG)

Table 36. Statistical analyses for **Figure 23.F**

Variables	Mixed ANOVA	Follow-up repeated-measures ANOVA (spindle extent [µm])	Pairwise comparison (Sidak)
Dependent variable: Spindle spatial extent (µm) **WS Factor:** LFP spindle oQuality (oQ1 to 5) **BS Factor:** Genotype (WT,KO)	**WS effect** (LFP spindle oQuality) $F_{4,40}$=57.3, *p*<*** (GG) **BS effect** (Genotype) $F_{1,5}$=0.45, *p*=0.53 **Spindle oQ* genotype** $F_{4,40}$=1.9, *p*=0.19	Effect of **spindle extent (µm)** in **WT** $F_{1,11}$= 18.45, *p*<** (GG)	100µm= a 300µm= a 500µm= b 700µm= b 900µm= c
		Effect of **spindle spatial extent (µm)** in **KO** $F_{1,11}$=27.09 *p*<*** (GG)	100µm= a 300µm= a 500µm= a,b 700µm= a,b 900µm= b

Table 37. Statistical analyses for **Figure 24.A**

Variables	Repeated measures ANOVA	Follow-up T-test (Sidak) (BS Factor)	Repeated Measures ANOVA (WS Factor)
Dependent variables: EEG power density (for each frequency bin (Freq=0:0.25:20) during epochs with detected spindles in the LFP **BS factor:** Genotype (WT,KO) **WS factor:** frequency (0:0.25:20 Hz)	**Genotype*Frequency** $F_{8,800}$=11.53, *p*<*** (GG)	*P*<* for: 0.5 to 3.25 Hz 9.5 to 17.5 All other T-tests *p*>*	**Effect of frequency in WT** $F_{1.9,5.9}$=29.52, p<*** (GG)
			Effect of frequency in KO $F_{2.8,14.3}$=21.4, *p*<*** (GG)

Table 38. Statistical analyses for **Figure 24.B**

Variables	Mixed ANOVA	Follow-up repeated-measures ANOVA (spindle extent [µm])	Pairwise comparison (Sidak)

Dependent variable: EEG sigma power. **WS Factor:** Spindle spatial extent (100, 300, 500,700, 900 µm) **BS Factor:** Genotype (WT,KO)	**Spindle extent * genotype** $F_{4,40}$=12.3.1, *p*<*** (GG)	Effect of **spindle oQuality** in **WT** *Linear effect* $F_{1,4}$= 44.9, *p*<***	oQ1= a oQ2= b oQ3= c,d oQ4= b,d oQ5= d
		Effect of **spindle oQuality** in **KO** $F_{1,5}$= 0.94, *p*=0.44 (GG)	oQ1= a oQ2= a oQ3= a oQ4= a oQ5= a

Table 39. Statistical analyses for **Figure 24.D**

Variables	Mixed ANOVA	Follow-up repeated-measures ANOVA (spindle extent [µm])	Pairwise comparison (Sidak)
Dependent variable: EEG sigma power. **WS Factor:** LFP spindle oQuality **BS Factor:** Genotype (WT,KO)	**LFP spindle oQuality * genotype** $F_{4,40}$=4.61, *p*<***	Effect of **spindle oQuality** in **WT** *Linear effect* $F_{1,4}$= 14.57, *p*<***	oQ1= a oQ2= a oQ3= a,c oQ4= b oQ5= b,c
		Effect of **spindle oQuality** in **KO** $F_{1,5}$= 0.82, *p*=0.56 (GG)	

Table 40. Statistical analyses for **Figure 24.E**

Variables	Independent T-test
Dependent variables: LFP slow-wave incidence **Grouping factor:** Genotype (WT,KO)	t_{11}=0.79, *p*=0.44

Table 41. Statistical analyses for

Figure 25.A

Variables	Independent T-test
Dependent variables: EEG slow-wave incidence **Grouping factor:** Genotype (WT,KO)	t_{11}=0.95, *p*=0.36

Table 42. Statistical analyses for

Figure 25.A

Variables	Independent T-test
Dependent variables: Percent of LFP spindles preceded by a slow-wave **Grouping factor:** Genotype (WT,KO)	T_{11}=0.83, *p*=0.45 (Equal variance not assumed)

Table 43. Statistical analyses for

***Figure 25*.C**

Variables	Independent T-test
Dependent variables: Percent of EEG spindles preceded by a slow-wave **Grouping factor:** Genotype (WT,KO)	T11=0.13, *p*=0.90

Table 44. Statistical analyses for

***Figure 25*.C**

Variables	Mixed ANOVA	Follow-up Repeated Measure (WS factor)	Pair-wise comparison	Follow up between-subject factor ANOVA (Sidak)
Dependent variable1: Percent of LFP spindles preceded by a slow-wave **BS factor:** Genotype (WT,KO) **WS factor:** LFP spindle *o-Quality* (oQ1 to 4) [not enough oQ5 spindles]	Effect **Genotype*oQuality** $F_{3,27}$=39.46, *p*<*	Effect of **spindle oQuality** in **WT** $F_{3,12}$=11.68, *p*<**	**WT:** Effect of *O-Quality* oQ1= a oQ2= b oQ3= c oQ4= b,c	**oQ1:** $F_{1,10}$=0.69, *p*=0.43
				oQ2: $F_{1,10}$=0.85, *p*=0.38
				oQ3: $F_{1,10}$=5.21, *p*<*
		Effect of **spindle oQuality** in **KO** $F_{3,15}$=0.97, *p*=0.44		**oQ4:** $F_{1,10}$=5.36, *p*<*

Table 45. Statistical analyses for

***Figure 25*.D**

Variables	Mixed ANOVA	Follow-up Repeated Measure (WS factor)	Pair-wise comparison	Follow up between-subject factor ANOVA (Sidak)
Dependent variable1: Percent of EEG spindles	Effect **Genotype*oQuality**	Effect of **spindle oQuality** in **WT**	**WT:** Effect of *O-Quality* oQ1= a	**oQ1:** $F_{1,10}$=2.32, *p*=0.16

preceded by a slow-wave **BS factor:** Genotype (WT,KO) **WS factor:** EEG spindle *o-Quality* (oQ 1 to 3) [not enough oQ4 or oQ5 spindles]	$F_{2,18}$=4.07, p<*	$F_{2,8}$=4.43, p<* Effect of **spindle oQuality** in **KO** $F_{2,10}$=1.07, p=0.38	oQ2= b oQ3= b	**oQ2:** $F_{1,10}$=1.87, p=0.20 **oQ3:** $F_{1,10}$=5.90, p<*

Table 46. Statistical analyses for

***Figure 25*.D**

Variables	Mixed ANOVA
Dependent variable1: Slow-wave activity (Baseline) **BS factor:** Genotype (WT,KO) **WS factor:** Zeitgeber Time (0-12h)	Effect **Genotype*ZT** $F_{11,99}$=1.67, p=0.19 **WS Effect** (Zeitgeber Time) $F_{11,99}$=6.24, p<*** (GG) **BS Effect** (Genotype) $F_{1,10}$=2.04, p=0.19

Table 47. Statistical analyses for **Figure 26.A**

Variables	Mixed ANOVA	Follow-up Repeated Measure (WS factor)
Dependent variable: Mean spindle *o-Quality* (LFP channel – layer 5) **BS factor:** Genotype (WT,KO) **WS factor:** Zeitgeber Time (0h – 12h)	Effect **Zeitgeber Time *Genotype** $F_{11,99}$=2.42, p<*	Effect **Zeitgeber Time** on **WT** $F_{1,10}$=4.26, p<** Effect **Zeitgeber Time** on **KO** $F_{1,10}$=0.97, p=0.43

Table 48. Statistical analyses for **Figure 26.A**

Variables	Mixed ANOVA
Dependent variable: Slow-wave activity (% of baseline) -(LFP layer 5 channel) **BS factor:** Genotype (WT,KO)	Effect **Zeitgeber Time *Genotype** $F_{5,45}$=2.52, p=0.050 (GG) **WS Effect** (ZT Time) $F_{5,45}$=23.56, p<*** (GG)

WS factor: Zeitgeber Time (7h – 12h)	**BS Effect** (WT vs KO) $F_{1,9}$=4.03, *p*=0.08 (GG)

Table 49. Statistical analyses for **Figure 26.B**

Variables	Mixed ANOVA	Follow-up Repeated Measure (WS factor)	Follow-up ANOVA (BS factor)
Dependent variable: Mean spindle *Incidence* (LFP layer 5 channel) **BS factor:** Genotype (WT,KO) **WS factor:** Sleep condition (Baseline, Recovery)	Effect **Sleep condition*Genotype** $F_{1,9}$=47.29, *p*<*** (GG)	Effect of **Sleep condition** (baseline vs recovery) in **WT** $F_{1,4}$=86.98, *p*<*** (GG)	**Sleep Baseline:** WT vs KO $F_{1,10}$=0.39, *p*=0.55
		Effect of **Sleep condition** (baseline vs recovery) in **KO** $F_{1,5}$=0.85, *p*=0.4 (GG)	**Sleep Deprivation** WT vs KO $F_{1,10}$=4.41, *p*=0.06

Table 50. Statistical analyses for **Figure 26.C**

Variables	Mixed ANOVA	Follow-up Repeated Measure (WS factor)	Follow-up ANOVA (BS factor)
Dependent variable: Mean spindle *o-Quality* (LFP layer 5 channel) **BS factor:** Genotype (WT,KO) **WS factor:** Sleep condition (Baseline, Recovery)	Effect **Sleep condition*Genotype** $F_{1,9}$=6.35, *p*<* (GG)	Effect of **Sleep condition** (baseline vs recovery) in **WT** $F_{1,4}$=10.78, *p*<* (GG)	**Sleep Baseline:** WT vs KO $F_{1,10}$=0.4, *p*=0.54
		Effect of **Sleep condition** (baseline vs recovery) in **KO** $F_{1,5}$=2.61, *p*=0.17 (GG)	**Sleep Deprivation** WT vs KO $F_{1,10}$=6.49, *p*<*

Table 51. Statistical analyses for **Figure 26.C**

Variables	Mixed ANOVA	Follow-up Repeated Measure (WS factor)	Follow up ANOVA (BS Factor) Sidak
Dependent variable:	Effect **Zeitgeber Time *Genotype**	Effect **Zeitgeber Time** on **WT**	Effect of genotype **7h** $F_{1,10=}$4.95, *p*<*

Slow-wave activity (% of baseline) - (LFP layer 6 channel) **BS factor:** Genotype (WT,KO) **WS factor:** Zeitgeber Time (7h – 12h)	$F_{5,45}$=4.99, p<** (GG)	$F_{1,4}$=7.09, p<* (GG)	Effect of genotype **8h** $F_{1,10}$=5.54, p<*
			Effect of genotype **9h** $F_{1,10}$=3.98, p=0.08
		Effect **Zeitgeber Time** on **KO** $F_{1,5}$=50.48, p<*** (GG)	Effect of genotype **10h** $F_{1,10}$=0.92, p=0.37
			Effect of genotype **11h** $F_{1,10}$=0.15, p=0.71
			Effect of genotype **12h** $F_{1,10}$=0.001, p=0.973

Table 52. Statistical analyses for **Figure 26.D**

Variables	Mixed ANOVA
Dependent variable: Mean spindle *Incidence* (LFP layer 6 channel) **BS factor:** Genotype (WT,KO) **WS factor:** Sleep condition (Baseline, Recovery)	Effect **Sleep condition*Genotype** $F_{1,10}$=0.18, p=0.68 (GG) **WS Effect** (baseline vs recovery) $F_{1,10}$=0.42, p=0.53 (GG) **BS Effect** (WT vs KO) $F_{1,10}$=4.03, p=0.08 (GG)

Table 53. Statistical analyses for **Figure 26.E**

Variables	Mixed ANOVA	Follow-up Repeated Measure (WS factor)
Dependent variable: Mean spindle *o-Quality* (LFP layer 6 channel) **BS factor:** Genotype (WT,KO) **WS factor:** Sleep condition (Baseline, Recovery)	Effect **Sleep condition*Genotype** $F_{1,9}$=0.15, p=0.47 (GG) **WS Effect** (baseline vs recovery) $F_{1,9}$=9.75, p<* (GG) **BS Effect** (WT vs KO) $F_{1,9}$=8.26, p<* (GG)	Effect of **Sleep condition** (baseline vs recovery) in **WT** $F_{1,4}$=7.68, p<* (GG)
		Effect of **Sleep condition** (baseline vs recovery) in **KO** $F_{1,5}$=9.69, p<* (GG)

Table 54. Statistical analyses for **Figure 26.E**

Variables	Mixed ANOVA	Follow-up Repeated Measure (WS factor)	Follow up ANOVA (BS Factor) Sidak

Dependent variable: Slow-wave activity (% of baseline) - (Frontal channel) **BS factor:** Genotype (WT,KO) **WS factor:** Zeitgeber Time (7h – 12h)	Effect **Zeitgeber Time *Genotype** $F_{5,45}$=0.98, *p*=0.39 (GG)	Effect **Zeitgeber Time** on **WT** $F_{5,25}$=127.83, *p*<***	Effect of genotype **7h** $F_{1,10}$=0.49, *p*=0.50
			Effect of genotype **8h** $F_{1,10}$=0.48, *p*=0.50
			Effect of genotype **9h** $F_{1,10}$=0.74, *p*=0.41
		Effect **Zeitgeber Time** on **KO** $F_{5,30}$=58.15, *p*<***	Effect of genotype **10h** $F_{1,10}$=9.07, *p*<**
			Effect of genotype **11h** $F_{1,10}$=19.74, *p*<***
			Effect of genotype **12h** $F_{1,10}$=5.97, *p*<*

Table 55. Statistical analyses for **Figure 26.F**

Variables	Mixed ANOVA
Dependent variable: Mean spindle *Incidence* (Frontal channel) **BS factor:** Genotype (WT,KO) **WS factor:** Sleep condition (Baseline, Recovery)	Effect **Sleep condition*Genotype** $F_{1,10}$=0.9, *p*=0.36 (GG) **WS Effect** (baseline vs recovery) $F_{1,10}$=3.22, *p*=0.10 (GG) **BS Effect** (WT vs KO) $F_{1,10}$=33.1, *p*<*** (GG)

Table 56. Statistical analyses for **Figure 26.G**

Variables	Mixed ANOVA	Follow-up Repeated Measure (WS factor)	Follow-up ANOVA (BS factor)
Dependent variable: Mean spindle *o-Quality* (Frontal channel) **BS factor:** Genotype (WT,KO) **WS factor:** Sleep condition (Baseline, Recovery)	Effect **Sleep condition*Genotype** $F_{1,9}$=5.15, *p*<* (GG)	Effect of **Sleep condition** (baseline vs recovery) in **WT** $F_{1,5}$=0.71, *p*=0.44 (GG)	**Sleep Baseline:** WT vs KO $F_{1,10}$=0.012, *p*=0.92
		Effect of **Sleep condition** (baseline vs recovery) in **KO** $F_{1,4}$=11.3, *p*<* (GG)	**Sleep Recovery:** WT vs KO $F_{1,10}$=8.60, *p*=0.01

Table 57. Statistical analyses for **Figure 26.G**

Variables	Mixed ANOVA	Follow-up Repeated Measure (WS factor)	Follow up ANOVA (BS Factor) Sidak
Dependent variable: Mean spindle *o-Quality* **BS factor:** Genotype (WT,KO) **WS factor:** NREM episode bin (1-5)	Effect **NREMbin *Genotype** $F_{4,32}$=4.62, *p*<***	Effect **NREM bin** on **WT** $F_{4,16}$=3.36, *p*<*	Effect of genotype NREM bin1 $F_{1,9=}$5.09, *p*=0.50
			Effect of genotype NREM bin2 $F_{1,9=}$0.01, *p*=0.92
			Effect of genotype NREM bin3 $F_{1,9=}$3.10, *p*=0.12
		Effect **Zeitgeber Time** on **KO** $F_{4,16}$=13.6, *p*<*	Effect of genotype NREM bin4 $F_{1,9=}$1.12, *p*=0.32
			Effect of genotype NREM bin5 $F_{1,9=}$9.69, *p*<*

Table 58. Statistical analyses for ***Figure 27*.D**

Variables	Mixed ANOVA	Pair-wise comparison (WS factor)
Dependent variable: Spatial reference memory performance: Plus-maze task **BS factor:** Genotype (WT,KO) **WS factor:** Training day	Effect **Trining day *Genotype** $F_{6,72}$=0.26, *p*=0.95 **WS effect** (Training day) $F_{6,72}$=22.94, *p*<*** $F_{1,12}$=190.45, *p*<*** (linear effect) **BS effect** (Genotype) $F_{1,12}$=0.15, *p*=0.71	Effect of training day D1= a D2= a D3= a D4= b D5= b, c D6= b, c D7= c

Table 59. Statistical analyses for **Figure 28.A**

Variables	T test	ANOVA (against zero mean)
Dependent variable: Spatial Memory: Object displacement task **Grouping variable:** Genotype (WT,KO)	t_{13}=0.69, *p*=0.95	$F_{2,26}$=4.03, *p*<* WT vs chance: *p*=0.022 KO vs chance: *p*=0.027

Table 60. Statistical analyses for **Figure 28.B**

APPRENDIX CHAPTER 5: STATISTIC TABLES

Abbreviations and notes:

- **WS**: within-subject factor.
- **BS**: between-subject factor.
- **GG**: Greenhouse-Geisser test used sphericity is not assumed (Mauchly's Test, $p<0.05$).
- *p<0.05, **p<0.001, ***p<0.0001.
- Note: tables are coloured to facilitate the discrimination of different analysis steps.

Variables	Factorial Repeated Measures ANOVA
Dependent variables: Percent of sounds played. **WS factor 1:** Conditions (Sham, stimulation) (500ms, 5kHz sounds) **WS factor 2:** Sleep/wake state (NREM, REM, Wake)	**Condition*Sleep/wake state:** $F_{11,44}=0.085$, $p=0.92$ **WS Factor 1** (Condition): $F_{1,4}=2.25$, $p=0.21$ **WS Factor 2** (Sleep/wake state): $F_{11,44}=119.7$, $p<$***

Table 61.

Variables	Factorial Repeated Measures ANOVA

Dependent variables: Time in NREM (min) **WS factor 1:** Conditions (Sham, stimulation) (500ms, 5kHz sounds) **WS factor 2:** Zeitgeber Time in hours (ZT)	**ZT*Condition:** $F_{11,44}$=0.74, p=0.69 **WS Factor 1** (ZT): $F_{11,44}$=1.43, p=0.19 **WS Factor 2** (Condition): $F_{1,4}$=0.009, p=0.93

Table 62. Statistical analyses for ***Figure 33***.C

Variables	Factorial Repeated Measures ANOVA
Dependent variables: Time in REM (min) **WS factor 1:** Conditions (Sham, stimulation) (500ms, 5kHz sounds) **WS factor 2:** Zeitgeber Time in hours (ZT)	**ZT*Condition:** $F_{11,44}$=1.04, p=0.42 **WS Factor 1** (ZT): $F_{11,44}$=1.40, p=0.18 **WS Factor 2** (Condition): $F_{1,4}$=0.001, p=0.98

Table 63. Statistical analyses for ***Figure 33***.D

.Variables	Factorial Repeated Measures ANOVA
Dependent variables: Incidence microarousals (per minute) **WS factor 1:** Conditions (Sham, stimulation) (500ms, 5kHz sounds) **WS factor 2:** Zeitgeber Time in hours (ZT)	**ZT*Condition:** $F_{11,44}$=1.42, p=0.24 **WS Factor 1** (ZT): $F_{11,44}$=2.79, p<* **WS Factor 2** (Condition): $F_{1,4}$=0.24, p=0.64

Table 64. Statistical analyses for ***Figure 33***.E

Variables	Factorial Repeated Measures ANOVA	Follow-up Repeated Measure (Condition-Sidak)	Follow-up Repeated Measure (ZT- Sidak)
Dependent variables: Sigma Power (10-15 Hz)	**ZT*Condition** $F_{11,44}$=3.8, p<** (GG)	**Effect of sham** $F_{11,44}$=6.92, p<** (GG) (Linear trend, p<**)	**ZT0-1** $F_{1,4}$=0.16, p=0.72
			ZT1-2: $F_{1,4}$=11.02, p<*
			ZT2-3: $F_{1,4}$=0.19, p=0.69
			ZT3-4: $F_{1,4}$=3.20, p=0.17
			ZT4-5: $F_{1,4}$=14.9, p<*

WS factor 1: Conditions (Sham, stimulation) (500ms, 5kHz sounds) **WS factor 2:** Zeitgeber Time in hours (ZT)		**Effect of stimulation** $F_{11,44}$=8.96, *p*<** (GG)	**ZT5-6:** $F_{1,4}$=7.62, *p*<*
			ZT6-7: $F_{1,4}$=0.23, *p*=0.67
			ZT7-8: $F_{1,4}$=0.17, *p*=0.71
			ZT8-9: $F_{1,4}$=15.06, *p*<*
			ZT9-10: $F_{1,4}$=1.97, *p*=0.26
			ZT10-11: $F_{1,4}$=31.87, *p*<**
			ZT11-12: $F_{1,4}$=1.46, *p*=0.31

Table 65. Statistical analyses for ***Figure 34***.A

Variables	**Factorial Repeated Measures ANOVA**	**Follow-up Repeated Measure (Condition- Sidak)**	**Follow-up Repeated Measure (ZT- Sidak)**
Dependent variables: Spindle incidence (per minute) **WS factor 1:** Conditions (Sham, stimulation) (500ms, 5kHz sounds) **WS factor 2:** Zeitgeber Time in hours (ZT)	**ZT*Condition** $F_{11,44}$=3.44, *p*<** (GG)	**Effect of sham** $F_{11,44}$=1.50, *p*=0.34 (GG)	**ZT0-1:** $F_{1,4}$=2.77, *p*=0.24
			ZT1-2: $F_{1,4}$=13.39, *p*<*
			ZT2-3: $F_{1,4}$=11.14, *p*<*
			ZT3-4: $F_{1,4}$=6.62, *p=0.12*
			ZT4-5: $F_{1,4}$=17.69, *p*<*
		Effect of stimulation $F_{11,44}$=5.37, *p*<*** (GG) (Cubic trend, *p*<**)	**ZT5-6:** $F_{1,4}$=15.16, *p*<*
			ZT6-7: $F_{1,4}$=0.48, *p*=0.56
			ZT7-8: $F_{1,4}$=10.61, *p*=0.07
			ZT8-9: $F_{1,4}$=0.057, *p*=0.83
			ZT9-10: $F_{1,4}$=5.83, *p*=0.14
			ZT10-11: $F_{1,4}$=18.7, *p*<*
			ZT11-12: $F_{1,4}$=0.29, *p*=0.64

Table 66. Statistical analyses for ***Figure 34***.B

Variables	**Factorial Repeated Measures ANOVA**	**Follow-up Repeated Measure (Condition- Sidak)**	**Follow-up Repeated Measure (ZT- Sidak)**
Dependent variables: Spindle *oQuality* **WS factor 1:** Conditions (Sham, stimulation) (500ms, 5kHz sounds)	**ZT*Condition** $F_{11,44}$=2.68, *p*<**	**Effect of sham** $F_{11,44}$=2.80, *p*<**	**ZT0-1:** $F_{1,4}$=3.63, *p*=0.13
			ZT1-2: $F_{1,4}$=6.30, *p*<*
			ZT2-3: $F_{1,4}$=0.007*p*=0.94
			ZT3-4: $F_{1,4}$=0.51, *p*=0.52
			ZT4-5: $F_{1,4}$=5.16, *p*=0.08
		Effect of stimulation $F_{11,44}$=1.41, *p*=0.26	**ZT5-6:** $F_{1,4}$=0.75, *p*=0.44
			ZT6-7: $F_{1,4}$=0.40, *p*=0.56
			ZT7-8: $F_{1,4}$=0.90, *p*=0.39

WS factor 2: Zeitgeber Time in hours (ZT)		(Cubic trend, p<*)	**ZT8-9:** $F_{1,4}$=0.05, p=0.83
			ZT9-10: $F_{1,4}$=10.79, p<*
			ZT10-11: $F_{1,4}$=1.70, p=0.26
			ZT11-12: $F_{1,4}$=1.086, p=0.36

Table 67. Statistical analyses for ***Figure 34***.C

Variables	Factorial Repeated Measures ANOVA	Follow-up Repeated Measure (Condition- Sidak)	Follow-up Repeated Measure (ZT- Sidak)
Dependent variables: Spindle duration **WS factor 1:** Conditions (Sham, stimulation) (500ms, 5kHz sounds) **WS factor 2:** Zeitgeber Time in hours (ZT)	**ZT*Condition** $F_{11, 44}$=1.17, p=0.28	**Effect of sham** $F_{11, 44}$=2.96, p<*	**ZT0-1:** $F_{1,4}$=6.6, p<*
			ZT1-2: $F_{1,4}$=6.16, p<*
			ZT2-3: $F_{1,4}$=2.2 p=0.21
			ZT3-4: $F_{1,4}$=0.24, p=0.65
			ZT4-5: $F_{1,4}$=5.71, p=0.05
		Effect of stimulation $F_{11, 44}$=2.37, p<* (Cubic trend, p<*)	**ZT5-6:** $F_{1,4}$=0.03, p=0.86
			ZT6-7: $F_{1,4}$=0.33, p=0.59
			ZT7-8: $F_{1,4}$=0.10, p=0.77
			ZT8-9: $F_{1,4}$=0.34, p=0.59
			ZT9-10: $F_{1,4}$=63.24, p<***
			ZT10-11: $F_{1,4}$=0.97, p=0.38
			ZT11-12: $F_{1,4}$=0.19, p=0.68

Table 68. Statistical analyses for ***Figure 34***.D

Variables	Factorial Repeated Measures ANOVA	Follow-up Repeated Measure (ZT- Sidak)
Dependent variable: Cumulative spindle incidence (per hour) **WS factor1:** Conditions (Sham, stimulation) - (500ms, 5kHz) **WS factor2:** ZT time (0-11h)	**Time*Condition:** $F_{11, 44}$=4.71, p<***	**ZT0-1:** $F_{1,4}$=5.18, p=0.08
		ZT1-2: $F_{1,4}$=10.6, p<*
		ZT2-3: $F_{1,4}$=2.36,p=0.20
		ZT3-4: $F_{1,4}$=1.63, p=0.27
		ZT4-5: $F_{1,4}$=0.009, p=0.92
		ZT5-6: $F_{1,4}$=0.002, p=0.97
		ZT6-7: $F_{1,4}$=0.19, p=0.68
		ZT7-8: $F_{1,4}$=1.14, p=0.35
		ZT8-9: $F_{1,4}$=1.84, p=0.25
		ZT9-10: $F_{1,4}$=1.49, p=0.29
		ZT10-11: $F_{1,4}$=1.38, p=0.31
		ZT11-12: $F_{1,4}$=1.33, p=0.31

Table 69. Statistical analyses for ***Figure 34***.E

Variables	Factorial Repeated Measures ANOVA	Follow-up Repeated Measure (ZT- Sidak)
Dependent variables: Slow-wave activity during NREM **WS factor1:** Conditions (Sham, stimulation) (500ms, 5kHz sounds) **WS factor2:** Zeitgeber Time in hours (ZT)	**ZT*Condition** $F_{11, 44}$=1.19, p=0.32 **Effect Condition** $F_{11, 44}$=0.47, p=0.54 **Effect ZT** $F_{11, 44}$=5.45, p<***	**All contrast p>*** **ZT0-1:** $F_{11, 44}$=4.71, p=0.06 **ZT1-2:** $F_{11,44}$=5.33, p=0.05

Table 70. Statistical analyses for ***Figure 34***.F

.Variables	Factorial Repeated Measures ANOVA
Dependent variables: Theta power during REM **WS factor1:** Conditions (Sham, stimulation) (500ms, 5kHz sounds) **WS factor2:** Zeitgeber Time in hours (ZT)	**ZT*Condition:** $F_{11, 44}$=1.43, p=0.20 **Effect Condition:** $F_{11, 44}$=0.58, p=0.65 **Effect ZT:** $F_{11, 44}$=6.32, p<***

Table 71. Statistical analyses for ***Figure 34***.G

Variables	Factorial Repeated Measures ANOVA
Dependent variables: Percent of sounds played. **WS factor 1:** Conditions (Sham, stimulation) (8-s, 5kHz sounds) **WS factor 2:** Sleep/wake state (NREM, REM, Wake)	**Condition*Sleep/wake state:** $F_{2,8}$=0.072, p=0.97 **WS Factor 1** (Condition): $F_{1,4}$=1.25, p=0.43 **WS Factor 2** (Sleep/wake state): $F_{2,8}$=99.8, p<***

Table 72.

Variables	Factorial Repeated Measures ANOVA	Follow-up Repeated Measure (Condition- Sidak)
Dependent variables: Log transformed LFP (Layer 4) power density	**Time*Condition** $F_{11, 44}$=9.17, p<***	p<* for frequencies 9.75 to 15.25 Hz

WS factor1: Frequency (0-30 Hz) **WS factor2:** Time from sound onset (8-s, 5kHz sounds)		16.75 Hz

Table 73. Statistical analyses for ***Figure 35***.D

Variables	Factorial Repeated Measures ANOVA	Follow-up Repeated Measure (Condition- Sidak)	Follow-up Repeated Measure (Time- Sidak)
Dependent variables: Spindle incidence (per minute) LFP L4 **WS factor1:** Conditions (Sham, stimulation) (8-s, 5kHz sounds) **WS factor2:** Time from sound onset	**Time*Condition** $F_{5,20}$=11.36, p<***	**Effect Sham** $F_{5,20}$=1.38, p=0.27 **Effect Stimulation** $F_{5,20}$=12.94, p<***	**T(-8):** $F_{1,5}$=13.11, p<* **T(0):** $F_{1,5}$=17.62, p<* **T(8):** $F_{1,5}$=7.49, p=0.05 **T(16):** $F_{1,5}$=0.93, p=0.39 **T(24):** $F_{1,5}$=26.59, p<*** **T(32):** $F_{1,5}$=21.86, p<***

Table 74. Statistical analyses for ***Figure 36***.A

Variables	Factorial Repeated Measures ANOVA	Follow-up Repeated Measure (Condition- Sidak)	Follow-up Repeated Measure (Time- Sidak)
Dependent variables: Sigma power during NREM in LFP (layer 4) **WS factor1:** Conditions (Sham, stimulation) (8-s, 5kHz sounds) **WS factor2:** Time from sound onset	**Time*Condition** $F_{5,20}$=31.43, p<***	**Effect Sham** $F_{5,20}$=0.69, p=0.63 **Effect Stimulation** $F_{5,20}$=37.80, p<***	**T(-8):** $F_{1,5}$=32.37, p<*** **T(0):** $F_{1,5}$=39.84, p<*** **T(8):** $F_{1,5}$=58.35, p<*** **T(16):** $F_{1,5}$=8.21, p<* **T(24):** $F_{1,5}$=48.84, p<*** **T(32):** $F_{1,5}$=52.81, p<***

Table 75. Statistical analyses for ***Figure 36***.B

Variables	Factorial Repeated Measures ANOVA	Follow-up Repeated Measure	Follow-up Repeated Measure

		(Condition- Sidak)	(Time- Sidak)
Dependent variables: Spindle *oQuality* LFP (L4) **WS factor1:** Conditions (Sham, stimulation) (8-s, 5kHz sounds) **WS factor2:** Time from sound onset	**Time*Condition** $F_{5,20}$=4.34, p<***	**Effect Sham** $F_{5,20}$=1.33, p=0.29 **Effect Stimulation** $F_{5,20}$=2.51, p<*	**T(-8-0):** $F_{1,5}$=1.28, p=0.29 **T(0-8):** $F_{1,5}$=1.47, p=0.26 **T(8-16):** $F_{1,5}$=1.75, p=0.22 **T(16-24):** $F_{1,5}$=7.76, p<* **T(24-32):** $F_{1,5}$=0.05, p=0.82 **T(32-40):** $F_{1,5}$=0.17, p=0.69

Table 76. Statistical analyses for ***Figure 36***.C

Variables	Factorial Repeated Measures ANOVA
Dependent variable: Cumulative spindle incidence (per hour) LFP Layer 4 **WS factor1:** Conditions (Sham, stimulation) - (8-s, 5kHz) **WS factor2:** ZT time (0-11h)	**Time*Condition:** $F_{11,55}$=1.09, p=0.39 **WS effect (Condition):** $F_{1,5}$=1.07, p=0.36 **WS effect (Time):** $F_{11,55}$=199.1, p<***

Table 77. Statistical analyses for ***Figure 36***.D

Variables	Factorial Repeated Measures ANOVA	Follow-up Repeated Measure (Time- Sidak)
Dependent variables: Slow-wave activity during NREM. LFP Layer 4 **WS factor1:** Conditions (Sham, stimulation) (8-s, 5kHz sounds) **WS factor2:** Time from sound onset	**Time*Condition:** $F_{5,20}$=1.48, p=0.24 **Effect Time:** $F_{5,20}$=0.87, p=0.52 **Effect Condition:** $F_{5,20}$=0.12, p=0.74	**All contrasts p>*** **T(16):** $F_{1,5}$=4.83, p<0.06

Table 78. Statistical analyses for ***Figure 36***.E

Variables	Factorial Repeated Measures ANOVA

Dependent variables: EMG variance **WS factor1:** Conditions (Sham, stimulation) (8-s, 5kHz sounds) **WS factor2:** Time from sound onset	**Time*Condition** $F_{5,20}$=1.64, p=0.21 **Effect Time** $F_{5,20}$=0.72, p=0.61 **Effect Condition** $F_{5,20}$=0.89, p=0.42

Table 79. Statistical analyses for ***Figure 36***.F

Variables	Factorial Repeated Measures ANOVA	Follow-up Repeated Measure (Condition- Sidak)	Follow-up Repeated Measure (Time- Sidak)
Dependent variables: Spindle incidence (per minute) frontal EEG **WS factor1:** Conditions (Sham, stimulation) (8-s, 5kHz sounds) **WS factor2:** Time from sound onset	**Time*Condition** $F_{5,20}$=9.36, p<***	**Effect Sham** $F_{5,20}$=5.38, p<* **Effect Stimulation** $F_{5,20}$=11.72, p<***	**T(-8):** $F_{1,5}$=0.99, p=0.42 **T(0):** $F_{1,5}$=7.12, p<* **T(8):** $F_{1,5}$=23.2, p<*** **T(16):** $F_{1,5}$=0.72, p=0.63 **T(24):** $F_{1,5}$=20.52, p<*** **T(32):** $F_{1,5}$=16.76, p<**

Table 80. Statistical analyses for ***Figure 37***.A

Variables	Factorial Repeated Measures ANOVA
Dependent variables: Spindle incidence (per minute). Infragranular LFP (layer 5B) **WS factor1:** Conditions (Sham, stimulation). (8-s, 5kHz sounds) **WS factor2:** Time from sound onset	**Time*Condition:** $F_{5,20}$=0.99, p=0.31 **Effect Condition:** $F_{5,20}$=0.82, p=0.49 **Effect Time:** $F_{5,20}$=1.01, p=0.18

Table 81. Statistical analyses for ***Figure 37***.B

Variables	Repeated Measures ANOVA	Pairwise comparisons (Sidak)

Dependent variables: Spindle duration (s). Granular Layer **WS factor:** Conditions (Sham, 12Hz clicks, 40Hz clicks)	**WS effect (Time)** $F_{2,16}$=5.86, p<*	**Sham:** a **12Hz:** b **14Hz:** a

Table 82. Statistical analyses for ***Figure 42***.C

Variables	Repeated Measures ANOVA	Pairwise comparisons (Sidak)
Dependent variables: Spindle oQuality. Granular layers **WS factor:** Conditions (Sham, 12Hz clicks, 40Hz clicks)	**WS effect (Time)** $F_{2,16}$=6.2, p<**	**Sham:** a **12Hz:** b **14Hz:** a

Table 83. Statistical analyses for ***Figure 42***.C

Variables	Repeated Measures ANOVA	Pairwise comparisons (Sidak)
Dependent variables: Spindle Incidence (per min). Granular layers **WS factor:** Conditions (Sham, 12Hz clicks, 40Hz clicks)	**WS effect (Time)** $F_{2,16}$=0.88, p=0.44	**Sham:** a **12Hz:** a **14Hz:** a

Table 84. Statistical analyses for ***Figure 42***.C

Variables	Repeated Measures ANOVA	Pairwise comparisons (Sidak)
Dependent variables: Spindle duration (s). Infragranular layers **WS factor:** Conditions (Sham, 12Hz clicks, 40Hz clicks)	**WS effect (Time)** $F_{2,16}$=3.6, p=0.05	**Sham:** a,b **12Hz:** a **14Hz:** b

Table 85. Statistical analyses for ***Figure 42***.D

Variables	Repeated Measures ANOVA	Pairwise comparisons (Sidak)
Dependent variables: Spindle oQuality. Infragranular layers **WS factor:** Conditions (Sham, 12Hz clicks, 40Hz clicks)	**WS effect (Time)** $F_{2,16}$=7.94, p<***	**Sham:** a **12Hz:** a **14Hz:** b (Sham vs 12 Hz p=0.05)

Table 86. Statistical analyses for ***Figure 42***.D

Variables	Repeated Measures ANOVA	Pairwise comparisons (Sidak)

Dependent variables: Spindle Incidence (per min). Infragranular layers **WS factor:** Conditions (Sham, 12Hz clicks, 40Hz clicks)	**WS effect (Time)** $F_{2,16}$=3.36, p=0.11 (GG)	**Sham:** a **12Hz:** a **14Hz:** a

Table 87. Statistical analyses for ***Figure 42***.D

Variables	Repeated Measures ANOVA	Pairwise comparisons (Sidak)
Dependent variables: Spindle duration (s). Frontal EEG **WS factor:** Conditions (Sham, 12Hz clicks, 40Hz clicks)	**WS effect (Time)** $F_{2,16}$=0.64, p=0.54	**Sham:** a **12Hz:** a **14Hz:** a

Table 88. Statistical analyses for ***Figure 42***.E

Variables	Repeated Measures ANOVA	Pairwise comparisons (Sidak)
Dependent variables: Spindle oQuality. Frontal EEG **WS factor:** Conditions (Sham, 12Hz clicks, 40Hz clicks)	**WS effect (Time)** $F_{2,16}$=0.34, p=0.71	**Sham:** a **12Hz:** a **14Hz:** a

Table 89. Statistical analyses for ***Figure 42***.E

Variables	Repeated Measures ANOVA	Pairwise comparisons (Sidak)
Dependent variables: Spindle Incidence (per min). Frontal EEG **WS factor:** Conditions (Sham, 12Hz clicks, 40Hz clicks)	**WS effect (Time)** $F_{2,16}$=1.99, p=0.18 (GG)	**Sham:** a **12Hz:** a **14Hz:** a

Table 90. Statistical analyses for ***Figure 42***.E

Variables	Repeated Measures ANOVA
Dependent variables: EMG variance **WS factor:** Conditions (sounds during S1 spindle vs sound in the absence of spindle)	**WS effect (Time)** $F_{1,6}$=3.44, p=0.062

Table 91. Statistical analyses for ***Figure 43.B***

BIBLIOGRAPHY

Achermann P, Borbély AA (1997) Low-frequency (< 1 hz) oscillations in the human sleep electroencephalogram. Neuroscience 81:213–222.

Achermann P, Borbély AA (1998) Coherence analysis of the human sleep electroencephalogram. Neuroscience 85:1195–1208.

Achermann P, Borbély AA (2003) Mathematical models of sleep regulation. Front Biosci 8.

Achermann P, Dijk DJ, Brunner DP, Borbély AA (1993) A model of human sleep homeostasis based on EEG slow-wave activity: Quantitative comparison of data and simulations. Brain Res Bull 31:97–113.

Achermann P, Olbrich E (2004) Oscillatory events in the human sleep EEG - Detection and properties. Neurocomputing 58–60:129–135.

Achermann P, Rusterholz T, Stucky B, Olbrich E (2019) Oscillatory patterns in the electroencephalogram at sleep onset. Sleep 42.

AESCHBACH D, BORBÉLY AA (1993) All-night dynamics of the human sleep EEG. J Sleep Res 2:70–81.

Aguilar DD, Strecker RE, Basheer R, McNally JM (2020) Alterations in sleep, sleep spindle, and EEG power in mGluR5 knockout mice. J Neurophysiol 123:22–33.

Alciatore DG (2002) Introduction to mechatronics and measurement systems, 2nd ed., 3rd ed. McGraw Hill.

Alfonsi V, D'Atri A, Gorgoni M, Scarpelli S, Mangiaruga A, Ferrara M, De Gennaro L (2019) Spatiotemporal dynamics of sleep spindle sources across NREM sleep cycles. Front Neurosci 13.

Amzica F, Steriade M (2000) Integration of low-frequency sleep oscillations in corticothalamic networks. Acta Neurobiol Exp (Wars) 60:229–245.

Anafi RC, Kayser MS, Raizen DM (2019) Exploring phylogeny to find the function of sleep. Nat Rev Neurosci 20:109–116.

Andrade KC, Spoormaker VI, Dresler M, Wehrle R, Holsboer F, Sämann PG, Czisch M (2011) Sleep spindles and hippocampal functional connectivity in human NREM sleep. J Neurosci 31:10331–10339.

Andrásfalvy BK, Smith MA, Borchardt T, Sprengel R, Magee JC (2003) Impaired regulation of synaptic strength in hippocampal neurons from GluR1-deficient mice. J Physiol 552:35–45.

Andrillon T, Nir Y, Staba RJ, Ferrarelli F, Cirelli C, Tononi G, Fried I (2011) Sleep spindles in humans: Insights from intracranial EEG and unit recordings. J Neurosci 31:17821–17834.

Ang G, McKillop LE, Purple R, Blanco-Duque C, Peirson SN, Foster RG, Harrison PJ, Sprengel R, Davies KE, Oliver PL, Bannerman DM, Vyazovskiy V V. (2018) Absent sleep EEG spindle activity in GluA1 (Gria1) knockout mice: relevance to neuropsychiatric disorders. Transl Psychiatry 8.

Antony JW, Paller KA (2017) Using oscillating sounds to manipulate sleep spindles. Sleep 40.

Antony JW, Piloto L, Wang M, Pacheco P, Norman KA, Paller KA (2018) Sleep Spindle Refractoriness Segregates Periods of Memory Reactivation. Curr Biol 28:1736-1743.e4 Available at: https://doi.org/10.1016/j.cub.2018.04.020.

Astori S, Wimmer RD, Lüthi A (2013) Manipulating sleep spindles - expanding views on sleep, memory, and disease. Trends Neurosci 36:738–748.

Astori S, Wimmer RD, Prosser HM, Corti C, Corsi M, Liaudet N, Volterra A, Franken P, Adelman JP, Lüthi A (2011) The Ca v3.3 calcium channel is the major sleep spindle pacemaker in thalamus. Proc Natl Acad Sci U S A 108:13823–13828.

Bannerman DM, Deacon RMJ, Brady S, Bruce A, Sprengel R, Seeburg PH, Rawlins JNP (2004) A comparison of GluR-A-deficient and wild-type mice on a test battery assessing sensorimotor, affective, and cognitive behaviors. Behav Neurosci 118:643–647.

Bannerman DM, Deacon RMJ, Seeburg PH, Rawlins JNP (2003) GluR-A-deficient mice display normal acquisition of a hippocampus-dependent spatial reference memory task but are impaired during spatial reversal. Behav Neurosci 117:866–870.

Bannerman DM, Sprengel R, Sanderson DJ, Mchugh SB, Rawlins JNP, Monyer H, Seeburg PH (2014) Hippocampal synaptic plasticity, spatial memory and anxiety. Nat Rev Neurosci 15:181–192 Available at: http://dx.doi.org/10.1038/nrn3677.

Barkus C, Feyder M, Graybeal C, Wright T, Wiedholz L, Izquierdo A, Kiselycznyk C, Schmitt W, Sanderson DJ, Rawlins JNP, Saksida LM, Bussey TJ, Sprengel R, Bannerman D, Holmes A (2012) Do GluA1 knockout mice exhibit behavioral abnormalities relevant to the negative or cognitive symptoms of schizophrenia and schizoaffective disorder? Neuropharmacology 62:1263–1272 Available at: http://dx.doi.org/10.1016/j.neuropharm.2011.06.005.

Barkus C, Sanderson DJ, Rawlins JNP, Walton ME, Harrison PJ, Bannerman DM (2014) What causes aberrant salience in schizophrenia? A role for impaired short-term habituation and the GRIA1 (GluA1) AMPA receptor subunit. Mol Psychiatry 19:1060–1070 Available at: http://dx.doi.org/10.1038/mp.2014.91.

Bartram J, Kahn MC, Tuohy S, Paulsen O, Wilson T, Mann EO (2017) Cortical Up states induce the selective weakening of subthreshold synaptic inputs. Nat Commun 8.

Battaglia FP, Sutherland GR, McNaughton BL (2004) Hippocampal sharp wave bursts coincide with neocortical “up-state” transitions. Learn Mem 11:697–704.

Beenhakker MP, Huguenard JR (2009) Neurons that Fire Together Also Conspire Together: Is Normal Sleep Circuitry Hijacked to Generate Epilepsy? Neuron 62:612–632.

Benca RM, Obermeyer WH, Thisted RA, Gillin JC (1992) Sleep and Psychiatric Disorders: A Meta-analysis. Arch Gen Psychiatry 49:651–668.

Bergmann BM, Winter JB, Rosenberg RS, Rechtschaffen A (1987) NREM sleep with low-voltage EEG in the rat. Sleep 10:1–11.

Bergmann TO, Mölle M, Diedrichs J, Born J, Siebner HR (2012) Sleep spindle-related reactivation of category-specific cortical regions after learning face-scene associations. Neuroimage 59:2733–2742.

Blume C, del Giudice R, Lechinger J, Wislowska M, Heib DPJ, Hoedlmoser K, Schabus M (2017) Preferential processing of emotionally and self-relevant stimuli persists in unconscious N2 sleep. Brain Lang 167:72–82.

Bódizs R, Gombos F, Kovács I (2012) Sleep EEG fingerprints reveal accelerated thalamocortical oscillatory dynamics in Williams syndrome. Res Dev Disabil 33:153–164.

Bonjean M, Baker T, Bazhenov M, Cash S, Halgren E, Sejnowski T (2012) Interactions between core and matrix thalamocortical projections in human sleep spindle synchronization. J Neurosci

32:5250–5263.

Bonjean M, Baker T, Lemieux M, Timofeev I, Sejnowski T, Bazhenov M (2011) Corticothalamic feedback controls sleep spindle duration in vivo. J Neurosci 31:9124–9134.

Bopp R, Holler-Rickauer S, Martin KAC, Schuhknecht GFP (2017) An ultrastructural study of the thalamic input to layer 4 of primary motor and primary somatosensory cortex in the mouse. J Neurosci 37:2435–2448.

Borbely AA (1980) Effects of light and circadian rhythm on the occurrence of REM sleep in the rat. Sleep 2:289–298.

Borbely AA (1982) A two process model of sleep regulation. Hum Neurobiol 1:195–204.

Borbély AA, Daan S, Wirz-Justice A, Deboer T (2016) The two-process model of sleep regulation: A reappraisal. J Sleep Res 25:131–143.

Born J, Feld GB (2012) Sleep to Upscale, Sleep to Downscale: Balancing Homeostasis and Plasticity. Neuron 75:933–935.

Born J, Rasch B, Gais S (2006) Sleep to remember. Neuroscientist 12:410–424.

Bouret S, Richmond XJ (2015) Sensitivity of locus ceruleus neurons to reward value for goal-directed actions. J Neurosci 35:4005–4014 Available at: http://www.ncbi.nlm.nih.gov/pubmed/7346592.

Broadbent NJ, Squire LR, Clark RE (2004) Spatial memory, recognition memory, and the hippocampus. Proc Natl Acad Sci U S A 101:14515–14520.

Bromberg MB, Penne JB, Stephenson BS, Young AB (1981) Evidence for glutamate as the neurotransmitter of corticothalamic and corticorubral pathways. Brain Res 215:369–374.

BuzsÁk G (1998) Memory consolidation during sleep: a neurophysiological perspective. J Sleep Res 7:17–23.

Buzsáki G (2004) Large-scale recording of neuronal ensembles. Nat Neurosci 7:446–451.

Buzsáki G, Anastassiou CA, Koch C (2012) The origin of extracellular fields and currents-EEG, ECoG, LFP and spikes. Nat Rev Neurosci 13:407–420.

Buzsáki G, Draguhn A (2004) Neuronal olscillations in cortical networks. Science (80-) 304:1926–1929.

Buzsáki G, Logothetis N, Singer W (2013) Scaling brain size, keeping timing: Evolutionary preservation of brain rhythms. Neuron 80:751–764.

Buzsáki G, Mizuseki K (2014) The log-dynamic brain: How skewed distributions affect network operations. Nat Rev Neurosci 15:264–278.

Buzsáki G, Moser EI (2013) Memory, navigation and theta rhythm in the hippocampal-entorhinal system. Nat Neurosci 16:130–138 Available at: http://www.nature.com/doifinder/10.1038/nn.3304%5Cnhttp://www.ncbi.nlm.nih.gov/pubmed/23354386.

Buzsáki G, Watson BO (2012) Brain rhythms and neural syntax: Implications for efficient coding of cognitive content and neuropsychiatric disease. Dialogues Clin Neurosci 14:345–367.

Bygrave AM, Jahans-Price T, Wolff AR, Sprengel R, Kullmann DM, Bannerman DM, Kätzel D (2019) Hippocampal–prefrontal coherence mediates working memory and selective attention at

distinct frequency bands and provides a causal link between schizophrenia and its risk gene GRIA1. Transl Psychiatry 9.

Campbell SS, Tobler I (1984) Animal sleep: A review of sleep duration across phylogeny. Neurosci Biobehav Rev 8:269–300.

Cantero JL, Atienza M, Stickgold R, Kahana MJ, Madsen JR, Kocsis B (2003) Sleep-Dependent θ Oscillations in the Human Hippocampus and Neocortex. J Neurosci 23:10897–10903.

Carskadon MA, Dement WC (2010) Normal Human Sleep: An Overview. In: Principles and Practice of Sleep Medicine: Fifth Edition, pp 16–26.

Carter ME, Yizhar O, Chikahisa S, Nguyen H, Adamantidis A, Nishino S, Deisseroth K, De Lecea L (2010) Tuning arousal with optogenetic modulation of locus coeruleus neurons. Nat Neurosci 13:1526–1535 Available at: http://dx.doi.org/10.1038/nn.2682.

Cirelli C, Tononi G (2008) Is sleep essential? PLoS Biol 6:1605–1611.

Cohrs S (2008) Sleep disturbances in patients with schizophrenia: Impact and effect of antipsychotics. CNS Drugs 22:939–962.

Contreras D, Destexhe A, Sejnowski TJ, Steriade M (1996) Control of spatiotemporal coherence of a thalamic oscillation by corticothalamic feedback. Science (80-) 274:771–774.

Contreras D, Destexhe A, Sejnowski TJ, Steriade M (1997a) Spatiotemporal patterns of spindle oscillations in cortex and thalamus. J Neurosci 17:1179–1196.

Contreras D, Destexhe A, Steriade M (1997b) Intracellular and computational characterization of the intracortical inhibitory control of synchronized thalamic inputs in vivo. J Neurophysiol 78:335–350.

Contreras D, Steriade M (1995) Cellular basis of EEG slow rhythms: A study of dynamic corticothalamic relationships. J Neurosci 15:604–622.

Contreras D, Steriade M (1996) Spindle oscillation in cats: The role of corticothalamic feedback in a thalamically generated rhythm. J Physiol 490:159–179.

Cote KA, Epps TM, Campbell KB (2000) The role of the spindle in human information processing of high-intensity stimuli during sleep. J Sleep Res 9:19–26.

Coyle JT (2006) Glutamate and schizophrenia: beyond the dopamine hypothesis. Cell Mol Neurobiol 26:365–384.

Crabtree G, Gogos JA (2014) Synaptic plasticity, neural circuits and the emerging role of altered short-term information processing in schizophrenia. Front Synaptic Neurosci 6.

Crochet S, Fuentealba P, Cissé Y, Timofeev I, Steriade M (2006) Synaptic plasticity in local cortical network in vivo and its modulation by the level of neuronal activity. Cereb Cortex 16:618–631.

Crunelli V, Cope DW, Hughes SW (2006) Thalamic T-type Ca2+ channels and NREM sleep. Cell Calcium 40:175–190.

Crunelli V, Lightowler S, Pollard CE (1989) A T-type Ca2+ current underlies low-threshold Ca2+ potentials in cells of the cat and rat lateral geniculate nucleus. J Physiol 413:543–561.

D'Agostino A, Castelnovo A, Cavallotti S, Casetta C, Marcatili M, Gambini O, Canevini M, Tononi G, Riedner B, Ferrarelli F, Sarasso S (2018) Sleep endophenotypes of schizophrenia: Slow waves and sleep spindles in unaffected first-degree relatives. npj Schizophr 4.

Daan S, Beersma DGM, Borbely AA (1984) Timing of human sleep: Recovery process gated by a circadian pacemaker. Am J Physiol - Regul Integr Comp Physiol 15.

Dang-Vu TT, Bonjean M, Schabus M, Boly M, Darsaud A, Desseilles M, Degueldre C, Balteau E, Phillips C, Luxen A, Sejnowski TJ, Maquet P (2011) Interplay between spontaneous and induced brain activity during human non-rapid eye movement sleep. Proc Natl Acad Sci U S A 108:15438–15443.

Dang-Vu TT, McKinney SM, Buxton OM, Solet JM, Ellenbogen JM (2010) Spontaneous brain rhythms predict sleep stability in the face of noise. Curr Biol 20.

David F, Schmiedt JT, Taylor HL, Orban G, Di Giovanni G, Uebele VN, Renger JJ, Lambert RC, Leresche N, Crunelli V (2013) Essential thalamic contribution to slow waves of natural sleep. J Neurosci 33:19599–19610.

De Vera L, González J, Rial R V. (1994) Reptilian waking EEG: slow waves, spindles and evoked potentials. Electroencephalogr Clin Neurophysiol 90:298–303.

De Vivo L, Bellesi M, Marshall W, Bushong EA, Ellisman MH, Tononi G, Cirelli C (2017) Ultrastructural evidence for synaptic scaling across the wake/sleep cycle. Science (80-) 355:507–510.

Deboer T (2013) Behavioral and electrophysiological correlates of sleep and sleep homeostasis. Curr Top Behav Neurosci 25.

Deleuze C, Huguenard JR (2016) Two classes of excitatory synaptic responses in rat thalamic reticular neurons. J Neurophysiol 116:995–1011.

Demanuele C, Bartsch U, Baran B, Khan S, Vangel MG, Cox R, Hämäläinen M, Jones MW, Stickgold R, Manoach DS (2017) Coordination of slow waves with sleep spindles predicts sleep-dependent memory consolidation in schizophrenia. Sleep 40:1–10.

Dement W, Kleitman N (1957) Cyclic variations in EEG during sleep and their relation to eye movements, body motility, and dreaming. Electroencephalogr Clin Neurophysiol 9:673–690.

Destexhe A, Bal T, Mccormick DA, Sejnowski TJ (1996) Ionic mechanisms underlying synchronized oscillations and propagating waves in a model of ferret thalamic slices. J Neurophysiol 76:2049–2070.

Destexhe A, Contreras D, Steriade M (1999) Spatiotemporal analysis of local field potentials and unit discharges in cat cerebral cortex during natural wake and sleep states. J Neurosci 19:4595–4608.

Destexhe A, McCormick DA, Sejnowski TJ (1993) A model for 8–10 Hz spindling in interconnected thalamic relay and reticularis neurons. Biophys J 65:2473–2477.

Devuyst S, Dutoit T, Didier JF, Meers F, Stanus E, Stenuit P, Kerkhofs M (2006) Automatic sleep spindle detection in patients with sleep disorders. In: Annual International Conference of the IEEE Engineering in Medicine and Biology - Proceedings, pp 3883–3886.

Dickey C, Sargsyan A, Madsen J, Eskandar E, Cash S, Halgren E (2020) Travelling spindles create necessary conditions for spike-timing-dependent plasticity in humans. bioRxiv:1–24.

Diering GH, Gustina AS, Huganir RL (2014) PKA-GluA1 coupling via AKAP5 controls AMPA receptor phosphorylation and cell-surface targeting during bidirectional homeostatic plasticity. Neuron 84:790–805 Available at: http://dx.doi.org/10.1016/j.neuron.2014.09.024.

Diering GH, Nirujogi RS, Roth RH, Worley PF, Pandey A, Huganir RL (2017) Homer1a drives

homeostatic scaling-down of excitatory synapses during sleep. Science (80) 355:511–515.

Dijk DJ (1995) EEG slow waves and sleep spindles: windows on the sleeping brain. Behav Brain Res 69:109–116.

Dijk DJ (2009) Regulation and functional correlates of slow wave sleep. J Clin Sleep Med 5.

Dijk DJ, Beersma DGM, Daan S (1987) EEG Power Density during Nap Sleep: Reflection of an Hourglass Measuring the Duration of Prior Wakefulness. J Biol Rhythms 2:207–219.

Dijk DJ, Hayes B, Czeisler CA (1993) Dynamics of electroencephalographic sleep spindles and slow wave activity in men: effect of sleep deprivation. Brain Res 626:190–199.

Duboué ER, Keene AC, Borowsky RL (2011) Evolutionary convergence on sleep loss in cavefish populations. Curr Biol 21:671–676.

Eastwood SL, Kerwin RW, Harrison PJ (1997) Immunoautoradiographic evidence for a loss of α-amino-3-hydroxy-5-methyl-4-isoxazole propionate-preferring non-N-methyl-D-aspartate glutamate receptors within the medial temporal lobe in schizophrenia. Biol Psychiatry 41:636–643.

Eastwood SL, McDonald B, Burnet PWJ, Beckwith JP, Kerwin RW, Harrison PJ (1995) Decreased expression of mRNAs encoding non-NMDA glutamate receptors GluRl and GluR2 in medial temporal lobe neurons in schizophrenia. Mol Brain Res 29:211–223.

Economo C V. (1930) Sleep as a problem of localization. J Nerv Ment Dis 71:249–259.

El-Brolosy MA, Stainier DYR (2017) Genetic compensation: A phenomenon in search of mechanisms. PLoS Genet 13.

Elton M, Winter O, Heslenfeld D, Loewy D, Campbell K, Kok A (1997) Event-related potentials to tones in the absence and presence of sleep spindles. J Sleep Res 6:78–83.

Erickson MA, Maramara LA, Lisman J (2010) A single brief burst induces GluR1-dependent associative short-term potentiation: A potential mechanism for short-term memory. J Cogn Neurosci 22:2530–2540.

Fang G, Chen Q, Cui J, Tang Y (2012) Electroencephalogram bands modulated by vigilance states in an anuran species: A factor analytic approach. J Comp Physiol A Neuroethol Sensory, Neural, Behav Physiol 198:119–127.

Farmer CA, Chilakamarri P, Thurm AE, Swedo SE, Holmes GL, Buckley AW (2018) Spindle activity in young children with autism, developmental delay, or typical development. Neurology 91:e112–e122.

Feinberg I, March JD, Floyd TC, Jimison R, Bossom-Demitrack L, Katz PH (1985) Homeostatic changes during post-nap sleep maintain baseline levels of delta EEG. Electroencephalogr Clin Neurophysiol 61:134–137.

Feldmeyer D, Brecht M, Helmchen F, Petersen CCH, Poulet JFA, Staiger JF, Luhmann HJ, Schwarz C (2013) Barrel cortex function. Prog Neurobiol 103:3–27 Available at: http://dx.doi.org/10.1016/j.pneurobio.2012.11.002.

Fernandez LMJ, Lüthi A (2020) Sleep Spindles: Mechanisms and Functions. Physiol Rev 100:805–868.

Fernandez LMJ, Vantomme G, Osorio-Forero A, Cardis R, Béard E, Lüthi A (2018) Thalamic reticular control of local sleep in mouse sensory cortex. Elife 7.

Ferrarelli F (2007) Reduced Sleep Spindle Activity in Schizophrenia Patients. Am J Psychiatry 164:483.

Ferrarelli F, Peterson MJ, Sarasso S, Riedner BA, Murphy MJ, Benca RM, Bria P, Kalin NH, Tononi G (2010) Thalamic dysfunction in schizophrenia suggested by whole-night deficits in slow and fast spindles. Am J Psychiatry 167:1339–1348.

Ferrarelli F, Tononi G (2016) What Are Sleep Spindle Deficits Telling Us About Schizophrenia? Biol Psychiatry 80:577–578 Available at: http://dx.doi.org/10.1016/j.biopsych.2016.08.012.

Ferrarelli F, Tononi G (2017) Reduced sleep spindle activity point to a TRN-MD thalamus-PFC circuit dysfunction in schizophrenia. Schizophr Res 180:36–43 Available at: http://dx.doi.org/10.1016/j.schres.2016.05.023.

Field A (2005) Andy Field - Discovering Statistics Using SPSS. Available at: http://doi.wiley.com/10.1111/j.1365-2648.2007.04270_1.x.

Finelli LA, Borbély AA, Achermann P (2001) Functional topography of the human nonREM sleep electroencephalogram. Eur J Neurosci 13:2282–2290.

Fisher SP, Cui N, McKillop LE, Gemignani J, Bannerman DM, Oliver PL, Peirson SN, Vyazovskiy V V. (2016) Stereotypic wheel running decreases cortical activity in mice. Nat Commun 7.

Fonnum F, Storm-Mathisen J, Divac I (1981) Biochemical evidence for glutamate as neurotransmitter in corticostriatal and corticothalamic fibres in rat brain. Neuroscience 6:863–873.

Franken P, Dijk DJ, Tobler I, Borbely AA (1991) Sleep deprivation in rats: Effects on EEG power spectra, vigilance states, and cortical temperature. Am J Physiol - Regul Integr Comp Physiol 261.

Freeman WJ (2006) Origin, structure, and role of background EEG activity. Part 4: Neural frame simulation. Clin Neurophysiol 117:572–589.

Fuchs EC, Zivkovic AR, Cunningham MO, Middleton S, LeBeau FEN, Bannerman DMM, Rozov A, Whittington MA, Traub RD, Rawlins JNP, Monyer H (2007) Recruitment of Parvalbumin-Positive Interneurons Determines Hippocampal Function and Associated Behavior. Neuron 53:591–604.

Funk CM, Honjoh S, Rodriguez A V., Cirelli C, Tononi G (2016) Local slow waves in superficial layers of primary cortical areas during REM sleep. Curr Biol 26:396–403.

Gais S, Mölle M, Helms K, Born J (2002) Learning-dependent increases in sleep spindle density. J Neurosci 22:6830–6834.

Geiser T, Hertenstein E, Fehér K, Maier JG, Schneider CL, Züst MA, Wunderlin M, Mikutta C, Klöppel S, Nissen C (2020) Targeting Arousal and Sleep through Noninvasive Brain Stimulation to Improve Mental Health. Neuropsychobiology 79:284–292.

Gemignani J, Agrimi J, Cheli E, Gemignani A, Laurino M, Allegrini P, Landi A, Menicucci D (2015) Pattern recognition with adaptive-thresholds for sleep spindle in high density EEG signals. Proc Annu Int Conf IEEE Eng Med Biol Soc EMBS 2015-November:594–597.

Genzel L, Dresler M, Cornu M, Jäger E, Konrad B, Adamczyk M, Friess E, Steiger A, Czisch M, Goya-Maldonado R (2015) Medial prefrontal-hippocampal connectivity and motor memory consolidation in depression and schizophrenia. Biol Psychiatry 77:177–186.

Gibbs EL, Gibbs FA (1962) Extreme spindles: Correlation of electroencephalographic sleep pattern

with mental retardation. Science (80-) 138:1106–1107.

Göder R, Graf A, Ballhausen F, Weinhold S, Baier PC, Junghanns K, Prehn-Kristensen A (2015) Impairment of sleep-related memory consolidation in schizophrenia: Relevance of sleep spindles? Sleep Med 16:564–569.

González-Rueda A, Pedrosa V, Feord RC, Clopath C, Paulsen O (2018) Activity-Dependent Downscaling of Subthreshold Synaptic Inputs during Slow-Wave-Sleep-like Activity In Vivo. Neuron 97:1244-1252.e5.

Gorgoni M, Lauri G, Truglia I, Cordone S, Sarasso S, Scarpelli S, Mangiaruga A, D'Atri A, Tempesta D, Ferrara M, Marra C, Rossini PM, De Gennaro L (2016) Parietal Fast Sleep Spindle Density Decrease in Alzheimer's Disease and Amnesic Mild Cognitive Impairment. Neural Plast 2016.

Gottesmann C (1996) The transition from slow-wave sleep to paradoxical sleep: Evolving facts and concepts of the neurophysiological processes underlying the intermediate stage of sleep. Neurosci Biobehav Rev 20:367–387.

Gottesmann C, Gottesman I (2007) The neurobiological characteristics of rapid eye movement (REM) sleep are candidate endophenotypes of depression, schizophrenia, mental retardation and dementia. Prog Neurobiol 81:237–250.

Granger AJ, Shi Y, Lu W, Cerpas M, Nicoll RA (2013) LTP requires a reserve pool of glutamate receptors independent of subunit type. Nature 493:495–500 Available at: http://dx.doi.org/10.1038/nature11775.

Grimsley JMS, Sheth S, Vallabh N, Grimsley CA, Bhattal J, Latsko M, Jasnow A, Wenstrup JJ (2016) Contextual modulation of vocal behavior in mouse: Newly identified 12 kHz "Mid-frequency" vocalization emitted during restraint. Front Behav Neurosci 10.

Hagler DJ, Ulbert I, Wittner L, Erőss L, Madsen JR, Devinsky O, Doyle W, Fabó D, Cash SS, Halgren E (2018) Heterogeneous origins of human sleep spindles in different cortical layers. J Neurosci 38:3013–3025.

Halassa MM, Acsády L (2016) Thalamic Inhibition: Diverse Sources, Diverse Scales. Trends Neurosci 39:680–693 Available at: http://dx.doi.org/10.1016/j.tins.2016.08.001.

Halassa MM, Siegle JH, Ritt JT, Ting JT, Feng G, Moore CI (2011) Selective optical drive of thalamic reticular nucleus generates thalamic bursts and cortical spindles. Nat Neurosci 14:1118–1120 Available at: http://dx.doi.org/10.1038/nn.2880.

Harlow JH (2004) Electric power transformer engineering.

Harrison PJ, McLaughlin D, Kerwin RW (1991) Decreased hippocampal expression of a glutamate receptor gene in schizophrenia. Lancet 337:450–452.

Hayat H, Regev N, Matosevich N, Sales A, Paredes-Rodriguez E, Krom AJ, Bergman L, Li Y, Lavigne M, Kremer EJ, Yizhar O, Pickering AE, Nir Y (2020) Locus coeruleus norepinephrine activity mediates sensory-evoked awakenings from sleep. Sci Adv 6.

He BJ (2014) Scale-free brain activity: Past, present, and future. Trends Cogn Sci 18:480–487.

Henin S, Borges H, Shankar A, Sarac C, Melloni L, Friedman D, Flinker A, Parra LC, Buzsaki G, Devinsky O, Liu A (2019) Closed-loop acoustic stimulation enhances sleep oscillations but not memory performance. eNeuro 6.

Henschke JU, Noesselt T, Scheich H, Budinger E (2015) Possible anatomical pathways for short-latency multisensory integration processes in primary sensory cortices. Brain Struct Funct

220:955–977.

Herreras O (2016) Local field potentials: Myths and misunderstandings. Front Neural Circuits 10.

Himanen SL, Virkkala J, Huhtala H, Hasan J (2002) Spindle frequencies in sleep EEG show U-shape within first four NREM sleep episodes. J Sleep Res 11:35–42.

Hoffman DA, Sprengel R, Sakmann B (2002) Molecular dissection of hippocampal theta-burst pairing potentiation. Proc Natl Acad Sci U S A 99:7740–7745.

Hofstetter JR, Lysaker PH, Mayeda AR (2005) Quality of sleep in patients with schizophrenia is associated with quality of life and coping. BMC Psychiatry 5.

Honjoh S, Sasai S, Schiereck SS, Nagai H, Tononi G, Cirelli C (2018) Regulation of cortical activity and arousal by the matrix cells of the ventromedial thalamic nucleus. Nat Commun 9.

Hooks BM, Mao T, Gutnisky DA, Yamawaki N, Svoboda K, Shepherd GMG (2013) Organization of cortical and thalamic input to pyramidal neurons in mouse motor cortex. J Neurosci 33:748–760.

Hudson JI, Lipinski JF, Keck PE, Aizley HG, Vuckovic A, Zierk KC, Pope HG (1993) Polysomnographic characteristics of schizophrenia in comparison with mania and depression. Biol Psychiatry 34:191–193.

Huguenard JR (1996) Low-threshold calcium currents in central nervous system neurons. Annu Rev Physiol 58:329–348.

Hunnicutt BJ, Long BR, Kusefoglu D, Gertz KJ, Zhong H, Mao T (2014) A comprehensive thalamocortical projection map at the mesoscopic level. Nat Neurosci 17:1276–1285.

Huupponen E, Gómez-Herrero G, Saastamoinen A, Värri A, Hasan J, Himanen SL (2007) Development and comparison of four sleep spindle detection methods. Artif Intell Med 40:157–170.

Huupponen E, Värri A, Himanen SL, Hasan J, Lehtokangas M, Saarinen J (2000) Optimization of sigma amplitude threshold in sleep spindle detection. J Sleep Res 9:327–334.

Ison JR, Allen PD, O'Neill WE (2007) Age-related hearing loss in C57BL/6J mice has both frequency-specific and non-frequency-specific components that produce a hyperacusis-like exaggeration of the acoustic startle reflex. JARO - J Assoc Res Otolaryngol 8:539–550.

Jensen KF, Killackey HP (1987) Terminal arbors of axons projecting to the somatosensory cortex of the adult rat. II. The altered morphology of thalamocortical afferents following neonatal infraorbital nerve cut. J Neurosci 7:3544–3553.

Johnson AW, Bannerman D, Rawlins N, Sprengel R, Good MA (2007) Targeted Deletion of the GluR-1 AMPA Receptor in Mice Dissociates General and Outcome-Specific Influences of Appetitive Rewards on Learning. Behav Neurosci 121:1192–1202.

Johnson AW, Bannerman DM, Rawlins NP, Sprengel R, Good MA (2005) Impaired outcome-specific devaluation of instrumental responding in mice with a targeted deletion of the AMPA receptor glutamate receptor 1 subunit. J Neurosci 25:2359–2365.

Jones EG (1975) Some aspects of the organization of the thalamic reticular complex. J Comp Neurol 162:285–308.

Jones EG (2009) Synchrony in the interconnected circuitry of the thalamus and cerebral cortex. Ann N Y Acad Sci 1157:10–23.

Jouvet M (1967) The states of sleep. Sci Am 216.

Kajikawa Y, Schroeder CE (2011) How local is the local field potential? Neuron 72:847–858 Available at: http://dx.doi.org/10.1016/j.neuron.2011.09.029.

Kandel A, Buzséki G (1997) Cellular-synaptic generation of sleep spindles, spike-and-wave discharges, and evoked thalamocortical responses in the neocortex of the rat. J Neurosci 17:6783–6797.

Karbowski J, Ermentrout GB (2002) Synchrony arising from a balanced synaptic plasticity in a network of heterogeneous neural oscillators. Phys Rev E - Stat Physics, Plasmas, Fluids, Relat Interdiscip Top 65.

Karimi A, Odenthal J, Drawitsch F, Boergens K, Helmstaedter M (2019) Cell-type specific innervation of cortical pyramidal cells at their apical tufts. bioRxiv:571695.

Katzner S, Nauhaus I, Benucci A, Bonin V, Ringach DL, Carandini M (2009) Local Origin of Field Potentials in Visual Cortex. Neuron 61:35–41.

Kerwin R, Patel S, Meldrum B (1990) Quantitative autoradiographic analysis of glutamate binding sites in the hippocampal formation in normal and schizophrenic brain post mortem. Neuroscience 39:25–32.

Killackey HP (1973) Anatomical evidence for cortical subdivisions based on vertically discrete thalamic projections from the ventral posterior nucleus to cortical barrels in the rat. Brain Res 51:326–331.

Kim D, Hwang E, Lee M, Sung H, Choi JH (2015) Characterization of topographically specific sleep spindles in mice. Sleep 38:85–96.

Kim J, Gulati T, Ganguly K (2019) Competing Roles of Slow Oscillations and Delta Waves in Memory Consolidation versus Forgetting. Cell 179:514-526.e13.

Kim U, McCormick DA (1998) The functional influence of burst and tonic firing mode on synaptic interactions in the thalamus. J Neurosci 18:9500–9516.

Kirov G et al. (2012) De novo CNV analysis implicates specific abnormalities of postsynaptic signalling complexes in the pathogenesis of schizophrenia. Mol Psychiatry.

Klinzing JG, Mölle M, Weber F, Supp G, Hipp JF, Engel AK, Born J (2016) Spindle activity phase-locked to sleep slow oscillations. Neuroimage 134:607–616.

Knoblauch V, Kräuchi K, Renz C, Wirz-Justice A, Cajochen C (2002) Homeostatic control of slow-wave and spindle frequency activity during human sleep: Effect of differential sleep pressure and brain topography. Cereb Cortex 12:1092–1100.

Knoblauch V, Martens WLJ, Wirz-Justice A, Cajochen C (2003) Human sleep spindle characteristics after sleep deprivation. Clin Neurophysiol 114:2258–2267.

Kouider S, Andrillon T, Barbosa LS, Goupil L, Bekinschtein TA (2014) Inducing task-relevant responses to speech in the sleeping brain. Curr Biol 24:2208–2214.

Krieger P, De Kock CPJ, Frick A (2017) Calcium dynamics in basal dendrites of layer 5a and 5b pyramidal neurons is tuned to the cell-type specific physiological action potential discharge. Front Cell Neurosci 11.

Krishnan GP, Rosen BQ, Chen JY, Muller L, Sejnowski TJ, Cash SS, Halgren E, Bazhenov M (2018) Thalamocortical and intracortical laminar connectivity determines sleep spindle properties. PLoS Comput Biol 14.

Krueger JM, Frank MG, Wisor JP, Roy S (2016) Sleep function: Toward elucidating an enigma. Sleep Med Rev 28:46–54.

Lajnef T, Chaibi S, Eichenlaub JB, Ruby PM, Aguera PE, Samet M, Kachouri A, Jerbi K (2015) Sleep spindle and K-complex detection using tunable Q-factor wavelet transform and morphological component analysis. Front Hum Neurosci 9:1–17.

Lampert T, Plano A, Austin J, Platt B (2015) On the identification of sleep stages in mouse electroencephalography time-series. J Neurosci Methods 246:52–64.

Landolt HP, Glatzel M, Blättler T, Achermann P, Roth C, Mathis J, Weis J, Tobler I, Aguzzi A, Bassetti CL (2006) Sleep-wake disturbances in sporadic Creutzfeldt-Jakob disease. Neurology 66:1418–1424.

Latchoumane CF V., Ngo HV V., Born J, Shin HS (2017) Thalamic Spindles Promote Memory Formation during Sleep through Triple Phase-Locking of Cortical, Thalamic, and Hippocampal Rhythms. Neuron 95:424-435.e6 Available at: http://dx.doi.org/10.1016/j.neuron.2017.06.025.

Lázár ZI, Dijk DJ, Lázár AS (2019) Infraslow oscillations in human sleep spindle activity. J Neurosci Methods 316:22–34.

Lecci S, Fernandez LMJ, Weber FD, Cardis R, Chatton JY, Born J, Lüthi A (2017) Coordinated infraslow neural and cardiac oscillations mark fragility and offline periods in mammalian sleep. Sci Adv 3.

Lee CC, Imaizumi K (2013) Functional convergence of thalamic and intrinsic projections to cortical layers 4 and 6. Neurophysiology 45:396–406.

Lein ES et al. (2007) Genome-wide atlas of gene expression in the adult mouse brain. Nature 445:168–176.

Leminen MM, Virkkala J, Saure E, Paajanen T, Zee PC, Santostasi G, Hublin C, Müller K, Porkka-Heiskanen T, Huotilainen M, Paunio T (2017) Enhanced memory consolidation via automatic sound stimulation during non-REM sleep. Sleep 40.

Lemus L, Hernández A, Luna R, Zainos A, Romo R (2010) Do sensory cortices process more than one sensory modality during perceptual judgments? Neuron 67:335–348.

Lesku JA, Roth TC, Amlaner CJ, Lima SL (2006) A phylogenetic analysis of sleep architecture in mammals: The integration of anatomy, physiology, and ecology. Am Nat 168:441–453.

Lips ES, Cornelisse LN, Toonen RF, Min JL, Hultman CM, Holmans PA, O'Donovan MC, Purcell SM, Smit AB, Verhage M, Sullivan PF, Visscher PM, Posthuma D (2012) Functional gene group analysis identifies synaptic gene groups as risk factor for schizophrenia. Mol Psychiatry 17:996–1006.

Liu D, Dan Y (2019) A Motor Theory of Sleep-Wake Control: Arousal-Action Circuit. Annu Rev Neurosci 42:27–46.

Loomis AL, Harvey EN, Hobart G (1935) Potential rhythms of the cerebral cortex during sleep. Science (80-) 81:597–598.

Loomis AL, Harvey EN, Hobart GA (1937) Cerebral states during sleep, as studied by human brain potentials. J Exp Psychol 21:127–144.

Lu J, Greco MA, Shiromani P, Saper CB (2000) Effect of lesions of the ventrolateral preoptic nucleus on NREM and REM sleep. J Neurosci 20:3830–3842.

Lustenberger C, Boyle MR, Alagapan S, Mellin JM, Vaughn B V., Fröhlich F (2016) Feedback-Controlled Transcranial Alternating Current Stimulation Reveals a Functional Role of Sleep Spindles in Motor Memory Consolidation. Curr Biol 26:2127–2136.

Lustenberger C, O'Gorman RL, Pugin F, Tüshaus L, Wehrle F, Achermann P, Huber R (2015) Sleep spindles are related to schizotypal personality traits and thalamic glutamine/glutamate in healthy subjects. Schizophr Bull 41:522–531.

Lustenberger C, Patel YA, Alagapan S, Page JM, Price B, Boyle MR, Fröhlich F (2018) High-density EEG characterization of brain responses to auditory rhythmic stimuli during wakefulness and NREM sleep. Neuroimage 169:57–68.

Lüthi A (2014) Sleep spindles: Where they come from, what they do. Neuroscientist 20:243–256.

Lüthi A, McCormick DA (1998) Periodicity of thalamic synchronized oscillations: The role of Ca2+-mediated upregulation of I(h). Neuron 20:553–563.

Maingret N, Girardeau G, Todorova R, Goutierre M, Zugaro M (2016) Hippocampo-cortical coupling mediates memory consolidation during sleep. Nat Neurosci 19:959–964 Available at: http://dx.doi.org/10.1038/nn.4304%5Cnhttp://10.1038/nn.4304%5Cnhttp://www.nature.com/neuro/journal/v19/n7/abs/nn.4304.html#supplementary-information.

Malinow R, Malenka RC (2002) AMPA receptor trafficking and synaptic plasticity. Annu Rev Neurosci 25:103–126.

Manoach DS, Mylonas D, Baxter B (2020) Targeting sleep oscillations to improve memory in schizophrenia. Schizophr Res 221:63–70.

Manoach DS, Pan JQ, Purcell SM, Stickgold R (2016) Reduced Sleep Spindles in Schizophrenia: A Treatable Endophenotype That Links Risk Genes to Impaired Cognition? Biol Psychiatry 80:599–608 Available at: http://dx.doi.org/10.1016/j.biopsych.2015.10.003.

Manoach DS, Stickgold R (2019) Abnormal Sleep Spindles, Memory Consolidation, and Schizophrenia. Annu Rev Clin Psychol 15:451–479.

Manoach DS, Thakkar KN, Stroynowski E, Ely A, McKinley SK, Wamsley E, Djonlagic I, Vangel MG, Goff DC, Stickgold R (2010) Reduced overnight consolidation of procedural learning in chronic medicated schizophrenia is related to specific sleep stages. J Psychiatr Res 44:112–120.

Marmion B (2007) The story of Q fever. IMVS Newsl 43:6–7 Available at: http://www.imvs.org/newsletters/PDFs/IMVS_NL_67.pdf.

Marshall L, Helgadóttir H, Mölle M, Born J (2006) Boosting slow oscillations during sleep potentiates memory. Nature 444:610–613.

Maruyama AT, Komai S (2018) Auditory-induced response in the primary sensory cortex of rodents. PLoS One 13:1–18.

Massé IO, Blanchet-Godbout S, Bronchti G, Boire D (2019) Afferent connections of the primary somatosensory cortex of the mouse for contextual and multisensory processing. bioRxiv:514414.

Massimini M, Ferrarelli F, Esser SK, Riedner BA, Huber R, Murphy M, Peterson MJ, Tononi G (2007) Triggering sleep slow waves by transcranial magnetic stimulation. Proc Natl Acad Sci U S A 104:8496–8501.

Massimini M, Huber R, Ferrarelli F, Hill S, Tononi G (2004) The sleep slow oscillation as a traveling

wave. J Neurosci 24:6862–6870.

Mayr O, Johnson SH (1976) The Origins of Feedback Control. J Dyn Syst Meas Control 98:204–204.

McCormick DA, Bal T (1994) Sensory gating mechanisms of the thalamus. Curr Opin Neurobiol 4:550–556.

McCormick DA, Bal T (1997) Sleep and arousal: Thalamocortical mechanisms. Annu Rev Neurosci 20:185–215.

McCormick DA, Feeser HR (1990) Functional implications of burst firing and single spike activity in lateral geniculate relay neurons. Neuroscience 39:103–113.

McNamara JO, Eubanks JH, McPherson JD, Wasmuth JJ, Evans GA, Heinemann SF (1992) Chromosomal localization of human glutamate receptor genes. J Neurosci 12:2555–2562.

McNamara P, Capellini I, Harris E, Nunn CL, Barton RA, Preston B (2008) The Phylogeny of Sleep Database: A New Resource for Sleep Scientists. Open Sleep J 1:11–14.

Mianné J, Chessum L, Kumar S, Aguilar C, Codner G, Hutchison M, Parker A, Mallon AM, Wells S, Simon MM, Teboul L, Brown SDM, Bowl MR (2016) Correction of the auditory phenotype in C57BL/6N mice via CRISPR/Cas9-mediated homology directed repair. Genome Med 8.

Mignot E (2008) Why we sleep: The temporal organization of recovery. PLoS Biol 6:661–669.

Miller JF, Neufang M, Solway A, Brandt A, Trippel M, Mader I, Hefft S, Merkow M, Polyn SM, Jacobs J, Kahana MJ, Schulze-Bonhage A (2013) Neural activity in human hippocampal formation reveals the spatial context of retrieved memories. Science (80-) 342:1111–1114.

Mineff EM, Weinberg RJ (2000) Differential synaptic distribution of AMPA receptor subunits in the ventral posterior and reticular thalamic nuclei of the rat. Neuroscience 101:969–982.

Miyawaki H, Billeh YN, Diba K (2017) Low activity microstates during sleep. Sleep 40.

Morison RS, Bassett DL (1945) Electrical Activity of the Thalamus and Basal Ganglia in Decorticate Cats. J Neurophysiol 8:309–314.

Moser MB, Moser EI (1998) Distributed encoding and retrieval of spatial memory in the hippocampus. J Neurosci 18:7535–7542.

Mureşan RC, Jurjuţ OF, Moca V V., Singer W, Nikolić D (2008) The oscillation score: An efficient method for estimating oscillation strength in neuronal activity. J Neurophysiol 99:1333–1353.

Murray Sherman S (2001) Tonic and burst firing: Dual modes of thalamocortical relay. Trends Neurosci 24:122–126.

Musall S, Von Pföstl V, Rauch A, Logothetis NK, Whittingstall K (2014) Effects of neural synchrony on surface EEG. Cereb Cortex 24:1045–1053.

Mylonas D, Baran B, Demanuele C, Cox R, Vuper TC, Seicol BJ, Fowler RA, Correll D, Parr E, Callahan CE, Morgan A, Henderson D, Vangel M, Stickgold R, Manoach DS (2020) The effects of eszopiclone on sleep spindles and memory consolidation in schizophrenia: a randomized clinical trial. Neuropsychopharmacology.

Naganuma F, Kroeger D, Bandaru SS, Absi G, Madara JC, Vetrivelan R (2019) Lateral hypothalamic neurotensin neurons promote arousal and hyperthermia. PLoS Biol 17.

Nathan AJ, Scobell A (2012) How China sees America.

Navarrete M, Schneider J, Ngo HV V., Valderrama M, Casson AJ, Lewis PA (2020) Examining the

optimal timing for closed-loop auditory stimulation of slow-wave sleep in young and older adults. Sleep 43:1–14.

Neimark MA, Andermann ML, Hopfield JJ, Moore CI (2003) Vibrissa resonance as a transduction mechanism for tactile encoding. J Neurosci 23:6499–6509.

Neske GT (2016) The slow oscillation in cortical and thalamic networks: Mechanisms and functions. Front Neural Circuits 9.

Ngo HV V., Claussen JC, Born J, Mölle M (2013a) Induction of slow oscillations by rhythmic acoustic stimulation. J Sleep Res 22:22–31.

Ngo HV V., Martinetz T, Born J, Mölle M (2013b) Auditory closed-loop stimulation of the sleep slow oscillation enhances memory. Neuron 78:545–553.

Ngo HV V., Seibold M, Boche DC, Mölle M, Born J (2019) Insights on auditory closed-loop stimulation targeting sleep spindles in slow oscillation up-states. J Neurosci Methods 316:117–124.

Niethard N, Ngo HV V., Ehrlich I, Born J (2018) Cortical circuit activity underlying sleep slow oscillations and spindles. Proc Natl Acad Sci U S A 115:E9220–E9229.

Nir Y, Mukamel R, Dinstein I, Privman E, Harel M, Fisch L, Gelbard-Sagiv H, Kipervasser S, Andelman F, Neufeld MY, Kramer U, Arieli A, Fried I, Malach R (2008) Interhemispheric correlations of slow spontaneous neuronal fluctuations revealed in human sensory cortex. Nat Neurosci 11:1100–1108.

Nir Y, Staba RJ, Andrillon T, Vyazovskiy V V., Cirelli C, Fried I, Tononi G (2011) Regional Slow Waves and Spindles in Human Sleep. Neuron 70:153–169 Available at: http://dx.doi.org/10.1016/j.neuron.2011.02.043.

Noben-Trauth K, Zheng QY, Johnson KR, Nishina PM (1997) mdfw: A deafness susceptibility locus that interacts with deaf waddler (dfw). Genomics 44:266–272.

Nunez PL, Srinivasan R (2009) Electric Fields of the Brain: The neurophysics of EEG.

O'keefe J, Nadel L (1979) Précis of O'Keefe & Nadel's The hippocampus as a cognitive map. Behav Brain Sci 2:487–494.

Olbrich E, Achermann P (2005) Analysis of oscillatory patterns in the human sleep EEG using a novel detection algorithm. J Sleep Res 14:337–346.

Olbrich E, Claussen JC, Achermann P (2011) The multiple time scales of sleep dynamics as a challenge for modelling the sleeping brain. Philos Trans R Soc A Math Phys Eng Sci 369:3884–3901.

Olbrich E, Landolt HP, Achermann P (2014) Effect of prolonged wakefulness on electroencephalographic oscillatory activity during sleep. J Sleep Res 23:255–262.

Olbrich E, Rusterholz T, LeBourgeois MK, Achermann P (2017) Developmental Changes in Sleep Oscillations during Early Childhood. Neural Plast 2017.

Oliveira AMM, Hawk JD, Abel T, Havekes R (2010) Post-training reversible inactivation of the hippocampus enhances novel object recognition memory. Learn Mem 17:155–160.

Ong JL, Lo JC, Chee NIYN, Santostasi G, Paller KA, Zee PC, Chee MWL (2016) Effects of phase-locked acoustic stimulation during a nap on EEG spectra and declarative memory consolidation. Sleep Med 20:88–97.

Pardey J, Roberts S, Tarassenko L, Stradling J (1996) A new approach to the analysis of the human sleep/wakefulness continuum. J Sleep Res 5:201–210.

Peyrache A, Battaglia FP, Destexhe A (2011) Inhibition recruitment in prefrontal cortex during sleep spindles and gating of hippocampal inputs. Proc Natl Acad Sci U S A 108:17207–17212 Available at: http://www.pubmedcentral.nih.gov/articlerender.fcgi?artid=3193185&tool=pmcentrez&rendertype=abstract.

Piantoni G, Halgren E, Cash SS (2017) Spatiotemporal characteristics of sleep spindles depend on cortical location. Neuroimage 146:236–245 Available at: http://dx.doi.org/10.1016/j.neuroimage.2016.11.010.

Picchioni D, Horovitz SG, Fukunaga M, Carr WS, Meltzer JA, Balkin TJ, Duyn JH, Braun AR (2011) Infraslow EEG oscillations organize large-scale cortical-subcortical interactions during sleep: A combined EEG/fMRI study. Brain Res 1374:63–72.

Pinault D (2004) The thalamic reticular nucleus: Structure, function and concept. Brain Res Rev 46:1–31.

Pinault D (2011) Dysfunctional thalamus-related networks in schizophrenia. Schizophr Bull 37:238–243.

Porkka-Heiskanen T, Kalinchuk A V. (2011) Adenosine, energy metabolism and sleep homeostasis. Sleep Med Rev 15:123–135.

Ralph MR, Foster RG, Davis FC, Menaker M (1990) Transplanted suprachiasmatic nucleus determines circadian period. Science (80-) 247:975–978.

Rasch B, Born J (2013) About sleep's role in memory. Physiol Rev 93:681–766 Available at: http://www.ncbi.nlm.nih.gov/pubmed/23589831%5Cnhttp://www.ncbi.nlm.nih.gov/pubmed/23589831.

Ray LB, Fogel SM, Smith CT, Peters KR (2010) Validating an automated sleep spindle detection algorithm using an individualized approach. J Sleep Res 19:374–378.

Rechtschaffen A (1998) Current perspectives on the function of sleep. Perspect Biol Med 41:359–390.

Rechtschaffen A, Bergmann BM (2002) Sleep deprivation in the rat: An update of the 1989 paper. Sleep 25:18–24.

Rechtschaffen A, Hauri P, Zeitlin M (1966) Auditory awakening thresholds in REM and NREM sleep stages. Percept Mot Skills 22:927–942.

Refinetti R, Wassmer T, Basu P, Cherukalady R, Pandey VK, Singaravel M, Giannetto C, Piccione G (2016) Variability of behavioral chronotypes of 16 mammalian species under controlled conditions. Physiol Behav 161:53–59.

Reisel D, Bannerman DM, Schmitt WB, Deacon RMJ, Flint J, Borchardt T, Seeburg PH, Rawlins JNP (2002) Spatial memory dissociations in mice lacking GluR1. Nat Neurosci 5:868–873.

Rial RV, Nicolau MC, Gamundí A, Akaârir M, Aparicio S, Garau C, Tejada S, Roca C, Gené L, Moranta D, Esteban S (2007) The trivial function of sleep. Sleep Med Rev 11:311–325.

Ripke S et al. (2014) Biological insights from 108 schizophrenia-associated genetic loci. Nature 511:421–427.

Ripperger JA, Jud C, Albrecht U (2011) The daily rhythm of mice. FEBS Lett 585:1384–1392.

Romberg C, Raffel J, Martin L, Sprengel R, Seeburg PH, Rawlins JNP, Bannerman DM, Paulsen O (2009) Induction and expression of GluA1 (GluR-A)-independent LTP in the hippocampus. Eur J Neurosci 29:1141–1152.

Rosanova M, Ulrich D (2005) Pattern-specific associative long-term potentiation induced by a sleep spindle-related spike train. J Neurosci 25:9398–9405.

Sakmann B (2017) From single cells and single columns to cortical networks: dendritic excitability, coincidence detection and synaptic transmission in brain slices and brains. Exp Physiol 102:489–521.

Sanchez-Vives M V., McCormick DA (2000) Cellular and network mechanisms of rhytmic recurrent activity in neocortex. Nat Neurosci 3:1027–1034.

Sanderson DJ, Good MA, Skelton K, Sprengel R, Seeburg PH, Rawlins JNP, Bannerman DM (2009) Enhanced long-term and impaired short-term spatial memory in GluA1 AMPA receptor subunit knockout mice: Evidence for a dual-process memory model. Learn Mem 16:379–386 Available at: http://learnmem.cshlp.org/cgi/doi/10.1101/lm.1339109.

Sanderson DJ, Hindley E, Smeaton E, Denny N, Taylor A, Barkus C, Sprengel R, Seeburg PH, Bannerman DM (2011) Deletion of the GluA1 AMPA receptor subunit impairs recency-dependent object recognition memory. Learn Mem 18:181–190 Available at: http://learnmem.cshlp.org/cgi/doi/10.1101/lm.2083411.

Sanderson DJ, McHugh SB, Good MA, Sprengel R, Seeburg PH, Rawlins JNP, Bannerman DM (2010) Spatial working memory deficits in GluA1 AMPA receptor subunit knockout mice reflect impaired short-term habituation: Evidence for Wagner's dual-process memory model. Neuropsychologia 48:2303–2315.

Saper CB, Chou TC, Scammell TE (2001) The sleep switch: Hypothalamic control of sleep and wakefulness. Trends Neurosci 24:726–731.

Saper CB, Fuller PM, Pedersen NP, Lu J, Scammell TE (2010) Sleep State Switching. Neuron 68:1023–1042.

Schabus M, Dang-Vu TT, Heib DPJ, Boly M, Desseilles M, Vandewalle G, Schmidt C, Albouy G, Darsaud A, Gais S, Degueldre C, Balteau E, Phillips C, Luxen A, Maquet P (2012) The fate of incoming stimuli during NREM sleep is determined by spindles and the phase of the slow oscillation. Front Neurol APR:1–11.

Schimicek P, Zeitlhofer J, Anderer P, Saletu B (1994) Automatic Sleep-Spindle Detection Procedure: Aspects of Reliability and Validity. Clin EEG Neurosci 25:26–29.

Schmitt WB, Deacon RMJ, Seeburg PH, Rawlins JNP, Bannerman DM (2003) A within-subjects, within-task demonstration of intact spatial reference memory and impaired spatial working memory in glutamate receptor-A-deficient mice. J Neurosci 23:3953–3958.

Schneider WT, Vas S, Nicol AU, Morton AJ (2020) Characterizing sleep spindles in sheep. eNeuro 7.

Schreiber T, Schmitz A (2000) Surrogate time series. Phys D Nonlinear Phenom 142:346–382.

Sejnowski TJ, Destexhe A (2000) Why do we sleep? Brain Res 886:208–223.

Sejnowski TJ, Paulsen O (2006) Network oscillations: Emerging computational principles. J Neurosci 26:1673–1676.

Sela Y, Krom AJ, Bergman L, Regev N, Nir Y (2020) Sleep differentially affects early and late neuronal responses to sounds in auditory and perirhinal cortices. J Neurosci 40:2895–2905.

Sela Y, Vyazovskiy V V., Cirelli C, Tononi G, Nir Y (2016) Responses in rat core auditory cortex are preserved during sleep spindle oscillations. Sleep 39:1069–1082 Available at: https://academic.oup.com/sleep/article-lookup/doi/10.5665/sleep.5758.

Shepherd JD, Huganir RL (2007) The cell biology of synaptic plasticity: AMPA receptor trafficking. Annu Rev Cell Dev Biol 23:613–643.

Sherin JE, Shiromani PJ, McCarley RW, Saper CB (1996) Activation of ventrolateral preoptic neurons during sleep. Science (80-) 271:216–219.

Sheroziya M, Timofeev I (2014) Global intracellular slow-wave dynamics of the thalamocortical system. J Neurosci 34:8875–8893.

Siegel JM (2005) Clues to the functions of mammalian sleep. Nature 437:1264–1271.

Siegel M, Donner TH, Engel AK (2012) Spectral fingerprints of large-scale neuronal interactions. Nat Rev Neurosci 13:121–134.

Sokolov BP (1998) Expression of NMDAR1, GluR1, GluR7, and KA1 glutamate receptor mRNAs is decreased in frontal cortex of “neuroleptic-free” schizophrenics: Evidence on reversible up-regulation by typical neuroleptics. J Neurochem 71:2454–2464.

Staresina BP, Bergmann TO, Bonnefond M, Van Der Meij R, Jensen O, Deuker L, Elger CE, Axmacher N, Fell J (2015) Hierarchical nesting of slow oscillations, spindles and ripples in the human hippocampus during sleep. Nat Neurosci 18:1679–1686 Available at: http://dx.doi.org/10.1038/nn.4119.

Steriade M (1991) Alertness, Quiet Sleep, Dreaming. In, pp 279–357.

Steriade M (1993) Cholinergic blockage of network- and intrinsically generated slow oscillations promotes waking and REM sleep activity patterns in thalamic and cortical neurons. Prog Brain Res 98:345–355.

Steriade M (2003) The corticothalamic system in sleep. Front Biosci 8.

Steriade M (2006) Grouping of brain rhythms in corticothalamic systems. Neuroscience 137:1087–1106.

Steriade M, Domich L, Oakson G (1986) Reticularis thalami neurons revisited: Activity changes during shifts in states of vigilance. J Neurosci 6:68–81.

Steriade M, Domich L, Oakson G, Deschenes M (1987) The deafferented reticular thalamic nucleas generates spindle rhythmicity. J Neurophysiol 57:260–273.

Steriade M, Dossi RC, Nunez A (1991) Network modulation of a slow intrinsic oscillation of cat thalamocortical neurons implicated in sleep delta waves: Cortically induced synchronization and brainstem cholinergic suppression. J Neurosci 11:3200–3217.

Steriade M, McCormick DA, Sejnowski TJ (1993a) Thalamocortical oscillations in the sleeping and aroused brain. Science (80-) 262:679–685.

Steriade M, Nunez A, Amzica F (1993b) A novel slow (< 1 Hz) oscillation of neocortical neurons in vivo: Depolarizing and hyperpolarizing components. J Neurosci 13:3252–3265.

Stickgold R (2005) Sleep-dependent memory consolidation. Nature 437:1272–1278.

Stone JM, Morrison PD, Pilowsky LS (2007) Glutamate and dopamine dysregulation in schizophrenia - A synthesis and selective review. J Psychopharmacol 21:440–452.

Takahashi YK, Kori H, Masuda N (2009) Self-organization of feed-forward structure and entrainment in excitatory neural networks with spike-timing-dependent plasticity. Phys Rev E - Stat Nonlinear, Soft Matter Phys 79.

Talley EM, Cribbs LL, Lee JH, Daud A, Perez-Reyes E, Bayliss DA (1999) Differential distribution of three members of a gene family encoding low voltage-activated (T-type) calcium channels. J Neurosci 19:1895–1911.

Tartar JL, Ward CP, McKenna JT, Thakkar M, Arrigoni E, McCarley RW, Brown RE, Strecker RE (2006) Hippocampal synaptic plasticity and spatial learning are impaired in a rat model of sleep fragmentation. Eur J Neurosci 23:2739–2748.

Telenczuk B, Dehghani N, Le Van Quyen M, Cash SS, Halgren E, Hatsopoulos NG, Destexhe A (2017) Local field potentials primarily reflect inhibitory neuron activity in human and monkey cortex. Sci Rep 7.

Tesler N, Gerstenberg M, Franscini M, Jenni OG, Walitza S, Huber R (2015) Reduced sleep spindle density in early onset schizophrenia: A preliminary finding. Schizophr Res 166:355–357.

Timofeev I, Chauvette S (2013) The spindles: Are they still thalamic? Sleep 36:825–826.

Timofeev I, Grenier F, Bazhenov M, Sejnowski TJ, Steriade M (2000) Origin of slow cortical oscillations in deafferented cortical slabs. Cereb Cortex 10:1185–1199.

Tobler I (2010) Phylogeny of Sleep Regulation. In: Principles and Practice of Sleep Medicine: Fifth Edition, pp 112–125.

Tobler I, Borbély AA (1986) Sleep EEG in the rat as a function of prior waking. Electroencephalogr Clin Neurophysiol 64:74–76.

Tobler I, Borbély AA, Groos G (1983) The effect of sleep deprivation on sleep in rats with suprachiasmatic lesions. Neurosci Lett 42:49–54.

Tononi G, Cirelli C (2003) Sleep and synaptic homeostasis: A hypothesis. Brain Res Bull 62:143–150.

Tononi G, Cirelli C (2006) Sleep function and synaptic homeostasis. Sleep Med Rev 10:49–62.

Tononi G, Cirelli C (2014) Sleep and the Price of Plasticity: From Synaptic and Cellular Homeostasis to Memory Consolidation and Integration. Neuron 81:12–34 Available at: http://dx.doi.org/10.1016/j.neuron.2013.12.025.

Tononi G, Riedner BA, Hulse BK, Ferrarelli F, Sarasso S (2010) Enhancing sleep slow waves with natural stimuli. Medicamundi 54:82–88.

Trachsel L, Tobler I, Borbely AA (1988) Electroencephalogram analysis of non-rapid eye movement sleep in rats. Am J Physiol - Regul Integr Comp Physiol 255.

Ujma P, Hajnal B, Bódizs R, Gombos F, Erőss L, Wittner L, Halgren E, Cash S, Ulbert I, Fabó D (2019) The laminar profile of sleep spindles in humans. bioRxiv:563221.

van Vugt MK, Sederberg PB, Kahana MJ (2007) Comparison of spectral analysis methods for characterizing brain oscillations. J Neurosci Methods 162:49–63.

Van Waterschoot T, Moonen M (2007) A pole-zero placement technique for designing second-order IIR parametric equalizer filters. IEEE Trans Audio, Speech Lang Process 15:2561–2565.

VanderPlas JT (2018) Understanding the Lomb–Scargle Periodogram. Astrophys J Suppl Ser 236:16.

VanRullen R (2011) Four common conceptual fallacies in mapping the time course of recognition.

Front Psychol 2.

Vogel-Ciernia A, Wood MA (2014) Examining object location and object recognition memory in mice. Curr Protoc Neurosci 2014:8.31.1-8.31.17.

Von Krosigk M, Bal T, McCormick DA (1993) Cellular mechanisms of a synchronized oscillation in the thalamus. Science (80-) 261:361–364.

Vorhees C V., Williams MT (2014) Assessing spatial learning and memory in rodents. ILAR J 55:310–332.

Vyazovskiy V V., Achermann P, Borbély AA, Tobler I (2004a) The dynamics of spindles and EEG slow-wave activity in NREM sleep in mice. In: Archives Italiennes de Biologie, pp 511–523.

Vyazovskiy V V., Cirelli C, Pfister-Genskow M, Faraguna U, Tononi G (2008) Molecular and electrophysiological evidence for net synaptic potentiation in wake and depression in sleep. Nat Neurosci 11:200–208 Available at: http://www.ncbi.nlm.nih.gov/pubmed/18204445.

Vyazovskiy V V., Faraguna U, Cirelli C, Tononi G (2009a) Triggering slow waves during NREM sleep in the rat by intracortical electrical stimulation: Effects of sleep/wake history and background activity. J Neurophysiol 101:1921–1931.

Vyazovskiy V V., Harris KD (2013) Sleep and the single neuron: The role of global slow oscillations in individual cell rest. Nat Rev Neurosci 14:443–451.

Vyazovskiy V V., Olcese U, Hanlon EC, Nir Y, Cirelli C, Tononi G (2011) Local sleep in awake rats. Nature 472:443–447 Available at: http://dx.doi.org/10.1038/nature10009.

Vyazovskiy V V., Olcese U, Lazimy YM, Faraguna U, Esser SK, Williams JC, Cirelli C, Tononi G (2009b) Cortical Firing and Sleep Homeostasis. Neuron 63:865–878 Available at: http://dx.doi.org/10.1016/j.neuron.2009.08.024.

Vyazovskiy V V., Riedner BA, Cirelli C, Tononi G (2007) Sleep homeostasis and cortical synchronization: II. A local field potential study of sleep slow waves in the rat. Sleep 30:1631–1642.

Vyazovskiy V V., Walton ME, Peirson SN, Bannerman DM (2017) Sleep homeostasis, habits and habituation. Curr Opin Neurobiol 44:202–211.

Vyazovskiy V, Achermann P, Borbély AA, Tobler I (2004b) Interhemispheric coherence of the sleep electroencephalogram in mice with congenital callosal dysgenesis. Neuroscience 124:481–488.

Wamsley EJ, Shinn AK, Tucker MA, Ono KE, McKinley SK, Ely A V., Goff DC, Stickgold R, Manoach DS (2013) The effects of eszopiclone on sleep spindles and memory consolidation in schizophrenia: A randomized placebo-controlled trial. Sleep 36:1369–1376.

Wamsley EJ, Tucker MA, Shinn AK, Ono KE, McKinley SK, Ely A V., Goff DC, Stickgold R, Manoach DS (2012) Reduced sleep spindles and spindle coherence in schizophrenia: Mechanisms of impaired memory consolidation? Biol Psychiatry 71:154–161 Available at: http://dx.doi.org/10.1016/j.biopsych.2011.08.008.

Warby SC, Wendt SL, Welinder P, Munk EGS, Carrillo O, Sorensen HBD, Jennum P, Peppard PE, Perona P, Mignot E (2014) Sleep-spindle detection: Crowdsourcing and evaluating performance of experts, non-experts and automated methods. Nat Methods 11:385–392.

Wen H, Liu Z (2016) Separating Fractal and Oscillatory Components in the Power Spectrum of Neurophysiological Signal. Brain Topogr 29:13–26.

Werth E, Achermann P, Borbély AA (1997) Brain topography of the human sleep EEG: Antero-posterior shifts of spectral power. Neuroreport 8:123–127.

Widmann A, Schröger E, Maess B (2015) Digital filter design for electrophysiological data - a practical approach. J Neurosci Methods 250:34–46.

Wiedholz LM, Owens WA, Horton RE, Feyder M, Karlsson RM, Hefner K, Sprengel R, Celikel T, Daws LC, Holmes A (2008) Mice lacking the AMPA GluR1 receptor exhibit striatal hyperdopaminergia and "schizophrenia-related" behaviors. Mol Psychiatry 13:631–640.

Wilson CJ, Groves PM (1981) Spontaneous firing patterns of identified spiny neurons in the rat neostriatum. Brain Res 220:67–80.

Wilson MA, McNaughton BL (1994) Reactivation of hippocampal ensemble memories during sleep. Science (80-) 265:676–679 Available at: http://www.sciencemag.org/cgi/doi/10.1126/science.8036517.

Wimmer RD, Astori S, Bond CT, Rovó Z, Chatton JY, Adelman JP, Franken P, Lüthi A (2012) Sustaining sleep spindles through enhanced SK2-channel activity consolidates sleep and elevates arousal threshold. J Neurosci 32:13917–13928 Available at: http://www.jneurosci.org/cgi/doi/10.1523/JNEUROSCI.2313-12.2012.

Wulff K, Gatti S, Wettstein JG, Foster RG (2010) Sleep and circadian rhythm disruption in psychiatric and neurodegenerative disease. Nat Rev Neurosci 11:589–599.

Xing D, Yeh CI, Shapley RM (2009) Spatial spread of the local field potential and its laminar variation in visual cortex. J Neurosci 29:11540–11549.

Xu M, Chung S, Zhang S, Zhong P, Ma C, Chang WC, Weissbourd B, Sakai N, Luo L, Nishino S, Dan Y (2015) Basal forebrain circuit for sleep-wake control. Nat Neurosci.

Yamadori A (1971) Role of the spindles in the onset of sleep. Kobe J Med Sci 17:97–111.

Yamawaki N, Borges K, Suter BA, Harris KD, Shepherd GMG (2014) A genuine layer 4 in motor cortex with prototypical synaptic circuit connectivity. Elife 3:e05422.

Yang C, Winkelman JW (2006) Clinical significance of sleep EEG abnormalities in chronic schizophrenia. Schizophr Res 82:251–260.

Zamanillo D, Sprengel R, Hvalby Ø, Jensen V, Burnashev N, Rozov A, Kaiser KMM, Köster HJ, Borchardt T, Worley P, Lübke J, Frotscher M, Kelly PH, Sommer B, Andersen P, Seeburg PH, Sakmann B (1999) Importance of AMPA receptors for hippocampal synaptic plasticity but not for spatial learning. Science (80-) 284:1805–1811 Available at: http://www.sciencemag.org/content/284/5421/1805.short.

Zamboni G, Perez E, Amici R, Jones CA, Parmeggiani PL (1999) Control of REM sleep: An aspect of the regulation of physiological homeostasis. Arch Ital Biol 137:249–262.

Zhou Y Di, Fuster JM (2004) Somatosensory cell response to an auditory cue in a haptic memory task. Behav Brain Res 153:573–578.